PHYSICAL AND NUMERICAL MODELLING FOR POWERHOUSE APPROACH AND TAILRACE DESIGNS

by

Marno R. Klein

A Thesis
Submitted to the Faculty of Graduate Studies
in Partial Fulfillment of the Requirements
for the Degree of

MASTER OF SCIENCE

Department of Civil and Geological Engineering
University of Manitoba
Winnipeg, Manitoba

© July, 1995

National Library
of Canada

Acquisitions and
Bibliographic Services Branch

395 Wellington Street
Ottawa, Ontario
K1A 0N4

Bibliothèque nationale
du Canada

Direction des acquisitions et
des services bibliographiques

395, rue Wellington
Ottawa (Ontario)
K1A 0N4

Your file *Votre référence*

Our file *Notre référence*

The author has granted an irrevocable non-exclusive licence allowing the National Library of Canada to reproduce, loan, distribute or sell copies of his/her thesis by any means and in any form or format, making this thesis available to interested persons.

L'auteur a accordé une licence irrévocable et non exclusive permettant à la Bibliothèque nationale du Canada de reproduire, prêter, distribuer ou vendre des copies de sa thèse de quelque manière et sous quelque forme que ce soit pour mettre des exemplaires de cette thèse à la disposition des personnes intéressées.

The author retains ownership of the copyright in his/her thesis. Neither the thesis nor substantial extracts from it may be printed or otherwise reproduced without his/her permission.

L'auteur conserve la propriété du droit d'auteur qui protège sa thèse. Ni la thèse ni des extraits substantiels de celle-ci ne doivent être imprimés ou autrement reproduits sans son autorisation.

ISBN 0-612-13257-9

Canada

Name _____

Dissertation Abstracts International is arranged by broad, general subject categories. Please select the one subject which most nearly describes the content of your dissertation. Enter the corresponding four-digit code in the spaces provided.

Civil Engineering
SUBJECT TERM

0	5	4	3
SUBJECT CODE

U·M·I

Subject Categories

THE HUMANITIES AND SOCIAL SCIENCES

COMMUNICATIONS AND THE ARTS
Architecture 0729
Art History 0377
Cinema 0900
Dance 0378
Fine Arts 0357
Information Science 0723
Journalism 0391
Library Science 0399
Mass Communications 0708
Music 0413
Speech Communication 0459
Theater 0465

EDUCATION
General 0515
Administration 0514
Adult and Continuing 0516
Agricultural 0517
Art 0273
Bilingual and Multicultural 0282
Business 0688
Community College 0275
Curriculum and Instruction 0727
Early Childhood 0518
Elementary 0524
Finance 0277
Guidance and Counseling 0519
Health 0680
Higher 0745
History of 0520
Home Economics 0278
Industrial 0521
Language and Literature 0279
Mathematics 0280
Music 0522
Philosophy of 0998
Physical 0523
Psychology 0525
Reading 0535
Religious 0527
Sciences 0714
Secondary 0533
Social Sciences 0534
Sociology of 0340
Special 0529
Teacher Training 0530
Technology 0710
Tests and Measurements 0288
Vocational 0747

LANGUAGE, LITERATURE AND LINGUISTICS
Language
- General 0679
- Ancient 0289
- Linguistics 0290
- Modern 0291

Literature
- General 0401
- Classical 0294
- Comparative 0295
- Medieval 0297
- Modern 0298
- African 0316
- American 0591
- Asian 0305
- Canadian (English) 0352
- Canadian (French) 0355
- English 0593
- Germanic 0311
- Latin American 0312
- Middle Eastern 0315
- Romance 0313
- Slavic and East European 0314

PHILOSOPHY, RELIGION AND THEOLOGY
Philosophy 0422
Religion
- General 0318
- Biblical Studies 0321
- Clergy 0319
- History of 0320
- Philosophy of 0322

Theology 0469

SOCIAL SCIENCES
American Studies 0323
Anthropology
- Archaeology 0324
- Cultural 0326
- Physical 0327

Business Administration
- General 0310
- Accounting 0272
- Banking 0770
- Management 0454
- Marketing 0338

Canadian Studies 0385
Economics
- General 0501
- Agricultural 0503
- Commerce-Business 0505
- Finance 0508
- History 0509
- Labor 0510
- Theory 0511

Folklore 0358
Geography 0366
Gerontology 0351
History
- General 0578
- Ancient 0579
- Medieval 0581
- Modern 0582
- Black 0328
- African 0331
- Asia, Australia and Oceania 0332
- Canadian 0334
- European 0335
- Latin American 0336
- Middle Eastern 0333
- United States 0337

History of Science 0585
Law 0398
Political Science
- General 0615
- International Law and Relations 0616
- Public Administration 0617

Recreation 0814
Social Work 0452
Sociology
- General 0626
- Criminology and Penology ... 0627
- Demography 0938
- Ethnic and Racial Studies 0631
- Individual and Family Studies 0628
- Industrial and Labor Relations 0629
- Public and Social Welfare 0630
- Social Structure and Development 0700
- Theory and Methods 0344

Transportation 0709
Urban and Regional Planning 0999
Women's Studies 0453

THE SCIENCES AND ENGINEERING

BIOLOGICAL SCIENCES
Agriculture
- General 0473
- Agronomy 0285
- Animal Culture and Nutrition 0475
- Animal Pathology 0476
- Food Science and Technology 0359
- Forestry and Wildlife 0478
- Plant Culture 0479
- Plant Pathology 0480
- Plant Physiology 0817
- Range Management 0777
- Wood Technology 0746

Biology
- General 0306
- Anatomy 0287
- Biostatistics 0308
- Botany 0309
- Cell 0379
- Ecology 0329
- Entomology 0353
- Genetics 0369
- Limnology 0793
- Microbiology 0410
- Molecular 0307
- Neuroscience 0317
- Oceanography 0416
- Physiology 0433
- Radiation 0821
- Veterinary Science 0778
- Zoology 0472

Biophysics
- General 0786
- Medical 0760

EARTH SCIENCES
Biogeochemistry 0425
Geochemistry 0996
Geodesy 0370
Geology 0372
Geophysics 0373
Hydrology 0388
Mineralogy 0411
Paleobotany 0345
Paleoecology 0426
Paleontology 0418
Paleozoology 0985
Palynology 0427
Physical Geography 0368
Physical Oceanography 0415

HEALTH AND ENVIRONMENTAL SCIENCES
Environmental Sciences 0768
Health Sciences
- General 0566
- Audiology 0300
- Chemotherapy 0992
- Dentistry 0567
- Education 0350
- Hospital Management 0769
- Human Development 0758
- Immunology 0982
- Medicine and Surgery 0564
- Mental Health 0347
- Nursing 0569
- Nutrition 0570
- Obstetrics and Gynecology .. 0380
- Occupational Health and Therapy 0354
- Ophthalmology 0381
- Pathology 0571
- Pharmacology 0419
- Pharmacy 0572
- Physical Therapy 0382
- Public Health 0573
- Radiology 0574
- Recreation 0575
- Speech Pathology 0460
- Toxicology 0383

Home Economics 0386

PHYSICAL SCIENCES
Pure Sciences
Chemistry
- General 0485
- Agricultural 0749
- Analytical 0486
- Biochemistry 0487
- Inorganic 0488
- Nuclear 0738
- Organic 0490
- Pharmaceutical 0491
- Physical 0494
- Polymer 0495
- Radiation 0754

Mathematics 0405
Physics
- General 0605
- Acoustics 0986
- Astronomy and Astrophysics 0606
- Atmospheric Science 0608
- Atomic 0748
- Electronics and Electricity 0607
- Elementary Particles and High Energy 0798
- Fluid and Plasma 0759
- Molecular 0609
- Nuclear 0610
- Optics 0752
- Radiation 0756
- Solid State 0611

Statistics 0463

Applied Sciences
Applied Mechanics 0346
Computer Science 0984
Engineering
- General 0537
- Aerospace 0538
- Agricultural 0539
- Automotive 0540
- Biomedical 0541
- Chemical 0542
- Civil 0543
- Electronics and Electrical 0544
- Heat and Thermodynamics 0348
- Hydraulic 0545
- Industrial 0546
- Marine 0547
- Materials Science 0794
- Mechanical 0548
- Metallurgy 0743
- Mining 0551
- Nuclear 0552
- Packaging 0549
- Petroleum 0765
- Sanitary and Municipal 0554
- System Science 0790

Geotechnology 0428
Operations Research 0796
Plastics Technology 0795
Textile Technology 0994

PSYCHOLOGY
General 0621
Behavioral 0384
Clinical 0622
Developmental 0620
Experimental 0623
Industrial 0624
Personality 0625
Physiological 0989
Psychobiology 0349
Psychometrics 0632
Social 0451

PHYSICAL AND NUMERICAL MODELLING FOR POWERHOUSE APPROACH AND TAILRACE DESIGNS

BY

MARNO R. KLEIN

A Thesis submitted to the Faculty of Graduate Studies of the University of Manitoba in partial fulfillment of the requirements of the degree of

MASTER OF SCIENCE

© 1995

Permission has been granted to the LIBRARY OF THE UNIVERSITY OF MANITOBA to lend or sell copies of this thesis, to the NATIONAL LIBRARY OF CANADA to microfilm this thesis and to lend or sell copies of the film, and LIBRARY MICROFILMS to publish an abstract of this thesis.

The author reserves other publication rights, and neither the thesis nor extensive extracts from it may be printed or other-wise reproduced without the author's written permission.

ABSTRACT

The purpose of this research project is to demonstrate the application of physical and numerical hydraulic models in the design of powerhouse approach and tailrace channels. The physical hydraulic model serves to provide pertinent information under a controlled environment that would not otherwise be available from the prototype; for example, to provide information regarding as yet unconstructed hydraulic facilities. These data may then be used to calibrate and verify a numerical model. This project demonstrates how a two-dimensional, depth-averaged, finite-element numerical model and a Froudian physical model may be applied in the design of forebay and tailrace channels of a hydro generating station. The case study used in this project is the proposed Manitoba Hydro Notigi Generating Station located on the Rat River in northern Manitoba. The thesis describes the procedure and theories involved in developing and testing both the physical and numerical models, and the application of these models for designing powerhouse forebay and tailrace channels. The aspects that relate to the design of powerhouse channels include: the choice of full or partial removal of the cofferdams, the design of the powerhouse approach and exit transitions, and the choice of overburden removal strategy. These aspects are investigated in terms of their impact on the hydraulic flow conditions around the powerhouse and in the downstream and upstream channels. The hydraulic considerations include headlosses, velocity distributions and their impact on ice formation and erosion, and flow patterns leading to air entrainment. The project concludes that the numerical model offers a good representation of the major flow characteristics, and that when used in conjunction with a physical model of the system it can be a very effective, economical and efficient tool in the design of powerhouse approach and tailrace channels.

ACKNOWLEDGMENTS

The completion of this work could not have been accomplished without the help and support of many people. I want to express sincere appreciation to Manitoba Hydro, and particularly to the Research and Development Committee, for making this project possible through initiation of the project, and for their financial support to this project. I would also like to extend particular thanks towards:

Dr. Barbara Lence, my advisor, for her continued guidance and support throughout not only my project work and thesis preparation, but also during my studies.

Mr. Philip Wang, project manager from Manitoba Hydro, for his technical support, direction and encouragement.

Mr. Dennis Lemke, also from Manitoba Hydro, for his willingness to share his insights and knowledge so that I might learn the aspects pertaining to hydraulic modelling that textbooks do not teach. Also, for the time and effort he contributed in the development and testing of the physical model.

Mr. Efrem Teklemarium, from Manitoba Hydro, for his participation and unobtrusive support throughout the project.

Mr. Paul Grover and Mr. Joe Groneveld, from Acres International Limited, for their part in helping me get started with using *FastTABS* by supplying me with helpful tips and sample data from the Conawapa Generating Station case study.

Mr. Stan Kaskiw, from the University of Manitoba, who spent vast amounts of time and sweat equity in making sure that all our needs were met.

Mr. Chris Maeder, President of BOSS International, who patiently offered technical guidance to my endless questions about *FastTABS*.

Finally, I would like to extend a special thanks to my dear wife, Esther, without whose continued encouragement and support, I would not be where I am today.

TABLE OF CONTENTS

LIST OF FIGURES

LIST OF TABLES

NOMENCLATURE

Symbol	Definition	Units
a	mechanical quantity expressed using dimensional analysis	–
a_o	elevation of the profile bottom	L
b_0	regression intercept	L/T
b_1	regression slope	–
C	Chezy roughness coefficient	–
F_{ip}, F_{im}	forces of inertia of the prototype and physical model	ML/T^2, F
F_{gp}, F_{gm}	gravitational forces of the prototype and physical model	ML/T^2, F
Fr	Froude number	–
g	gravitational acceleration	L/T^2
h, d	water depth	L
h_T	energy head to the turbines	L
h_L	other head losses (i.e., friction)	L
H	head of water above V-notched weir	L
L	unit of length	L
m	number of water level data points	–
M	unit of mass	M
N_i	the numerical model velocity estimates for i observations	L/T
$\overline{N}$	the average numerical model velocity estimates	L/T
N'	the numerical model water level measurements	L
P_i	the physical model velocity measurements for i observations	L/T
$\overline{P}$	the average physical model velocity measurements	L/T
P'	the numerical model water surface estimates	L
Q	discharge	L^3/T
r^2	coefficient of determination	–
R	hydraulic radius	L
Re	Reynolds number	–
T, t	unit of time	T
u	horizontal flow velocity in the x-direction	L/T
v	horizontal flow velocity in the y-direction	L/T
V	velocity	L/T
x	distance in the x-direction (longitudinal to the flow direction)	L
y	distance in the y-direction (lateral to the flow direction)	L
Δz	difference in water levels	L
α, β, γ	constants for dimensionless analysis	–
ε_{ij}	turbulent exchange coefficient in all directions	FT/L^2
ε_{xx}	normal turbulent exchange coefficient in the x-direction	FT/L^2

Symbol	Definition	Units
ε_{xy}	tangential turbulent exchange coefficient in the x-direction	FT/L^2
ε_{yx}	normal turbulent exchange coefficient in the y-direction	FT/L^2
ε_{yy}	tangential turbulent exchange coefficient in the y-direction	FT/L^2
λ_l	model scale	–
μ	dynamic viscosity	$M/(TL)$
ρ	fluid density	M/L^3

GLOSSARY OF TERMS

air entrainment The drawing of air down through a vortex into the intake of the powerhouse.

boundary conditions The flows and water surface elevations applied to the boundaries of a numerical model.

causeway A raised roadway across wet ground or water.

coefficient of determination The measure of the strength of linear association in a regression analysis.

cofferdam A watertight enclosure from which water is pumped to expose the bottom of a body of water and permit construction of a power generating station or dam.

computational hydraulics The approach of mathematically simulating the hydraulics of a river system using computers and computer programs.

critical depth The depth of water for which specific energy is minimum.

critical flow The discharge of water through a channel for which the specific energy is minimum.

critical velocity The velocity of water for which specific energy is minimum.

draft tube The conduit in a powerhouse through which the water is discharged.

dynamic flow The flow condition where velocity varies in magnitude or direction with time.

element The space defined by a set of nodes or end points representing a small segment of the material or substance being modelled.

finite-element mesh A grid of nodes and elements representing a body of water.

finite-element method The method used to solve differential equations by approximating them as algebraic terms interpolated over a grid.

fixed bed model A physical model in which the riverbed is permanent.

forebay The reservoir or channel upstream of a power generating station from which water passes to the turbines.

Froude number The dimensionless parameter to characterize flow governed by gravitational forces.

full gate discharge The maximum flow capacity through a powerhouse.

headloss A change in water surface elevation or energy between two points in a hydraulic system.

hotstart The execution of the *FastTABS* numerical model using information generated from a previous execution of the model.

hydro generating station The comprehensive term for all structures necessary for utilizing a selected power site to generate electricity from a water source.

intakes The conduits where the water enters the powerhouse for power generation.

invert The bottom of a channel or excavation.

isotropic The condition in which the hydraulic properties of a system are equal in all directions.

laminar flow The movement of fluid particles in a smooth path and in thin layers over adjacent layers.

Manning's *n* A coefficient of riverbed roughness.

minimum supply level The lowest allowable water level in the forebay of a hydro power station.

model calibration The process of parameter estimation using known data for model input and output.

model verification The process of comparing parameter estimates against a new set of field data once the numerical model has been calibrated.

moveable bed model A physical model in which the riverbed materials of the model are scaled to prototype riverbed materials and are transported through the process of erosion and deposition.

node A grid point identified by coordinate referencing and used to store geometric and hydraulic information in a finite-element mesh.

outliers The data points that fall an "unusually large" distance beyond the scatter of the remaining data points.

overburden The surface material overlying the bedrock.

powerhouse main structure of a hydro power generating station, housing the generating units and the pertaining installations.

prototype The original model or system on which a model is patterned.

Reynolds number The dimensionless parameter to characterize flow governed by viscous forces.

riprap The stones or rock used to protect shoreline or riverbed overburden material from erosion.

scour The removal of riverbed overburden material by flow of water.

similitude The theory and art of predicting prototype performance from model observations.

spillway A passage for surplus water to run over or around an obstruction such as a dam.

spinning up The technique by which the boundary conditions or parameter values in *FastTABS* are changed using a series of revisions to achieve the desired solution for calibration or verification of the numerical model.

steady-state flow A flow condition in which the velocity at any point does not vary in magnitude or direction with time.

subcritical flow The discharge of water at which the depth is greater than critical depth and the velocity is less than the critical velocity.

supercritical flow The discharge of water at which the depth is less than critical depth and the velocity is greater than the critical velocity.

tailrace The channel downstream of the power generating station.

trash racks The steel grating at powerhouse intakes used to prevent floating debris from entering the powerhouse.

turbine A mechanical device which produces power by diverting water through blades of a rotating wheel which turns a shaft to drive generators.

turbulent exchange coefficient A constant of proportionality in the relationship between the lateral turbulent stresses and the mean velocity gradients in a column of water.

turbulent flow A flow condition in which fluid particles move in non-uniform, random patterns.

vortices The flows for which the streamlines are concentric circles.

weir A dam or structure used to raise the water level or divert the flow.

1. INTRODUCTION

1.1 Objective

The objective of the research presented in this thesis is to apply physical and numerical modelling in a combined fashion to aid in the design of powerhouse approach and tailrace channel designs. In addition, the adequacy of the results from numerical models of such systems is analyzed, and improvements to the numerical model are investigated to provide better simulation of prototype conditions. The physical model is used primarily to simulate prototype flows and to calibrate and verify the numerical models. It also serves to analyze general flow characteristics and the effects of several flow conditions, such as scour and deposition of the overburden, that are beyond the capability of the numerical model. The numerical model may be used as an inexpensive, efficient, and long-term way of predicting the effects on flow of various powerhouse approach and tailrace channel design alternatives long after the physical model has been removed.

1.2 Background

The hydraulic flow characteristics upstream and downstream of powerhouses are important considerations in the design of hydro generating stations. The hydraulic conditions in the forebay and the tailrace are strongly affected by the design of the channel itself. Some of the factors influencing the flow include the presence of cofferdam remnants, transitions at the powerhouse intake and draft tube exits, approach and tailrace slopes, and, of course, the boundary conditions imposed on the system. One particularly significant consideration in designing the approach channel at some sites is to economi-

cally minimize the headlosses across the upstream cofferdam remnant so that the potential energy for the generating station is maximized. The approach channel must be designed so as to provide an acceptable flow pattern that will not create air-entraining vortices upstream of the intakes. It should also be designed so as to avoid oblique flow at the trash racks causing headlosses. The velocities in this reach must be kept low enough to avoid erosion and transportation of the granular bed material into the powerhouse. The velocities in the forebay are also crucial to the formation of a competent ice cover in the early winter season. A competent ice cover in the forebay mitigates the problem of ice blockage at the trash racks. Downstream of the powerhouse, the tailrace channel must be designed to provide the lowest feasible water level at the draft tube exits to maximize power production.

The use of physical models has historically been a reliable way of predicting the effect of various channel design configurations on the flow characteristics of a system. With advances in computing abilities to solve mathematical or numerical models of such systems, the field of computational hydraulics has developed into an active area of research and application. If properly calibrated and verified, numerical models are economical and efficient tools for solving hydrodynamic problems and for looking at many different alternatives. On the other hand, one must be aware that hydraulic numerical models are typically designed and limited in their usage to predict only certain phenomena, such as flow velocities and water surface elevations. Any attempt to incorporate all the variables or factors that influence flow into a model, such that it can be used to simulate every phenomenon relating to river hydraulics, could result in a very cumbersome and complex

numerical model requiring an enormous amount of field data to arrive at a solution. Simplifying a numerical model, by concentrating on a particular phenomenon and by making a few approximations, allows for greater efficiency and reduced data requirements. By combining the efforts of physical and numerical models in the design of a proposed scenario, not only can a reliable computer model be developed, but many different design alternatives can be investigated and physically verified in a cost efficient manner. In this project, the physical model is used to provide pertinent hydraulic information for a proposed hydraulic system that has not yet been constructed, and to use this information to calibrate and verify a numerical model. The numerical model can then be used to economically and efficiently investigate many different alternatives. The advantages of using the calibrated numerical model at this stage include greater consistency and precision for comparing various alternatives, increased efficiency, and a long-term life-span. Once a suitable design alternative has been achieved, the physical model can then be used to verify this alternative and to investigate any additional phenomena beyond the limitations of the numerical model. This helps to avoid any costly corrective measures that may otherwise be required for the prototype after construction. The approach of applying numerical and physical models to powerhouse channel designs is best demonstrated using a case study.

1.3 Case Study of the Notigi Generating Station

The proposed Manitoba Hydro Notigi Generating Station on the Rat River in northern Manitoba is the test case for this project (see Figure 1.1). The site currently consists of a dam and a control structure which is used to regulate the flow from the Churchill River Diversion through the Rat River, and hence the Burntwood River, in Manitoba. The

flow conditions for this site are based on the assumption that the proposed Wuskwatim Generating Station on the Burntwood River downstream of the Notigi dam has not yet been constructed. These flow conditions are referred to in this thesis as pre-Wuskwatim flow conditions. The successful development of a computer model in this application would provide the tools and methodology for analyzing similar projects on different river systems, and for further investigations of detailed design alternatives for the Notigi Generating Station.

The site of the proposed Notigi Generating Station, as illustrated in Figure 1.2, will make use of existing structures to minimize costs of construction. The existing main dam will be used as the upstream cofferdam. The downstream cofferdam is to be located in the same vicinity as the old causeway used for construction of the main dam. The existing spillway will continue to divert flow during the construction phase. Once the construction of the powerhouse is complete, the downstream cofferdam will be partly removed to provide an adequate powerhouse discharge channel. The upstream cofferdam will also be partly removed to create a suitable intake channel for the powerhouse. The existing Provincial Road 391 will be re-routed across the generating station.

For the Notigi Generating Station case study, only limited field data describing the bed material at this site are available. Based on an exploration program conducted in 1969 (Manitoba Hydro, 1978), the Rat River at the existing main dam, upstream of the proposed powerhouse, has a boulder pavement of coarse gravel and boulders being underlain by a deposit of silty sand with numerous gravel or silt layers. In the vicinity of the proposed powerhouse, just downstream of the main dam, 5 m of very dense sand over 3.5 m

of very dense sandy gravel rests on bedrock of pegmatite and granite-pegmatite. The downstream cofferdam site is characterized by a layer of highly plastic clay of unknown thickness.

The issues of primary concern in this study of the proposed Notigi Generating Station are the hydraulic conditions in the approach and the tailrace channels and how these are affected by various channel design alternatives and boundary conditions. The channel design options that are investigated in this study include various upstream and downstream cofferdam removal schemes, transitions at the powerhouse intake and draft tubes, and various overburden removal schemes in the tailrace. The design considerations, mentioned earlier, are evaluated by estimating velocities and water levels throughout the approach and tailrace channels using physical and numerical models.

1.4 Scope of Work

This thesis describes several aspects of the development, testing, and analysis of physical and numerical models and their combined use. In Chapter 2, a theoretical review of physical and numerical modelling techniques, practices, applications, and limitations is presented, and a discussion of the search for and acquisition of the hydraulic numerical model is given. Chapter 3 describes the steps and issues involved in developing the numerical model. Chapter 4 provides an overview of some of the aspects involved in the construction of the comprehensive physical model in the Hydraulics Laboratory at the University of Manitoba. Next, the tests on the physical model that generate the data needed to calibrate and verify the numerical model are described in Chapter 5. Chapter 6 explains the calibration and verification process for the numerical model. Chapter 7

presents the results of the calibration and verification of the numerical model with the physical model test data. This chapter also demonstrates various applications of the numerical model for the selection of the best design alternatives. Chapter 8 concludes the work of this project and offers some recommendations relating to the use of numerical and physical models.

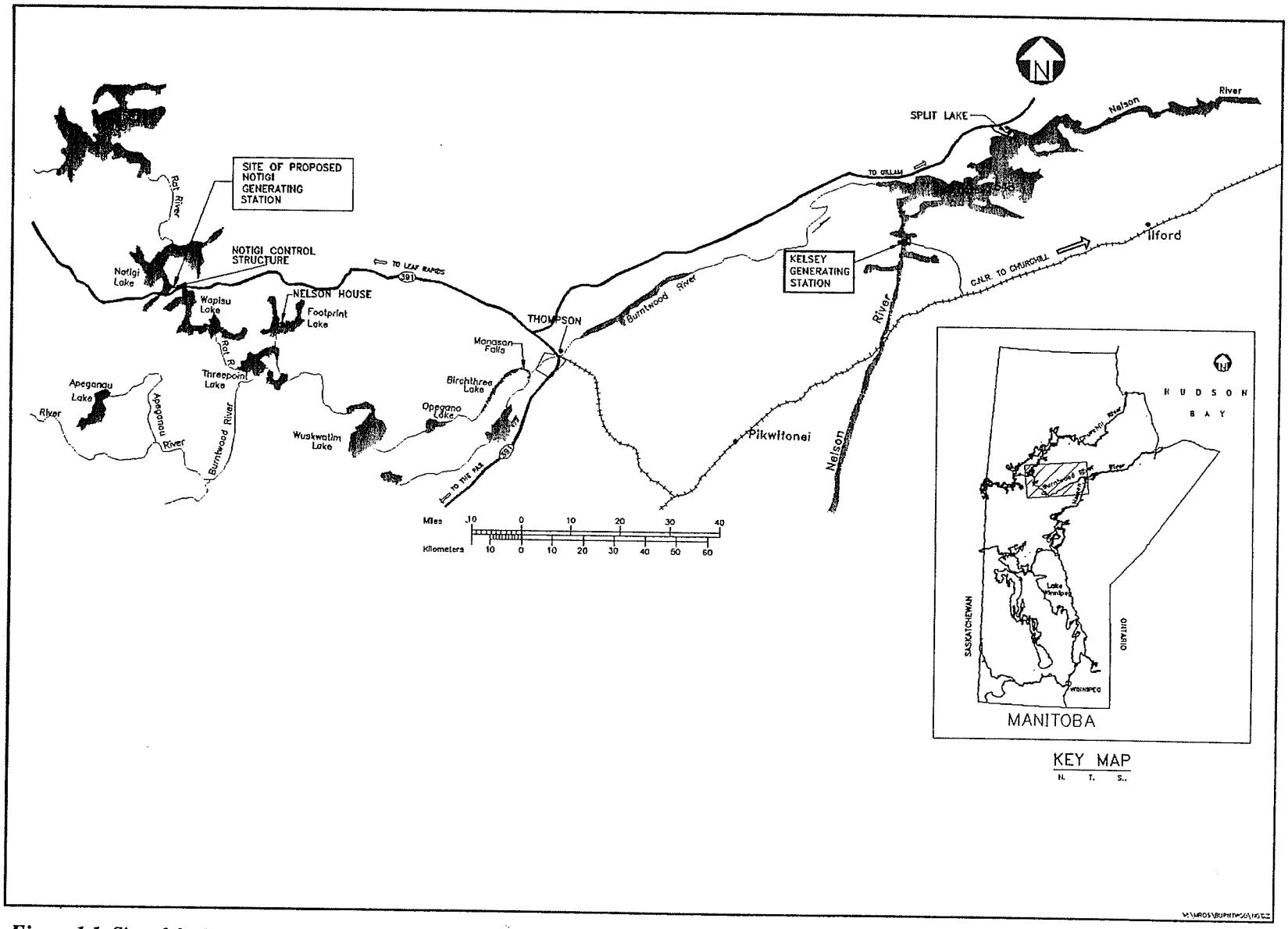

Figure 1.1 Site of the Proposed Notigi Generating Station

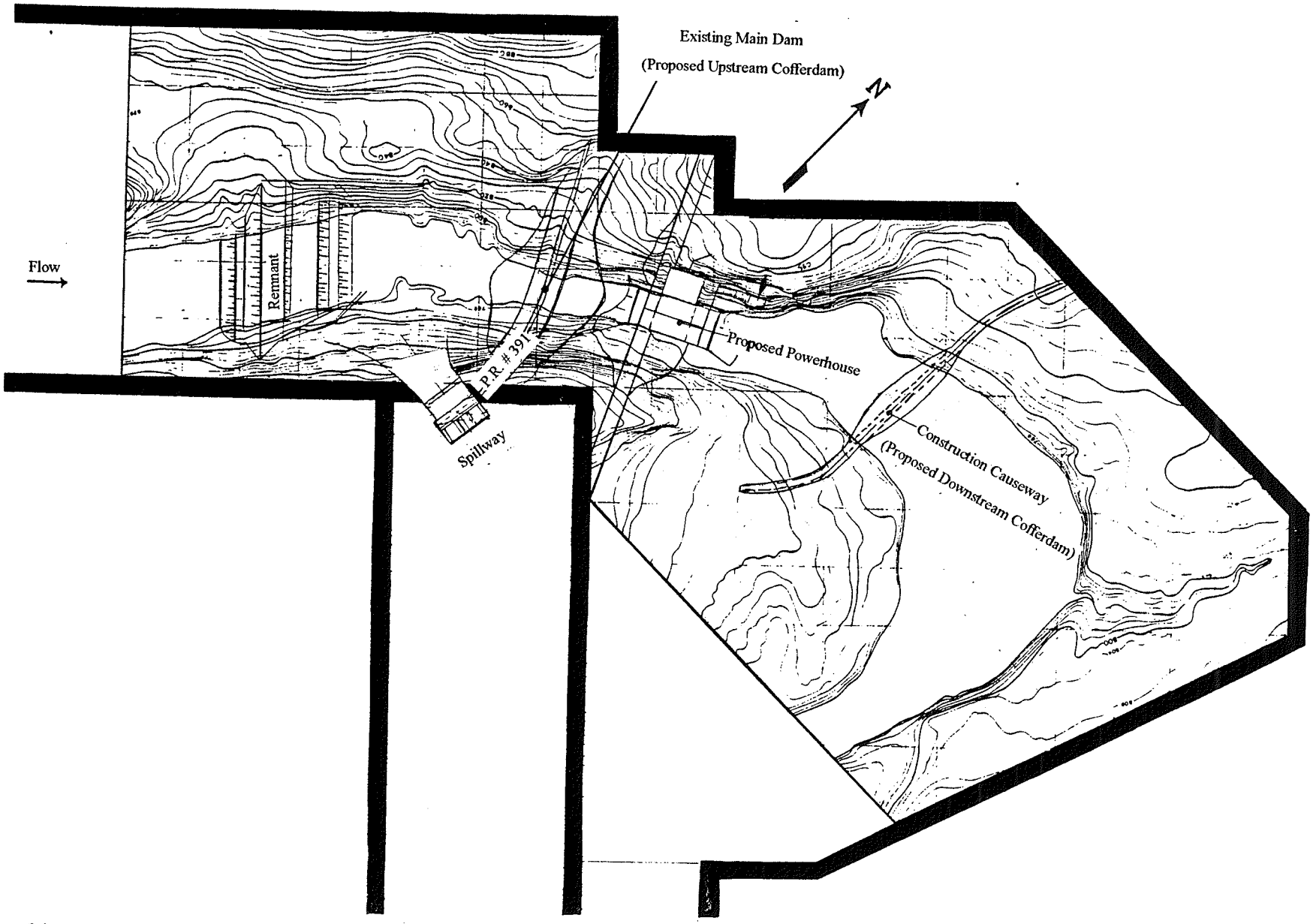

Figure 1.2 Layout of the Physical Model of the Proposed Notigi Generating Station showing Model Boundary, Cofferdams, Spillway and Hydro Dam.

2. THEORETICAL AND PRACTICAL REVIEW OF PHYSICAL AND NUMERICAL HYDRAULIC MODELS

Much of what is written about physical and numerical modelling of hydrodynamic systems treats these approaches as two separate alternatives to analyzing a system. Physical models are commonly based on a prototype situation in the field and the tests conducted with the physical model are used to derive pertinent information that would otherwise be difficult, if not impossible, to attain. Numerical models are also commonly developed based on field data and are used to further investigate other flow or design alternatives. Literature that combines the efforts of both physical and numerical modelling, particularly in the study of powerhouse approach and tailrace channel designs, is rare. The following sections review the theory and concepts cited in the literature that relate to both physical and numerical models. The chapter closes with a brief description of the selection of the numerical model used in this project.

2.1 Literature Review

2.1.1 Physical Model Studies

The use of physical models in hydraulic engineering has a long history. One of the first successfully used scale models was developed by Osborne Reynolds who designed and operated a tidal model of the River Mersey in 1885 at Manchester University, England (Novak and Cábelka, 1981). Since then, the use of physical models has developed into a somewhat specialized field of science. Today, models can vary as to the phenomena being modelled, the use of fixed or moveable beds, the scale, and perhaps the distortion of the

model, and the mathematical theory on which the physical model is based (Liggett, 1994; Novak and Cábelka, 1981; and Yalin, 1971). The basic principles upon which most physical models are based remain common. They are the Theory of Dimensional Analysis and of Similitude. Cursory overviews of the Theory of Dimensional Analysis and Similitude are provided here in order to better appreciate both the capabilities, as well as the limitations, of physical models.

2.1.1.1 Dimensional Analysis

The basis of the Theory of Dimensional Analysis is that any mechanical quantity, such as energy, force, velocity, and density, can be defined using three fundamental entities, length *(L)*, time *(T)*, and mass *(M)* (Yalin, 1971). The units of a mechanical quantity a can be expressed as a function of the fundamental entities by

$$[a] = L^{\alpha} T^{\beta} M^{\gamma} \qquad [2.1]$$

where α, β, and γ are simply constants. If at least one of these exponents is not zero, the quantity a is said to be a dimensional quantity. If the exponents are all zero, the quantity a is referred to as a dimensionless quantity. Table 2.1 provides a list of the dimensions and the constants α, β, and γ for some common quantities frequently used in hydraulic modelling.

The Theory of Dimensional Analysis has two major applications: the simplification of equations involving a large number of mechanical parameters, and the development of criteria for similitude (Henderson, 1966). One approach to simplifying the number of parameters that is commonly used in Dimensional Analysis is the application of Buckingham's π Theorem (Novak and Cábelka, 1981). Buckingham's π Theorem transforms the

relationship describing the mechanical quantities of a particular problem into another relatively simpler relationship between a smaller number of dimensionless numbers. There are numerous dimensionless numbers introduced as more parameters are added. One dimensionless number that is appropriate when gravitational forces prevail in free-surface fluid transport is the well-known Froude number, *Fr*:

$$Fr = \frac{v}{\sqrt{gL}} \qquad [2.2]$$

where v is the velocity of the fluid, g is the force of gravity, and L is a characteristic length, such as depth. If the action of internal friction, or viscosity, μ, significantly affects the flow, then another dimensionless number is introduced as the Reynolds number, *Re*:

$$Re = \frac{vL\rho}{\mu} \qquad [2.3]$$

where ρ represents the fluid density, and all other variables are defined above. In open channel flow, it has been shown that the Froude number plays a significant role in the appropriate flow equations (Novak and Cábelka, 1981). The Reynolds number plays a more limited role in open channel flow, particularly when the flow is on a large scale, for since the Reynolds number is an inverse measure of the effect of viscosity, it has the least influence when the viscosity is largest (Henderson, 1966). There are many other dimensionless numbers that are used in fluid mechanics (Liggett, 1994), but these do not apply to the case study of the Notigi Generating Station. The Theory of Dimensional Analysis is not limited to simplifying multi-variable equations, but it also serves as an integral tool for the concept of hydraulic similitude (Novak and Cábelka, 1981).

2.1.1.2 Theory of Similitude

Hydraulic research involving the use of scale physical models is based on the Theory of Similitude. Similitude uses fundamental equations of fluid motion to relate a physical model of a system to the prototype, or actual system, so that the behavior of the physical model can be used to predict the behavior of the prototype. The equations of similarity are derived using Dimensional Analysis. The numerical values of a dimensionless number remain the same in all systems of fundamental units (e.g., the SI system). As a result, all dimensionless functional relationships representing the laws governing mechanical phenomena would remain the same for different scales (Yalin, 1971). This is the basis for the development and application of scaled physical models. Hydraulic modelling is usually based on achieving *geometric* (form), *kinematic* (motion), and *dynamic* (force) *similarity* (Yalin, 1971). Two systems, a physical model and a prototype, that are related to each other in terms of a length ratio are referred to as being *geometrically similar*. If two systems are related by both length and time ratios, they are considered *kinematically similar*. Two systems that are related to each other by length, time and mass ratios are referred to as *dynamically similar*. For true *dynamic similarity*, the ratio of prototype force to model force must be equal for all of the types of forces that are present. The forces relating to fluid mechanics are caused by gravity, pressure, viscosity, capillary forces, volumetric elasticity, and inertia. No fluid can simultaneously give the same ratio of prototype force to model force for all of these types of forces, and consequently true dynamic similitude is impossible to achieve. However, for systems in which some of these forces are negligible, physical models can be used to achieve acceptable similitude of

certain properties of a phenomenon without achieving true *dynamic similitude* (Yalin, 1971).

In most open channel flow systems, the governing force affecting flow is gravity. The assumption is that the other forces do not affect the flow in either the prototype or the physical model. In the flow of a real (viscous) fluid, however, the forces of inertia always act simultaneously with gravity. *Dynamic similitude* requires that the ratio of inertial forces and the gravitational forces are equal for both the prototype and the physical model (Novak and Cábelka, 1981), as shown in Equation 2.4:

$$\left(\frac{F_{ip}}{F_{im}}\right)=\left(\frac{F_{gp}}{F_{gm}}\right) \qquad [2.4]$$

or rearranging

$$\left(\frac{F_i}{F_g}\right)_p=\left(\frac{F_i}{F_g}\right)_m \qquad [2.5]$$

where F_{ip} and F_{im} are the forces of inertia of the prototype and physical model, respectively, and F_{gp} and F_{gm} are the corresponding forces due to gravity. This relationship of forces is the fundamental basis for what is called a Froude model. The inertia force is given as the product of mass and acceleration while the gravity force is the product of mass and gravitational acceleration, g, thereby allowing either side of Equation 2.5 to be written as:

$$\frac{(\rho L^3)(L/T^2)}{(\rho L^3)g} \qquad [2.6]$$

where T is time. Since T is equal to L/v, Equation 2.6 can be simplified to:

$$\frac{v^2}{gL} \qquad [2.7]$$

which is the Froude number squared. Substituting Equation 2.7 into both sides of Equation 2.5 yields:

$$\left(\frac{v^2}{gL}\right)_p = \left(\frac{v^2}{gL}\right)_m \qquad [2.8]$$

Therefore, the requirement for similarity of flow between the physical model and the prototype is that the Froude number must be equal for the physical model and the prototype. Equation 2.8 is the fundamental basis for the Froude model. From Equation 2.8, the following Froude scale ratios can be derived for a given geometric scale (L_p/L_m) and can be used to relate measurements in the physical model and the prototype:

$$\left.\begin{aligned} &\textit{Velocity}, && \frac{v_p}{v_m} = \left(\frac{L_p}{L_m}\right)^{1/2} \\ &\textit{Discharge}, && \frac{Q_p}{Q_m} = \left(\frac{L_p}{L_m}\right)^{2\frac{1}{2}} \\ &\textit{Time}, && \frac{T_p}{T_m} = \left(\frac{L_p}{L_m}\right)^{1/2} \\ &\textit{Mass}, && \frac{M_p}{M_m} = \left(\frac{L_p}{L_m}\right)^{3} \\ &\textit{Force}, && \frac{F_p}{F_m} = \left(\frac{L_p}{L_m}\right)^{3} \end{aligned}\right\} \qquad [2.9]$$

The subscripts p and m indicate that the quantity is for the prototype and the physical model, respectively. Scale ratios for other quantities can also be derived from equating the Froude numbers.

As was mentioned previously, achieving a small scale, completely *dynamically similar* hydraulic model may not be possible due to severe restrictions of a physical, technical, or economic nature. For practical and economic reasons, most physical models use water, thus prohibiting the proper scaling of density and viscosity, and since both physical model and prototype are on the same planet, proper scaling of the gravitational force is impractical. The alternative is to use a physical model that demonstrates *incomplete similitude* (Liggett, 1994). According to Liggett (1994), *incomplete similitude* "represents a situation in which the desired phenomena are dynamically similar but other features of the flow are not." *Incomplete similitude* means, for example, that of the three fundamental proportionalities, length, time, and mass, only the first proportionality can be applied. The implication is that, for relatively small physical models, while *geometric similarity* is maintained, total *dynamic* and *kinematic similarities* are not. The basic objective, knowing that the realization of *dynamically similar* behavior of all properties is impossible, is to attempt to ensure the *dynamic similarity* of at least those properties which are to be measured or observed. A physical model that is based on *incomplete similitude*, where only a certain group of properties are adequately reproduced, should never be used to predict the behavior of properties other than the group.

Incomplete similitude can be applied in hydraulic modelling of open channel flows when the Froude numbers in both the physical model and prototype are large enough that viscous effects can be ignored. This means that the flow regimes in both the physical model and the prototype are rough turbulent. The flow regime is turbulent if the viscous forces are weak relative to the inertial forces, and consequently water particles move in

irregular paths which are neither smooth nor fixed (Chow, 1959). Laminar flow, on the other hand, is when the viscous forces are strong relative to the inertial forces such that water particles appear to move in definite smooth paths, and infinitesimally thin layers of fluid seem to slide over adjacent layers (Chow, 1959). There is a significant difference in the energy losses between laminar and turbulent flow regimes. In most natural rivers, only turbulent conditions prevail, and therefore the physical model scale must be large enough to maintain a turbulent flow regime. Yalin (1971) suggests that this condition is always satisfied provided the model scale, λ_l, is greater than a certain lower limit determined by the prototype value of the Reynolds number, Re_p, as shown in Equation 2.10.

$$\lambda_l >\approx \left(\frac{70}{Re_p}\right)^{\frac{2}{3}} \qquad [2.10]$$

The features of flow separation and surface resistance are more or less independent of the Reynolds number as long as the physical model Reynolds number is high enough to ensure turbulent flow. Since in a Froude model, the major influence on flow in an open channel is gravity, other forces, such as frictional resistance of a viscous liquid and capillary forces, either do not affect the flow or are negligible. For the Froude model to be valid, it is suggested that minimum limiting values be observed in the design of typical open channel flow models (Novak and Cábelka, 1981). These limiting values are:

1) The head of a nappe on a sharp-edged notched weir must be greater than or equal to 60 mm, for the measured shape of the nappe to be capable of extrapolation to greater scales.
2) The length of a surface wave on the physical model must be greater than or equal to 17 mm.
3) The velocity at the water surface of the physical model must be greater than or equal to 230 mm/s in order that gravity waves might occur.

4) The depth of flow in the physical model be greater than 15 mm to eliminate the effect of capillary and surface tension.

These guidelines are particularly important in the modelling of spillways, resistance of flow around piers, and waves.

Another type of similitude that may be considered is *approximate similitude*. *Approximate similitude* is when "the objective of exactly modelling the desired phenomena must be abandoned and the model has to be constructed so as to obtain the best practical approximation" (Liggett, 1994). As the scale of the physical model is reduced and other forces, such as viscous effects, have an increased influence on the flow, then the measurements of velocity or depth can be distorted by scale effects. In other words, the forces influencing the flow in the physical model are not the same as those in the prototype, thereby yielding *approximate similitude*. If the model scale is such that small depths lead to laminar flow, while the flows in the prototype are turbulent, then even *approximate similitude* is not attainable. It is therefore necessary to choose a physical scale model large enough to properly simulate the phenomena under investigation, to minimize errors due to scale effects, and to insure measurement accuracy.

One common approach in dealing with *approximate similitude* in small scale physical models is to use a distorted model (Liggett, 1994). Common types of distorted models use techniques that include the vertical exaggeration, slope distortion by tilting the model, and riverbed roughness distortion (Henderson, 1966). In all cases of distorted physical models, while *geometric similitude* is abandoned, *partial dynamic similitude* is preserved; even this is only an *approximate similarity* according to the criteria of similarity for prevailing forces (Novak and Cábelka, 1981). The results obtained from a distorted

physical model, as opposed to a true physical model, are usually limited to the objective (i.e., such as, to observe scaled depth, scaled velocity, or surface roughness) for which the physical model was planned. There are several advantages as well as disadvantages to using a distorted physical model (U.S. Department of the Interior, 1980). The advantages are:

1) Sufficient tractive force can be developed to produce bedload movement with a reasonably small physical model and available model sediment;
2) Water surface slopes are exaggerated and therefore easier to determine;
3) The width and length of the physical model can be held within economical limits for the required depth;
4) Operation is simplified by use of a smaller physical model; and
5) Turbulent prototype flow can be modelled.

The disadvantages are:

1) Velocities may not be correctly reproduced in magnitude and direction;
2) Some of the flow details are not correctly reproduced;
3) Slopes of cuts and fills are often too steep to be molded in sand or erodible material;
4) There is an unfavorable psychological effect on the observer who views distorted models; and
5) Boundary roughness may need to be distorted to produce similarity.

Complete similarity in all geometric aspects of the physical model, particularly bed roughness and sediment transport, may be difficult, if not impossible, to achieve. Scaling down the granular material in a river is not simply a matter of selecting a grain size that is the length scale times smaller than the average river grain diameter. Not only may this particular bed material be difficult to obtain, but the friction in a river bed is influenced by many other factors as well, including bed configuration. For this reason, it may be necessary to use a sand or another model boundary that is rougher than the scaled down

prototype boundary should be (Yalin, 1971). In the attempt to meet the friction criterion, the goal of maintaining similarity in sediment transport often becomes unattainable. The grain size for adequate roughness may not be the same as for sediment transport. The forces and mechanics involved in scour and deposition are rather complicated and consequently the investigation of sediment transport in hydraulic research typically concentrates on qualitative rather than quantitative forces (Novak and Cábelka, 1981).

2.1.2 Numerical Model Studies

The use of mathematical models in hydraulic engineering has undergone significant advancement with the implementation of efficient computers. Not only has the computer provided new and powerful means to solve traditional problems, it has also been useful in identifying new or previously ignored hydraulic problems by forcing engineers to evaluate and address any other relevant factors that might improve the simulation (Lai et. al., 1980). It has also inspired new perspectives with respect to some of the basic concepts and accepted understandings of flow characteristics. Consequently, the discipline of computational hydraulics has expanded to utilize many varieties of mathematical formulations to a vast range of applications.

Although many mathematical methods have been employed in the past, new and better methods are continually being developed. Some of the more common numerical techniques still being used today to solve the governing partial differential flow equations include: the finite-difference method (Abbott and Basco, 1989); the finite-element method (Pinder and Gray, 1977; Lee and Froehlich, 1986); and the finite-volume method (Patankar, 1980). No single method is ideal in terms of applicability, accuracy, and cost,

and all of the methods have their strengths and weaknesses (Williams, 1993). For example, one significant advantage that the finite-element method has over the finite-difference method, particularly in two-dimensional, depth-averaged flow problems, is that "it allows the user greater flexibility in defining geometric features such as the boundaries of a water body, channels, islands, dikes, and embankments" (Lee and Froehlich, 1986). Lee and Froehlich (1986) provide a detailed summary of the published literature dealing with the application of the finite-element method to solving the equations of two-dimensional surface water flow in the horizontal plane.

Hydraulic numerical models are currently being used in numerous applications. Some of the applications, to name a few, include estuary studies (Cheng, 1981), flood plain analyses (Gurule, 1981; Lesleighter, 1983), flood control and routing analyses (Noble and Narum, 1981), flood forecasting (Fread, 1981), water quality modelling (Thomann and Mueller, 1987), and flow pattern investigations (Östberg and Johansson, 1992). In the area of channel and river designs, the approach has been to develop numerical models based on intuition and experience, and, if available, data collected in the field. The data requirements for numerical models are often quite extensive and therefore costly (Williams, 1993). Without proper calibration and verification based on actual field data, the application of a numerical model is limited to subjective or qualitative analyses. Gee and MacArthur (1981) demonstrate the use of a numerical model to provide quick visualizations of flow fields near structures, without verification. A similar usage of a numerical model is applied to investigate various approach channel design alternatives for the proposed Conawapa Generating Station in Manitoba (Grover, 1989). The models in these

cases serve to provide preliminary estimates of the hydraulics in various channel design options which need to be validated at some later date.

One way to acquire the data necessary for calibrating and verifying a numerical model, when field data are unavailable, is to make use of physical models. Even though physical models also require field data for calibration and verification, as long as the model fulfills the criteria of similarity and limiting conditions according to the nature of the problem under investigation, the phenomena of interest can be expected to be a reasonable estimate for the prototype. The data required for calibration and verification of a numerical model should be reliable and sufficiently detailed. A physical model allows the phenomenon of interest to be observed, measured, and recorded under a controlled environment and to the level of detail required to adequately develop a numerical model. A calibrated and verified numerical model can then be used as an efficient tool to investigate the particular hydraulic phenomenon of interest for a range of design alternatives under various boundary conditions. The combined use of physical and numerical models offers several advantages that the solitary use of either a physical or numerical model cannot afford. These are:

1) a numerical model that is calibrated and verified to physical model data offers a greater degree of reliability than a non-verified numerical model that is based on subjective intuition;
2) a physical model offers, as was previously stated, a reliable, affordable, and controlled way of collecting data, to be used to calibrate and verify the numerical model, for conditions that may not exist in the prototype;
3) a numerical model can be used to quickly assess the hydraulic impacts for a large quantity of design and boundary conditions, which are useful for channel optimization;
4) estimates based on a numerical model for a particular design or flow condition can be verified with a physical model while the physical model is still available; and

5) after the deconstruction of a physical model, a numerical model can continue to be used for further investigations with a reasonable degree of confidence.

In this thesis, the approach of using combined physical and numerical modelling is applied in the design of powerhouse approach and tailrace channels. A similar approach is used by Östberg and Johansson (1992) to investigate the flow patterns at intakes of a number of Swedish water power stations. The purpose of their investigation is to verify the calculation method by comparing the results from a physical model with those from a two- and three-dimensional model called *PHOENICS* and to investigate the limits of that model in open waterways. The *PHOENICS* program uses the finite-volume technique to calculate the flow characteristics. The authors conclude that the three-dimensional model yields good agreement with the physical model in terms of velocity and eddy distributions, and that the two-dimensional model gives a poorer but adequate representation of the flow patterns. The approach of using both physical and numerical models is also implemented by the engineering firm of Crippen Acres Wardrop, Inc., in collaboration with Manitoba Hydro, to investigate the hydraulics of the approach area upstream of the proposed Manitoba Hydro Conawapa Generating Station (Grover, 1989). They use the mathematical model *RMA* to perform the analysis. The preliminary results from the numerical model give an indication of the potential for other cofferdam removal alternatives to be investigated in greater detail in a comprehensive physical model.

2.2 Numerical Model Selection

The selection of a suitable numerical model to study open channel flow is based on numerous considerations and requirements. Much of the emphasis in the past has been

focused primarily on the development and testing of various mathematical-numerical simulation schemes. However, while the selection of a sound mathematical-numerical technique is of great importance, it is also appropriate to recognize that simulation models are not an end in themselves. The intended purpose of numerical models is "to depict hydraulic phenomena and to provide information, insight, and data to a model user and ultimately to a decision maker" (Lai et. al., 1980). Some key aspects, identified by Lai et. al. (1980), that should be considered in the selection of a hydraulic numerical model include the following:

1) the ability to simulate, with minimal distortion, the wide range of flows encountered in the prototype channels;
2) the ability to permit schematization of a range of complex prototype conditions, for example, variable channel conveyance and cross-sectional properties, channel overbank storage, lateral inflows, branching channels, and networks of channels;
3) the ability to generate accurate results repeatably by means of a stable, convergent, and numerically reliable computational scheme;
4) the ability to provide a high degree of computational efficiency; and
5) the ability to facilitate functional, user-oriented modelling by interacting with an operational data-handling system.

There are also other considerations that can be added to this list including the ease with which the model may be implemented and maintained on a computer system, and the immediate and long term costs.

In this project, the search for a suitable numerical model that would be applicable for river hydraulics involved the investigation of several computer programs. Two of these programs, examined in the initial stages of this project, are listed and compared in Appendix A. The first program, *Finite-Element Surface Water Modelling System, 2-D in the*

Horizontal Plane (*FESWMS-2DH*), is available from WEST Consultants, Inc. The other program, *FastTABS,* is marketed and supported by BOSS Corporation. Both programs implement finite-element techniques and can solve various complex problems involving shallow water flow. The comparison in Appendix A includes some preliminary information, such as addresses, contact personnel, costs, computer requirements, and programs included in the package. The remainder of the evaluation compares various program characteristics and capabilities including the following: types of model applications, unit systems, types of flow regimes and conditions, element configurations, methodology for solving equations, material properties, coefficients and parameters, output information, and graphical capabilities. Some of the program capabilities are not available at this time but may be incorporated in a future version. The *FastTABS* model is appealing because it incorporates a versatile graphical interface to display and edit the finite-element mesh, it has a variety of finite-element mesh generation and interactive editing tools available, it is easy to use, it has excellent technical support, and it is continually being upgraded and enhanced. On the other hand, the *FESWMS-2DH* program offers the capacity to handle a greater variety of flow conditions than *FastTABS.* For the focus of this project, the positive aspects for using *FastTABS* outweigh the negative and therefore it is selected over *FESWMS-2DH.*

Dimensional Quantity	α	β	γ	Dimensional Quantity	α	β	γ
Length	1	0	0	Stress (pressure)	-1	-2	1
Time	0	1	0	Density	-3	0	1
Mass	0	0	1	Specific Weight	-2	-2	1
Velocity	1	-1	0	Viscosity	-1	-1	1
Acceleration	1	-2	0	Kinematic Viscosity	2	-1	0
Volumetric Flow Rate	3	-1	0	Work (energy)	2	-2	1
Force (weight)	1	-2	1	Power	2	-3	1

Table 2.1 *Common dimensional quantities for hydraulics*

3. DEVELOPMENT OF THE NUMERICAL MODEL

Numerical models afford powerful and inexpensive ways of analyzing and solving traditional hydraulic problems. This chapter provides a general introduction to the two-dimensional, shallow water hydraulics simulation program called *FastTABS* (BOSS Corporation, 1993), as well as a brief overview of how the program is used.

3.1 The *FastTABS* Hydraulics Simulation Program

3.1.1 Background

FastTABS is a graphical pre- and post-processor which includes, and is designed to be used in conjunction with, a set of *TABS* hydraulic programs (BOSS Corporation, 1993). *FastTABS* was developed by the Engineering Computer Graphics Laboratory at Brigham Young University (1993) and is currently being marketed and supported by BOSS Corporation in Madison, Wisconsin. The two components of the *TABS* system, *RMA-2* and *RMA-4*, were developed by the United States Army Corps of Engineers Waterways Experiment Station. The *RMA-2* program is a two-dimensional, depth-averaged, free surface, finite-element program for solving hydrodynamic problems. The *RMA-4* program, used to model contaminant transport, is not utilized for this study. Both programs are coded for numerical solution by the finite-element method using Galerkin's method of weighted residuals (Pinder and Gray, 1977) and the resulting nonlinear system of equations are solved with the Newton-Raphson solution technique (Pinder and Gray, 1977). In a typical application, *FastTABS* is used to construct a finite-element mesh of the water body being modelled, to apply a set of boundary conditions, and to interpret the results

from *RMA-2*. A finite-element mesh is made up of nodes and elements that represent a physical structure or body of water. Figure 3.1 shows a sample mesh of a hypothetical river section. The nodes are points that define the geometry of the mesh, and the elements are the triangular and quadrilateral patches, formed by connecting a set of nodes, that define the mesh topography. The *RMA-2* program is used to perform the hydrodynamic analysis, thereby generating one or more solution files containing the water surface elevation and flow velocity at each node in the mesh. These solution files are interpreted by *FastTABS* to produce various types of contour and vector plots.

3.1.2 Depth-Averaged Flow Equations

The *RMA-2* program uses a finite-element mesh representing a body of water such as a river, harbor or estuary to compute the water levels and velocities. *RMA-2* can perform both steady-state and transient solutions. The program assumes that the fluid is incompressible, Newtonian, and maintains constant physical properties. The mathematical equations that govern two-dimensional, depth-averaged flow are obtained by applying the conservation of mass and momentum laws to a water column. These equations are summarized by BOSS Corporation (1993) as follows:

$$\frac{\partial h}{\partial t} + \frac{\partial (uh)}{\partial x} + \frac{\partial (vh)}{\partial y} = 0 \qquad [3.1]$$

$$\underset{(1)}{\left\{\frac{\partial u}{\partial t} + u\frac{\partial u}{\partial x} + v\frac{\partial u}{\partial y}\right\}} + \underset{(2)}{\left\{g\left(\frac{\partial h}{\partial x} + \frac{\partial a_o}{\partial x}\right)\right\}} - \underset{(3)}{\left\{\frac{\varepsilon_{xx}}{\rho}\frac{\partial^2 u}{\partial x^2} + \frac{\varepsilon_{xy}}{\rho}\frac{\partial^2 u}{\partial y^2}\right\}} + \underset{(4)}{\left\{\frac{g\,u}{C^2 h}\sqrt{u^2 + v^2}\right\}} = 0 \qquad [3.2]$$

$$\underbrace{\left\{\frac{\partial v}{\partial t}+u\frac{\partial v}{\partial x}+v\frac{\partial v}{\partial y}\right\}}_{(1)}+\underbrace{\left\{g\left(\frac{\partial h}{\partial y}+\frac{\partial a_o}{\partial y}\right)\right\}}_{(2)}$$

$$-\underbrace{\left\{\frac{\varepsilon_{yx}}{\rho}\frac{\partial^2 v}{\partial x^2}+\frac{\varepsilon_{yy}}{\rho}\frac{\partial^2 v}{\partial y^2}\right\}}_{(3)}+\underbrace{\left\{\frac{g\,v}{C^2 h}\sqrt{u^2+v^2}\right\}}_{(4)}=0 \qquad [3.3]$$

where x = distance in the x-direction (longitudinal to flow direction) [L],
u = horizontal flow velocity in the x-direction [L/T],
y = distance in the y-direction (lateral to flow direction) [L],
v = horizontal flow velocity in the y-direction [L/T],
t = time [T],
g = acceleration due to gravity [L/T^2],
h = water depth [L],
a_o = elevation of the profile bottom [L],
ρ = fluid density [M/L^3],
ε_{xx} = normal turbulent exchange coefficient in the x-direction [FT/L^2],
ε_{xy} = tangential turbulent exchange coefficient in the x-direction [FT/L^2],
ε_{yx} = normal turbulent exchange coefficient in the y-direction [FT/L^2],
ε_{yy} = tangential turbulent exchange coefficient in the y-direction [FT/L^2], and
C = Chezy roughness coefficient converted from Manning's roughness coefficient, n *(i.e.,* $C = R^{1/6}/n$, where R is the hydraulic radius).

Equation 3.1 represents the conservation of mass, and states that the net change of the volume in a water column of unit width and length, with respect to time is equal to the volume rate of flow in the x and y directions. Equations 3.2 and 3.3 summarize the conservation of momentum expressions for which the sum of all external forces acting on a fixed quantity of matter is equal to the time rate of change of linear momentum of the matter (Newton's Second Law of Motion). The external forces acting on a vertical column of water include: hydrostatic pressure forces, indicated as term (2); turbulence indicated as term (3); and drag forces or bed shear stress, indicated as term (4). Other

forces that could come into play if the body of water is large enough but are not included in Equations 3.2 and 3.3 are wind shear stress, and Coriolis forces.

3.1.3 Parameters in FastTABS

The parameters that are considered of primary interest for this project is the turbulent exchange coefficient, ε_{ij}, and the roughness coefficient, Manning's n. The ε_{ij} coefficient (also called eddy viscosity) is used to describe the turbulent stresses in the momentum equations. These turbulent stresses are tractive (or frictional) forces acting on the vertical faces of a water column, as shown in Figure 3.2, and are caused by the horizontal transport of momentum by turbulent motion. For two-dimensional, depth-averaged flow equations there are four turbulent related stresses acting on a column of water, as defined in Equation 3.2 and 3.3. The units of the ε_{ij} coefficient is the ratio of force-time and length squared (e.g., N-s/m^2 or lbf-s/ft^2). The ε_{ij} , by definition, represents a constant of proportionality in the relationship between the lateral turbulent stresses and the mean velocity gradients, as originally formulated by Boussinesq (Schlicting, 1968). The ε_{ij} is similar in principle to the coefficient of molecular viscosity, but deviates in that it is not solely a property of the fluid but depends also on the state of turbulent motion, and therefore may vary significantly from one point to another or with time (Lee and Froehlich, 1986). In most hydrodynamic applications, isotropic conditions are assumed in order to simplify the modelling process, and all four directional components of ε_{ij} (i.e. ε_{xx}, ε_{xy}, ε_{yy}, and ε_{yx}) are assigned the same value (Larock, 1981). This is unrealistic for complex flows, and therefore, directional ε_{ij}'s are sometimes used to define turbulent

momentum transport. It is important to be aware of the fact that these coefficients are not entirely based on physical processes but also include "numerical viscosity" which arises from the numerical approximation. All numerical models incorporate some degree of numerical viscosity approximation.

Factors that affect the ε_{ij} both numerically and physically are mesh spacing, the local flow depth and flow velocity, contractions or expansions in the water body, and the dynamic nature of the problem. In the *TABS* Primer of the *FastTABS* User's Manual (Boss Corporation, 1993), it is suggested that "as a general rule, the coefficients should be kept as low as possible without introducing stability problems." Initially, the model requires that an artificially high ε_{ij} be assigned in order to produce a stable solution. However, these initial settings will typically not properly model flow distributions, flow separations, and eddy currents. Calibration then involves lowering the ε_{ij} for a particular set of flow conditions in consecutive runs until the results from the numerical model achieve the highest agreement with the data from the physical model. The best results typically occur at a ε_{ij} that is slightly higher than the ε_{ij} for which the model becomes unstable. Generally, the higher the flow, the higher the ε_{ij}. To accurately calibrate and verify a model, the ε_{ij} coefficient should be determined for a range of flows in areas of constant depth under steady-state conditions. Table 3.1 shows a list of suggested initial values ε_{ij} taken from the *FastTABS* User's Manual (Boss Corporation, 1993).

Manning's n is the roughness coefficient and is assigned based on the physical properties of bed materials and certain geometric considerations. Chow (1959) provides some

guidance for the assignment of these values for a variety of river scenarios. In determining the value of Manning's n, four general approaches are commonly practiced. They are:

1) having an understanding of the factors that affect n, and thereby acquiring a basic knowledge of the problem and narrowing the wide range of guesswork;
2) consulting a table of typical n values for various types of channels;
3) examining and becoming familiar with the appearance of some typical channels whose roughness coefficients are known; and
4) using an analytical approach based on theory and available physical data.

Even though, in reality, the value of Manning's n is highly variable and dependent on a large number of factors, it is common in certain applications to assume that a channel has a single value of n for all occasions. Appendix B includes tables from Chow (1959) showing common roughness coefficient values. Based on the limited field data available for the Notigi Generating Station case study, and using the roughness coefficient tables as a guide, a suitable range of Manning's n is chosen to be between 0.025 and 0.040 for this case study.

3.1.4 Data Requirements

The data requirements for *FastTABS* are relatively minimal. Geometrical data describing the bathymetry of the channel bottom, based on field surveys or contour maps, is necessary to construct the finite-element mesh. The model requires the user to assign boundary conditions for the mesh. Boundary conditions are typically entered as an incoming flow rate or velocity at one end of the mesh and an exit head or water surface elevation at the other end of the mesh. Calibration and verification of the model requires additional field data including depth measurements and velocity magnitudes and directions at various key locations.

3.2 Modelling Process

3.2.1 Mesh Construction

The first step in determining a hydrodynamic solution using *RMA-2* is to construct a finite-element mesh representing the bathymetry of the region being modelled. *FastTABS* offers various tools that assist in developing and editing a mesh in accordance with some general guidelines. As was defined earlier, a finite-element mesh is made up of nodes and elements. Nodes can be read from a geometry file or created interactively. For the numerical modelling performed for this project, a survey of the laboratory model provided the basic nodal information used in *FastTABS*. The data from the survey was converted to prototype scale and used in the development of the mesh.

New elements may be built interactively using the element tools in *FastTABS*. Elements can also be created automatically using *rectangular* or *triangular patches*, the *triangulation* command, or the *Mesh from Polygon* command. There are four types of elements that can be created:

1) three node, linear, triangles;
2) six node, quadratic, triangles;
3) four node, linear, quadrilaterals; and
4) eight node, quadratic, quadrilaterals.

FastTABS performs several checks when a new element is constructed. Each new element is checked to see if it is ill-formed, if it is overlapping any adjacent elements, and if the element conforms to the type of the other elements (i.e., if the elements are all linear or all quadratic). The quality of the mesh can also be displayed and improved upon by using the

Mesh Quality Options in the display options dialogue. The program's help menu lists the quality criteria as follows (BOSS Corporation, 1993):

1) The *Minimum Interior Angle* criterion checks all of the interior angles of an element. If an interior angle is less than the user specified minimum angle entered in the text edit field, then that element is flagged;.
2) The *Ambiguous Gradient* criterion checks quadrilateral elements for equal elevation values on opposite corners. If opposite corners of an element are found to have the same elevation, then that element is flagged;
3) The *Concave Quadrilateral* criterion checks for those elements that are not convex in shape. If a quadrilateral element has an interior angle that is greater than or equal to 180 degrees, then that element is flagged;
4) The *Maximum Slope* criterion checks the slope of each element edge. If the slope of an element edge is greater than the user specified value entered in the text edit field, then that element is flagged; and
5) The *Element Area Change* criterion checks each element to ensure that it does not violate the 50% rule. If an element is smaller in area than 50% (or an amount specified in the text edit fields) of one of the surrounding elements, then that element is flagged.

The degree to which the mesh conforms to these quality criteria contributes to the viability of the solution. In the development of both the upstream and downstream meshes for the Notigi Generating Station site, the *Maximum Slope* and the *Element Area Change* criteria were the most difficult to satisfy. The suggested *Maximum Slope* criterion parallel to the direction of flow is approximately 1:10 (or 0.10) and anything greater violates the mild slope assumption and influences the results. The bottom slope measured in the direction perpendicular to the direction of flow can be steeper than 1:10 without causing significant problems. The slopes of the cofferdam remnant and the approach and tailrace channels have design slopes between 1:1.5 and 1:4, which exceed the mild slope assumption. To limit problems resulting under such conditions, it is suggested that a dense mesh be

provided in areas with high velocity gradients, high bottom slope, and high boundary curvature. Caution needs to be exercised in evaluating the results in such zones as there is a higher potential for stability and accuracy problems. It is also important to note that *RMA-2* is unable to model supercritical flow and therefore scenarios leading to such conditions should be avoided.

Adhering to the 50% *Element Area Change* criterion requires practice and some experience. In this project, the finite-element meshes were created using a technique that combines the automatic triangulation function with the manual formation and editing of elements on an individual basis. The meshes are based on a detailed survey of the physical model along with estimates based on interpolation between measured locations. The high relief in the riverbed made it difficult to maintain reasonable transitions in element sizes. One suggestion for dealing with such a problem is to use the *Mesh from Polygon* command in *FastTABS* for creating and modifying meshes. This command allows an existing mesh to be used as a background mesh over which the elevations at the nodes of a new mesh are interpolated. The difficulty with this method is in preserving the locations and edges of fixed formations such as the cofferdam or the tailrace expansion. Another approach is to use consistent grid spacing when conducting the original survey and to add extra nodes in areas that need more detail or resolution. This would assist in maintaining the mesh quality during formation and editing of the grid. For this study, all the factors affecting mesh quality were applied as best as possible and no further analyses were performed as to the sensitivity of the model to various degrees of mesh quality.

The design of the mesh is one of the most important aspects in the construction of numerical models. While the mesh needs to comply with the quality criteria listed earlier, which affects the model stability, it also needs to have sufficient resolution, which impacts the solution accuracy. The *FastTABS* User's Manual (BOSS Corporation, 1993) states that "meshes must have sufficient resolution to define the physical surface to be modelled but also enough to solve for the velocity and water depth gradients on the interior of the mesh." According to David T. Williams of WEST Consultants:

> The grid resolution (fineness or coarseness), departure of grid lines from orthogonality (non-rectangular grid) and the rate of change of grid spacing (long grids to short or vice versa) greatly control the accuracy of the solution (Williams, 1993).

The approach to achieving the proper resolution for a particular mesh would be to execute the *FastTABS* model for a given mesh configuration and suitable parameter values, to re-execute the model with finer mesh configurations, and to compare the results of these consecutive model executions. If at some grid configuration further reduction in grid spacing does not cause any change in the flow results, then the grid spacing is adequate. *FastTABS* allows the user to define as many as 3000 elements and an upgraded version of the program can be provided for meshes larger than 3000 elements. The only limitation on the size of the mesh is the computer memory. For this study, the downstream portion of the numerical model contains 334 elements and 953 nodes while the upstream portion of the numerical model contains as many as 639 elements and 1770 nodes. The mesh is developed with greater refinement in zones where the riverbed exhibits relatively high gradients in elevation. As was mentioned earlier, achieving the proper degree of mesh resolution requires the use of suitable parameter values, but until the numerical model has

been calibrated and verified, these parameter values are unknown. For this reason, and because of time constraints, evaluation of the sensitivity and suitability of various degrees of mesh resolution is left for future considerations. Increasing the mesh density solves many of the stability and accuracy problems associated with *RMA-2* but there is a drawback. The greater the density of the mesh, the greater the computational time. With the development of more powerful computers, the potential size and density of mesh designs has increased dramatically. The trade-off between computational time and the refinement necessary to achieve accurate results is essentially accomplished by trial and error.

The way that a mesh is numbered is also an important consideration in the design process. Each node and element in the mesh is given a number by which it is referenced. *FastTABS* can be used to automatically renumber the nodes and elements according to a variety of numbering sequences. The order in which the nodes and elements are numbered can produce drastically different solution times. The status of the numbering sequence is represented by two parameters, the maximum node half-band width and the maximum element front width. These parameters are related to the relative difference in the adjacent node and element numbers, and essentially, they give an indication or measure of how well the elements in the mesh are numbered. The solution time for *RMA-2* is proportional to the total number of nodes times the square of the element front width. The numbering sequence that minimizes the element front width is therefore preferred.

All of the information describing the finite-element mesh geometry is saved by *FastTABS* in an ASCII text file. A sample geometry file is shown in Figure 3.3. Each line of the file provides information or commands to the program and the two or three letter code

at the beginning of the line signifies the type of data contained on that line. For example, the *T1* to *T3* lines are reserved for titles; The *GF* line is an optional mesh debugging control; the *SI* line indicates whether or not the System International units are used; the *$L* line sets up the input and output files; the *GO* line is used for reordering the way the mesh is numbered; the *GE* lines indicate to the program that the following numbers in that line identify the element number, the order of the nodes making up that element, and the material ID; and the *GNN* lines list the node numbers followed by the x, y, and z coordinate reference. Since the ASCII geometry file is generated and saved directly by *FastTABS*, the user generally has no need to examine or alter the file using a text editor. The geometry file format, as well as listing of all the data cards and their descriptions, are summarized in the *FastTABS* User's Manual (BOSS Corporation, 1993).

3.2.2 Assigning Boundary Conditions

The next step, after creating a finite-element mesh, is to assign boundary conditions for the mesh. Boundary conditions are in the form of discharge rates or velocities and water surface elevations. *FastTABS* allows the boundary conditions to be specified interactively or manually using a text editor. Normally, the discharge or the velocity boundary conditions are applied to the boundary where the water enters the model and the water surface elevation boundary conditions are applied to the boundary where the water exits the model. In the upstream model of the Notigi Generating Station case study, these boundary conditions are reversed. If a boundary condition has not been explicitly specified for a boundary node, the node is assumed to be a "no-flow" boundary and the flow direction is considered parallel to the boundary. Boundary conditions can be designated

for individual boundary nodes or for an entire string of nodes. In situations where prototype boundary conditions are not available, it is important to ensure that boundary conditions are well-posed. Another guideline is to make sure that the boundary conditions are far from the area of study to avoid overconstraining the results.

In addition to boundary conditions, a set of material properties or parameters are also necessary to define the hydrodynamic model. Each element is assigned a material ID which is used as an index to the list of parameters. The parameters assigned to each element include four ε_{ij} coefficients and one Manning's n value. A more detailed discussion of the values for these parameters is included in Chapter 6.

Another important component of the boundary condition file is the initial condition of the average initial water surface elevation, which is important in determining the stability of ensuing simulations. *FastTABS* automatically assigns a default value for the initial condition using the value of the water level boundary condition. If the initial condition causes instability, a technique called "spinning up" the model can be used to solve this problem. The process involves first using boundary conditions that are stable, then gradually changing the boundary conditions to the desired values using a series of revisions.

The boundary conditions and the parameters necessary to define the hydrodynamic problem are, for the most part, entered interactively into an ASCII boundary condition file using *FastTABS*. The boundary condition file also includes default values, based on a typical, steady-state problem, for the model controls and additional information, such as the water temperature, the system of units, the output control, the type of analysis (i.e.,

static or dynamic), the number of iterations, and the depth convergence criterion. If changes are needed to be made, the boundary condition files may be edited manually using a text editor. An example of a boundary condition file used in modelling the downstream portion of the Notigi Generating Station case study is shown in Figure 3.4. The layout is similar to that of the geometry file, with each line providing information or commands to the program. The data types are defined in the *FastTABS* User's Manual (BOSS Corporation, 1993), but in general, the *TI* to *T3* lines are again reserved for titles; the *TRN* line provides a list of nodes for which a special trace summary is printed out; the *SI* and *$L* lines are the same as in the geometry file; the *TR* line controls the trace printout; the *GC* line identifies geometry and continuity check lines; the *TZ* line is used to control the computation time; the *TI* line sets the number of iterations and convergence criterion; *FT* sets the water temperature in degrees Celsius; the *IC* line defines the initial water level conditions; the *EV* line defines the turbulent exchange coefficients and Manning's n for each element type; the *BQL* and the *BHL* lines assign the boundary discharge and boundary water surface elevation conditions to a set of nodes; and the *REV* line is used to revise the boundary conditions or the coefficients.

3.2.3 Executing the Model

Executing the model is essentially a two step process. Once the mesh has been constructed and boundary conditions have been defined, the program *GFGEN* must be executed. *GFGEN* is the **G**eometry **F**ile **GEN**eration Program, or in other words, the geometry pre-processor for *RMA-2*. *GFGEN* reads the ASCII geometry file and converts it to a binary file that is input to *RMA-2*. *GFGEN* also generates an ASCII output file

summarizing the geometric information, the renumbering process, and any errors that may have been encountered relating to the design of the mesh. When executing *GFGEN*, the program prompts for the input and output file names to be used.

The next step in the modelling process is to execute the program *RMA-2*. *RMA-2* reads the ASCII boundary condition file and the binary geometry file and then computes the hydrodynamic solution. Figure 3.5 illustrates the possibilities of data flow within the *RMA-2* model. There are three primary forms of output from *RMA-2*, each of which serve a distinct purpose. *RMA-2* can produce something called a HOTSTART binary file which is used to preserve the critical information at the end of one simulation and to become the HOTSTART input file for the initial conditions of a continuous run. The second form of output is the RESULTS binary solution file which contains the velocity, depth, and water surface elevation information for each time step used in post-processing by *FastTABS*. The third form of output by *FastTABS* is the ASCII File which provides the solutions in tabulated form. The ASCII output is available in three forms: 1) the processing information on the screen in interactive mode or in the log-file for batch mode; 2) the full printout file summarizes the complete data input and output; and 3) the special nodal summary summarizes the output for selected nodes in the mesh. Execution of *RMA-2* simply requires the names of input and output files to be entered. The time required for *RMA-2* to complete a solution may vary from a few seconds to many hours depending on the size and resolution of the mesh as well as the speed of the computer.

3.2.4 Post-Processing with FastTABS

FastTABS may be used as a post-processor to read the binary solution files generated by *RMA-2* and to graphically display the results of the flow analysis. The solution files generated by *RMA-2* contain head and flow data for either steady-state or dynamic solutions. Besides the hydrodynamic solution files, there are potentially three additional types of solution files. The concentration files generated by *RMA-4* contain concentration information (e.g., pollutant and sediment load). The residual files (not yet available with the current version of *FastTABS*) contain error estimates for each node. The deposition rate files (also not yet available with the current version of *FastTABS*) contain a value representing the rate of deposition over a given time interval for each node. The display of the solution files depends on the type of data, vector or scalar. Vector type data can be displayed as vectors while scalar type data can be viewed as contour plots. The scalar data include water surface elevation, water depth, river bed bathymetry, velocity magnitude, and Froude number. *FastTABS* can produce various forms of contour plots of the scalar data. The appearance of the contours can be varied in terms of the colour, labels, and type (e.g., one can use normal curvi-linear contours, color filled contours, or cubic spline contours). Only one type of data can be contoured at once. Another useful way of presenting the results is by flow vectors. Each node has an associated velocity magnitude and direction and can therefore be displayed as a vector. *FastTABS* allows the user to control the size, shape, and color of the velocity vectors. *FastTABS* provides many other tools for post-processing which allow numerous options in the appearance of the solution.

In the case where dynamic solutions are generated, the results, over a range of time steps, can be displayed using the "time history" option. Time history data are presented in the form of plots showing the variation of a solution data type, such as water surface elevation or velocity, at selected nodes over a period of time. Dynamic solutions can also be viewed in an animated sequence. Each time step of the dynamic solution file is plotted and presented sequentially as an animation of the changing flow conditions. These features are not used in this project since the tests are based on steady-state conditions. Another feature of *FastTABS*, similar to animation, is the particle trace film loop. This shows an animated perspective of the flow or particle trace lines under steady-state conditions. This tool may be helpful in visualizing and identifying critical flow patterns, such as vortex formation or flow separation.

The post-processing tools available in *FastTABS* are essentially used to gain both a qualitative as well as a quantitative perspective of the solution. Often, a cursory view of the plots may indicate whether or not the results are reasonable. Specific information can be gathered using the *FastTABS* interface by zooming in on an area or nodal point. This analysis is useful in validating the numerical model against a set of field data.

Condition	Turbulent Exchange Coefficient, ε_{ij} [lb.-sec/ft^2]	Turbulent Exchange Coefficient, ε_{ij} [N-sec/m^2]
shallow river (slow currents)	5-25	240-1200
shallow river (fast currents)	25-50	1200-2400
deep estuary (small elements)	50-100	2400-4800
deep estuary (large elements)	200-300	9500-14400
wetland with tidal wetting and drying	100-200	4800-9500
flow separation around structures	1-5	50-240

Table 3.1 *Typical values of turbulent exchange coefficients (BOSS Corporation, 1993). (1 lb-sec/ft^2 = 47.8791 N-sec/m^2)*

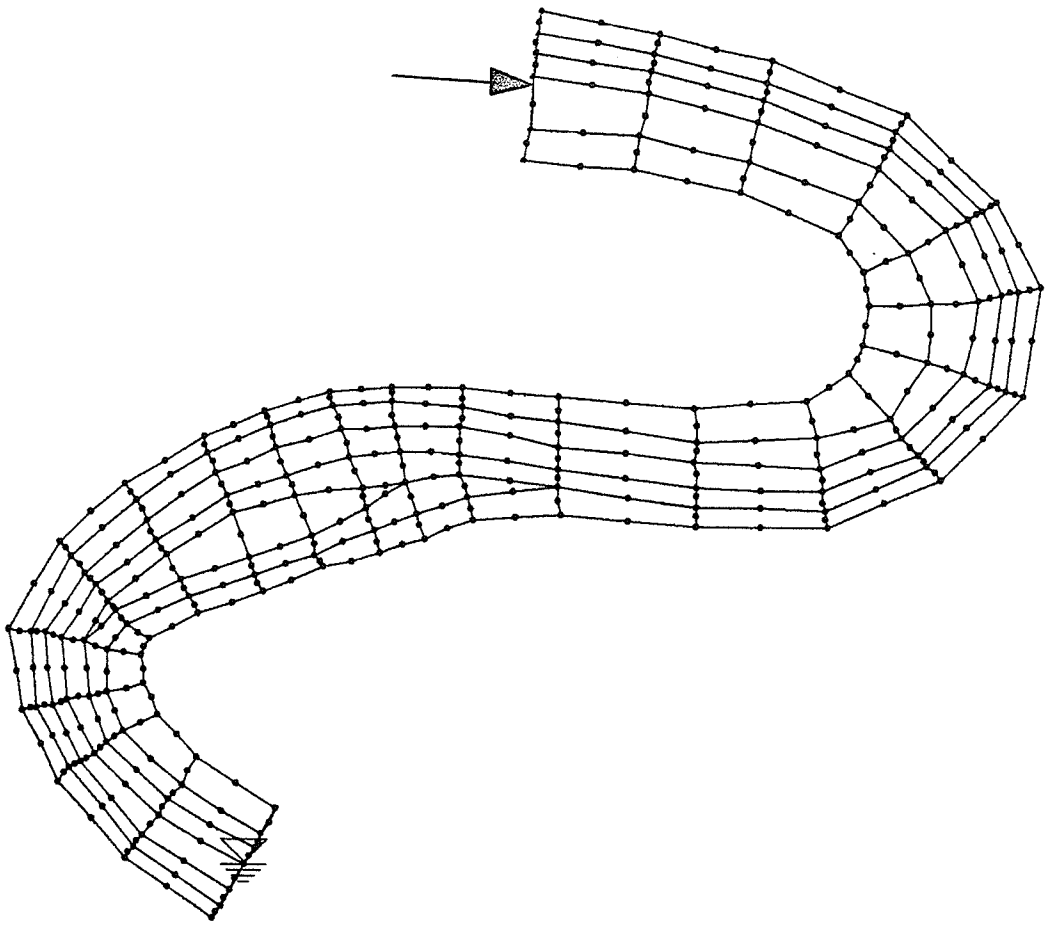

Figure 3.1 *Sample Finite-element Mesh*

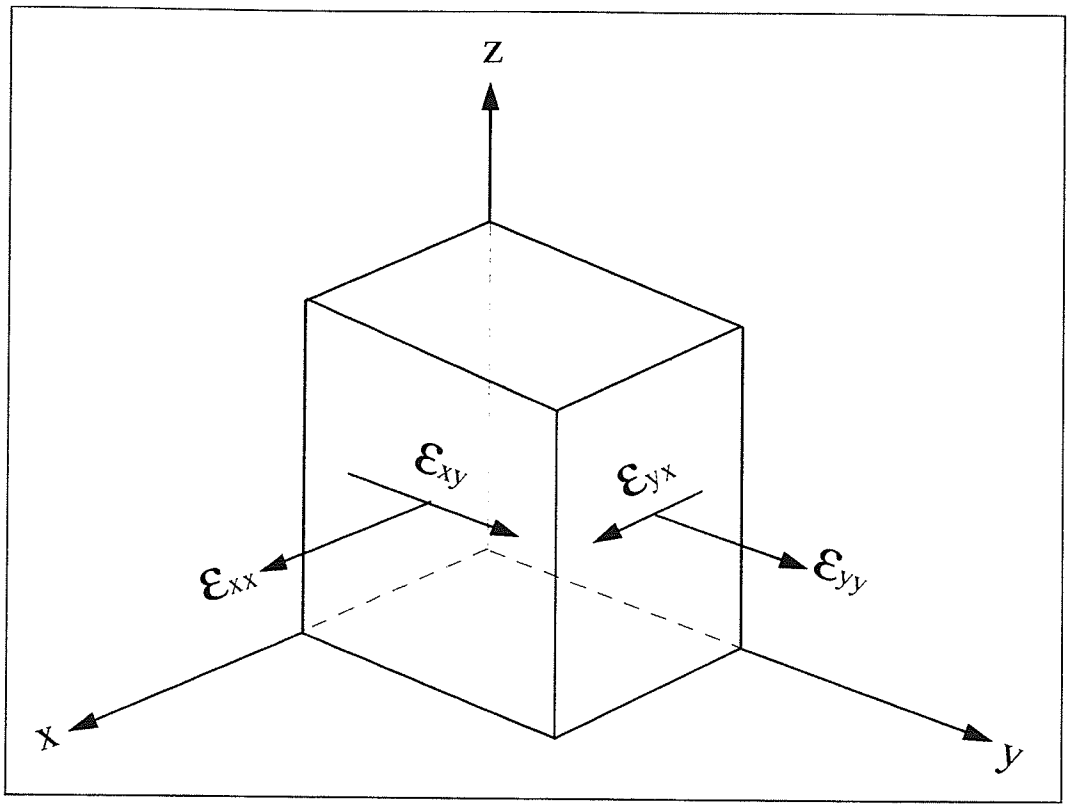

Figure 3.2 *Turbulent exchange coefficients acting on a column of water*

```
T1
T2  Notigi - Overburden BOC case
T3  No Cofferdam
GF  1
SI  1
$L  3 0 6 0
GO  1     1   8   7   13   12   18   17
GO   23   22   -1
GE     1     7     6     5     4     3     2     1     8     1    0.0
GE     2    12    11    10     9     5     6     7    13     1    0.0
GE     3    17    16    15    14    10    11    12    18     1    0.0
GE     4    22    21    20    19    15    16    17    23     1    0.0
GE     5     3    30    29    28    27    26    25    24     1    0.0
.
.
.
GNN     1 -6.4598216e+000   -1.1832040e+002   2.2500000e+002
GNN     3 5.8990000e+000   -1.1650000e+002   2.2519000e+002
GNN     5 7.3700000e+000   -1.2554070e+002   2.2499000e+002
GNN     7 -4.7513704e+000   -1.2738834e+002   2.2500000e+002
GNN    10 8.9500000e+000   -1.3525000e+002   2.2498000e+002
GNN    12 -3.1086289e+000   -1.3717908e+002   2.2500000e+002
GNN    15 1.0530000e+001   -1.4495940e+002   2.2496000e+002
GNN    17 -1.7944356e+000   -1.4716694e+002   2.2500000e+002
GNN    20 1.2000000e+001   -1.5400000e+002   2.2503000e+002
.
.
.
```

Figure 3.3 Sample geometry file

```
T1  Notigi - Case DC2b, downstream with cofferdam
T2  Invert = 242 m, bottom width = 131 m
T3  Q = 1100cms, d/s wsel = 245.6m , n = 0.040
TRN   33  116  225  318  369  512  722  783  792  890
SI  1
$L  0  0  60  64  0  3  59
TR  0  -1  0  1  0
GC   5   1   7   12   17   22
GC   12   343   345   348   351   421   360
GC   300   302   251   197   136   139
GC   11   538   540   543   481   428   369
GC   318   260   262   265   268
GC   13   627   631   564   566   503   505
GC   444   446   449   452   455   458
GC   391
TZ  0.000000  0.000000  0  0  0
TI  10  0  0.001000  0.000000
FT  17.000000
IC  245.60  0.000000  0.250000
EV   1      1800.00    1800.00    1800.00    1800.00     0.040000
EV   2      1800.00    1800.00    1800.00    1800.00     0.055000
BQL   1   1100.00   0.16
BHL   8   245.60
REV  Lower Turbulent exchange Coefficients
EV   1      1500.00    1500.00    1500.00    1500.00     0.040000
EV   2      1500.00    1500.00    1500.00    1500.00     0.055000
REV  Lower Turbulent exchange Coefficients
EV   1      1200.00    1200.00    1200.00    1200.00     0.040000
EV   2      1200.00    1200.00    1200.00    1200.00     0.055000
.
.
.
END  simulation at time = 0.0
STOP
```

Figure 3.4 Sample boundary condition file

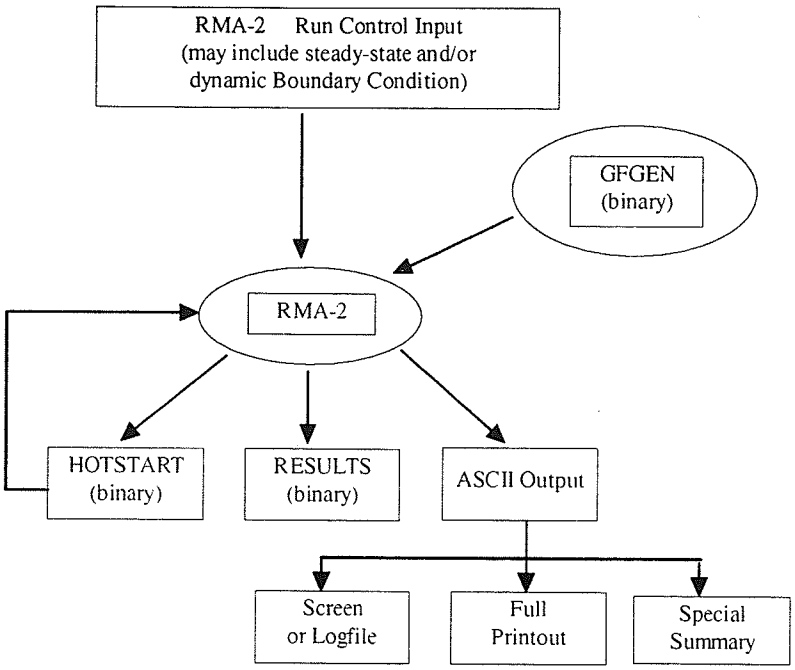

Figure 3.5 *Data flow chart for the RMA-2 model*

4. CONSTRUCTION OF THE PHYSICAL MODEL

This chapter describes several of the important components and design considerations necessary in the construction of the physical model. In modelling hydraulic systems with physical models, often the physical model is applied to investigate a hydromechanical phenomenon and is calibrated and verified based on a set of field data collected under different sets of flow conditions. Since the objective of this study is to calibrate and verify a numerical model under situations in which little or no field data exist, a physical model is used in this case to represent field conditions. This assumes that reliance on the Theory of Similitude is reasonable for velocity and head data, as the scale model is based on a Froude model approach. This project investigates scenarios involving the powerhouse structure, the spillway, and the different sets of cofferdam removal schemes (as was shown in Figure 1.2), that as yet do not exist in the field. The information gained from the physical model may then be used to develop a numerical model which may be applied in an inexpensive and efficient way to investigate a wide range of alternatives before and after the physical model has been removed.

4.1 Design Criteria and Constraints

Designing a physical model requires not only an assessment of the necessary information that is sought, but also a comprehension of the criteria and limitations that affect the design of the model. The degree of similarity between the physical model and the prototype is typically subjected to restrictions of a physical, technical, and economical nature, as was mentioned in Chapter 2. The selection of the model scale and its boundaries is based

on a trade-off between a large scale model that can successfully meet the similarity criteria requirements, and the physical or economical limitations of the laboratory. The issues of primary interest in this study of powerhouse approach and tailrace channel designs are the flow velocities and the headlosses through the cofferdam remnants (see Figure 1.2). Choosing a scale that also permits the accurate simulation of erodible beds and of vortices is secondary for this case study. After extensive investigation of all the modelling objectives and constraints, the constraint that had the greatest impact on the selection of the model scale was the space limitations of the laboratory. The largest, undistorted model that could fit into the hydraulics laboratory, that could encompass the main area of interest, and, at the same time, meet most of the desired similarity requirements was a model scale of 1:100. All references to measurements in this report are considered to be in prototype scale, unless otherwise indicated. In evaluating the possible use of a distorted model, the disadvantages outweigh the advantages, described in Chapter 2, and therefore an undistorted model is used. With the selection of a 1:100 scale, it is recognized that certain areas of the model, especially the shallow, low velocity zones, may not meet Froude model requirements of similar flow regimes and velocity estimates in such areas may be less than what they might be in the prototype. The issues of greatest interest to this project deal with flows in the main channel where the depths and velocities tend to be greater. Therefore, while the ability of the model to exhibit *incomplete similitude* (i.e., similitude of only the flow characteristics) in these areas is possible, the model will at least be able to provide *approximate similitude* of the flow phenomena.

4.2 Elements of the Physical Model

4.2.1 Bedrock and Overburden

The physical model bedrock was constructed by filling a template grid system, based on bedrock contour maps, with sand and coating it with a layer of concrete, as shown in Figure 4.1. According to field investigations, the riverbed consists of material ranging from a boulder pavement of coarse gravel to a very dense sand to a layer of highly plastic clay, depending on the location. The entire range of bed materials is represented in the physical model by using sand of average grainsize diameter 0.4 mm (i.e., 0.04 m prototype scale) as overburden. A particle size distribution curve of the model sand is included in Appendix B. The sand is compacted and shaped to represent the prototype topography, based on contour maps of the overburden, using inverted templates, as shown in Figure 4.2. This material is suitable in that it provides a reasonable representation of the roughness but also provides an indication of where critical scouring may start to occur. The physical model was initially constructed as a movable bed model to investigate the possible scour and deposition associated with the cofferdam removal alternatives. After qualitative investigations of this phenomenon, the model was then transformed into a semi-fixed bed model so that the numerical model could be calibrated and verified based on a consistent set of physical model conditions. Although contour maps of the area provided the information needed to shape the overburden, the relief in some areas, such as the downstream river channel and in the vicinity of the powerhouse, had to be estimated.

The calibration and verification of the two-dimensional, depth-averaged, numerical hydraulic model *FastTABS* using a moveable bed system is not appropriate. In order for

the numerical model to provide a reasonable simulation of the hydraulic behavior in the physical model, each change in the physical topography would have to be replicated in the mesh of the computer model. This requires that the changes due to scouring and deposition would need to be recorded as they occur. Clearly, this is both difficult and time consuming. Another inconvenience with a moveable bed model is artificial erosion that occurs during the filling and emptying of the model. These physical model difficulties led to changing the physical model from a moveable bed to a semi-fixed bed model. This was accomplished by sifting a light coating of cement or mortar mix over the sand, wetting the surface with a mist of water, and allowing the surface to dry to a crust. Modifications in the layout of the semi-fixed overburden can be accomplished fairly conveniently.

4.2.2 Powerhouse and Spillway

The proposed powerhouse structure at the Notigi Generating Station site is designed to house two horizontal bulb turbines. The maximum power output, at a full gate discharge (FGD) in summer of 1100 m^3/s and a full supply level (FSL) of 257.4 m in the forebay, is 115 MW at a gross head of 11.9 m. The existing spillway is regulated by three control gates and has a maximum discharge capacity of 1650 m^3/s. The physical models of both the spillway and the powerhouse are constructed from plexi-glass, as shown in Figure 4.3 and Figure 4.4, respectively. The shape and scale of the intake and draft tube for the prototype plant are replicated so that the flow lines within the intake and draft tube might be approximately simulated. The discharge through the powerhouse model is controlled by sliding plates filled with holes mounted in the powerhouse mid-section, approximately where the turbines would be situated. Several wire screens are also placed

immediately downstream of the control plates but upstream of the draft tube to help remove energy from the system. These screens assist in distributing what would otherwise be a 'jet' flow through the draft tube. The powerhouse model is calibrated for FGD conditions by making fine adjustments to the opening through the powerhouse until the water surface elevation achieves steady-state. The total energy dissipated by the powerhouse model represents the energy that would be absorbed by the turbines plus the sum of all other frictional and transitional losses.

4.2.3 Cofferdams

The proposed cofferdams in the physical model are fabricated to offer a range of design alternatives for testing. Wood and concrete modules are used as the basic components for the cofferdams because this allows for quick and easy changes in the design. Figure 4.5 shows the downstream cofferdam with wood modules in the excavated portion for easy removal. The upstream cofferdam, shown in Figure 4.6, displays the combined use of wood and concrete to form various width and invert design alternatives. The physical model cofferdams do not use scaled prototype material for two reasons: 1) the cofferdams are impervious and hence, flow through the structure is not of relevance; and 2) the primary focus of this work is on the impact that various cofferdam removal alternatives have on the flow and head characteristics in the approach and tailrace regions, and consequently local effects caused by cofferdam roughness can be ignored.

4.2.4 Model Controls and Instrumentation

The data requirements of the test program, for the cofferdam excavation alternatives described in detail in Chapter 5, and for calibration and verification of the numerical model

described in Chapter 6, include water levels, discharges, and velocities (magnitude and direction) for different approach and tailrace channel designs and boundary conditions. Flow patterns and erosion are also observed and documented, but only as qualitative measures.

4.2.4.1 Water Level Measurements

The water levels in river systems are typically a function of the flow entering the system and the backwater results created by downstream restrictions. An adjustable tailgate located at the downstream end of the model allows for control of the water levels in the tailrace and, in a secondary way, in the forebay. Water levels are measured using manual point gauges. Permanent, non-mobile, point gauges are mounted in the following locations:

1) the upstream end of the model, to indicate the forebay level;
2) the powerhouse for measurement by the intake and beside the draft tube, as shown in Figure 4.7; and
3) the downstream end of the model, to indicate the tailrace water levels, as shown in the top right hand corner of Figure 4.8.

Mobile point gauges are required to measure water levels at various locations in the approach and tailrace regions. This is accomplished by a point gauge mounted to a laterally moving instrument wagon on a longitudinally moving bridge, as shown in Figure 4.8 and Figure 4.9. To eliminate possible sag effects caused by the long span of the moveable bridge, the point gage is read using a surveyor's level. Although the point gauges are graduated in 0.1 mm increments (0.01 m in prototype) the accuracy of the measurements using this technique is $\pm$ 0.025 m (in prototype). The mobile point gauge also allows for a comprehensive survey of the river topography for longitudinal, lateral,

and vertical dimensions, in x, y, and z coordinates, respectively. The rails for and the mobile bridge itself are marked in 10 cm increments for longitudinal and lateral coordinates.

4.2.4.2 Discharge Measurements

Discharge measurements are made using a 90° V-notched weir, as shown in Figure 4.10, and the following equation (U.S. Department of the Interior, 1975):

$$Q = 1.342H^{2.48} \qquad [4.1]$$

where Q is the discharge in m^3/s and H is the head of the water in m above the V-notch. The flow entering the model is controlled by a butterfly valve downstream of the laboratory pump as well as a separate valve on a bypass drain for fine tuning, shown in Figure 4.11. The discharge scale ratio, defined by Equation 2.9, is the geometric scale raised to the power of 5/2. Thus, a prototype FGD of 1100 m^3/s is represented in the physical model by a discharge of 0.011 m^3/s. From Equation 4.1, the head above the V-notch weir for a discharge of 0.011 m^3/s is 0.1441 m, which is measured using a fixed point gauge mounted upstream of the V-notch weir. Adjustments in the opening through the powerhouse allow control of flow until steady-state at the desired forebay level is reached. The flow through the spillway is used only for emergency releases, and therefore 100% of the flow passes through the model powerhouse under steady-state testing conditions.

4.2.4.3 Velocity Measurements

Flow velocities in the river, approach channel, and tailrace are measured by a Kent Lea Miniflow Probe, also called a mini-propeller current meter. The general direction of each measurement is determined by evaluating with a protractor the angle that a sub-

merged thread makes with the longitudinal x axis (counter clockwise to the x axis). The velocity magnitudes are converted from the frequency readout of the measurements by calibrated conversion equations provided for the meter. The mini-propellor is attached to the point gauge on the instrument wagon, as is shown in Figure 4.9, allowing readings anywhere in the model as well as velocity readings at specified depths. For physical model water depths, d, greater than 7 cm, the depth-averaged velocity is the average of the velocity readings at $0.2d$ and $0.8d$. The velocity at $0.6d$ represents the depth averaged velocity for depths less than 7 cm.

4.2.4.4 Flow Patterns and Erosion

Flow patterns and erosion behavior provide supplementary information to the tests and are therefore qualitative in nature. The flow patterns are defined with the aid of dye tracing to permit efficient appraisal of the flow conditions. This is particularly useful in identifying zones of flow separation and eddy behavior. Erosion is monitored in terms of the velocities associated with certain design alternatives that cause erosion of the bed material. Difficulties in operating a moveable bed model and simulating it with a numerical model, as described earlier, led to converting the model to a semi-fixed bed model by applying a light coating of concrete cement.

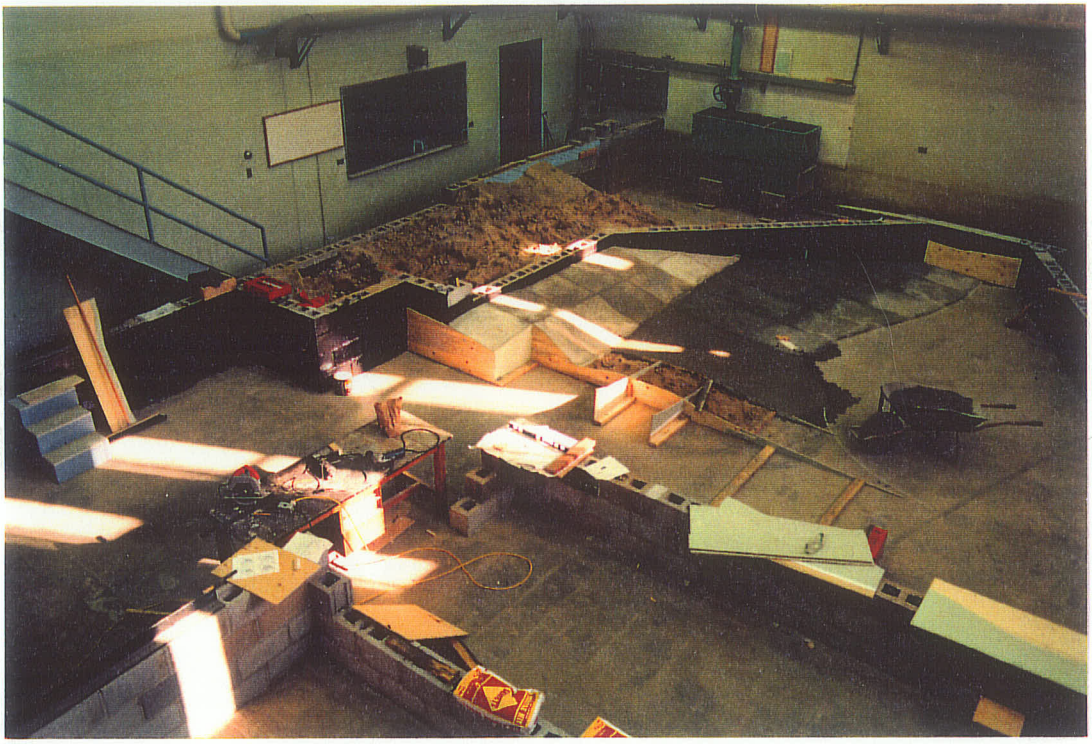

Figure 4.1 *Construction of the physical model for the Notigi Generating Station showing formation of bedrock using templates, sand, and concrete.*

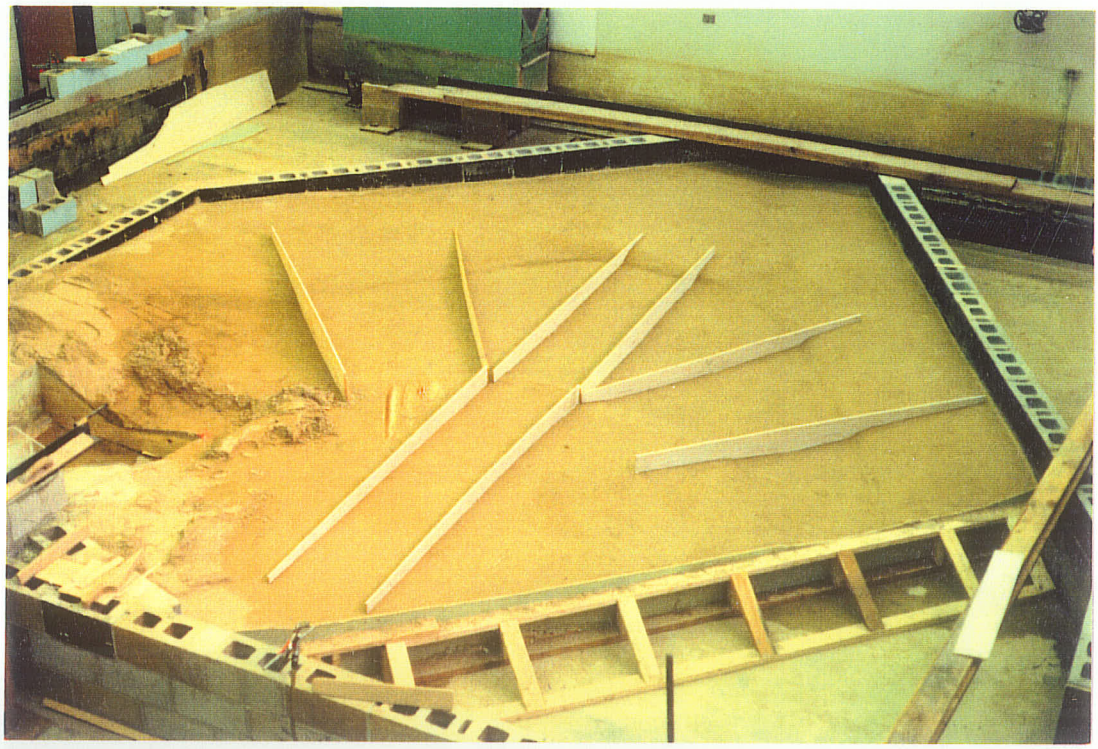

Figure 4.2 *Shaping the downstream overburden using inverted templates resting on elevation pins.*

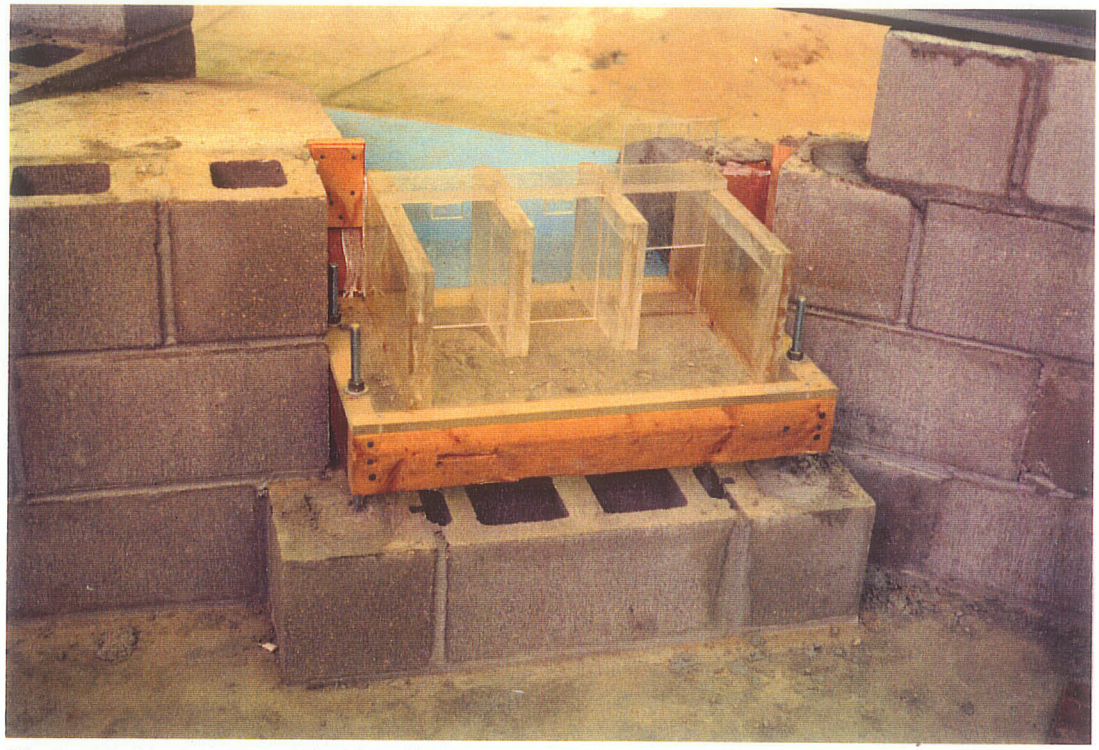

Figure 4.3 *Plexi-glass model of the spillway structure.*

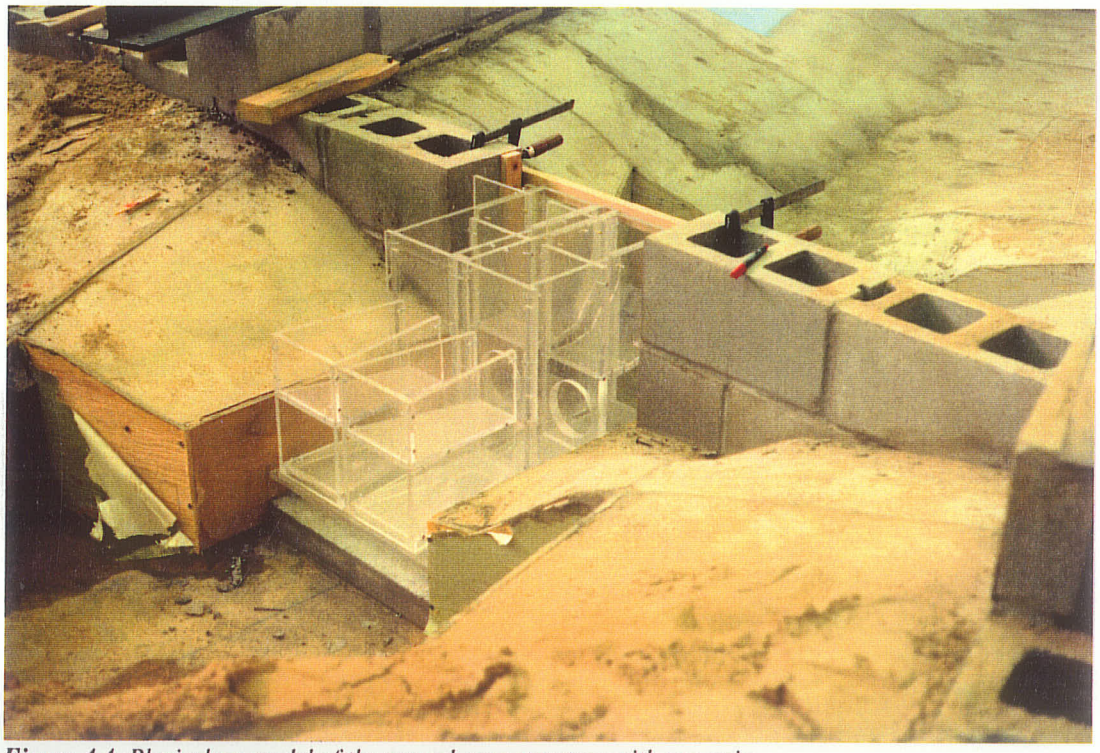

Figure 4.4 *Plexi-glass model of the powerhouse structure with two units.*

Figure 4.5 *Downstream cofferdam constructed with wood and concrete modules for easy adjustments to excavation widths and elevations.*

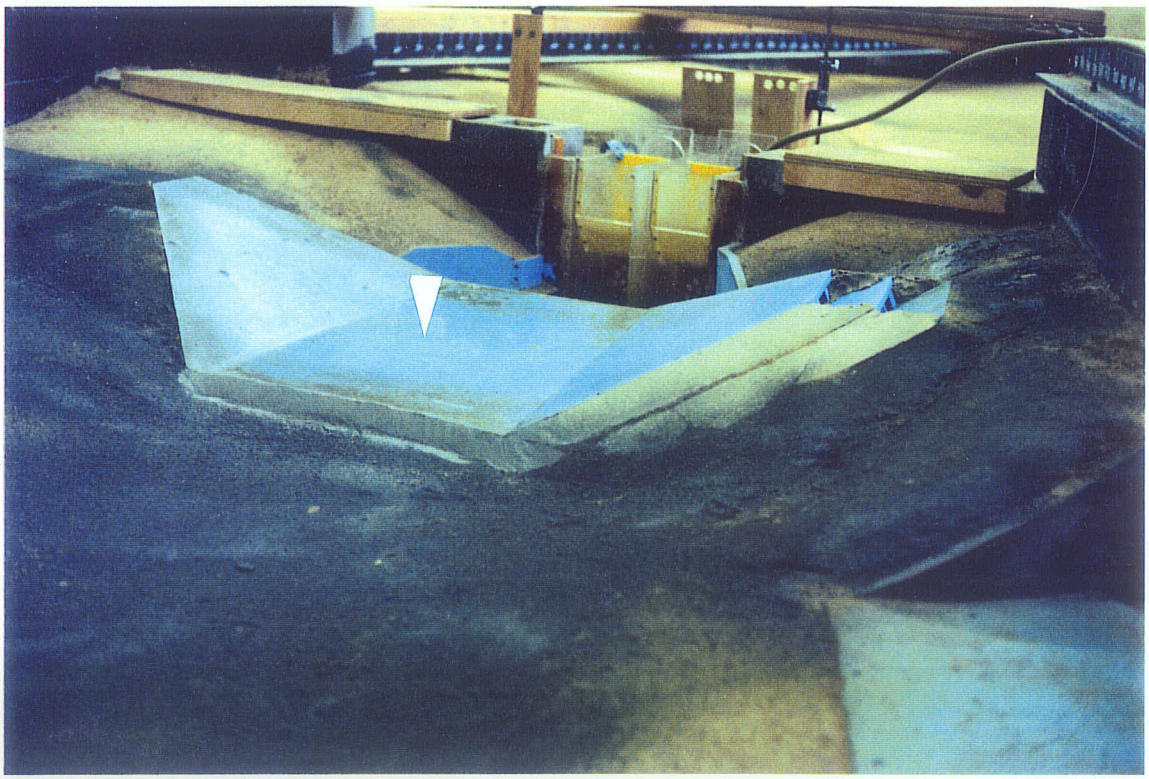

Figure 4.6 *Upstream cofferdam composed of wood and concrete modules for easy adjustments of excavation widths and inverts.*

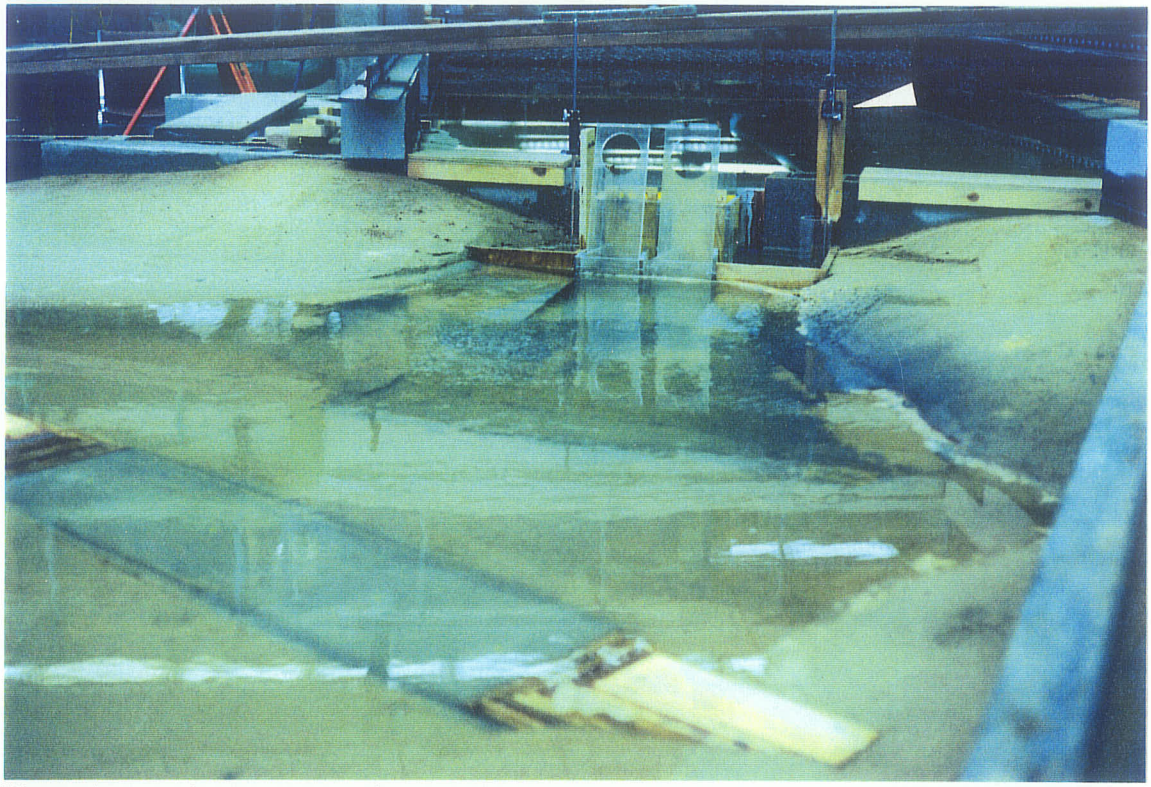

Figure 4.7 *Fixed point gauge to the right of the powerhouse used for measuring water surface elevations by the intake and beside the draft tube.*

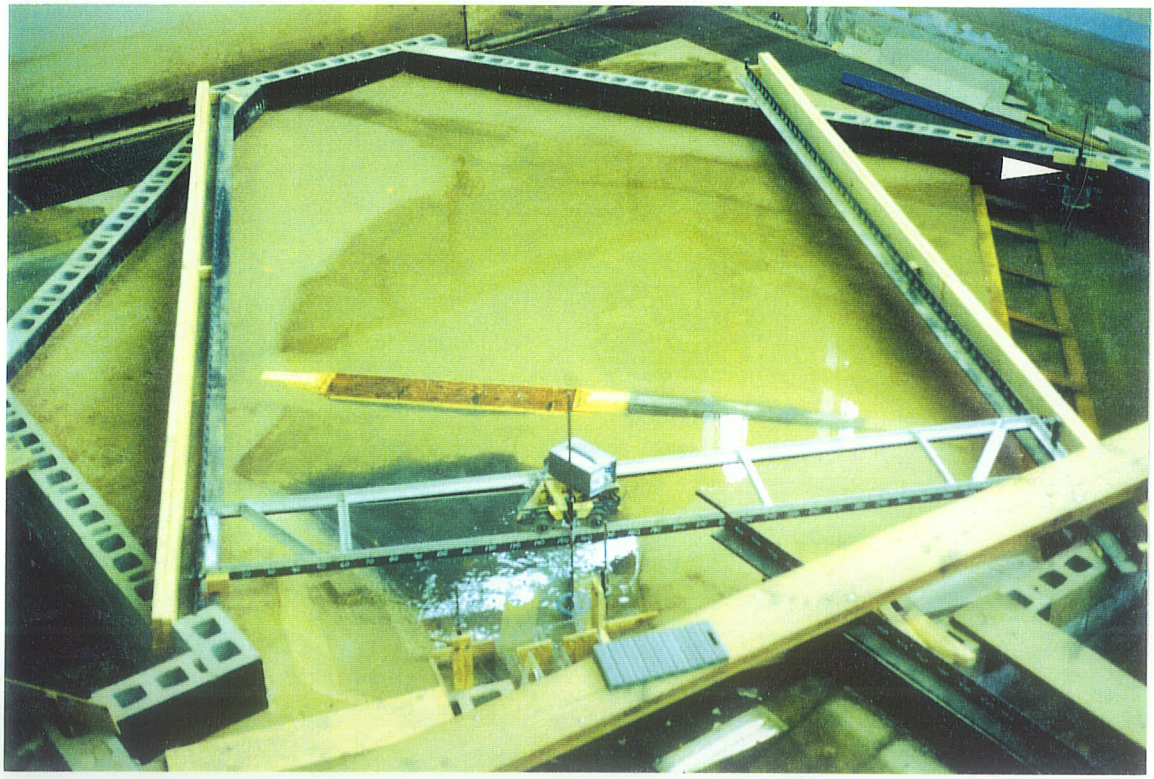

Figure 4.8 *Tailrace channel with a fixed point gauge mounted at the downstream end of the model, seen in the top right*

Figure 4.9 *View of the point gauge and mini-flow current meter mounted to the instrument wagon on a mobile bridge.*

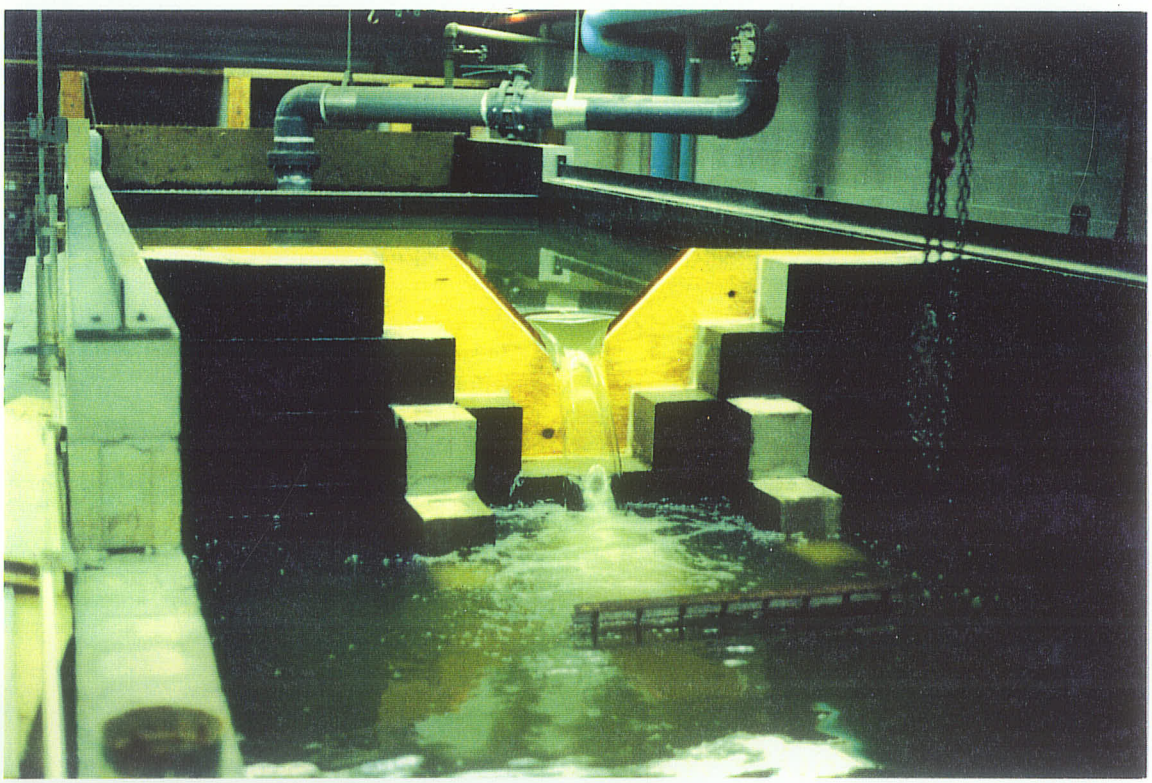

Figure 4.10 *Flow into the model measured by the V-notched weir.*

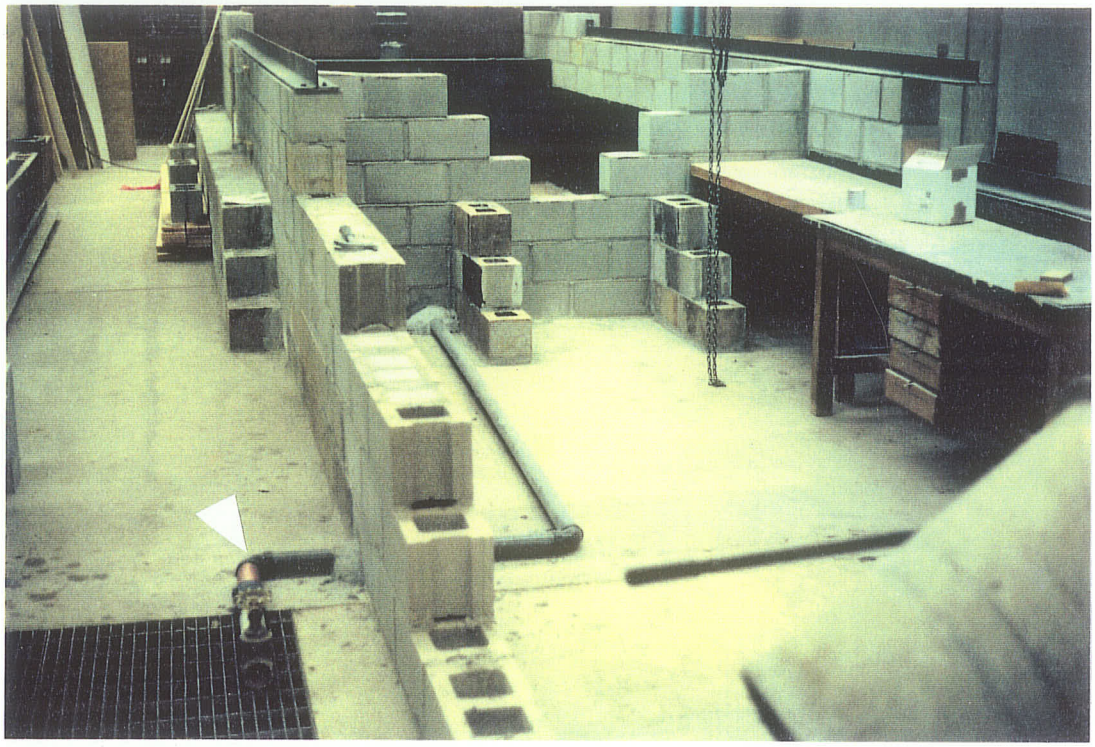

Figure 4.11 *By-pass drain coming from the V-notched weir tank to allow for fine tuning of the control of discharge into the model.*

5. TESTING OF THE PHYSICAL MODEL

5.1 Information to be Gained

The main purpose of the physical model is to provide hydraulic information for various powerhouse approach and tailrace design alternatives that can be used to calibrate and verify the numerical model. Flow velocities and water surface elevations are measured throughout the physical model and compared to numerical model estimates to evaluate headlosses and velocities affecting ice formation and erosion. The physical model is also used to get a qualitative impression of erosion and any significant flow patterns under different boundary conditions.

5.2 Design Alternatives

The design of the powerhouse approach and tailrace channels involves several different variables. The most significant variable, in terms of the impact on the hydraulic conditions, is the degree and configuration of cofferdam removal. Another factor is the contraction angle excavated in the bedrock of the approach channel and the expansion angle excavated in the bedrock of the tailrace channel. The zone downstream of the powerhouse and upstream of the cofferdam is also investigated qualitatively in terms of the impact of overburden removal.

There are essentially two removal schemes for the downstream cofferdam, referred to as the Removal Schemes *DC(a)* and *DC(b)*. Removal Scheme *DC(a)*, as shown in Figure 5.1, has a bottom width of approximately 113 m that lies within the confines of the main channel, and side slopes of 1:2 (vertical:horizontal). Scheme *DC(a)* is tested for three

different inverts: 1) 244.0 m; 2) 242.0 m; and 3) 240.0 m. These inverts are selected to be below the minimum tailwater level for pre-Wuskwatim conditions of around 245.0 m, and thus provide a suitable range of alternatives. The second alternative, Removal Scheme *DC(b)* is also shown in Figure 5.1 and is designed to allow for the expansion of flow leaving the powerhouse. Removal Scheme *DC(b)* differs from *DC(a)* in that the excavation is widened by 18 m to accommodate a flow expansion of 3:1 (longitudinal:lateral). Other reasons for including this alternative are to accommodate the fact that the axes of the cofferdam and the powerhouse are not parallel, to minimize energy losses due to contraction and expansion of flow through the cofferdam opening, and to prevent rotational flow patterns upstream of the remnant.

The removal schemes for the upstream cofferdam, referred to as Removal Schemes *UC*, follow a similar arrangement as the downstream schemes, as indicated in Figure 5.2. Removal Scheme *UC(a)* represents the widest bottom width that fits within the bounds of the main upstream channel. Removal Scheme *UC(b)*, decreases the bottom width by 10 m, and Removal Scheme *UC(c)* reduces the bottom width by another 10 m. The side slopes for all of these cases are set at 1:2. Each Removal Scheme is further subdivided into three invert elevations: 1) 239.8 m; 2) 242.8 m; and 3) 245.4 m. The design alternative having an invert of 239.8 m and the widest bottom width cuts into the river bank and is not considered. This combination of widths and inverts permits the testing of eight different cofferdam removal alternatives. These design options are designed so that all of the inverts are well below the MSL in the forebay of 254.2 m. The area through the remnant should also be large enough to yield low velocities for ice formation and to

mitigate erosion. The range of bottom widths combined with the invert options provide a reasonable range of testing conditions for this case study.

The flow patterns and powerhouse efficiency are also dependent on the type of transitions upstream of the intake and downstream of the draft tube. The powerhouse is situated so that the intake and draft tube inverts are below the bedrock by as much as 10 m. The contraction and expansion of the bedrock excavation in the approach and tailrace zones are varied by using two alternatives. The expansion in the tailrace has either a 3:1 expansion (Expansion Scheme *TR3:1)* or no expansion (Expansion Scheme *TR0*). Figure 5.3 shows the concrete modules used to produce the no expansion alternative. The upstream transition was to have similar alternatives with either an approach contraction of 1.5:1 or no contraction excavated in the bedrock. The proximity of the cofferdam to the powerhouse is such that the 1.5:1 approach contraction would coincide with the edge of the cofferdam slope, as indicated in Figure 5.4. Consequently, the 1.5:1 contraction was eliminated and only the no contraction case was examined for all design alternatives.

Another design aspect in the tailrace channel involves evaluating the hydraulics for various overburden removal alternatives. The velocity in the tailrace between the powerhouse and the cofferdam tends to be high enough for significant scouring to occur in the overburden. The fact that the tailrace immediately downstream of the powerhouse is still in a very narrow section of the river, and that the pre-Wuskwatim water levels are rather low, contribute to the high velocities in this reach. The scouring and resulting deposition could change the river bottom in such a way that it severely alters the flow patterns, even

to the point of increasing the head at the powerhouse. In order to deal with this problem, the overburden downstream of the powerhouse is removed to an elevation of approximately 231 m in two stages. The original design for the downstream overburden (Overburden Removal Scheme *DOB*), as illustrated in Figure 5.5, shows the bedrock excavation rise at a 1:5 slope until the natural river bed is reached. Removal of the overburden for the first stage (Overburden Removal Scheme *DOB1*) begins at the interface of the bedrock and the overburden for a length of about one-third the distance to the cofferdam. This excavation is joined to the natural river bed with a 1:3 slope. The second stage of downstream overburden removal (Overburden Removal Scheme *DOB2*) continues at the same invert to approximately two-thirds of the distance to the cofferdam and rises to the natural river bed with a 1:3 slope.

5.3 Boundary Conditions

For this case study, the physical model is tested under the same boundary conditions in all but one case. By using the same boundary conditions, the impact that various design alternatives have on the hydraulic characteristics can be assessed for design purposes. This is also important in calibrating and verifying the numerical model. With the same boundary conditions, the numerical model can be calibrated and verified for a range of design alternatives. The numerical model also needs to be verified for a different boundary condition to establish the range of model applicability.

The boundary conditions selected for the tests in the physical model are listed in Table 5.1. Boundary Condition (1) is used for the majority of the tests while Boundary Condition (2) is used for verification of the numerical model. The first boundary condition is a

FGD of 1100 m^3/s with a FSL in the forebay of 257.4 m for open water summer flows. The second boundary condition uses a significantly lower flow representing the long term summer mean flow of 867 m^3/s and a forebay elevation at the MSL of 254.2 m. The water levels in the tailrace represent the pre-Wuskwatim levels during summer for the corresponding flows. These boundary conditions offer a reasonable range of flow conditions under which the design alternatives can be tested. Another useful test would be to set the boundary conditions at a maximum discharge and a minimum forebay elevation, as might occur during the winter season. Unfortunately, time constraints did not permit testing of these additional extremes in boundary conditions.

5.4 Test Scenarios

The tests scenarios for the physical model are conducted in two separate sets: the downstream reach tests and the upstream reach tests. The focus in this study is not on the powerhouse itself, but rather on the relative impacts of changes in channel designs on the upstream or downstream hydraulic conditions. Moreover, the numerical model is not capable of simulating flow through a powerhouse and can therefore only be applied for the two distinct models of the upstream and downstream systems. On the other hand, it is important to recognize that the upstream and downstream sections are not totally independent of one another. The water levels in the forebay are influenced by the head in the tailrace. Conversely, for constant flow conditions, the forebay level does not have a significant impact on the tailrace water level. Thus, for tests conducted in the upstream reach under the same boundary conditions, it is important that the boundary conditions in the downstream reach be kept constant.

The test scenarios that are executed in the physical model are summarized in Tables 5.2 and 5.3 for the downstream and upstream sections of the model, respectively. Each scenario is defined by a design alternative, the model variables, and the applied boundary conditions. The first column identifies the design alternative being tested. The design alternatives for the downstream reach include three overburden removal alternatives, three inverts for two different cofferdam removal widths, and two tailrace expansion alternatives. For the upstream reach the design alternatives include the complete removal of the upstream cofferdam and various inverts for the three cofferdam removal widths. Each design alternative is assigned a reference code or design designation, shown in the second column, to aid in the data management. The third column identifies the model variables. In Table 5.2, the model variables for the downstream model include the bottom width, the invert elevation, the degree of overburden removal, and the choice of tailrace expansion. Similarly, the upstream model variables in Table 5.3 include the cofferdam bottom width and invert, as well as the approach contraction. The fourth column indicates the level of detail of the tests in terms of the number of velocity and head data that are collected in the physical model and also can be identified for comparison in the numerical model. The larger data sets are used for calibration and verification of the numerical model whereas the smaller data sets are used for supplementary verification of the computer model. The final column summarizes the boundary conditions for each test, in terms of a discharge and a downstream water surface elevation for the downstream model, as shown in Table 5.2, or a discharge and an upstream water surface elevation for the upstream model, as shown in Table 5.3.

5.5 Summary of the Physical Modelling Test Results

Although the data collected from the physical model are primarily used in the calibration and verification of the numerical model, they also serve to identify the hydrodynamic response due to various combinations of boundary conditions and channel designs. The information gained from the model is in the form of quantitative measurements as well as qualitative observations.

5.5.1 Quantitative Results

5.5.1.1 Downstream Model

The tests in the tailrace region of the model, as previously summarized, encompass three distinct design issues. They include the following: 1) overburden removal; 2) cofferdam removal scheme; and 3) tailrace expansion. The tables in Appendix C summarize the velocity and water surface elevation measurements for all the downstream tests. These measurements are helpful in identifying the hydraulic response to changes in both design and boundary conditions. The tests involving the first design issue, removal of the overburden, are intended to investigate the impact of this feature on the velocity and head in the tailrace zone just downstream of the powerhouse. Measurements for three overburden removal schemes are made only in the area of concern, that being the section of river between the powerhouse and the downstream cofferdam site. Unfortunately, neither the mini-propeller meter nor the point gauge could provide consistent and meaningful measurements in this turbulent zone and consequently the data for these scenarios had to be disregarded. Several interesting observations did come out of these tests though, as will be described in Section 5.5.2.

The tests dealing with the second design issue, cofferdam removal schemes, reveal some useful relationships in terms of the hydraulic characteristics. The most critical impact of the downstream cofferdam is with respect to the water level near the powerhouse. One way of illustrating this behavior is by plotting the relative headloss, or net water surface elevation, across the cofferdam, as shown in Figure 5.6. This plot describes, for two cofferdam removal schemes, the difference in the water level just upstream of the cofferdam to a point near the downstream end of the model. The difference in the water level across Removal Scheme *DC(a)* is greater than the wider Removal Scheme *DC(b)*. There is a significant decrease in the net water level of as much as 1.17 m when lowering the invert from 244 m to 242 m whereas lowering the invert another two metres to an invert of 240 m yields a decrease in the water level of only 0.22 m. The cofferdam removal scheme also has an impact on the velocities that may be experienced through the opening. Figure 5.7 compares the average velocity through the upstream cofferdam to the cofferdam invert for the two widths, Removal Schemes *DC(a)* and *DC(b)*, for a discharge of 1100 m^3/s and a downstream water level of 245.5 m. The dashed line indicates the average velocity in the vicinity of the cofferdam excavations, but with no cofferdam in place. The average velocity through the remnant is as high as 3.7 m/s for Removal Scheme *DC(a)*, while complete removal of the cofferdam would only reduce the average velocity in the cofferdam vicinity to about 1.2 m/s. For the cases tested, there is a greater reduction in the average velocity by lowering the invert excavation than there is by widening the excavation.

The third design issue is to evaluate the effect that the tailrace expansion has on the flow characteristics. As was described earlier, only two alternatives are investigated: Expansion Scheme *TR3:1* having an expansion of 3:1 and Expansion Scheme *TR0* having no expansion. All other factors, such as boundary conditions and cofferdam alternatives, remain the same between the two tests. The results agree with theory in that the expansion yields higher water levels and lower velocities between the powerhouse and the downstream cofferdam. Figure 5.8 displays the water surface elevation profile along the centerline of the main channel for the two expansion design alternatives. The water levels upstream of the cofferdam are higher for Expansion Scheme *TR3:1*, and although the associated velocities in this zone would be lower, they are not low enough to cancel the effect of the increased head. In other words, the total energy head in the Expansion Scheme *TR3:1* tends to be slightly higher than the Expansion Scheme *TR0*. The obvious negative effect of using the Expansion Scheme *TR0* is that the higher velocities may cause downstream scouring.

Figure 5.8 shows another interesting condition that occurs just downstream of the draft tube. The low water surface elevation right at the powerhouse is a phenomenon that can occur at a submerged abrupt outlet. In situations where the area of the tailrace channel is of finite dimensions in comparison with the area of the submerged outlet, "there will be a conversion of part of the velocity head in the pipe to the elevation head in the channel" (Kells and Smith, 1988). Kells and Smith (1988) refer to this as *recovery* and claim that it can amount to as much as 50% of the velocity head. The recovery is maximum when the ratio of the area of the submerged outlet to the area of the tailrace channel

downstream of the outlet is 0.5, and equal to 0.5 times the outlet velocity head. The total energy level at the face of the draft tube is the water level at that point plus the outlet velocity head. At some point downstream of the powerhouse, the water level is recovered to the equilibrium water level as velocities become more uniform with depth and as the channel widens.

5.5.1.2 Upstream Model

The velocity and water surface elevation measurements for all the upstream tests are summarized in Appendix D. The data collected from the physical model are used to calibrate and verify the numerical model. Proper assessment of the impact of various cofferdam removal strategies would require that all other model variables, specifically the boundary conditions, remain constant. Unfortunately, testing in the upstream reach proved somewhat challenging due to unstable boundary conditions and low velocities, as is described in Section 5.5.3. As a result, a comparison of velocities and water levels for various cofferdam removal strategies yields, at best, general tendencies. A comparison of the difference in water surface elevation from the upstream end of the model to the powerhouse offers a more relative perspective of the impact that various design alternatives have on headlosses. Figure 5.9 compares the net water levels for the different cofferdam removal options. The net water surface elevation across the upstream cofferdam ranges from 0.05 m to 0.0 m. These differences in water surface elevation are quite small when compared to the downstream model. Obviously, changing the boundary conditions, for example, to a significantly lower forebay elevation while maintaining the

discharge, can dramatically increase the headlosses across the cofferdam, but such scenarios could not be fit into the testing schedule.

The velocity through the cofferdam is significant in monitoring the onset of erosion. Figure 5.10 gives an indication of the maximum and approximate mean depth-averaged velocities that occur through the upstream cofferdam for various design alternatives. These results are for the boundary conditions of a discharge of 1100 m^3/s and a forebay level of 257.55 m. The solid indicators represent the maximum velocity that is measured through the cofferdam and the hollow indicators represent the approximate average velocity through the cofferdam. Lowering the invert results in a marked decrease in the velocity. The solid line indicates the maximum allowable velocity below which erosion of riverbed material will not be of significance. A maximum velocity criterion of 1 m/s is selected for the river bed material based on observations from the physical model as well as maximum permissible velocity tables referenced by Chow (1959). The prototype cofferdam material probably consists of granular and random rockfill ranging in average particle size from 0.01 m to 0.1 m, for which the maximum permissible velocities range between 1.0 m/s to 3.0 m/s, respectively (Chow, 1959). For the cases tested, the maximum velocity experienced through the upstream cofferdam was approximately 1.4 m/s thereby indicating that erosion may occur for particles smaller than 0.02 m. It is clear that other boundary conditions may yield higher velocities leading to greater erosion, and therefore such conditions would have to be considered in a more rigorous channel design analysis.

5.5.2 *Qualitative Observations*

There are several additional observations that may be made from the tests of both the upstream and downstream models. The issues of interest include flow patterns, turbulence, and erosion. The flow downstream of the powerhouse in the natural riverbed tends to have higher velocities along the inside bend of the main channel. With the cofferdam remnant in place, the design alternative having a bottom width within the main channel, Removal Scheme *DC(a)*, tends to force the higher velocities further to the outside of the bend than when there is no cofferdam, as is shown in Figure 5.11. This could lead to erosion of the outer river bank. The wider design alternative, Removal Scheme *DC(b)*, allows the flow to follow its natural course. Also, the choice of cofferdam removal may result in differences in the separation of flow at the remnant ends. In particular, the flow through the narrower option, Removal Scheme *DC(a)*, experiences greater separation at the upstream corners of the protruding remnant (see Figure 5.12). The more prominent the separation of flow, the greater the headloss through the cofferdam. This means that the water levels immediately downstream of the powerhouse would be higher, and consequently the powerhouse would have less potential head needed for power production. The separation is also confirmed by the sand deposit pattern from the remnant towards the mid-channel, as illustrated in Figure 5.13. The sand trail on the south side (the left sand trail in Figure 5.13) deviates from the direction of flow by turning inwards whereas the trail from the north remnant (the right sand trail in Figure 5.13) is parallel to the direction of flow.

The separation of flow through the upstream cofferdam is less obvious than the downstream scenarios because of the slower velocities in this portion of the model. However, with the use of tracer dyes, the degree of separation is more clearly defined, as shown in Figure 5.14. The flow tends to circle back into the flow along the inside face of the cofferdam excavation. This pattern is fairly consistent for all remnant alternatives. Vertical separation also occurs at the downstream edge of the excavation invert as shown in Figure 5.15. The forces that cause separation of flow may eventually erode the corners of the cofferdam remnant in the field, depending on the materials used for the cofferdam, until the physical boundary conforms to a shape of natural transition.

Another flow pattern of interest is the formation of eddies or vortices. Vortices near the intakes to the powerhouse may lead to air entrainment which decreases the discharge capacity thereby reducing the powerhouse efficiency. Although the scale of the physical model does not allow accurate simulation of vorticy formation, any vortices that do occur in the physical model can be assumed to occur in the prototype scale. On the other hand, the absence of any vortices in the model does not indicate that there will be no vortices in the prototype. Large scale circular flow patterns were observed on either side of the powerhouse intakes between the upstream cofferdam and the main dam for FGD and FSL. These large scale eddies are well out of the main flow and do not give any indication that air entrainment will become a problem. The powerhouse axis is perpendicular to the direction of flow and therefore the eddies are forced to spread to the outside, well beyond the range of the intakes. Changes in the upstream cofferdam widths within the limits chosen do not have a significant impact on the location of the large scale eddies. Simi-

larly, large circular flow patterns were observed between the downstream cofferdam and the powerhouse. The eddies that appear downstream of the powerhouse do not have any negative effects on the power production of the generating station.

The flow downstream of the powerhouse differs significantly from the upstream section in the degree of turbulence that is experienced. The flow from the draft tube exits in the form of a submerged jet which rapidly expands the moment it leaves the draft tube. Much of the expansion occurs in the vertical direction thereby producing significant swelling and rough water at the surface. A two-dimensional depth-averaged approximation of this flow is rather incomplete and, because of the variability of the turbulent flow, may also be inaccurate. The flow appears to stabilize somewhat, that is, become more two-dimensional, by the time it reaches the natural river bed at the end of the overburden excavation.

In order to maintain similitude between the physical model and the prototype, the total energy absorbed by the powerhouse in both cases must be comparable. The model simplifies the energy removal by adding 'friction' to the system until the appropriate scaled headlosses are achieved. During the initial powerhouse calibration, it was recognized that even though the flow through the powerhouse remained constant, the velocity distribution at the draft tube exits would vary. Although the physical model of the powerhouse does not contain a scaled turbine, the wire mesh screens and plates with adjustable opening sizes, used to remove energy, produced velocity distributions that were similar to results from field studies of low-head turbines (Staubli and Deniz, 1994). The investigation by Staubli and Deniz (1994) on flow non-uniformities at draft tube exits, states that there may

be a considerable loss of kinetic energy at the exit of the draft tubes which accounts for a substantial proportion of the available head. The authors also state that the range of velocity distributions through the draft tube is highly dependent on the gate opening. Although the analysis of draft tube flow kinetics is beyond the scope of this project, it is important to acknowledge the significance of variable velocity distributions in the design of draft tubes.

A qualitative investigation of erosion of the overburden is conducted for the down-stream portion of the model, in part, to identify the velocity corresponding to the onset of sediment scouring for the model bed material. This velocity is then used as a suggested upper limit at which erosion could occur in the prototype with similar material properties. The tailrace channel is initially tested for the 'no overburden removal' alternative (Overburden Removal Scheme *DOB*), as was described in Section 5.2. Severe scouring occurs at the point where the bedrock and overburden meet, and a dune or ridge of bed material is deposited across the downstream channel. Figure 5.16 and Figure 5.17 show the magnitude of the erosion that occurs in the physical model under a prototype discharge of 1100 m^3/s. A retaining wall is constructed along the north bank to prevent slope failure. One approach to mitigate the erosion occurring in the channel is to line the leading edge of the overburden with a 15-20 m wide band of riprap (see Figure 5.18). The riprap represents rock having a maximum diameter of 1 m, and is placed so that it follows the same bathymetry as the 'no overburden removal' option. The riprap succeeds only in transferring the scour problem to the downstream edge of the riprap, but to a lesser degree than the unprotected riverbed (see Figure 5.19).

A second attempt at dealing with the erosion problem is to remove a section of the overburden to an elevation of 231 m. The first consideration, referred to as Overburden Removal Scheme *DOB1*, has the overburden removed to one-third of the distance to the downstream cofferdam, as shown in Figure 5.5 and Figure 5.20. The unprotected river-bed experiences erosion similar to the Overburden Removal Scheme *DOB*, only with less sand being transported (see Figure 5.21). Adding a 10 m wide band of riprap along the leading edge does little to correct the problem (see Figure 5.22 and Figure 5.23). The second stage of overburden removal, referred to as Overburden Removal Scheme *DOB2*, has the overburden removed to two-thirds of the distance to the cofferdam. A slightly wider band of riprap is placed along the leading edge (see Figure 5.24). This time, even though there is still erosion downstream of the riprap, the transported sediment is not deposited onto the downstream natural riverbed (see Figure 5.25). The tests of these scenarios conclude that the high velocities near the channel bottom, resulting from the submerged jets leaving the powerhouse as well as from the narrow cross-sectional area of the reach immediately downstream of the powerhouse, will cause significant erosion of the riverbed in the tailrace. The tests also indicate that erosion of the bed material can be considered insignificant for velocities less than approximately 1 m/s. In order to conduct the remaining tests and gather the needed information suitable for calibrating and verifying a numerical model, the overburden is converted to a semi-fixed bed by applying a light coating of cement and allowing it to harden to a crust (see Figure 5.26). The riprap alternative was abandoned as it is likely not feasible for the Notigi Generating Station field site.

5.5.3 Limitations Related to Data Collection

The equipment used to conduct the tests in the physical model have limitations in terms of accuracy. The variability in some of the properties being measured also adds to the uncertainty in the data. Operation of the model presents certain variabilities that need to be taken into account, as well.

The accuracy of the instrumentation used to measure elevations and velocities are sufficient for what is being measured. The point gauges, although capable of reading to within 0.01 cm (0.01 m in prototype scale), are only accurate in these tests to ±0.025 cm. This is because the readings are taken using a transit in order to compensate for the sag in the moving instrument bridge and any irregularities in the rails that support it. In most areas of the model, particularly in the upstream reach, the water surface is fairly calm allowing for accurate readings of the instruments. On the other hand, the readings in some of the downstream sections can be off by as much as 0.1 cm due to the turbulent nature of the water surface.

The calibrated mini-propeller meter is capable of measuring velocities ranging between 4 cm/s (0.4 m/s in prototype scale) and 130 cm/s (13 m/s in prototype scale). In order for the reading to represent the proper velocity magnitude, the propeller needs to be positioned into the direction of flow. The maximum recorded velocity in the model was approximately 50 cm/s (5.0 m/s in prototype scale) occurring at the draft tube outlet. The velocities in some portions of the model were less than 4 cm/s and if a reading was still possible, the velocity was calculated by extrapolating the calibrated frequency curve for

the meter to as low as 3.4 cm/s. Velocities less than this are recorded as zero. The error induced by this procedure is relatively small in terms of the velocity magnitude. The accuracy decreases further by the fact that, in many parts of the model, the flows being measured are turbulent. This means that the direction of flow is constantly changing, thereby causing fluctuations in the velocity readings. To compensate, the velocities are time averaged. Even then, however, some turbulent zones cause significant fluctuations. The accuracy of the mini-propeller is ±0.3 cm/s (±0.03 m/s prototype) under steady flow conditions, but can be as poor as ±15 cm/s (±1.5 m/s prototype) under very turbulent conditions. The latter scenario occurs only in the three-dimensional flow zone downstream of the powerhouse draft tube exits.

The other dimension recorded for qualitative analysis, along with the velocity magnitude, is the velocity direction. The direction of flow is measured using a submerged thread and a protractor mounted to the velocity gauge. The accuracy of these readings are, at best, ±2 degrees but can be out by as much as ±15 degrees due to the wide fluctuations. The directional component of the velocity data serves mainly to provide a qualitative representation of the flow patterns in the numerical model.

Maintaining steady and consistent boundary conditions while operating the model is not straight forward. The flow into the model can be held to within ±5 m^3/s in prototype scale, provided that minor adjustments are made throughout the testing process. The flow through the powerhouse, on the other hand, is extremely sensitive to the degree of opening controlled by the plates and screens. In other words, very minor changes in the openings could result in a very different headloss across the powerhouse. Any sediment

or fine materials in the water could easily get lodged in the screen mesh thereby closing off some of the opening. Over time, slight adjustments would need to be made to maintain a constant forebay. Another factor that influenced the water levels, especially in the fore-bay, is the degree of model saturation. After filling the model with water, it is observed that during the early tests for a particular day, the water levels stay well below the desired forebay elevation for a constant flow and fixed powerhouse opening. After several hours, the water levels gradually rise and even surpass the desired level. This problem might be avoided by keeping the model filled at all times. Unfortunately, the model is not totally water tight and after a day or two, empties completely. These fluctuations in the water level affect mainly the forebay, due to the nature of the boundary conditions. The actual boundary conditions for all the upstream tests show some variability, as is shown by the range of upstream water level boundary conditions in Table 5.3, therefore making it difficult to compare the effects of various channel designs on the hydrodynamics of the system. The results are still useful in calibrating and verifying the numerical model, which can then be used to recreate these scenarios under consistent boundary conditions.

Boundary Condition	Discharge (m^3/s)	Forebay Water Surface Elevation (m)	Tailwater Elevation (m)
(1)	1100	257.4 ± 0.5	245.5 ± 0.2
(2)	867	254.2 ± 0.1	244.5 ± 0.1

Table 5.1 *Boundary conditions for model tests*

Design Alternatives	Design Designation	Model Variables				Level of Detail [2]		Boundary Conditions	
		Bottom Width (m) [1]	Invert Elevation (m)	Overburden Removal	Tailrace Expansion	Number of Velocity Data	Number of Head Data	Flow (m^3/s)	Downstream Head (m) [3]
Downstream Overburden Removal	DOB	-	-	Original	3:1	74	-	1100	245.5
	DOB1	-	-	1/3	"	15	8	"	245.67
	DOB2	-	-	2/3	"	24	8	"	245.67
Downstream Cofferdam Removal Scheme (a)	DC1a	121 (113)	244	2/3	3:1	-	10	1100	245.52
	DC2a	112.5 (113)	242	"	"	-	10	"	245.58
	DC3a	105.5 (113)	240	"	"	72	10	"	245.6
	"	"	"	"	"	68	10	867	244.67
Downstream Cofferdam Removal Scheme (b)	DC1b	139.1 (131)	244	2/3	3:1	-	9	1100	245.58
	DC2b	131 (131)	242	"	"	73	10	"	245.6
	DC3b	123.5 (131)	240	"	"	-	10	"	245.67
Tailrace Expansion	TR3:1	105.5 (113)	240	2/3	3:1	(DC3a)	10	1100	245.62
	TR0	105.5 (113)	"	"	0	7	10	"	245.62

Table 5.2 *Summary of the Downstream Test Scenarios*

(1) The first value is the actual bottom width while the bracketed value represents the average bottom width for a removal scheme.

(2) The level of refers to the number of comparable data points on both the physical and numerical models. The tests consisting of large data sets are used for calibration and verification of the numerical model, whereas the smaller data sets are used for supplementary verification.

(3) The downstream head is the water surface elevation measured near the downstream end of the model at coordinates (386, -355.2) and is used as the boundary head for the downstream numerical model.

Design Alternatives	Design Designation	Model Variables			Level of Detail		Boundary Conditions	
		Bottom Width (m) (1)	Invert Elevation (m)	Approach Contraction	Number of Velocity data	Number of Head data	Flow (m^3/s)	Upstream Head (m) (2)
No Cofferdam	UOB	-	-	1.5:1	25	8	1100	257.92
Cofferdam Removal Scheme (a)	UC2a	70	242.8	0	9	11	1100	257.61
	UC3a	80	245.4	"	11	11	"	257.75
Cofferdam Removal Scheme (b)	UC1b	50	240	0	30	11	1100	257.56
	UC2b	60	242.8	"	9	11	"	257.56
	UC3b	70	245.4	"	11	11	"	257.52
Cofferdam Removal Scheme (c)	UC1c	40	240	0	11	11	1100	257.26
	UC2c(i)	50	242.8	"	30	11	"	257.97
	UC2c(ii)	"	"	"	9	11	"	257.56
	UC3c	60	245.4	"	30	11	"	257.45
	"	"	245.4	"	26	11	867	254.02

Table 5.3 Summary of the Upstream Test Scenarios

(1) Removal scheme (a) represents the widest excavation alternative, scheme (b) represents the middle of the alternatives, and scheme (c) represents the narrowest of the alternatives.

(2) The upstream head is the water surface elevation measured near the upstream edge of the model at node (41, 100) and is taken as the input boundary head for the upstream numerical model.

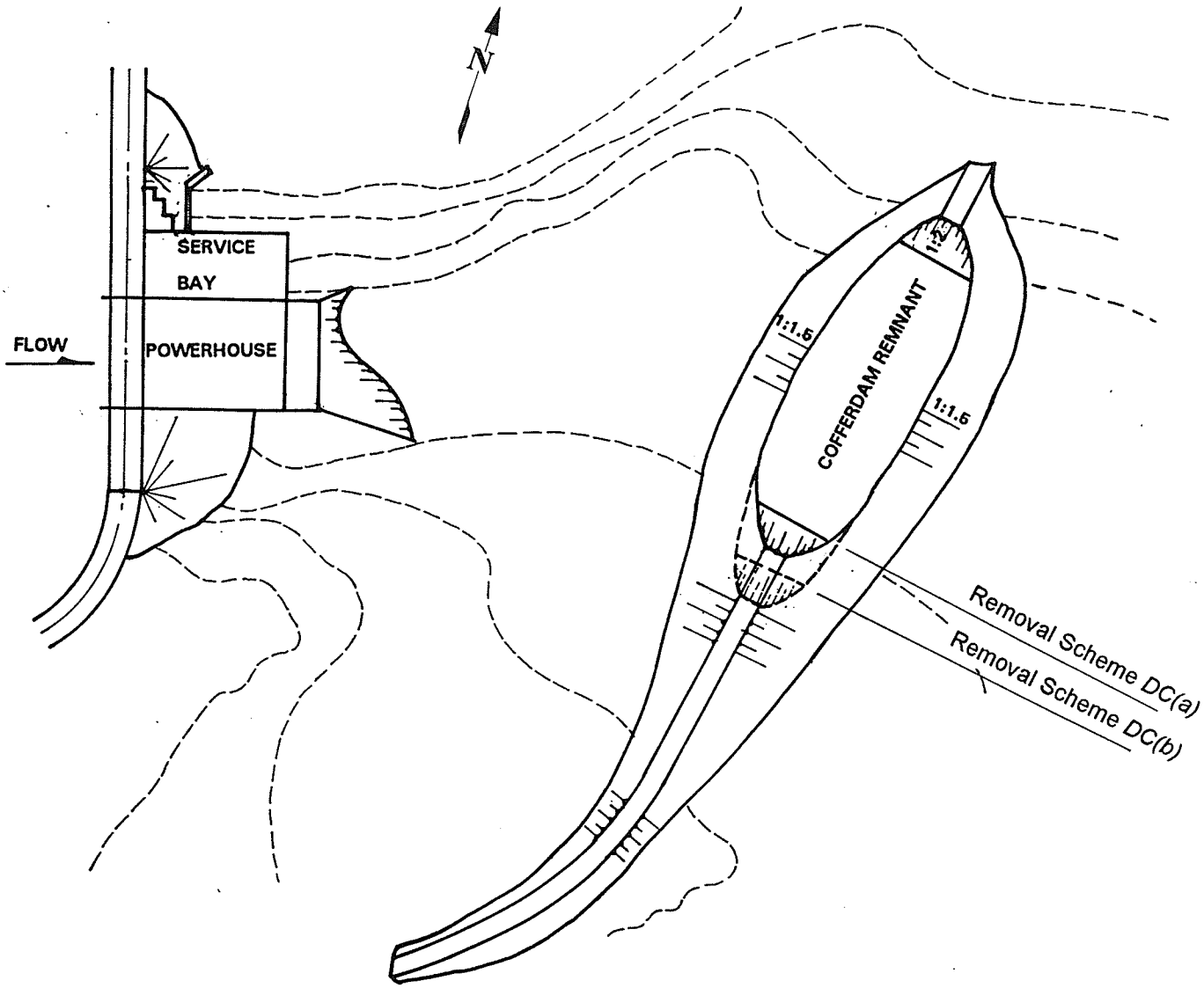

Figure 5.1 Removal Schemes for the Downstream Cofferdam

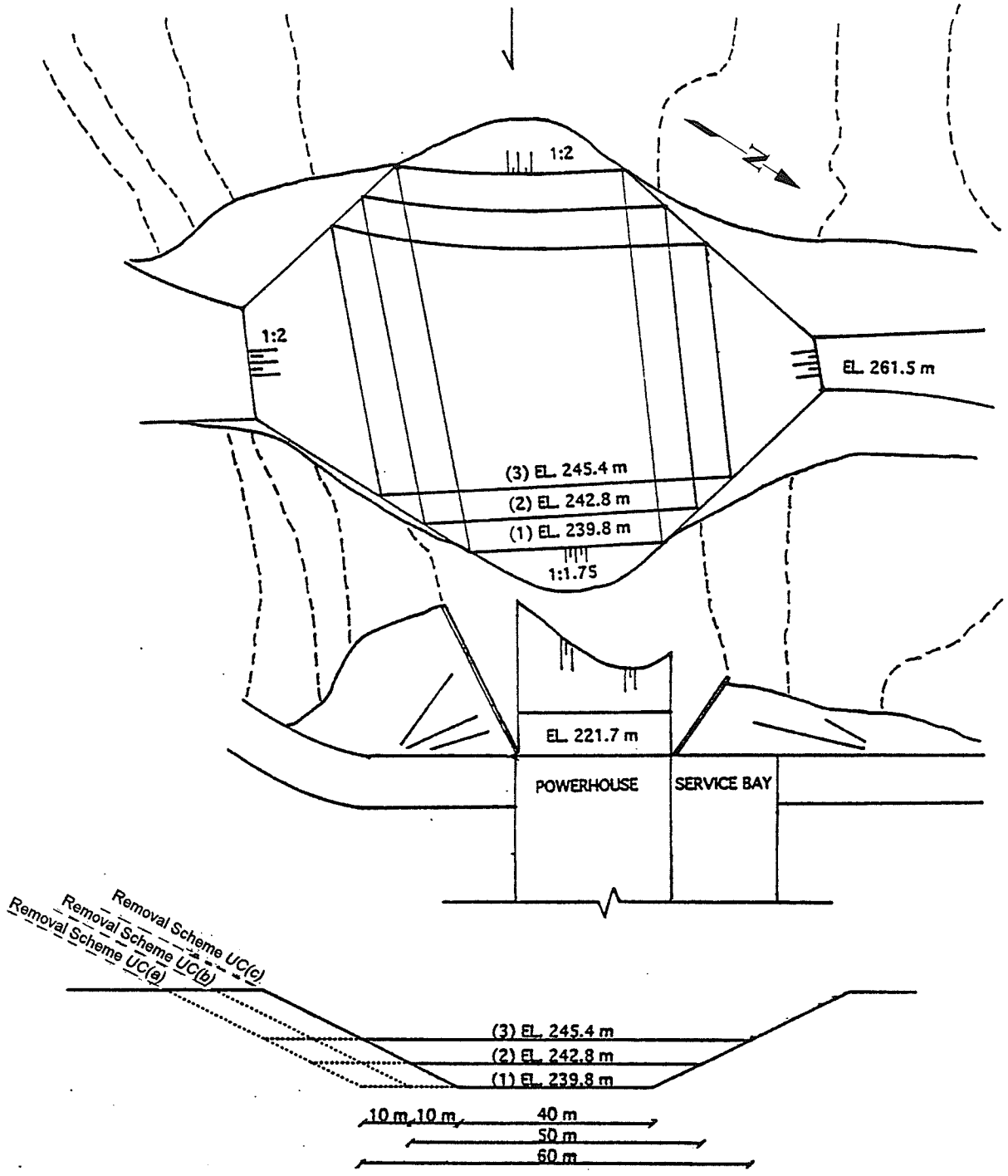

Figure 5.2 Removal Schemes for the Upstream Cofferdam

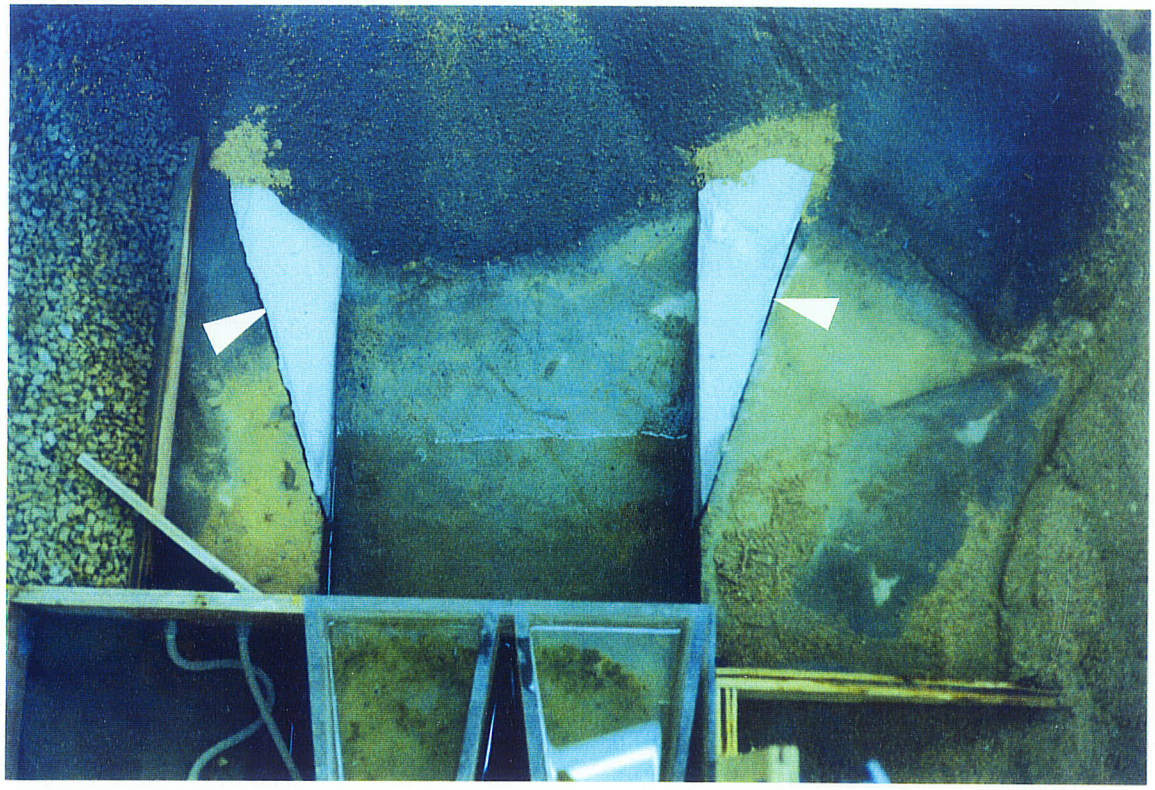

Figure 5.3 *Downstream expansion alternatives using concrete modules; no-contraction with blocks in place, 3:1 expansion with blocks removed.*

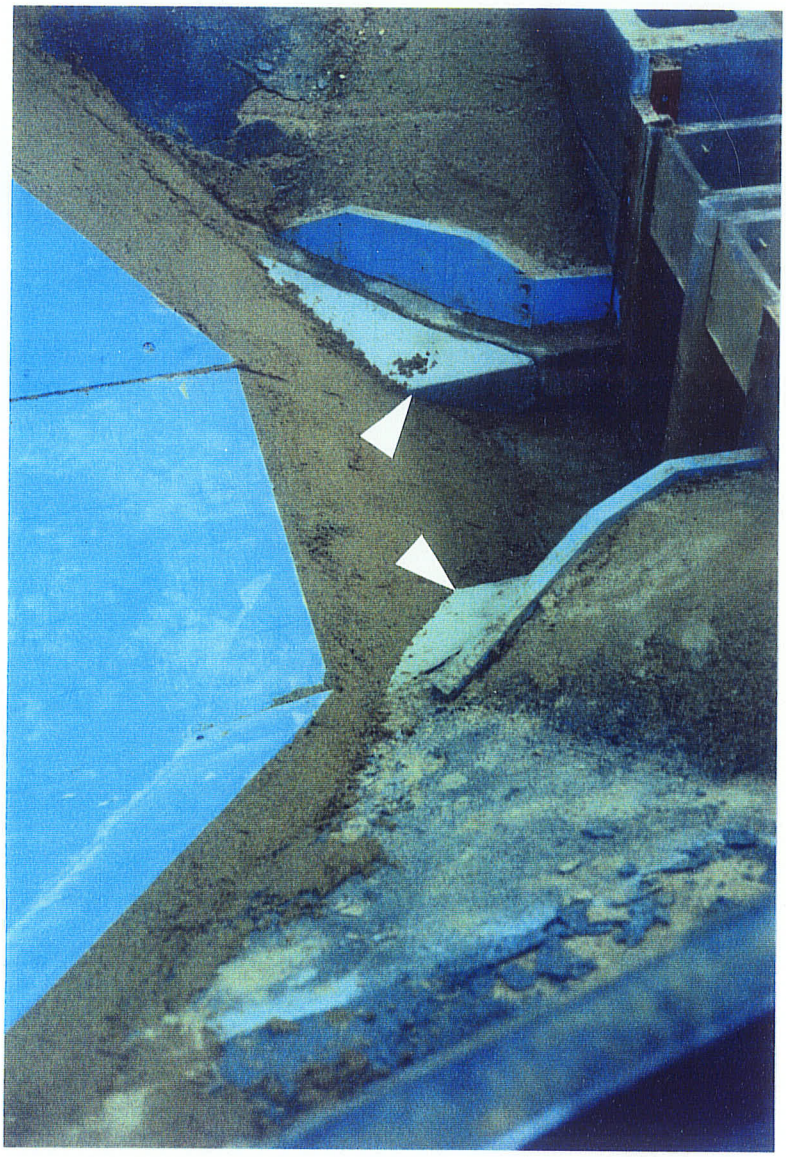

Figure 5.4 *Upstream cofferdam in close proximity to powerhouse thereby obstructing the intent of the 1.5:1 contraction at the intake; default is the no-contraction scenario shown.*

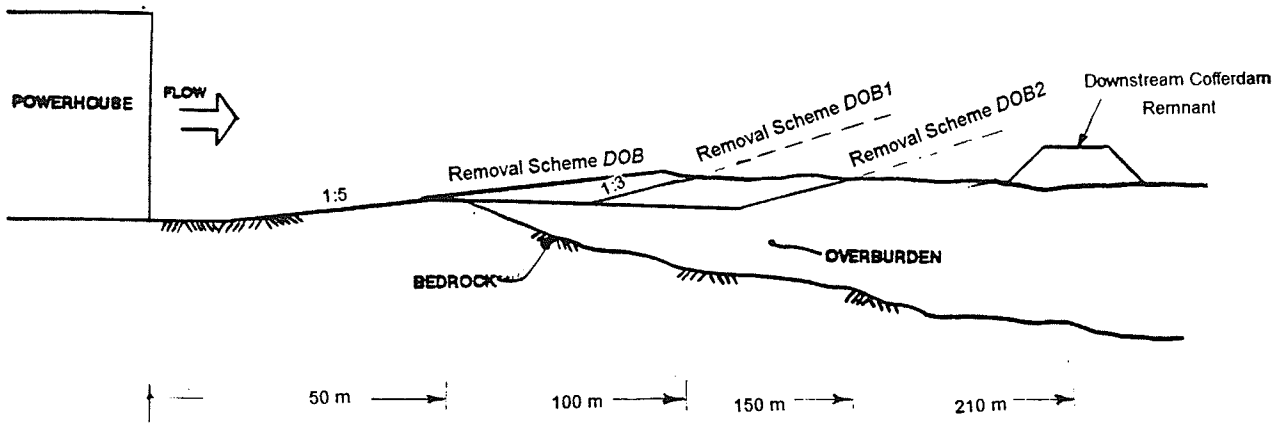

Figure 5.5 Tailrace Channel Overburden Removal Alternatives

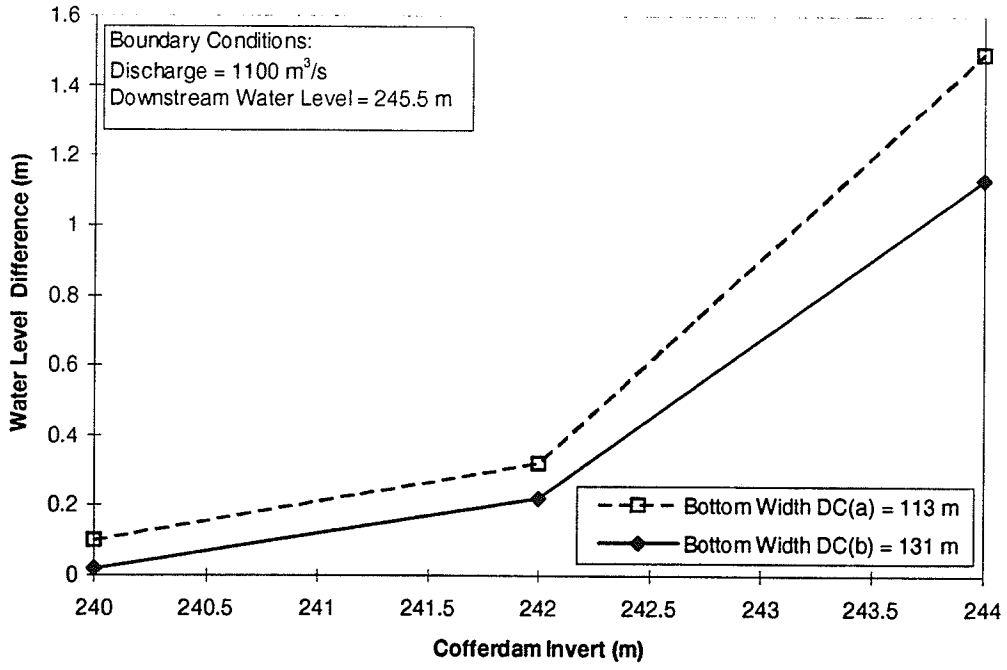

Figure 5.6 Water Level Difference Across the Downstream Cofferdam

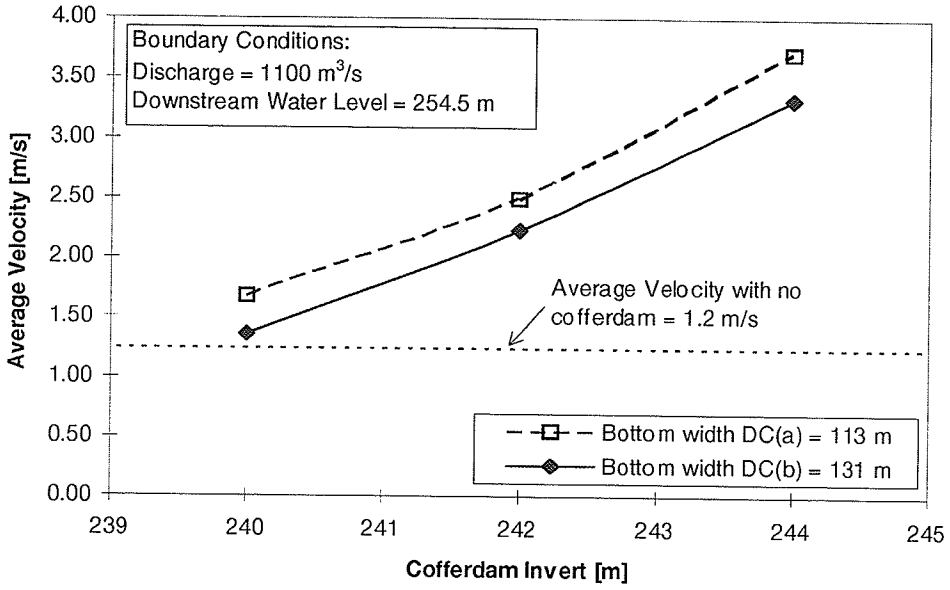

Figure 5.7 Average velocity through the downstream cofferdam

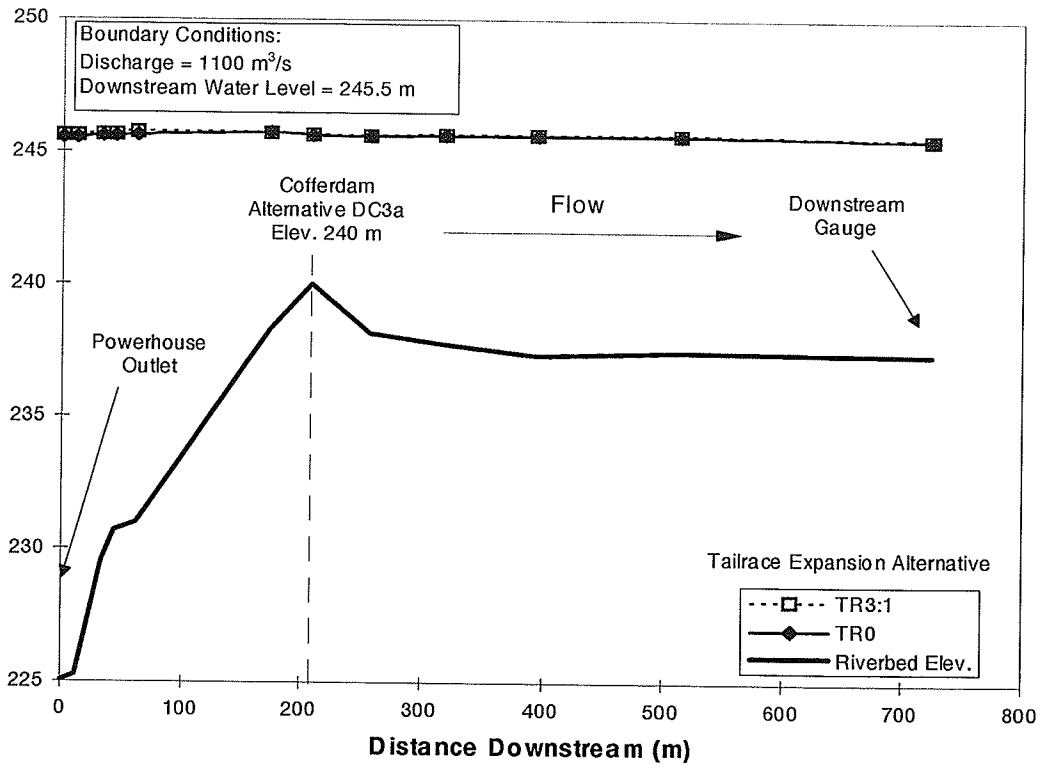

Figure 5.8 Water surface elevation profile for two tailrace expansion design alternatives

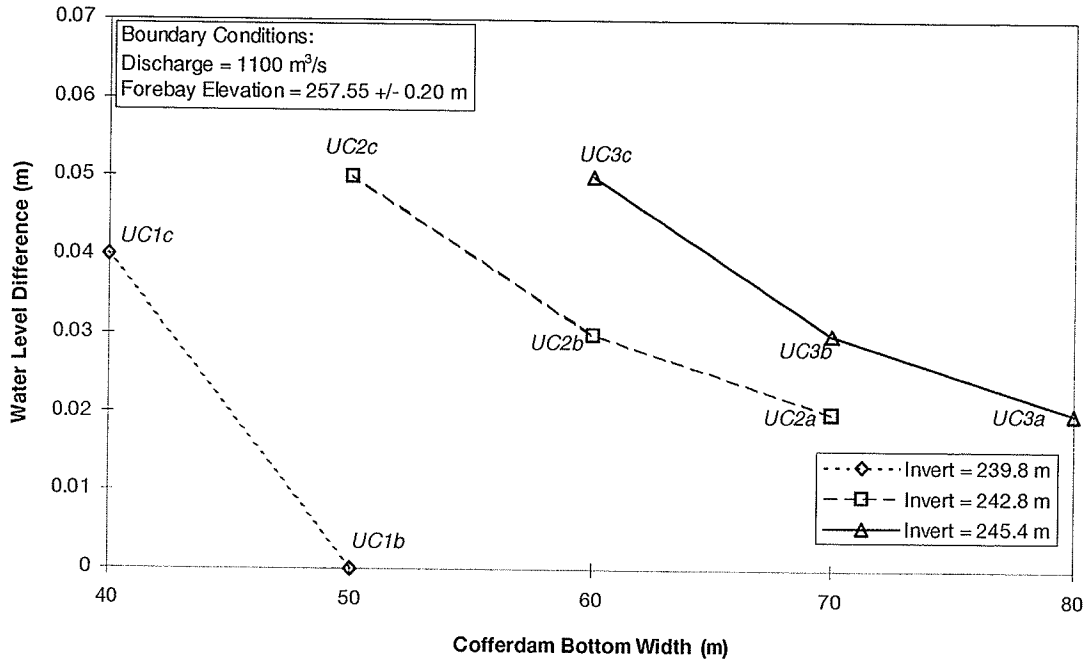

Figure 5.9 *Water level difference across the upstream cofferdam*

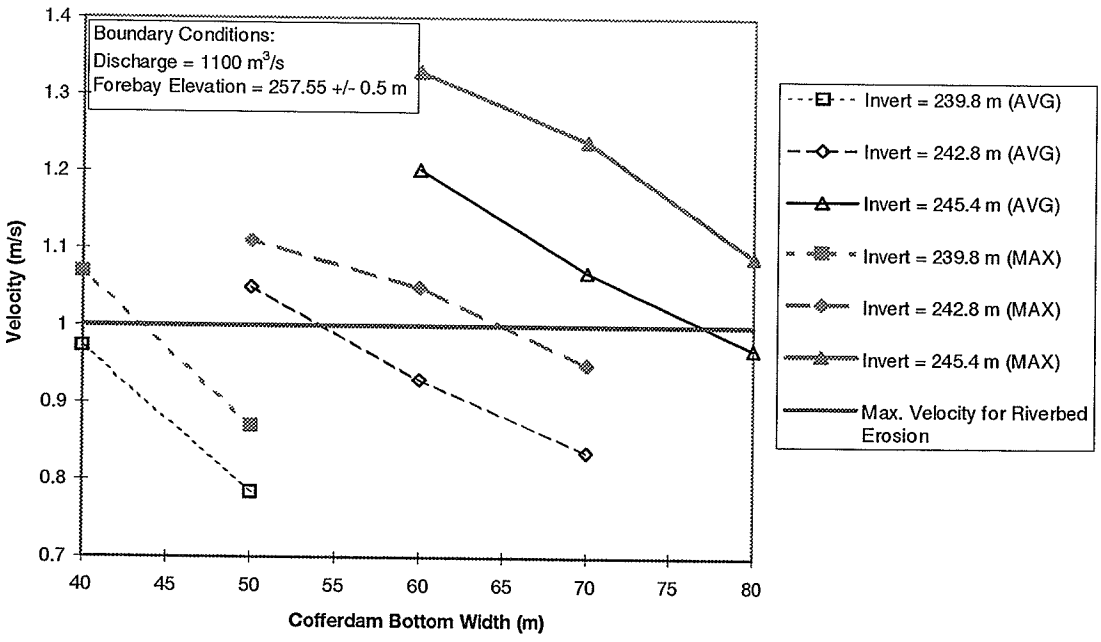

Figure 5.10 *Maximum and approximate mean depth-averaged velocities through the upstream cofferdam*

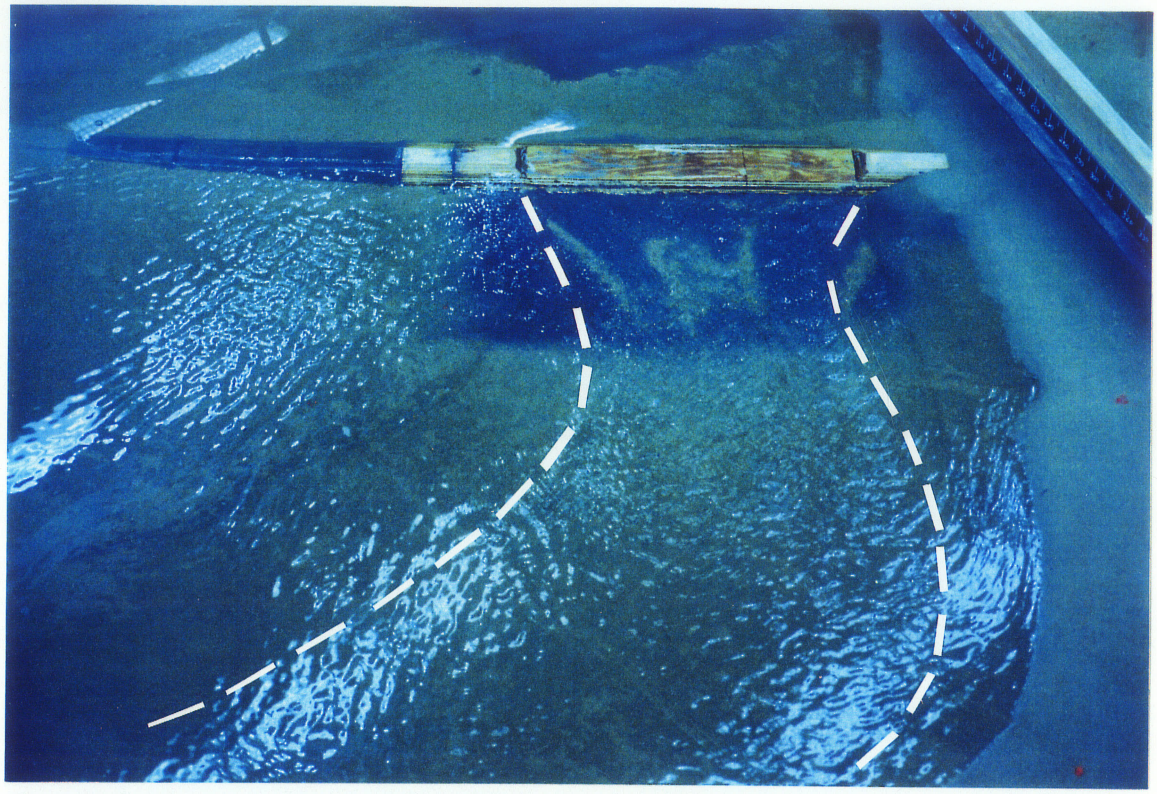

Figure 5.11 *Flow across the narrower cofferdam Removal Scheme DC(a) forces the main flow to travel wider to the outside (to the right) of the river bend.*

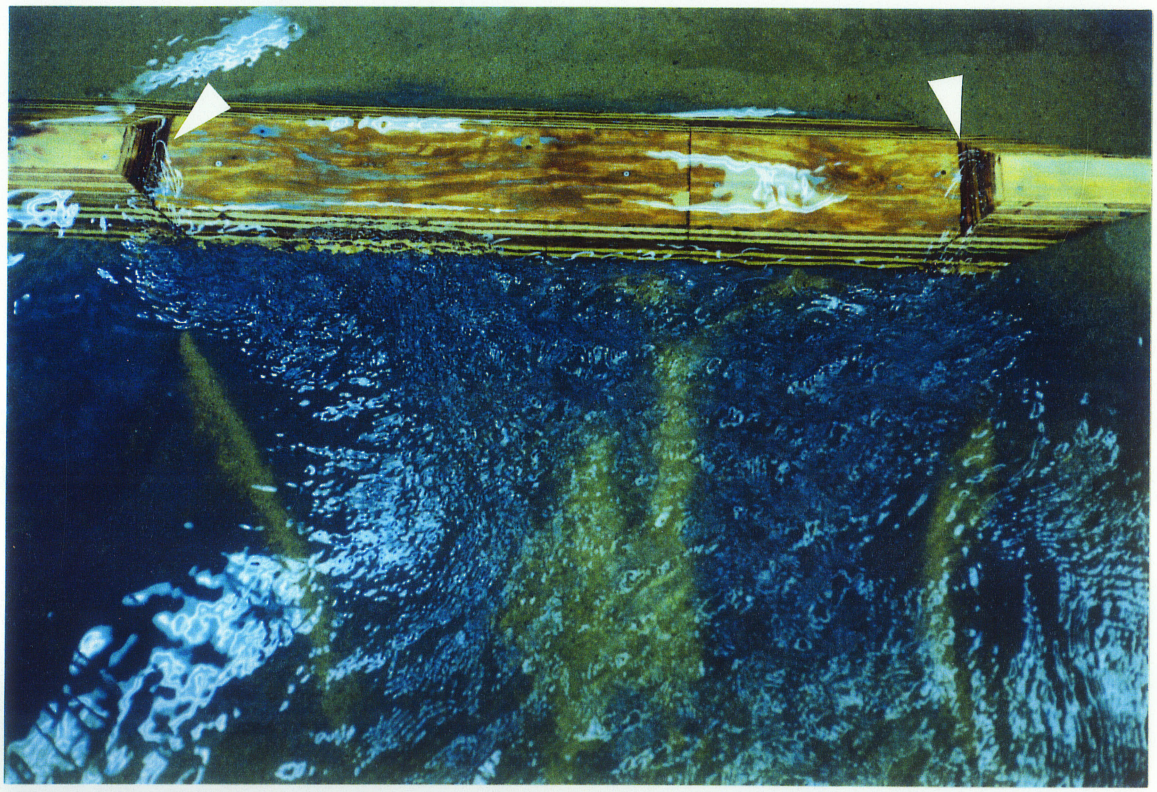

Figure 5.12 *Turbulence downstream of cofferdam Removal Scheme DC(a), with an invert 244 m, and flow separation occurring at the upstream corners of the cofferdam remnant.*

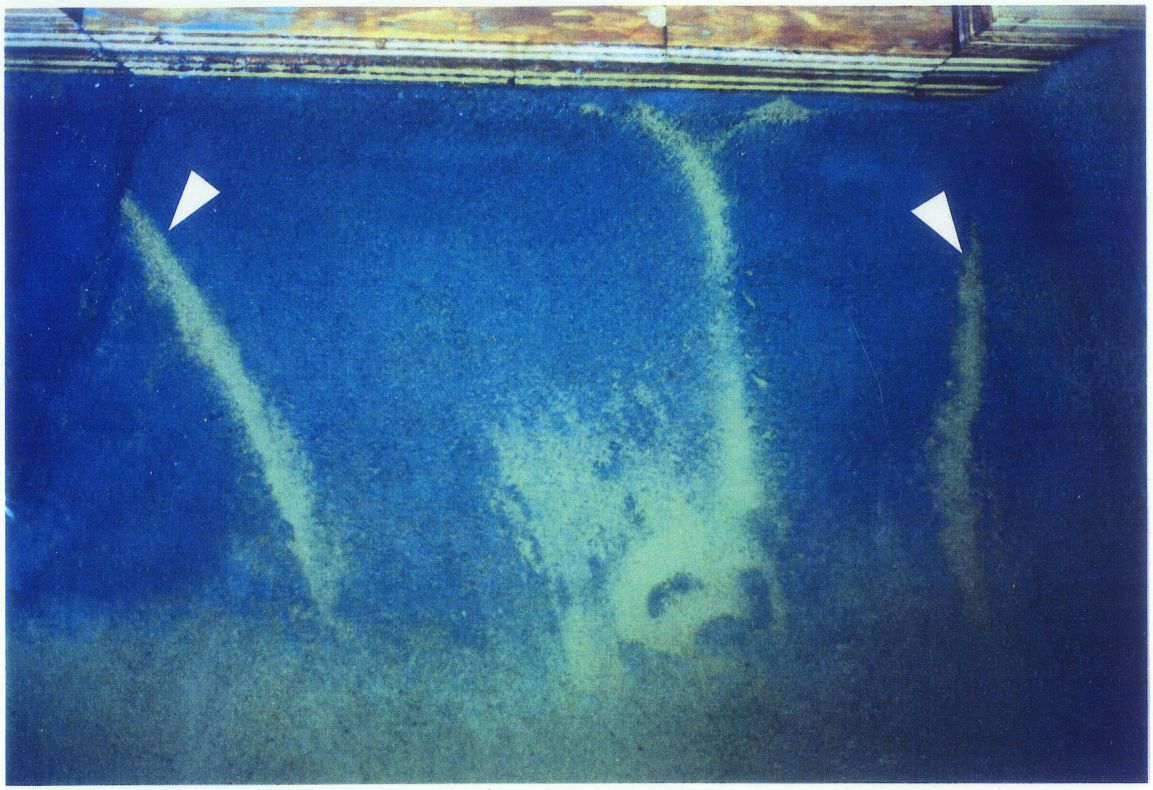

Figure 5.13 *Sand deposits give indication of direction of flow at the downstream side of the downstream cofferdam Removal Scheme DCa.*

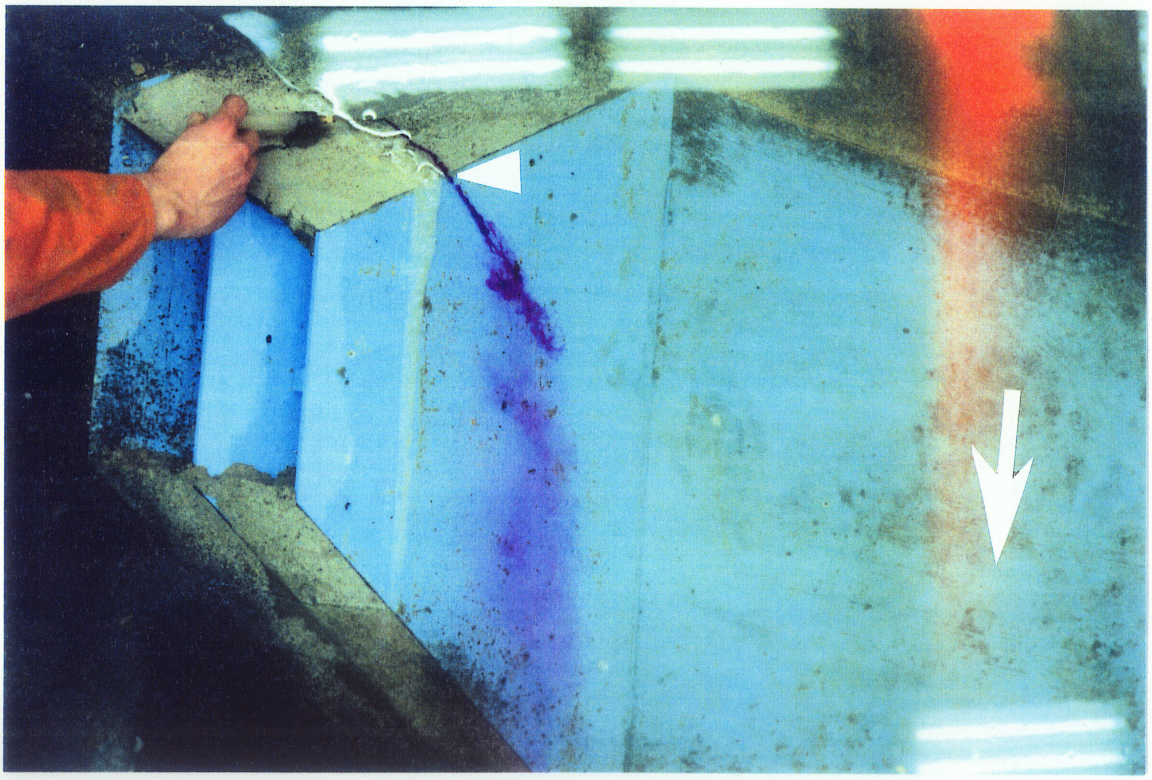

Figure 5.14 *Separation of flow at the upstream edge of the cofferdam Removal Scheme UC3c seen by using tracer dye.*

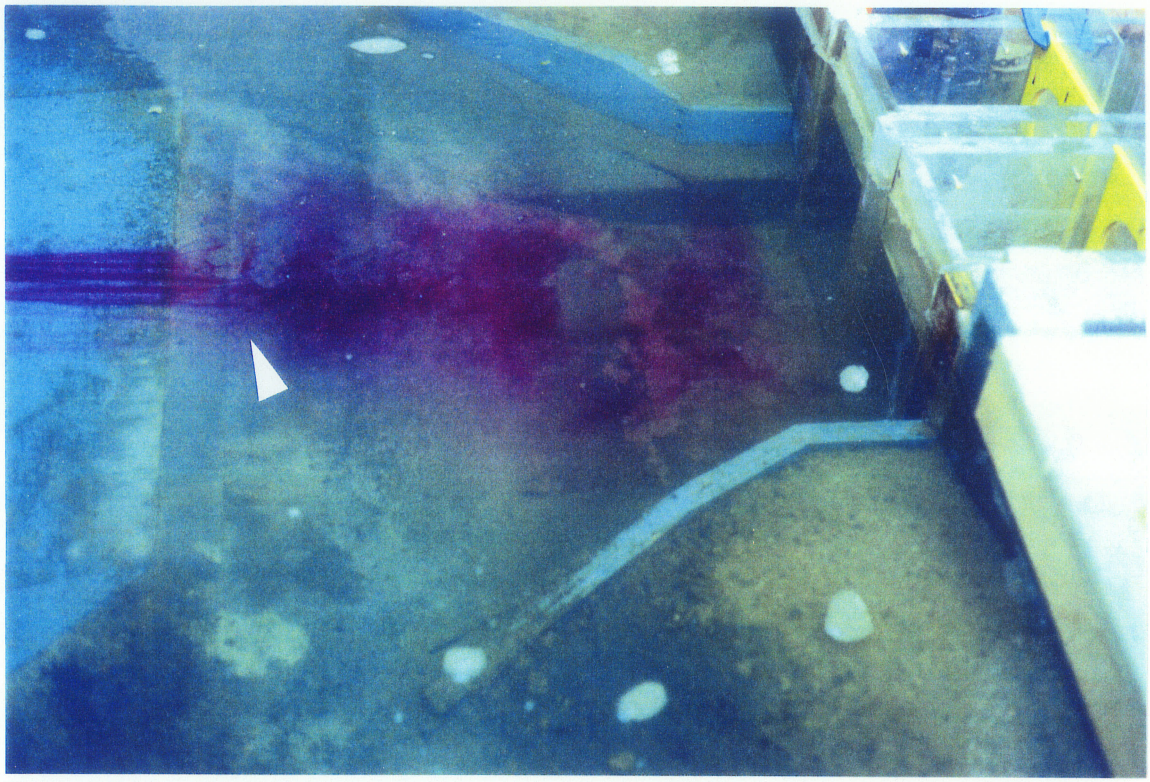

Figure 5.15 *Vertical flow separation at the downstream invert edge of the upstream cofferdam Removal Scheme UC3c.*

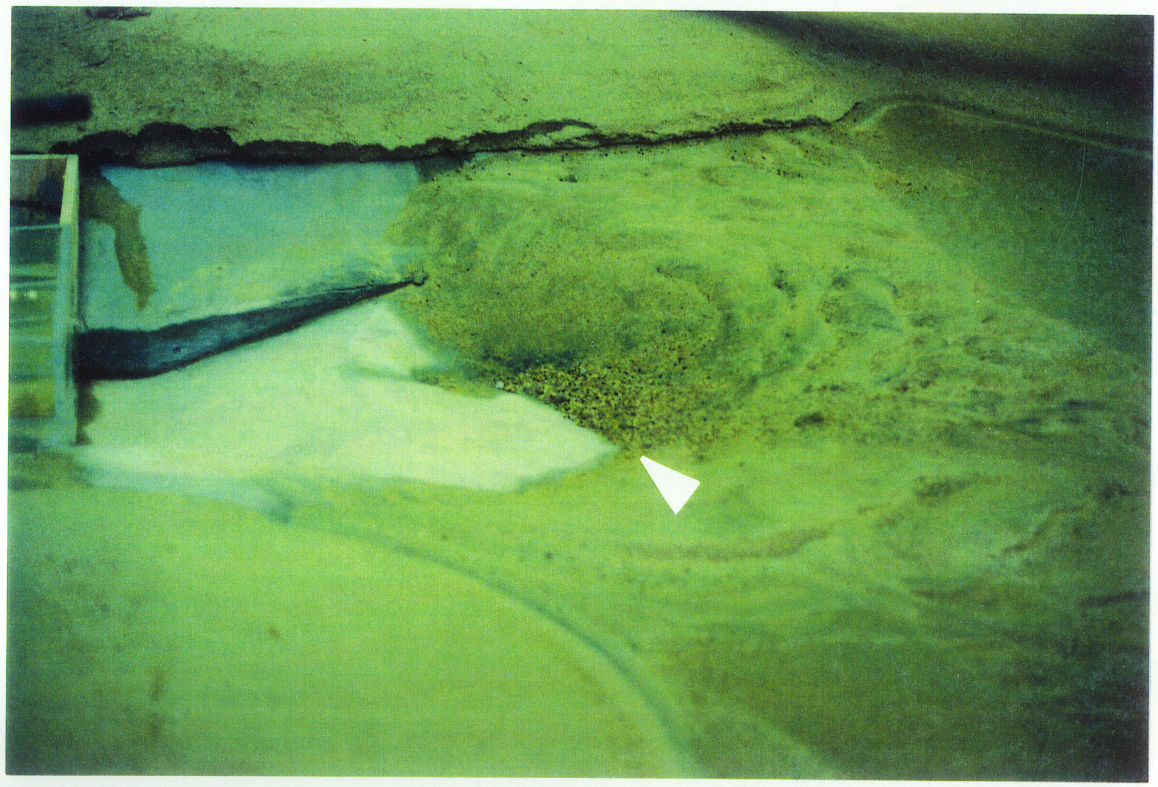

Figure 5.16 *Erosion of original overburden downstream of the powerhouse: the initial slope was an extrapolation of the 1:5 bedrock slope.*

Figure 5.17 *Erosion of the overburden downstream of the powerhouse.*

Figure 5.18 *Retaining wall and riprap (less than 1 m diameter, prototype scale) to mitigate erosion in the tailrace.*

Figure 5.19 *Erosion of the downstream overburden, even with riprap in place.*

Figure 5.20 *Looking downstream from the powerhouse at the overburden Removal Scheme DOB1 where the overburden is removed to one-third the distance to the powerhouse to an invert of 231 m (no riprap).*

Figure 5.21 *Erosion of the overburden Removal Scheme DOB1.*

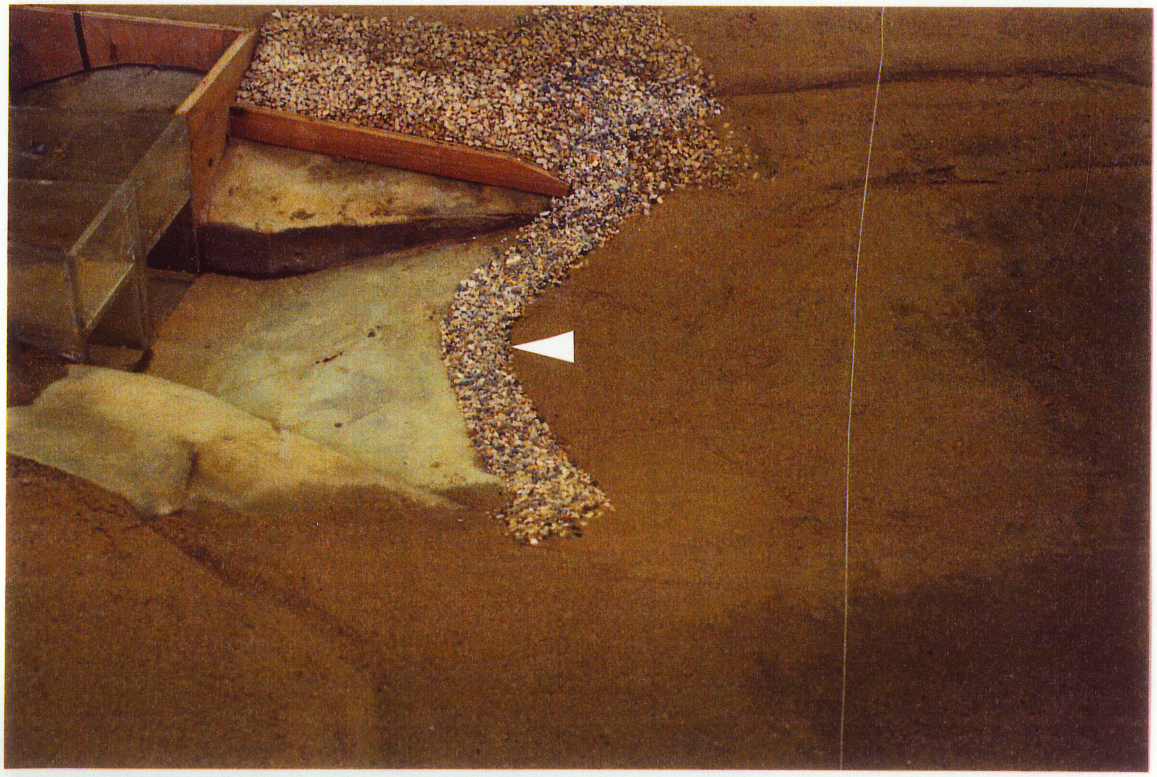

Figure 5.22 *Riprap added to the overburden Removal Scheme DOB1.*

Figure 5.23 *Erosion of the overburden Removal Scheme DOB1, in spite of the riprap.*

Figure 5.24 *Overburden Removal Scheme DOB2 where the overburden is removed to two-thirds the distance to the downstream cofferdam to an invert of 231 m, with riprap at the leading edge.*

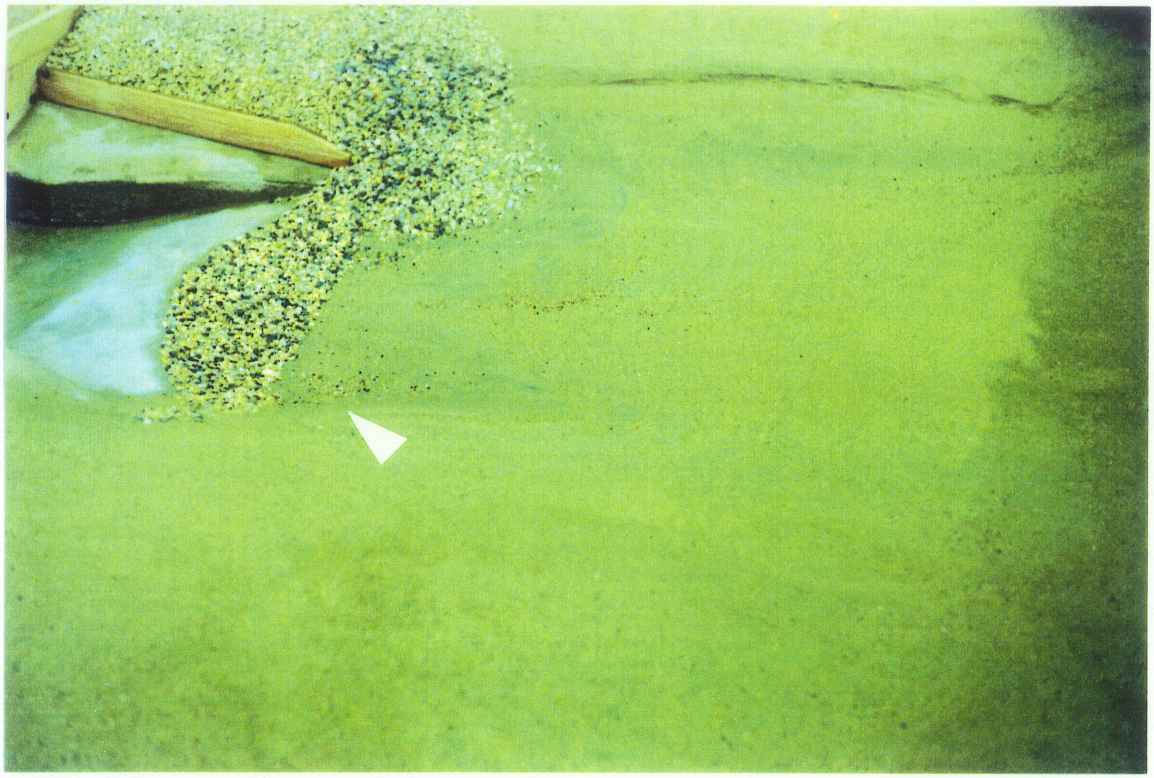

Figure 5.25 *Erosion of the overburden Removal Scheme DOB2, with riprap, is less than for the overburden Removal Scheme DOB1.*

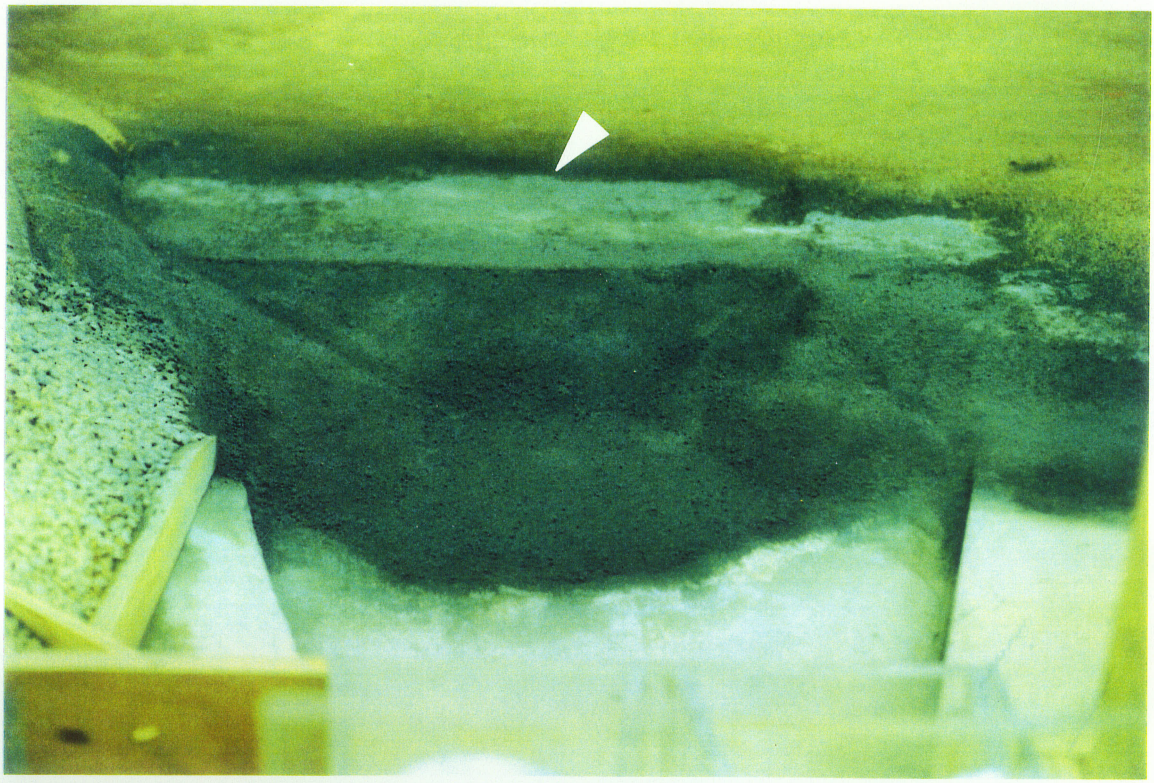

Figure 5.26 *Cement dusting created a semi-fixed bed model for consistent testing conditions.*

6. CALIBRATION AND VERIFICATION OF THE NUMERICAL MODEL

The basic requirement for any numerical model is that it should reproduce correctly the behavior of the situation being modelled and that it should do so without violating any biological, chemical, or physical principles of the system being modelled. Essentially, the model must be consistent with reality. Calibration is the process of estimating appropriate model coefficients and other inputs, so that the model can be used to accurately simulate the prototype or field response. The success of the solution to a numerical model depends on the appropriate choice of model coefficients and the correct application of the equations representing the system. A calibrated model is verified when it is able to simulate a field response for different sets of boundary conditions or system input conditions. The verified model can then be used to predict the field response for a variety of potential scenarios of system input conditions.

The numerical model calibration and verification for the proposed Notigi Generating Station is divided into two separate sets of conditions, one representing the tailrace channel downstream of the powerhouse, and the second representing the approach channel upstream of the powerhouse.

6.1 Basic Concepts for Calibration

6.1.1 Parameters

The parameters of a model are those coefficients or rates used in expressions that relate model inputs and boundary conditions to the predicted field response. Often, exact

values are not available for such coefficients. Model calibration involves estimating these parameters so that the model accurately simulates the field situation. In defining a hydrodynamic model, *FastTABS* requires a set of system parameters, also referred to as material properties by the *FastTABS* User's Manual (BOSS Corporation, 1993), to be assigned. These are: 1) the turbulent exchange coefficient, ε_{ij}; and 2) the Manning's n value. The definitions and applications of these parameters have been provided in Chapter 3.

6.1.2 System and Model Design Options

The configuration of either the approach or tailrace channel is alterable with respect to several aspects. For the cases investigated, the system design options includes allowing for: 1) various cofferdam excavation alternatives; 2) various overburden removal alternatives in the tailrace; and 3) various degrees of expansion in the tailrace and of contraction in the approach channels. These design alternatives have been described in detail in Chapter 5.

While incorporating the design alternatives into the numerical model it is important to adhere to the fundamental mesh design principles discussed in Chapter 3. The impact that changes in mesh density and element configuration may have on the solution requires that, for consistency, the mesh incorporate all the possible design alternatives into one mesh. This means that the number of nodes and elements in all the cases would remain essentially the same. The longitudinal and lateral position of all of the nodes would remain constant and only the vertical reference would vary for certain nodes in the mesh to represent changes in the design. This also allows consistent reference to specific nodes corresponding to measurements taken in the physical model.

6.1.3 Boundary Conditions

Besides the model and system design, various boundary conditions can be imposed upon the models as well. In some applications where no boundary conditions from field data are available, it would be important to ensure that the boundary conditions assigned to the numerical model are well-posed. For a typical riverine system, this means specifying a downstream water surface elevation and an upstream discharge. In this project, the flow and water surface elevation conditions assigned to each case throughout the calibration and verification process correspond to the field conditions measured in the physical model. The boundary conditions used in all the tests have been described in Chapter 5.

6.1.4 Numerical Model Output

The numerical model is used to compute water surface elevations and flow velocities at nodal points in a finite-element mesh representing a body of water. This information is compared with the field data collected from the physical model to calibrate and verify the numerical model. The data produced by the numerical model at each node include: 1) velocity magnitude; 2) velocity in the x-direction; 3) velocity in the y-direction; 4) water surface elevation; 5) flow; and 6) depth of the water. This information can also be used to generate Froude numbers. The data collected from the physical model include velocity magnitude and direction, and water surface elevation data at various locations throughout the model that coincide with nodal points in the numerical model. The tests having the greatest number of data points are used for calibration purposes. The velocity data are collected at various locations throughout the entire model, as described in Chapter 4, whereas water surface elevations are only taken along the center line of the main

channel. The large number and range in values of velocity measurements suggests that the model should be calibrated with the velocity data. The water surface elevation data are then used for additional validation of the numerical model. Although the direction of the velocity was measured in the physical model, the accuracy of this information is believed to be poor. For simplification of the calibration process, the velocity magnitudes are selected as the basis for calibration while the directional component is evaluated on a qualitative basis.

6.1.5 Criteria for Calibration and Verification of the Numerical Model

There are many possible ways to measure the numerical model performance. The choices also depend on the data being used. In this work, the measure of performance for calibrations based on the velocity data is the result of linear regression analysis, using the method of least squares, for plots of velocity magnitudes generated by the numerical model (N) against corresponding values measured in the physical model (P). Figure 6.1 shows a sample comparison of velocity magnitudes between the physical and numerical models, as well as the regression and the desired perfect fit lines through the data. The criteria used in the calibration process are: 1) the coefficient of determination, r^2; 2) the intercept of the regression line, b_0; and 3) the slope of the regression line, b_1, for the linear relationship between N and P. The coefficient r^2 provides a measure of the strength of linear association between P and N. A direct computational formula for r^2 is:

$$r^2 = \frac{\left[\sum\left(P_i - \overline{P}\right)\left(N_i - \overline{N}\right)\right]^2}{\sum\left(P_i - \overline{P}\right)^2 \sum\left(N_i - \overline{N}\right)^2} \qquad [6.1]$$

where P_i = the physical model velocity measurements,
N_i = the numerical model velocity estimates,
$\overline{P}$ = the average physical model velocity measurements,
$\overline{N}$ = the average numerical model velocity estimates, and
i = the number of observations.

The limiting values for r^2 are as follows:

1) If all the numerical data fall on the fitted regression line, then $r^2 = 1$; and
2) If the data points are so scattered that the slope of the fitted regression line is $b_1 = 0$, then there is no linear relationship between P and N, and $r^2 = 0$.

The slope term, b_1, indicates the change in the mean of the probability distribution of N per unit increase in P. The intercept, b_0, gives the mean probability distribution of N at $P = 0$. The objective in the calibration of the numerical model is to strive for the best possible agreement to the physical data. A perfect agreement between the physical and numerical models would result in regression statistics of $r^2 = 1$, $b_0 = 0$, and $b_1 = 1$, indicated in Figure 6.1 by the dotted line labeled *perfect fit*.

Other criteria were investigated as to their usefulness in the calibration of the velocity data. These included standard error of the N estimate, standard error of the intercept and slope, the t-statistic for the intercept and slope, and the t-test for the mean difference. It was decided that none of these criteria could provide any extra information that would be beneficial in the calibration process.

The water surface elevation data are compared by evaluating the differences (or error) between the physical and numerical models. This approach is used because the water level values do not change very much. One statistical comparison is given by the relative error for water surface elevation data. Unfortunately, the calculated errors tend to be extremely small in comparison with the large values of water surface elevation, and therefore relative

error may be misleading. Another measure of the error is the root mean squared error. It is simply an estimator for the standard deviation. The root mean squared error is statistically well-behaved and provides a direct measure of model error. Equation 6.2 shows the definition of the root mean squared error, *rmse*.

$$rmse = \sqrt{\frac{\sum (P_i' - N_i')^2}{m}} \qquad [6.2]$$

where P_i' = the physical model water level measurements,
N_i' = the numerical model water surface estimate, and
m = the number of data points.

This criterion is used to provide additional verification of the numerical model rather than as another parameter for calibration.

6.2 Model Calibration

6.2.1 Introduction

The purpose of model calibration is to produce a model that can accurately and reasonably reproduce certain behaviors occurring in the prototype. The process of calibration is defined by Thomann and Mueller (1987) as:

> The first stage testing or tuning of a model to a set of field data, preferably a set of field data not used in the original model construction; such tuning to include a consistent and rational set of theoretically defensible parameters and inputs.

The calibration process in this study can be broken down into a series of steps. Figure 6.2 shows the principal steps used to calibrate the model for a single scenario. The first step involves selecting the appropriate design and boundary conditions, those being the same as

for the physical system being modelled. The mesh in the numerical model should represent the geometric layout of the physical model converted to prototype scale. When the appropriate choices for the model reach, excavation alternatives, and flow conditions have been determined, the values for the parameters of Manning's n and ε_{ij} are set. The Manning's n is initially held constant while ε_{ij} is varied. If a high enough ε_{ij} has not been initially set, determining a starting value for ε_{ij} may then involve several trial runs, each time increasing ε_{ij} until the model converges to a solution.

The model is executed by using *RMA-2*, the actual finite-element program within *FastTABS* for solving the hydrodynamic problem. Using the depth-averaged flow equations, the program proceeds to calculate the velocity and the water surface elevation at every single node in the mesh. Several iterations are usually required to comply with conservation of mass and momentum. When the maximum change in water surface elevation, from one iteration to the next, is less than the convergence limit, the model is considered to have converged to a solution for the given set of parameters. Having produced a solution of velocity and water surface elevation data at every node in the mesh, the values measured in the physical model are compared and the regression statistics for velocity magnitude comparisons are evaluated.

The calibration process continues by executing the model again for a lower value of the ε_{ij} coefficient. The procedure is simplified in *FastTABS* by using the technique described in Chapter 3 as spinning up the model. This technique involves gradually reducing the ε_{ij} coefficient using a series of revisions. The ε_{ij} coefficient should only be lowered as

long as a stable solution is achieved. There comes a point where oscillation or instability begins to take place and further reduction will cause the model to diverge. For each ε_{ij}, the converged solution set is used to evaluate the regression statistics of the coefficient of determination, r^2, slope, b_1, and intercept, b_0.

The actual value for Manning's n is not known and therefore a reasonable range of values needs to be tested. The entire process, executing the model with revisions and evaluating the regression criteria, is repeated for other values of Manning's n. The values of Manning's n evaluated include 0.025, 0.030, 0.035, and 0.040.

The final step in the calibration process is to identify the values of ε_{ij} and Manning's n which yield the best regression criteria. The objectives, as previously stated, are to have r^2 and b_1 approaching 1.0, and to have b_0 be as near to 0.0 as possible. In some cases, these objectives oppose one another and examination of the trade-offs among them is necessary. For each Manning's n, a 'best' ε_{ij} is chosen. From this set of solutions, the parameter values associated with the highest quality of criteria can be considered as the calibrated settings for that particular case.

6.2.2 Calibration Example for a Downstream Case

An understanding of the calibration process may be obtained by following an example. The process is illustrated for one downstream design alternative and boundary condition, but a similar procedure has been applied to every other scenario that is calibrated. Summaries of all the downstream and the upstream model calibration and verification processes are included in Appendix E and Appendix F, respectively.

The scenario used in this example is the scenario with the downstream cofferdam Removal Scheme *DC3a* under full flow conditions. The design and boundary conditions for this case are summarized as follows:

1) Cofferdam excavation invert = 240 m, and bottom width within the main channel = 113 m;
2) Overburden in the tailrace removed to 2/3 the distance to the cofferdam to an elevation of approximately 231 m; and
3) FGD = 1100 m^3/s and a downstream water surface elevation of 245.6 m.

Figure 6.3 shows the mesh of the downstream reach with the boundary conditions for the cofferdam Removal Scheme *DC3a*. The next step is to assign values for the parameters. Let Manning's n be set to 0.025 for the first set of computations. An initial value for the ε_{ij} coefficient should be high enough to provide a stable solution. For this scenario, a good starting point is in the range of 1500 N-s/m^2. The ε_{ij} coefficient is then gradually lowered to 650 N-s/m^2, at which point the model becomes unstable, using a revision process while holding Manning's n constant. The model is executed and the regression statistics are determined for each of the solutions. The regression statistics are calculated by regressing the 72 velocity magnitude data collected from the physical model for this case against the corresponding output from the numerical model. This procedure is repeated for n = 0.030 and 0.035. The behavior of each regression statistic is plotted against ε_{ij} for each Manning's n, as shown in Figures 6.4, 6.5 and 6.6. Figure 6.4 shows that as ε_{ij} is lowered, r^2 is reduced. For ε_{ij} less than 1150 N-s/m^2, increasing Manning's n results in a higher value of r^2. On the other hand, lowering ε_{ij} yields an improvement in b_0

and b_1, as shown in Figure 6.5 and Figure 6.6. Increasing Manning's n worsens b_0 and b_1 for ε_{ij} values greater than 700 N-s/m^2.

Finding an acceptable calibrated solution requires an evaluation of the trade-off between the objectives, that is comparing r^2 against b_0 and b_1. Figures 6.7, 6.8, and 6.9 show the trade-off curves of the regression statistics, normalized by the percentage of the statistic's range, for each value of Manning's n. As the normalized value of r^2 is reduced, there comes a point where both b_0 and b_1 reach their best values. A balanced trade-off occurs at the point where the degree of improvement in one criterion (i.e., the magnitude of change in the value of the normalized criterion) equals the degree of degeneration in the other criterion. For n equal to 0.025, the best trade-off, indicated in Figure 6.8, is for the point corresponding to a ε_{ij} value of 800 N-s/m^2. Also, analyses of the trade-offs for Manning's n values of 0.030 and 0.035, shown in Figures 6.8 and 6.9, yield ε_{ij} coefficients of 650 N-s/m^2 and 375 N-s/m^2, respectively. The general tendency appears to be that as Manning's n is increased, the value of the most acceptable ε_{ij} is decreased.

At this stage of the calibration process, the choice of the best values of the parameters has been reduced to the number of Manning's n cases tested, in this case three. Selection of the calibrated parameters is a simple matter of identifying the parameters corresponding to the highest r^2 and b_1, and to the lowest b_0. Table 6.1 shows a summary of the regression statistics associated with the best ε_{ij} for every Manning's n. The best values for r^2, b_0, and b_1 all correspond to the Manning's n of 0.025 and ε_{ij} of 800 N-s/m^2. These values

represent the calibrated parameters for the cofferdam Removal Scheme *DC3a* at a discharge of 1100 m^3/s and a downstream water surface elevation of 245.5 m.

A comparison of how well the velocity data generated by the numerical model agree with the data measured in the physical model is best illustrated by a scatter plot. Figure 6.10 depicts this comparison for velocity magnitudes converted to prototype scale. The velocities range from zero to 2 m/s, in prototype scale. A certain amount of scatter can be expected. Reasons for such deviations are discussed later in this chapter. The numerical velocities are based on the numerical model and the calibrated parameters. For this data set, the regression line represents the best fit through the points. A perfect agreement between the physical and numerical data would be a 45° line (where $r^2 = 1$, $b_0 = 0$, and $b_1 = 1$), as represented by the dashed line.

6.3 Model Verification

6.3.1 Introduction

The common approach to model verification is to apply the calibrated model, including the estimated parameter values, to additional field data, preferably under different boundary conditions, and to examine the validity of the model response. The methodology used to verify the model of the Notigi Generating Station case study is described in this section. For each scenario tested in the physical model having sufficient data, a calibrated numerical model is generated. If the calibrated parameters for all the scenarios are reasonably similar, then the cases are verified against each other using each of the calibrated parameters. The set of results leading to the best overall regression statistics is selected as the final calibrated model used in the final results for all the cases. On the

other hand, scenarios having calibrated parameters that are significantly different, indicate that a model having only one set of calibrated parameters can not adequately simulate all prototype scenarios. This could potentially lead to several models, each calibrated to a different range of design or boundary conditions. Under these circumstances, to make the assumption that a single calibrated model is capable of providing reasonable simulation of prototype hydrodynamics for all types of design alternatives and boundary conditions would not only be an over-simplification, but also inaccurate.

Further verification of the model is employed by comparing the test results from additional data sets. Typically, these include scenarios having smaller data sets not used for calibration purposes (see Tables 5.2 and 5.3). The regression statistics for the velocity magnitude data for smaller data sets will be of lesser merit than the large data sets. For this reason, the verification of the smaller data sets is used as a qualitative indicator of the validity of the model.

The model is also evaluated by how well it replicates some of the other data characteristics. Although the model is calibrated based on velocity magnitudes, it is only viable if there is also reasonable agreement in the velocity direction or flow patterns. This information is evaluated on a qualitative basis, with the objective of attaining reasonable replication of depth-scaled eddies and flow patterns. A more quantitative comparison of velocity direction can be conducted, but in the interest of time, it was felt that, due to the degree of uncertainty in these data, this information would not contribute any significant benefit to this project. The model is also evaluated by how well it simulates the water

surface elevations. Due to the limited quantity and the nature of these data, this information can only offer a supplementary comparison for verification of the numerical model.

Having established the methodology for model verification, the following two sections elucidate and summarize the verification process for the downstream and upstream models.

6.3.2 Verification Summary for the Downstream Model

Verification for the downstream reach of the Notigi Generating Station case study model is described here. Of the tests performed on the physical model, three test scenarios qualify as being large enough to be used as a basis for verification. A fourth scenario, representing complete removal of the cofferdam, was also investigated, but the estimated parameter, ε_{ij}, for this scenario was significantly different from the first three, thereby falling outside the range of comparability with the remaining scenarios. The scenarios all have comparable data sets of velocity magnitudes. Two design alternatives are tested under similar flow conditions and one of the design alternatives is tested for a second flow condition. The scenarios are outlined in Table 6.2. Scenarios 1 and 2 both have the cofferdam Removal Scheme *DC3a*, representing the excavation in the downstream cofferdam with an invert of 240 m and a bottom width inside the confines of the main river channel of 113.5 m. The flows tested for these two cases range from the FGD capacity of 1100 m^3/s with a downstream water surface elevation of 245.6 m, to a summer mean flow of only 867 m^3/s with a downstream water surface elevation of 244.67 m. The third scenario incorporates cofferdam Removal Scheme, *DC2b*, representing the downstream

cofferdam with a wider excavation of 131 m and a corresponding invert of 242 m. The FGD conditions are applied in this scenario.

As described earlier, a calibrated model is developed for each of the three scenarios. Table 6.3 summarizes the values for the parameters and regression statistics for each of the calibrated cases. For every calibrated scenario, the remaining two scenarios are used to verify that particular model (i.e., using the estimated parameters). The regression statistics for the verification cases are included in Table 6.3 as well. The first column identifies the scenario, as defined in Table 6.2. Each scenario is calibrated and used in verification, as tabulated in the second column. The third and fourth columns indicate the parameter values used for calibration and verification. The final three columns summarize the regression statistics derived from comparing the numerical velocity estimates to the physical velocity measurements. Calibrating the numerical model for Scenario 1 yields a ε_{ij} of 800 N-s/m^2 and a Manning's n of 0.025. The range of ε_{ij} values tested starts from 1500 N-s/m^2 down to 650 N-s/m^2. Scenarios 2 and 3 are used to verify the calibrated model and parameter estimates. The regression statistics for all three scenarios are then averaged. By the same approach, average regression criteria are determined using the calibrated models for Scenarios 2 and 3 as well. A comparison of these averages reveals that the model that performs the best for all three cases would result in an estimated ε_{ij} of 850 N-s/m^2 and a Manning's n of 0.035. The average r^2, b_0, and b_1 values of the three models show only marginal variability. Therefore, any one of the models could potentially be as reliable as the next.

The other aspects of verification involve analyzing the flow patterns and the water surface elevations. The flow patterns generated by the numerical model can be illustrated by a velocity vector plot. Figure 6.11 shows the flow pattern for the downstream section of the Notigi Generating Station case study for the cofferdam Removal Scheme *DC3a* at FGD. The vectors indicate the depth-averaged velocity magnitude by their size and the direction of flow by their direction. The density of the vectors merely reflects the density of the mesh configuration. The numerical model appears to simulate the major eddies and flow patterns based on observations of the tests performed in the physical model. Appendix G contains velocity vector and contour plots for all other downstream scenarios.

The water surface elevation data gathered from the physical model consists of ten data points distributed along the center of the main channel. These are compared to corresponding water surface elevations estimated by the numerical model. Figure 6.12 illustrates the comparison of these data in profile. The actual change in water surface elevation across the cofferdam Removal Scheme *DC3a* for the defined flow conditions is 0.1 m (in prototype scale). The reach immediately upstream of the cofferdam shows the best agreement between the physical and numerical models. The sections where the models appear to differ represent physical phenomena that the mathematical model is not designed to reproduce. For example, in the zone just downstream of the powerhouse, the flow is a very complex, three-dimensional, submerged, turbulent jet flow, and should not be simulated with a two-dimensional, depth-averaged flow model such as *FastTABS*. The accuracy of the physical measurements in this particular zone is $\pm$ 0.1 m due to the turbulent water surface. Under the circumstances, the difference of 0.17 m between the physi-

cal and numerical water surface elevations in this zone is due in part to limitations in physical measurements as well as poor numerical approximation in a three-dimensional flow zone. The reach downstream of the cofferdam also displays some discrepancy. In this region the flow follows a bend in the river and, being a relatively flat-bottomed channel, the flow deviates from the two-dimensional, depth-averaged assumption required by the numerical model. Another cause for this problem is that the boundary condition defining the downstream water surface elevation is located too near the area of study. The model, as it is set up, forces the water surface elevation at the downstream end of the model to be equal to that measured in the laboratory. A better numerical design practice would be to apply the boundary condition further downstream so that there is better agreement in the area of study. A similar trend in the profile comparison occurs for each of the other tests conducted.

A measure of how well the physical model and numerical model water surface elevation data compare is the root mean squared error of the numerical model water level estimates, defined earlier in this chapter. Even with the apparent differences in water surface elevations, the value of this error is less than 0.1 m for all cases, using the calibrated model. The actual root mean squared errors for each of the scenarios are tabulated in the calibration and verification summary table included in Appendix E.

Additional water surface elevation tests for other design alternatives are examined with the calibrated model. Comparison of these data with that from the physical model shows a similar tendency to that demonstrated in Figure 6.12. The model is unable to simulate the flows for the designs having an excavation invert of 244 m or higher because

the flow conditions through these cofferdams approach critical depth, and the *RMA-2* program is not applicable to supercritical flow problems.

6.3.3 Verification Summary for the Upstream Model

For the basic calibration of the upstream model, three design alternatives are compared under essentially similar sets of boundary conditions, and one of the design alternatives is tested using a different set of boundary conditions. The design and boundary conditions for these four scenarios are summarized in Table 6.4. As before, each of the scenarios are calibrated individually using the velocity magnitude as a basis for comparison. The first three cases are operated under similar flow conditions; the flow being at FGD of 1100 m^3/s and an upstream forebay water surface elevation of approximately 257.6 m. The fourth scenario uses the cofferdam Removal Scheme *UC3c* but under a reduced flow of 867 m^3/s and a lower forebay of 245.4 m. Calibration of these data sets yields parameters and regression statistics listed in Table 6.5. The first three scenarios all result in the same conclusion, that ε_{ij} is 2800 N-s/m^2, out of a test range from 4000 N-s/m^2 down to about 2600 N-s/m^2, and that Manning's n is 0.040. In the fourth scenario, a significantly higher ε_{ij} of 5800 N-s/m^2 is required, out of a test range from 7000 N-s/m^2 down to 5650 N-s/m^2. The ε_{ij} coefficient for the upstream model is generally larger than that determined for the downstream model. This may appear confusing considering the fact that in the upstream reach, the flows appear calm and slow because of the depth, whereas in the downstream reach, the flows are comparably faster and more turbulent due to shallower conditions. The main factor influencing the difference between the two sets

of ε_{ij} values is the constriction imposed on the flow in the upstream reach. In the upstream reach, the flow is contracted as it goes through the cofferdam and ultimately into the powerhouse, while in the downstream reach, the flow expands from the powerhouse and again through the cofferdam. The reason for a higher ε_{ij} in the upstream reach of Scenario 4, is that the water surface elevation is lowered considerably, from 257.59 m to 254.2 m. The numerical model views this scenario as a significantly different hydrodynamic situation. The numerical model for the upstream section of the Notigi Generating Station is therefore calibrated for a variety of design alternatives but only for a limited range of flow conditions. Based on Scenarios 1 to 3, the calibrated parameters are a ε_{ij} of 2800 N-s/m^2, and a Manning's n of 0.04.

The numerical model is confirmed, as was the case for the downstream model, by ensuring that the flow patterns and eddies are representative of the prototype. The vector plot in Figure 6.13 shows the velocity vectors for the cofferdam Removal Scheme *UC3c* under FGD and FSL flow conditions. Appendix H contains velocity vector and contour plots for all other upstream scenarios. Even with a significantly higher value for ε_{ij}, the numerical model simulates the flow patterns very well for all of the test scenarios, based on observations in the physical model.

Verification using the upstream water surface elevation provides additional support to validity of the model. Comparison with the physical model data is somewhat difficult due to the unsteady nature of the physical model. As described in Chapter 5, the water surface elevation data was collected after the velocity data for each test scenario, and in that time,

the water level could not be held constant due to model saturation and powerhouse flow control inconsistencies. Even though only 11 water level data points were collected, the instability of the model skewed some of the results, making it difficult to evaluate the relative impacts of design changes. In light of this, the numerical model is executed under slightly different boundary conditions for each of the water surface elevation tests than for the velocity tests. One of the comparisons for water surface elevation is plotted in Figure 6.14. The excavation design alternative used in this profile is for a bottom width of 50 m and an invert of 242.8 m. Assigning an upstream water surface elevation in the numerical model has a strong influence on how well the rest of the profile compares. The difference between the numerical and physical elevations, at most 0.06 m for this case, occurs between the upstream cofferdam and the powerhouse where 3-D effects are prevalent. Even with the stability problems, the value for the root mean squared error for the water levels in each of the calibrated cases is less than 0.03 m, indicating an excellent agreement.

Additional tests for other design alternatives consist of fewer velocity data, concentrated mostly in the reach between the powerhouse and above the upstream cofferdam. This zone, representing the area of interest for design of the cofferdam excavation, also experiences complex 3-D flows. The calibrated model is applied to each of these cases and the criteria for velocity and water levels are evaluated to see how well the model performs under theses circumstances. A detailed summary of this analysis is included in Appendix F. It should be noted that in some of the cases, where the water level was slightly lower than the levels used for calibration, the ε_{ij} could not be reduced to the calibrated value of 2800 N-s/m^2. For each design alternative under similar flow condi-

tions, the model shows good agreement, as indicated by the regression statistics and root mean squared errors.

Manning's n	Turbulent Exchange Coefficient	Regression Statistics		
		Coefficient of Determination, r^2	Intercept, b_0	Slope, b_1
0.025	800	0.7594	0.2139	0.7680
0.030	650	0.7578	0.2186	0.7615
0.035	375	0.7367	0.2149	0.7651

Table 6.1 *Regression statistics associated with the calibrated parameters for cofferdam Removal Scheme DC3a.*

Scenarios	Design Alternative	Cofferdam Excavation		Flow [m^3/s]	Downstream Water Level [m]	Number of Velocity Data
		Invert [m]	Bottom Width [m]			
1	DC3a	240	113.5	1100	245.6	72
2	DC3a	"	"	867	244.67	68
3	DC2b	242	131	1100	245.6	73

Table 6.2 *Design and boundary conditions for the downstream model calibration and verification*

Scenario	Operation	Parameters		Regression Statistics (for velocity magnitude)		
		ε [N-s/m^2]	Manning's n	r^2	b_0	b_1
1	Calibration	800	0.025	0.7594	0.2139	0.7680
2	*Verification*	"	"	0.7900	0.1530	0.7690
3	*Verification*	"	"	0.6130	0.2520	0.8020
			Average	0.7208	0.2063	0.7797
2	Calibration	650	0.03	0.7912	0.1514	0.7665
1	*Verification*	"	"	0.7580	0.2190	0.7610
3	*Verification*	"	"	0.6052	0.2438	0.7975
			Average	0.7181	0.2047	0.7750
3	Calibration	850	0.035	0.6838	0.1361	0.8645
1	*Verification*	"	"	0.7710	0.2490	0.7320
2	*Verification*	"	"	0.8030	0.1590	0.7530
			Average	**0.7526**	**0.1814**	**0.7832**

Table 6.3 *Summary of calibration and verification parameters and criteria for the downstream model*

Scenario	Design Alternative	Cofferdam Excavation Invert [m]	Cofferdam Excavation Bottom Width [m]	Flow [m^3/s]	Upstream Water Level [m]	Number of Velocity Data
1	UC1b	240	50	974	257.56	30
2	UC2c	242.8	50	1100	257.66	30
3	UC3c	245.4	60	1100	257.59	30
4	UC3c	"	"	867	254.02	26

Table 6.4 Design and boundary conditions for the upstream model calibration and verification

Scenario	Parameters: ε ($N\text{-}s/m^2$)	Parameters: Manning's n	Regression Statistics (for Velocity Magnitudes): r^2	b_0	b_1
1	2800	0.04	0.7872	0.1143	0.7089
2	2800	0.04	0.8435	0.1132	0.9265
3	2800	0.04	0.8627	0.1532	0.7559
4	5800	0.04	0.7908	0.1848	0.8134

Table 6.5 Summary of calibration parameters and criteria for the upstream model

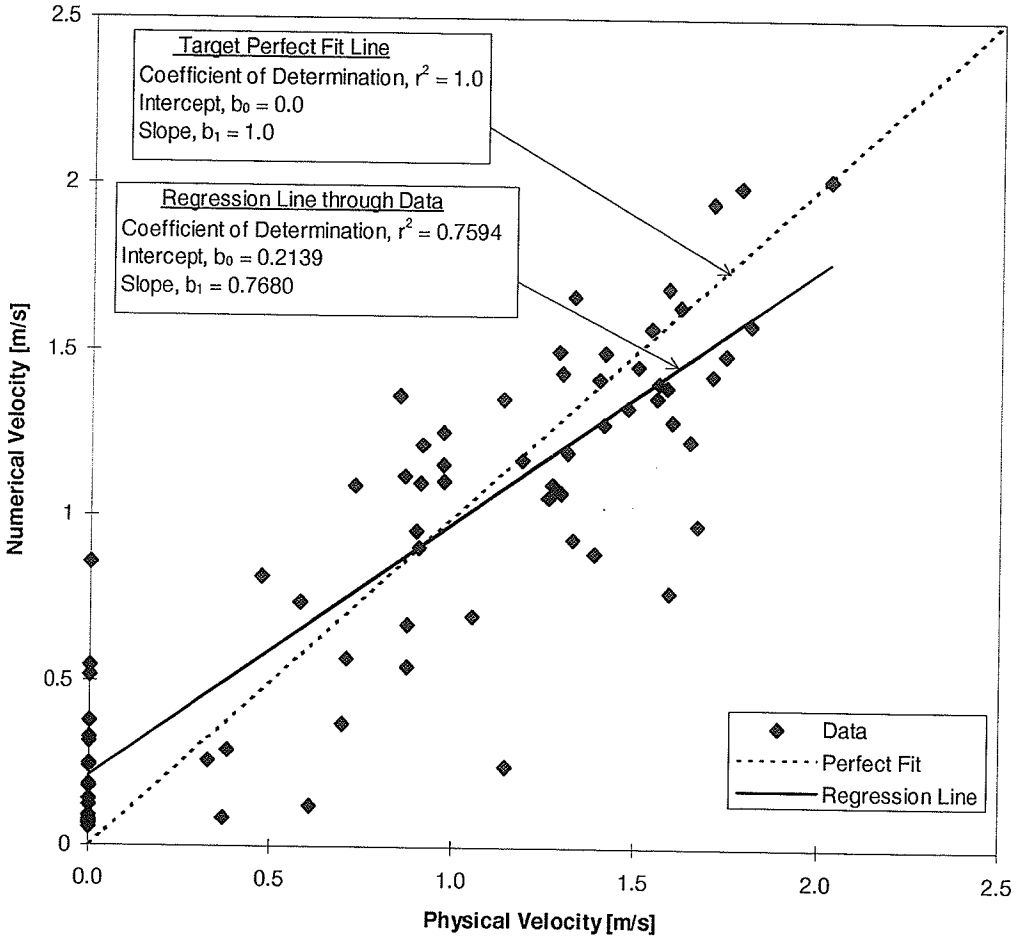

Figure 6.1 *Sample scatter plot comparing numerical and physical velocity magnitudes, and showing the fitted regression line through the data*

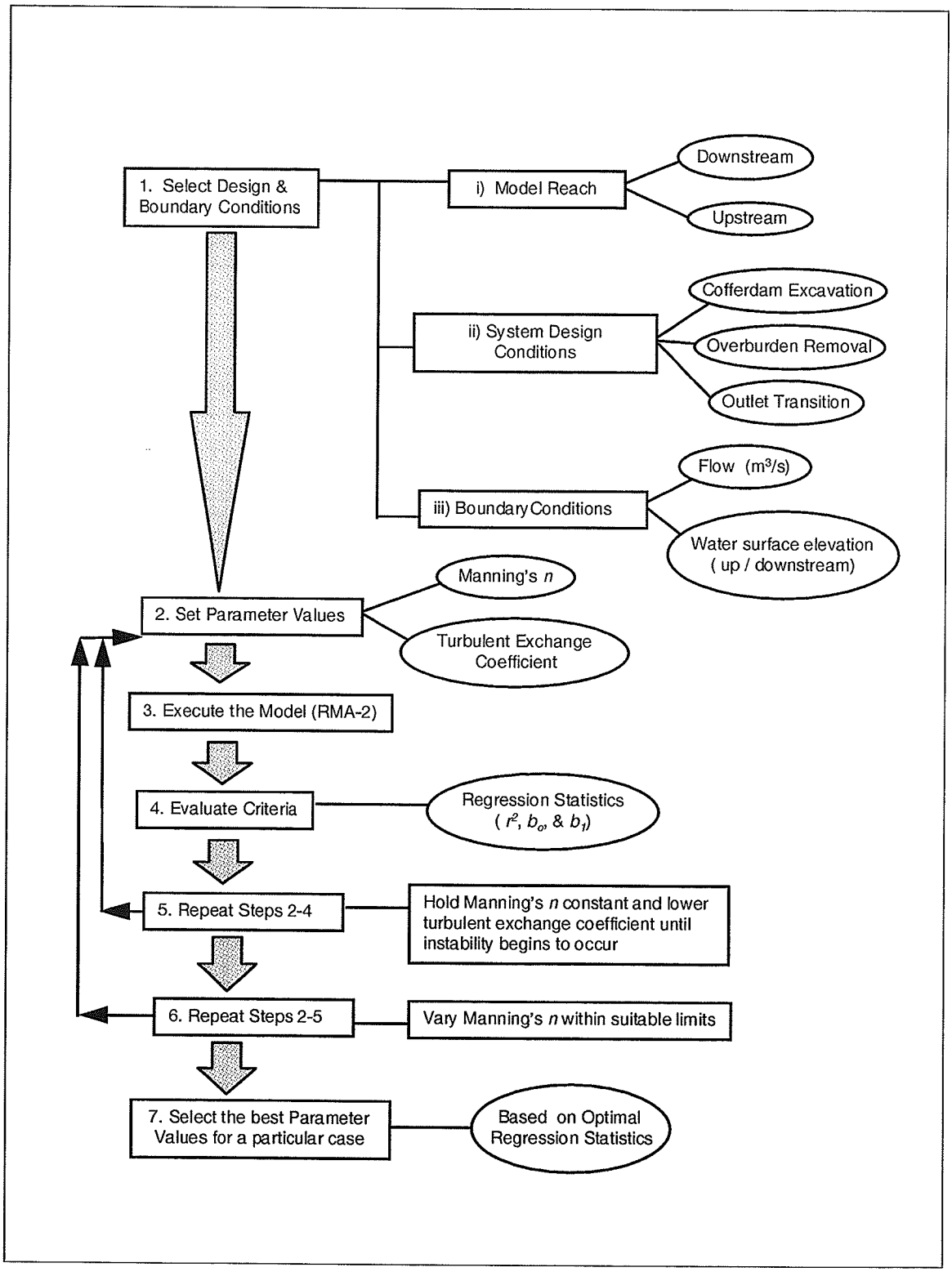

***Figure 6.2** Principal steps for the calibration process*

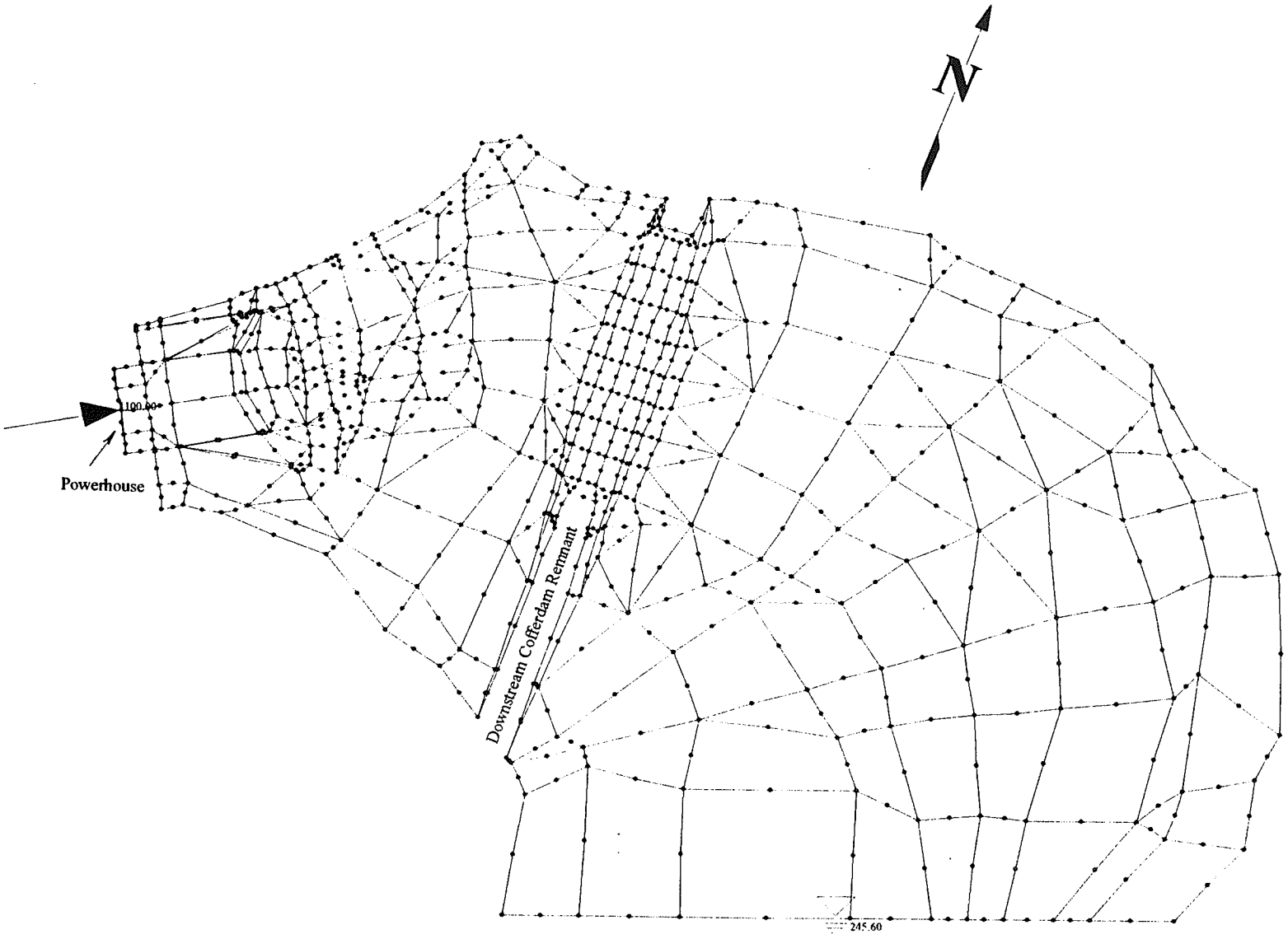

***Figure 6.3** Mesh and Boundary Conditions for Design Alternative DC3a of the Downstream Reach*

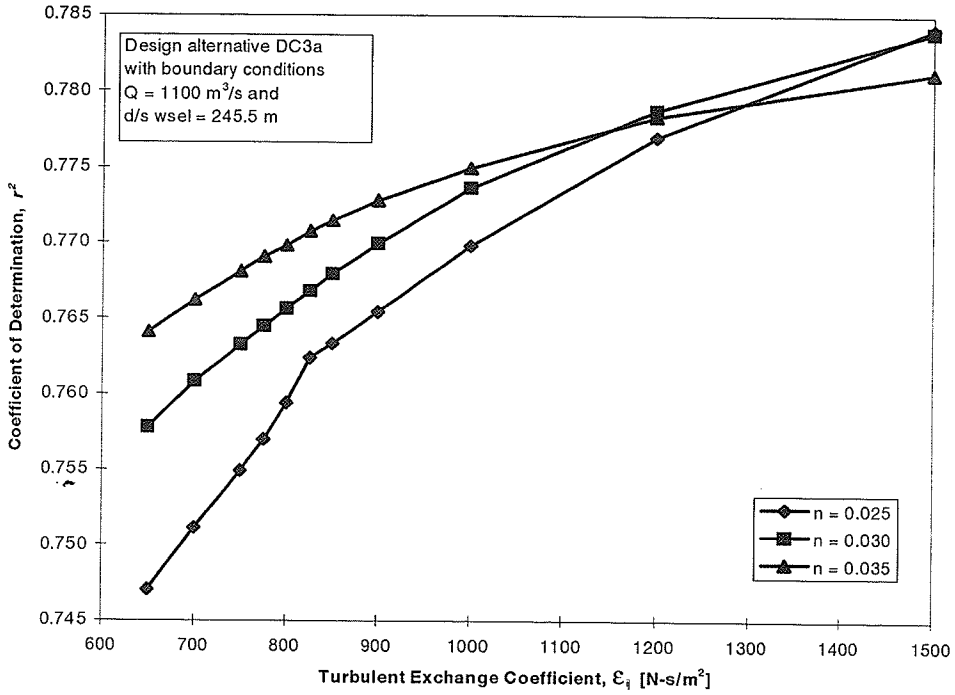

Figure 6.4 *The coefficient of determination, r^2, from comparisons of velocity magnitudes vs. turbulent exchange coefficient, ε_{ij}, for cofferdam Removal Scheme DC3a.*

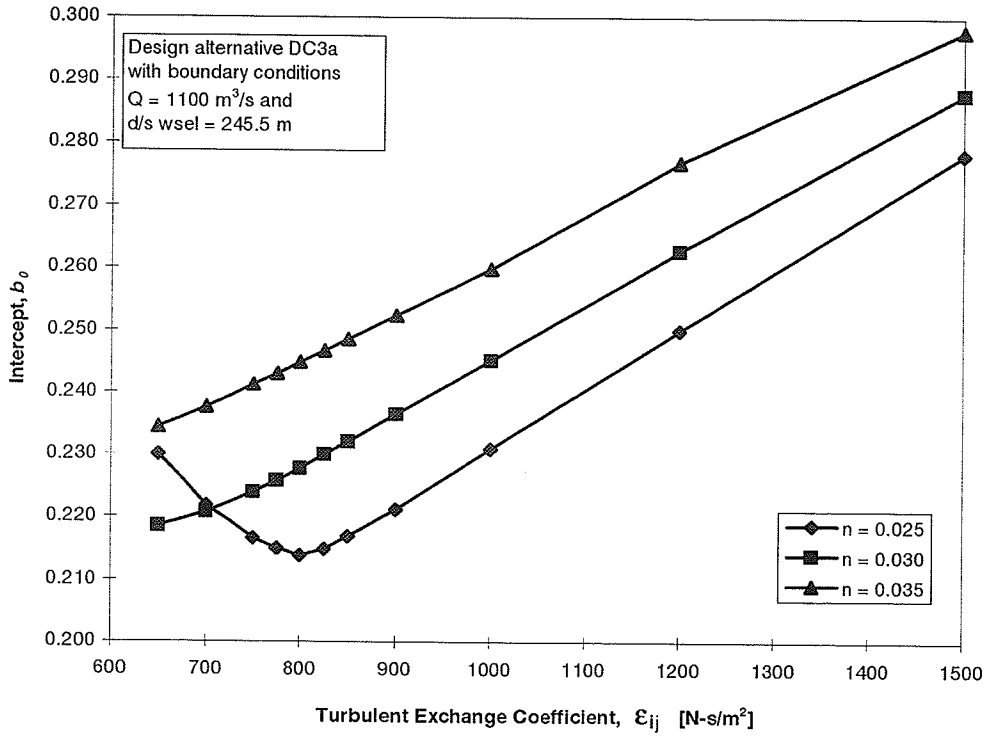

Figure 6.5 *Intercept, b_0, from comparisons of velocity magnitudes vs. turbulent exchange coefficient, ε_{ij}, for cofferdam Removal Scheme DC3a.*

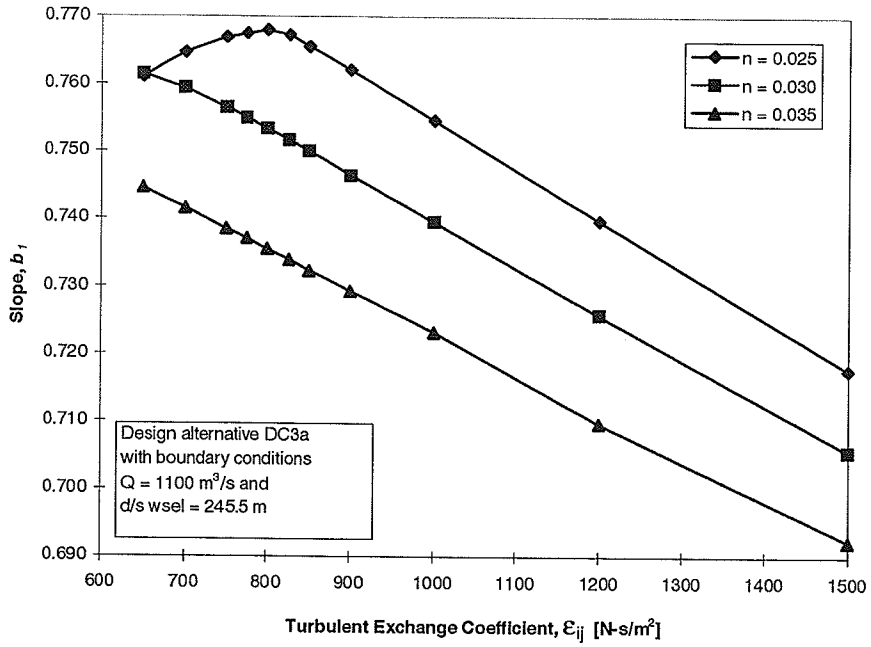

Figure 6.6 *Slope, b_1, from comparisons of velocity magnitudes vs. turbulent exchange coefficient, ε_{ij}, for cofferdam Removal Scheme DC3a*

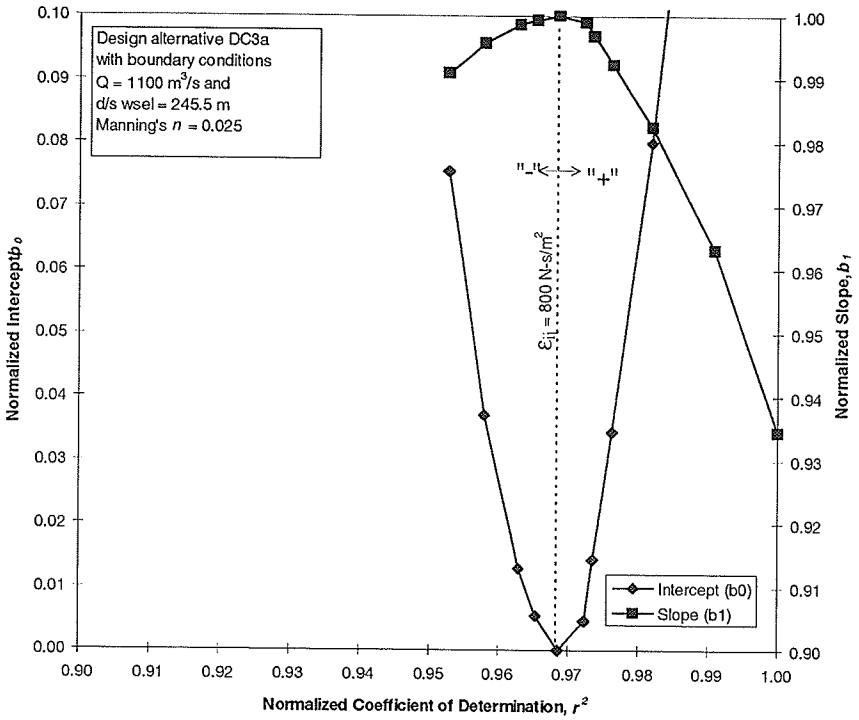

Figure 6.7 Normalized trade-off of regression statistics for Manning's n = 0.025 and cofferdam Removal Scheme DC3a

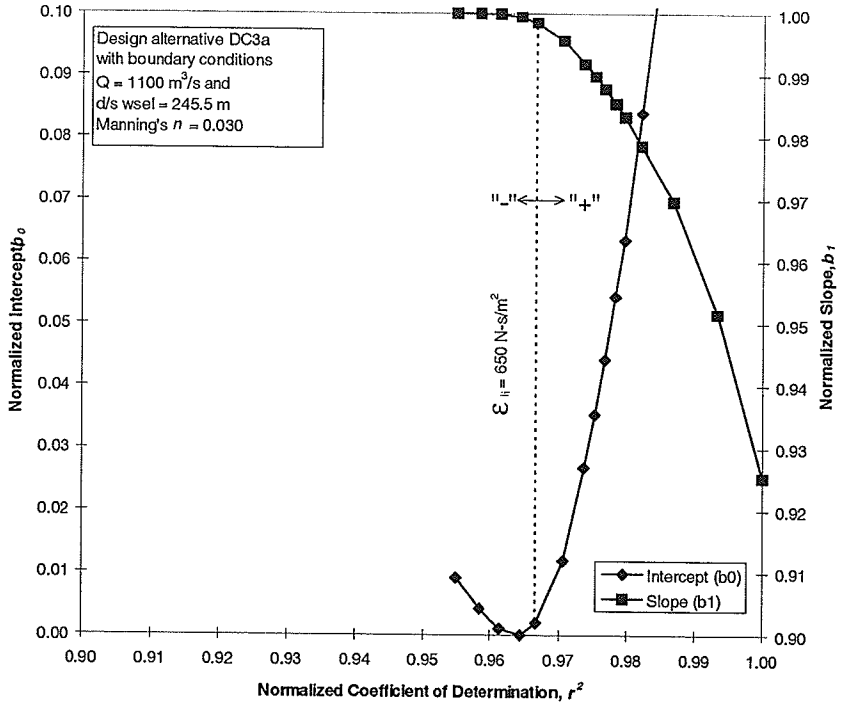

Figure 6.8 Normalized trade-off of regression statistics for Manning's n = 0.030 and cofferdam Removal Scheme DC3a

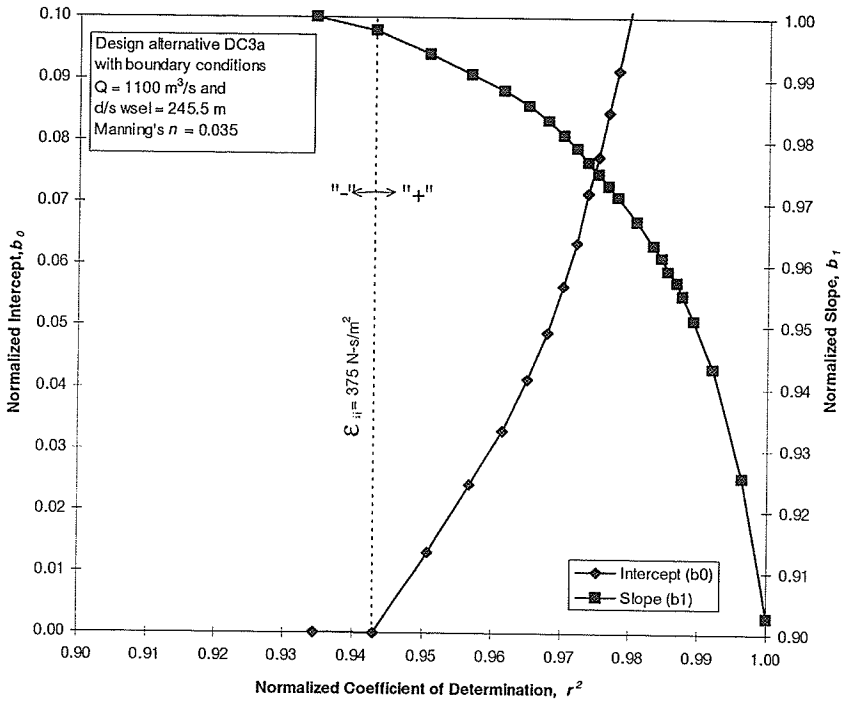

Figure 6.9 *Normalized trade-off of regression statistics for Manning's n = 0.035 and cofferdam Removal Scheme DC3a*

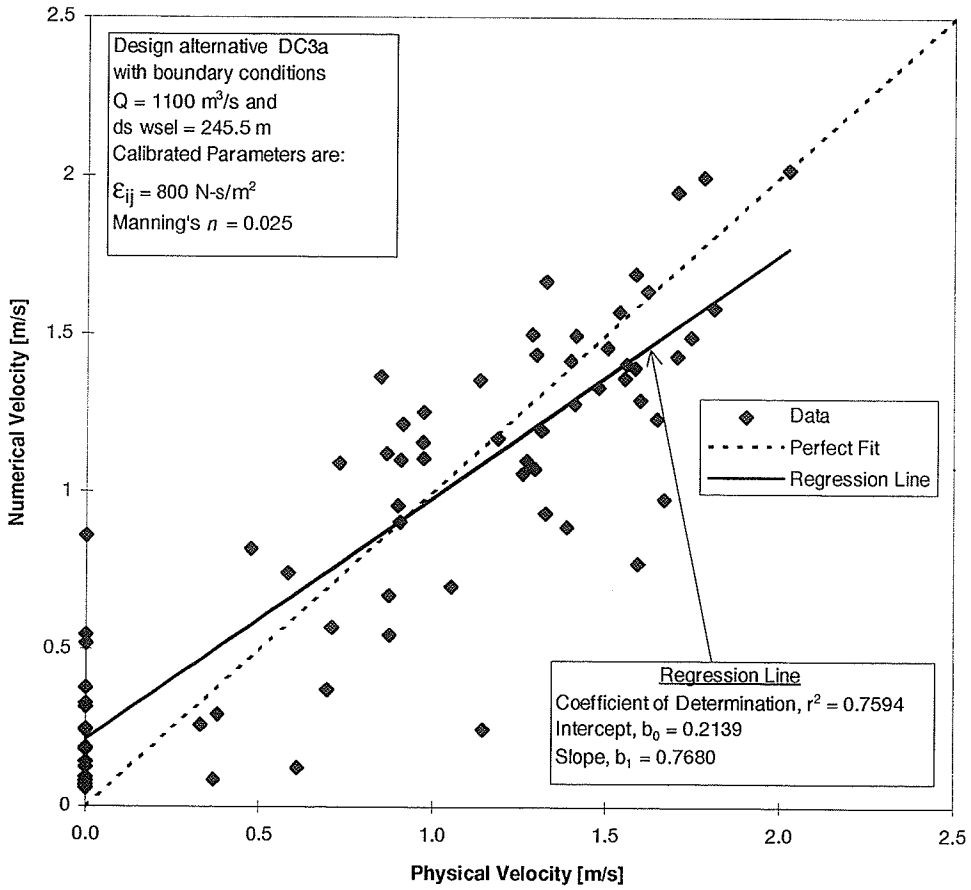

Figure 6.10 *Scatter plot comparing numerical and physical velocity magnitudes for cofferdam Removal Scheme DC3a*

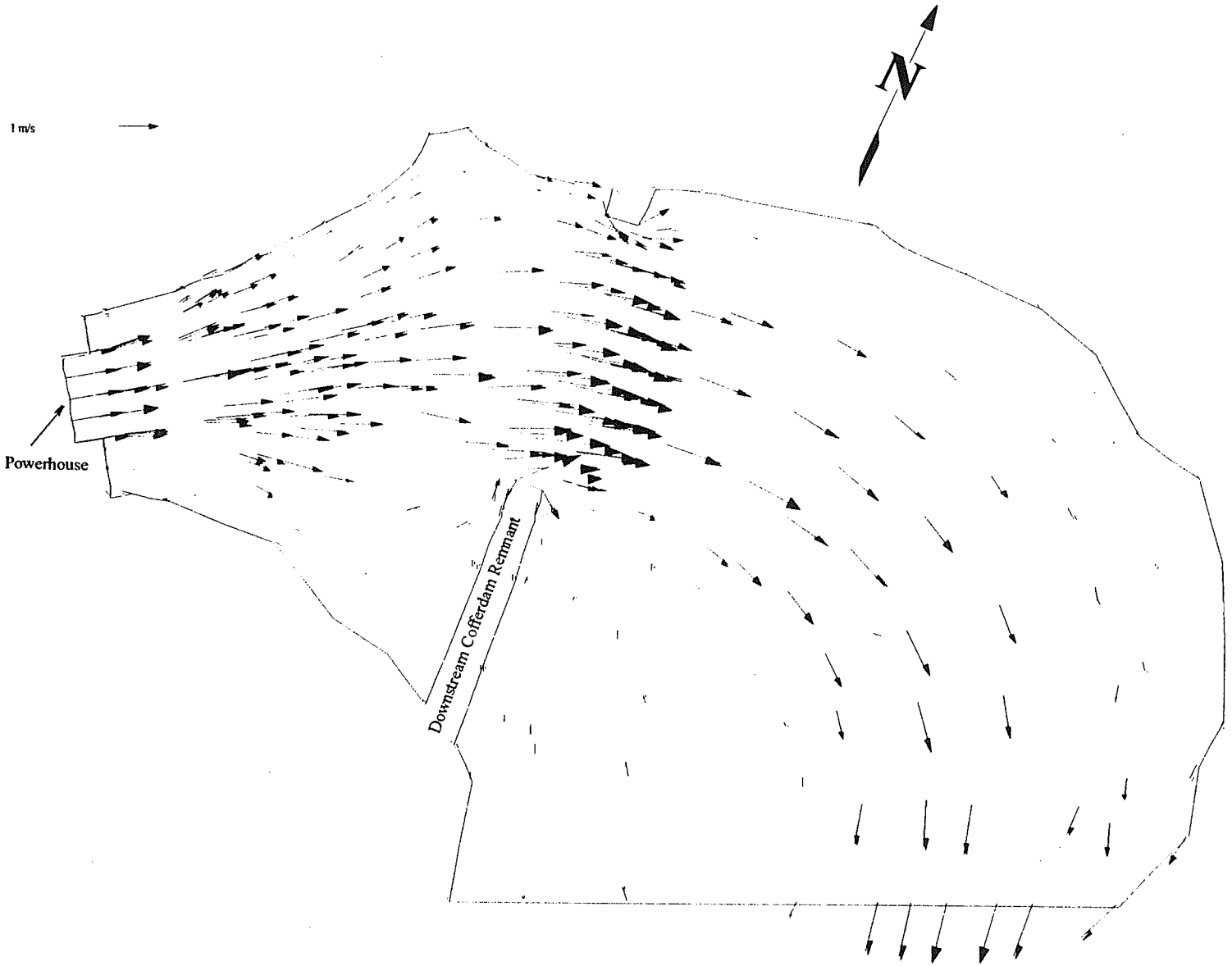

Figure 6.11 *Velocity Vector Plot for Cofferdam Removal Scheme DC3a at Full Gate Discharge*

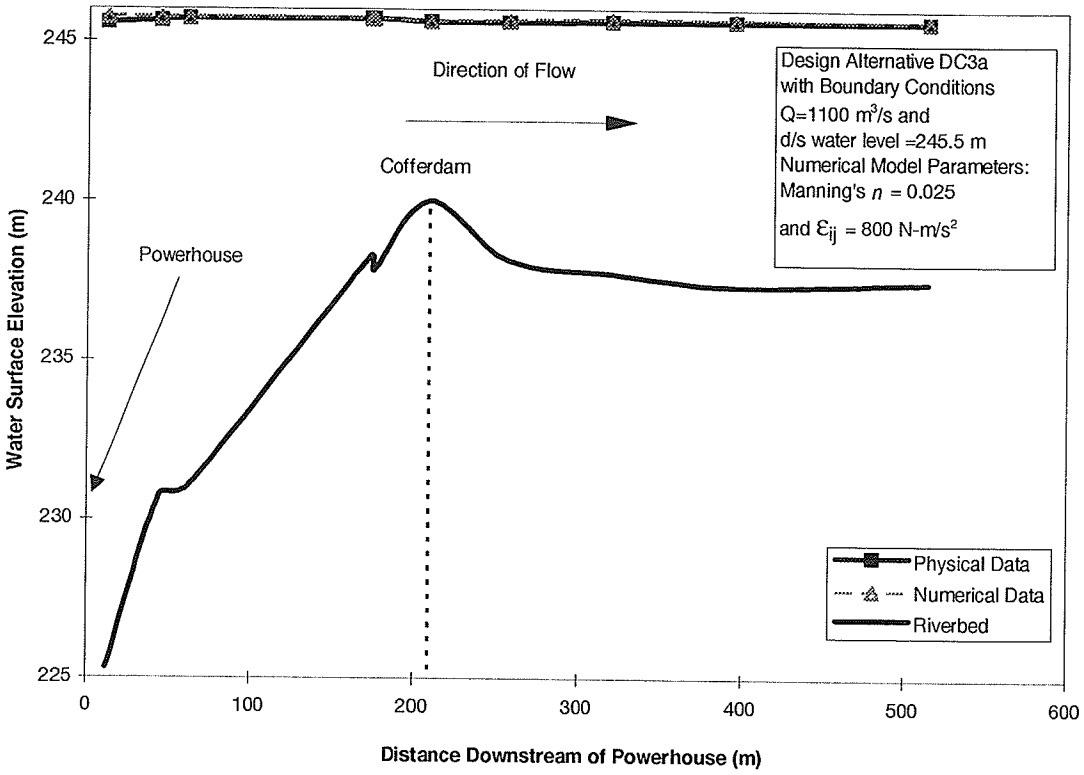

Figure 6.12 *Physical and numerical water surface elevation along the centerline of the downstream channel for cofferdam Removal Scheme DC3a*

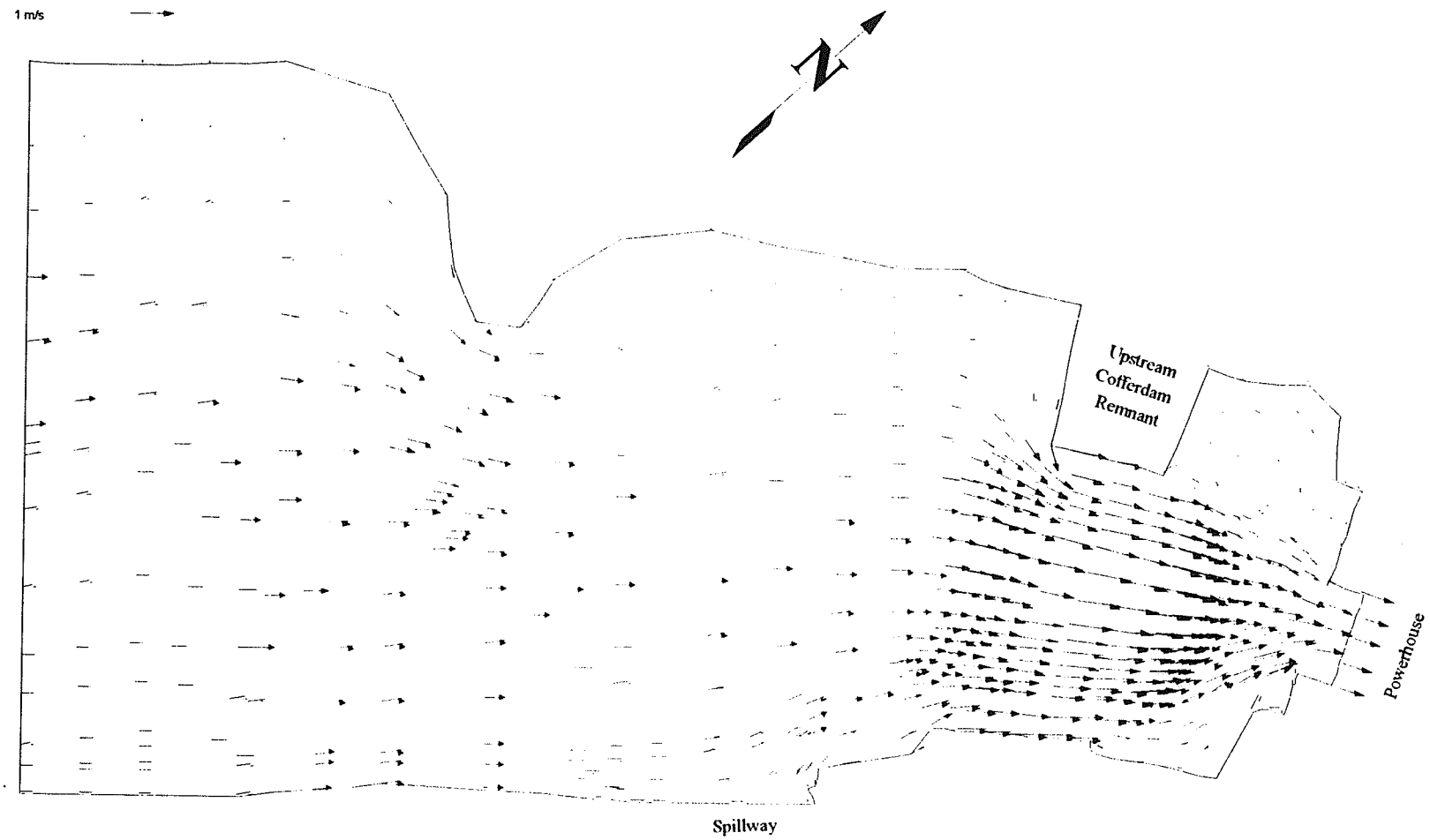

Figure 6.13 *Velocity Vector Plot for Cofferdam Removal Scheme UC3c under FGD*

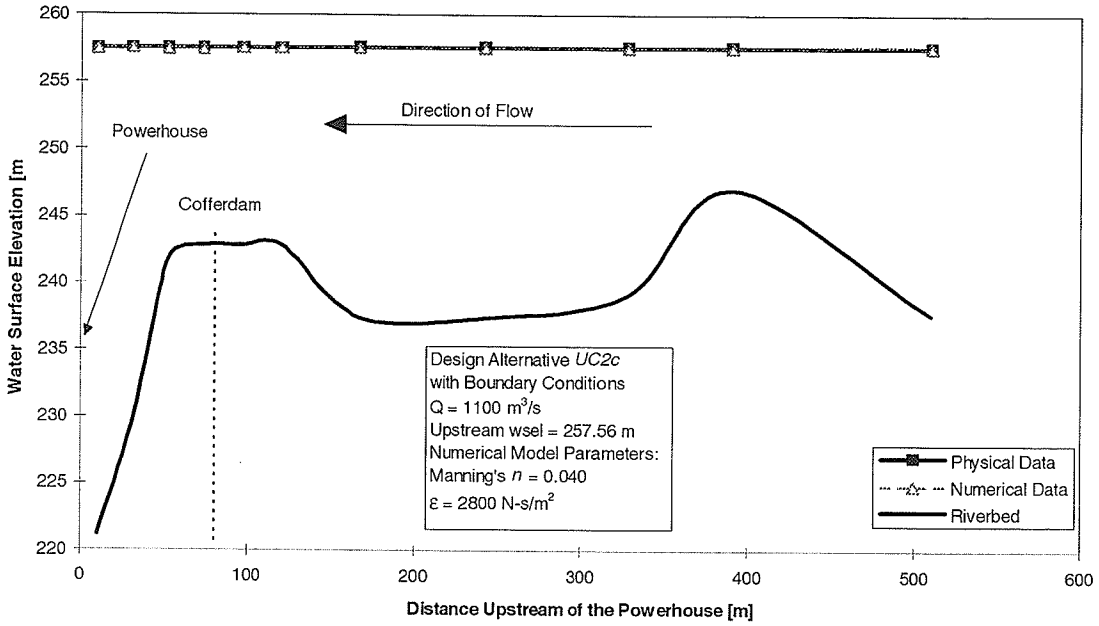

Figure 6.14 *Physical and numerical water surface elevation along the centerline of the upstream channel for cofferdam Removal Scheme UC2c*

7. APPLICATIONS AND ANALYSIS OF THE RESULTS

The numerical model can be useful in numerous applications, as long as the user is aware of the limitations and the behavior of the model system. This chapter addresses the accuracy and sensitivity of the numerical model and provides an explanation for some of the scatter in the data. It is also important to recognize that the calibrated model is only valid under a specific range of operating conditions. In light of these guidelines, it is demonstrated that the model can be applied to various issues relating to the design of the approach and tailrace channels.

7.1 Model Accuracy and Sensitivity

The question of model accuracy can best be addressed by including a discussion of the various factors influencing the numerical solution. An appreciation for the degree of sensitivity of the model results to these factors is also necessary. Depending on the specific purpose of the model, a higher or lower level of accuracy may be required. In the previous chapter, the velocity magnitude is used as the basis for the calibration and verification process. Further support is acquired by evaluation of the velocity directions, water surface elevations, and additional test cases. As was noted, the scatter plot, in Figure 6.10, showing a sample comparison between the physical model and numerical model velocities, contains a fair amount of scatter. Subsequent investigation revealed a series of reasons for these discrepancies.

The physical model data, to which the numerical model solutions are compared, are considered to be as representative of the prototype. The laboratory model, as described in

Chapter 4, is based on a Froudian model having a scale of 1:100. The assumption is that the condition of flow in both the prototype and the physical model is governed exclusively by gravity and that other forces, such as viscosity and capillary forces, either do not affect the flow or that their effect may be neglected. This assumption may not be valid in some of the shallow and slower flow sections of the physical model studied in this work. For example, a few of the points measured in the physical model showed a velocity near zero and a depth of less than 2 cm, conditions that obviously include capillary forces. The numerical model is developed to represent the prototype scale, not the laboratory model scale. Therefore, the numerical model may appear to over-estimate the velocity in regions where capillary or viscous forces are occurring. It is then possible that the numerical model may actually provide a truer indication of the prototype velocities in such zones. This could be part of the reason why the regression statistics consistently show a positive intercept and a slope slightly less than one.

The accuracy of the physical model velocity data is limited in a number of ways. As discussed in Chapter 5, the mini-propeller used to measure velocity only provides a reasonable reading for velocities greater than 4 cm/s, which represents 0.4 m/s in prototype scale. Some of the data points represent sites where the propeller did not spin and it was assumed that the velocity was zero. The numerical model, on the other hand, may still generate a value for the velocity at that point, albeit, close to zero. These points are included in the regression analyses to provide a full range of the velocities and to maintain consistency throughout the tests. Again, this phenomenon tends to skew the statistics somewhat.

There are some velocity data points in the comparison between the physical and numerical models that appear to be outliers. Although a portion of the discrepancy might be attributed to an error in physical measurements, some zones in the system may also be experiencing complex flow conditions such as turbulence or vertical separation. The numerical model attempts to represent such zones by depth-averaged flows. For some of these points the model appears to be successful, but this is more likely a coincidence than a precise estimate. The numerical model is also operated under the assumption that a single ε_{ij} value can apply over the entire model. This is an unrealistic assumption, as was discussed in Chapter 3, and can lead to poor velocity estimates by the numerical model. A calibrated numerical model can be fine-tuned by adjusting the values for the ε_{ij} for individual elements in the mesh so that the velocity estimates better reflect the physical measurements. This process requires some expertise and engineering judgment. These type of discrepancies can be positive or negative, and thus tend to decrease the value of the coefficient of determination, r^2.

Another cause for some of the scatter is due to the way the mesh has been constructed. The degree to which the guidelines for mesh construction are followed, described in Chapter 3, can have a significant impact on the viability of the solution. An analysis of the average difference in velocities between the physical and numerical models reveals that there is a higher margin of error for the downstream section than for the upstream section of the system. Appendices E and F contain the physical model and numerical model velocities and residual statistics for every case tested for the downstream and upstream scenarios, respectively. The average absolute difference in velocity magni-

tude between the physical and numerical models for all of the downstream tests is 0.23 m/s, while for the upstream tests, it is only 0.09 m/s. Similarly, the average absolute maximum difference for all of the downstream tests is 0.66 m/s while for the upstream cases, it is 0.25 m/s. This can be attributed, in part, to the fact that the upstream mesh is of a higher quality than the downstream mesh.

A greater level of detail, or refinement, is applied to the upstream model in order to provide adequate representation of the relief. It is acknowledged that both the upstream and downstream meshes have some elements which fail to meet every criterion for element quality. There are a few elements that violate either the minimum angle, the maximum slope, or the element area change criteria. The numerical model calculates the velocity and water surface elevation at each node based on the information available at any adjacent nodes. Deviating from the criteria for element quality makes it difficult for the model to maintain continuity, resulting in a questionable solution. Some of the outliers identified in the scatter plots, as well as differences in the water surface elevation profiles, correspond to nodes associated with lower quality elements. For example, the velocity being interpolated at the common nodes for two elements of very different sizes or shapes is based on the values and positions of the adjacent nodes, and therefore is not the result of a balanced interpolation. Some of the mesh problems, such as failure to meet the interior angle and element area change criteria, can be improved upon, but the time for such an undertaking was not available and deemed not necessary in the areas of concern for this case study. The minimum slope criteria, on the other hand, could not be maintained due to the nature of the river bed topography.

7.2 Range of Operation

A calibrated numerical model is often limited to a set range of operating conditions. Pursuing flow conditions or design alternatives beyond the scope of the calibrated model can lead to invalid solutions. A model that can be applied to a large range of operating conditions is considered robust. The robustness of a model depends on how sensitive the solution is to the parameters under different design and flow conditions. The flow chart in Figure 7.1 offers a simplified perspective of model robustness. The model parameters are tuned or calibrated so that the best solution is achieved. The sensitivity of the solution to Manning's n and to ε_{ij} can influence the confidence level of the model. Similarly, the degree to which the calibrated parameters depend upon the flow or boundary conditions imposed on the system also affects the confidence level. For example, if the value of the calibrated parameter shows a high dependence on the imposed boundary conditions, the parameters may be considered very sensitive. In other words, small changes in the boundary conditions can necessitate significant changes in the calibrated parameters. Conversely, large variation in the boundary conditions that lead to minor impacts on the calibrated parameters, implies that the parameters are not sensitive to changes in boundary conditions. Thus, a robust model is one that can successfully simulate the desired characteristics under various flow or boundary conditions.

An analysis of the results throughout the calibration process reveals that there is a rather low sensitivity on the part of the velocity or water surface elevation data to changes in either ε_{ij} or Manning's n. Manning's n is tested for the reasonable range, between 0.025 and 0.040, for which the velocity varies by as much as 0.1 m/s and the water surface

by as much as 0.02 m at any one point. Although the ε_{ij} coefficient is evaluated for a large range of values, the corresponding impact on the solution is minor. For example, in the upstream model section, changing the value of ε_{ij} by 1000 N-s/m^2 results in a change in average velocity of about 0.1 m/s and a change in water surface elevation of 0.06 m. Therefore, the effect on the solution due to changes in ε_{ij} value by even 500 N-s/m^2 near the point of the calibrated value, are considered to be negligible.

There is a mixed relationship between the parameters and the set of flow or boundary conditions applied to the model. The value of the calibrated ε_{ij} is found to be dependent on the boundary conditions imposed. Manning's *n*, on the other hand, shows only minor dependence on the flow conditions, which is expected. The selection of the best ε_{ij} value depends physically upon the water surface elevation, the flow, and the channel or coffer-dam design configuration, and numerically upon the mesh spacing. A significant factor affecting the range of appropriate ε_{ij} values is the overall expansive or contractive nature of the channel. The flow in the downstream channel tends to widen or expand leading to a lower ε_{ij} value. The upstream reach forces the flow to contract through the cofferdam excavation and then again into the powerhouse thus requiring a higher ε_{ij} value. The calibrated ε_{ij} for the upstream section under FGD is 2800 N-s/m^2 whereas in the down-stream section, the calibrated ε_{ij} is only 850 N-s/m^2. The other aspect that has an impact on the calibrated value of the ε_{ij} coefficient is the maximum velocity in the mesh. There is a direct relationship between the velocity and the value of ε_{ij} at a point. From theory, the

velocity in the model is also a function of the flow and water surface elevations or depth. Thus, an analysis of all of the tests conducted confirms the conceptual relationship between the value of ε_{ij} and the water surface elevation for increasing flows. Increasing the velocity, either by increasing the flow or decreasing the water level, necessitates a higher exchange coefficient.

Most of the scenarios used in the calibration of the numerical model of the upstream and downstream sections were such that the velocities together with the channel contraction, or expansion, yielded similar ε_{ij} values. Although a slight change in the flow conditions, or channel designs, may require a potentially different value for the ε_{ij}, applying the calibrated value, or a value for which the solution can converge, may still yield a reasonable result. This is because changes of as much as 500 N-s/m^2 in the coefficient have only a negligible impact on the velocity and water level solutions. Consequently, attempting to model scenarios experiencing different velocities, and water surface elevations, than the calibrated situation would require substantially different ε_{ij} values. The calibrated parameters of the numerical model are valid and can generate viable results provided the model is operated within a specified range of boundary conditions. In general, the flow conditions and design alternatives can only be modified to the extent that there are no significant changes in the magnitude and directions of the velocity vectors. Specifically, the downstream model is valid for flows between 867 m^3/s and 1100 m^3/s, for downstream water levels between 244.7 m and 245.6 m, and for cofferdam inverts less than 242 m and bottom widths between 113 m and 131 m. The upstream model is found to be more

sensitive to changes in the boundary conditions. For a constant flow of 1100 m^3/s, the upstream water level should be kept between 257.3 m and 257.7 m. At the same time, the upstream excavation alternatives should be restricted to having a bottom width of between 40 m and 80 m and an invert between 240 m and 245.4 m. Further changes in these flow conditions should be such that the velocities in the system do not exceed 1.2 m/s. Scenarios that yield lower velocities are still valid as long as the ε_{ij} cannot be reduced by more than 500 N-s/m^2 below the calibrated level. Any tests conducted outside the specified range of the calibrated models are speculative in nature and are not verified.

Reasonable, but not verifiable, solutions can still be generated for tests outside the specified range by using a slightly different approach. The traditional calibration and verification approach, as has been illustrated, is to identify the values for the parameters that offer the best solutions for a range of operating conditions. It is suggested that the methodology, described as spinning up the model in Chapter 6, can lead to reasonable solutions for tests that extend beyond the range of the calibrated model. The ε_{ij} values are lowered by a series of revisions to the point where oscillation or instability in continuity begins to occur. These oscillations can be detected in the numerical model with the aid of continuity lines, referred to in the numerical model as 'GC strings.' *RMA-2* calculates the flow rate at each continuity line for each iteration and writes it as a percentage in the solution file. The *FastTABS* manual suggests that "the results can be expected to be reasonable if the percentage of oscillation is less than about 1.0%" (BOSS Corporation, 1993). Instability also is exhibited in the maximum change in velocity and water surface elevation per iteration. With each iteration, the maximum difference in velocity or water

level should be decreasing or converging. It is observed that the best ε_{ij} value for a set of data corresponds to the point where the solution can no longer converge. In other words, further reduction in the ε_{ij} value only causes the maximum difference in velocity or water level to oscillate and diverge and ultimately become unstable. Establishing this convergence point depends upon the step size of reduction in the value of ε_{ij}. Even if the selected ε_{ij} coefficient is not the best value for a particular case, the coefficients in this model can be off by even 500 N-s/m^2 with negligible impact on the solution. The calibrated and verified models add support to the viability of these extrapolated scenarios. Thus, as long as the general modelling guidelines (see Chapter 3) are observed, and by making use of the spinning up technique, the numerical model can conceivably offer reasonable solutions for a significant range of flow conditions and design alternatives, even without having adequate calibration data.

7.3 Approaches for Determining the Best Design

The designs of the approach and tailrace channels are influenced by several factors. The main design criteria for the tailrace channel is the minimization of the headloss at the downstream side of the powerhouse. The factors that influence the headloss in the tailrace include the downstream cofferdam removal alternatives, the boundary conditions, the overburden removal, and the degree of scour and deposition of the tailrace riverbed material. The principal design criteria to be considered for the approach channel include the headloss across the cofferdam remnant, the flow distribution at the intake, the potential for stable ice formation in the forebay, and the potential for erosion of the riverbed.

The key factors that affect these criteria include the upstream cofferdam design alternative, the boundary conditions, and the design of the intake. The relative location and alignment of the powerhouse and the cofferdams to each other and in the river channel can also have a significant impact on the hydraulic behavior of the system. Although such changes can be modelled both in the laboratory setting and with *FastTABS*, it is assumed in this project that the locations for the powerhouse and cofferdams are fixed. The following sections describe the preliminary investigations that have been conducted for the primary design criteria to demonstrate the potential applications of the numerical model.

7.3.1 Ice Formation in the Forebay

One objective in the design of the approach channel is a stable ice cover formation in the forebay during winter to prevent frazil ice generation. The ice cover in rivers and streams is often initiated by smaller crystals that form in fast moving, supercooled water. These crystals rise to the surface and combine there to form frazil ice, a spongelike structure having an adhesive nature. According to Pariset and Hausser (1961), in reaches where the velocity is low (0.15 - 0.3 m/s), an ice cover will develop from the banks by lateral propagation of frazil ice. When the velocity in the river is 0.38 m/s or higher, the ice cover is formed by accumulation against a downstream obstruction. The ice floes will be drawn under the leading edge of a downstream ice cover when the velocity exceeds 0.69 m/s. Frazil ice can cause problems for hydroelectric plants by adhering to screens and trash racks at the intakes and severely restricting or even completely blocking their inflow. If the frazil ice is allowed to flow through the turbine, it may, under extremely cold conditions, adhere to the blades and the interior walls, thereby reducing the blade

efficiency. Forming and maintaining a stable ice cover prevents frazil ice from forming (Perham, 1983), and consequently these types of problems can be avoided.

The criterion commonly used to determine the potential for forming a stable ice cover is a maximum Froude number of 0.07 in the approach channel during freeze-up. In the upstream river section, the velocity and Froude number tends to reach the highest value through the cofferdam remnant. The Froude number can be calculated from the measurements taken on the physical model. The numerical model generates Froude numbers at every node in the mesh. Figure 7.2 shows a contour map of Froude numbers that has been produced by *FastTABS* for the upstream cofferdam Removal Scheme *UC1c*, having an invert of 239.8 m and a bottom width of 40 m, under FGD and FSL. Froude contour plots for the other upstream scenarios are included in Appendix H. The Froude number through the cofferdam Removal Scheme *UC1c* ranges between 0.06 and 0.075. This is approximately within the critical range for which a stable ice cover can still form. Higher Froude number values occur near the leading edges of the cofferdam remnant where there is separation of flow. In the zone just upstream of the cofferdam, the Froude number is only about 0.035 to 0.04, well below the maximum level required for an ice cover. These results are based on the boundary condition having a discharge of 1100 m^3/s and a forebay level of 257.56 m. Flows at freeze-up are typically lower, usually less than 963 m^3/s, and the forebay level may be as low as the MSL of 254.2 m. Such boundary conditions may yield Froude numbers that are very different from the scenarios tested and should therefore be investigated in greater detail as part of the process in designing the approach channel. The advantage of seeing a two-dimensional plot of Froude number contours is

that problem areas can quickly be identified and addressed. Many different design alternatives can be tested for various flow conditions and with the aid of the Froude number contour plots, the best design can be selected.

The comparison of the Froude numbers for various cofferdam excavation alternatives under the same flow conditions can be performed for a single point in the mesh. Although such a comparison may not represent the whole picture, it does provide a useful description of the relationship between the design alternative and the Froude number. Figure 7.3 depicts such a comparison, as generated by the numerical model, for a point near the center of various cofferdam design alternatives for a single flow condition. Under a FGD of 1100 m^3/s and a forebay elevation of 257.56 m, only three of the cases experience Froude numbers below 0.07 near the center of the cofferdam excavation. Again, the flows and forebay levels are usually lower during freeze-up than those used to test the model. Decreasing the flow would yield lower velocities and consequently lower Froude numbers. On the other hand, lowering the forebay may yield higher velocities and consequently higher Froude values. The tests performed in this analysis have been limited, due to time constraints, to only three excavation inverts with varying bottom widths under one set of flow conditions. Many other combinations of designs and flow conditions can be examined, using the numerical model, in establishing the cofferdam removal requirements. Thus, *FastTABS* can be applied, by producing contour plots and detailed nodal summaries of the solution, in the evaluation of a river system's ability to form a stable ice cover during the freeze-up period. This may also prove useful in assessing the feasibility and

placement of an ice boom structure upstream of the remnant, at a location where the velocity and Froude number are low enough to aid in the formation of a stable ice cover.

7.3.2 Erosion

Another factor that needs to be considered, particularly in the design of the approach channel, is erosion of the bed material. There are several reasons why erosion in the up-stream river bed is not acceptable. Suspended particles of a large enough size can shorten the life of, and inflict considerable damage to, the turbines. Significant volumes of bed material transported into the powerhouse can also make the turbines less efficient. Although the river bed will erode in areas of high velocities until it has reached a state of equilibrium, the resulting change in bed topography may impose a flow pattern that could diminish the performance of the generating station. The eroded material will settle in areas where the velocities are lower and potentially create dunes, thereby causing a backwater effect at the powerhouse.

Both physical and numerical models can be used to investigate potential erosion zones. There are two approaches that can be taken to study erosion in the physical model. Scaled bed material can be used in a moveable-bed model and the actual erosion can be observed and documented for various flow conditions. A physical model with a fixed-bed may be used to estimate the erosion by comparing the velocity measurements to the velocity required to initiate sediment transport for an average particle size. This project used a semi-fixed bed model as described in Chapter 4. The current version of *FastTABS* does not perform sediment transport modelling, so the estimated velocities are used to evaluate zones that would be prone to erosion. The criterion used to determine whether

or not erosion will take place is the maximum permissible velocity, as was discussed in Chapter 5. This represents the greatest mean velocity that will not cause erosion of the channel bed.

The areas of potential erosion can easily be identified by viewing the velocity contour plots produced by *FastTABS*. An example of such a plot is shown in Figure 7.4. The upstream cofferdam in this illustration shows the cofferdam Removal Scheme *UC2b* having an invert of 242.8 m and a bottom width of 60 m. Under a flow of 1100 m^3/s and a forebay level of 257.56 m, the maximum velocities occur in the central portion of the excavation near the downstream edge of the cofferdam. The velocities are slightly in excess of 1.0 m/s near the invert edge closest to the powerhouse. For this scenario, it is unlikely for there to be erosion of the cofferdam since the velocities necessary to initiate bed motion for random rockfill tend to range between 1.0 m/s to 3.0 m/s (see Chapter 5). In analyzing the velocity contour results, it is important to keep in mind that these represent depth averaged values. The actual profile of the velocity distribution with depth, for a typical channel section, would show a higher velocity near the surface and a lower velocity near the river bed. Nevertheless, for areas indicating velocities significantly greater than 1 m/s, there may still be a probability of erosion. In such areas, it may be necessary to provide some protection against erosion.

The selection of the best cofferdam excavation design can be simplified by comparing the maximum velocity through the excavation, as generated by the numerical model, for the various design alternatives. Figure 7.5 shows the maximum velocity through the upstream cofferdam as estimated by both the physical and numerical models. The flow

conditions for these results are, as before, for a discharge of 1100 m^3/s and a forebay water level of 257.56 m. The maximum velocity for each case occurs at the downstream edge of the excavation, closest to the powerhouse. Although only one of the design alternatives falls below the maximum velocity criterion for erosion riverbed material, they are well all below a critical velocity of 3 m/s required to initiate movement of particles greater than 0.1 m in size. Other scenarios of boundary conditions and design alternatives may yield higher velocities for which remedial measures may be required to mitigate any serious erosion.

7.3.3 Channel Optimization for Power Production

The key factor influencing the generating station's ability to produce electricity is the energy head. The energy head represents the potential energy available to the power house, generally resulting from the difference between the upstream and downstream water levels. The simplest approximation defining the energy head available for power generation is based on Bernoulli's Energy Equation, as shown by Equation 7.1.

$$h_T = \Delta z + \frac{V_1^2 - V_2^2}{2g} - h_L \qquad [7.1]$$

Equation 7.1 states that the energy head available to the turbines, h_T, is equal to the difference in water levels, Δz, between the upstream and downstream sections, plus the difference in velocity head, $(V_1^2-V_2^2)/\ 2g$, resulting from the difference in velocities entering and leaving the powerhouse, less the remaining head losses (i.e., friction losses), h_L, all in metres. Figure 7.6 provides a visual description of the variables involved Equation 7.1. The Energy Grade Line, EGL, refers to the total head in metres.

The presence of a cofferdam remnant in either the forebay or the tailrace channel can have a negative impact on the power production capability of the generating station. A significant headloss across the upstream cofferdam can reduce the potential energy for the turbines. Likewise, a headloss over the downstream cofferdam will create a backwater effect and thereby reduce the potential energy of the powerhouse. The approach taken in this project is to evaluate the impact of various cofferdam removal strategies on the water surface elevations immediately upstream and downstream of the powerhouse. The assumption is that any change in water level, in either the upstream or the downstream models, will be reflected as principal impacts on the energy potential of the power generating station. The best cofferdam removal scheme, from the perspective of power production, is the one which provides the greatest benefits resulting from reduced headlosses.

The results from the numerical model provide a consistent basis by which the cofferdam headlosses can be evaluated. Although the results from the physical model were useful in calibrating and verifying the numerical model, the water level results were too variable or uncertain to be of use for this analysis due to scale and operational difficulties. However, the numerical results can overcome this inconsistency by assigning constant boundary conditions for each of the design alternatives. The contour plots of the water surface provide a good sense of how the water differential is distributed for each individual scenario. Also, the net water surface elevation for all of the design alternatives may be used as a way to compare the impact that varying the cofferdam design has on the water levels.

Figure 7.7 provides an example of the upstream water level contour plot for the upstream cofferdam Removal Scheme *UC2c* as generated by *FastTABS*. The water levels directly in front of the intakes may not be accurate because the model cannot represent complex, three-dimensional, submerged intake flows with a simple, depth-averaged, open channel flow. Similar water surface elevation contour plots are generated for the other upstream design alternatives and are included in Appendix H. The water surface elevation contour plots for the downstream model, included in Appendix G, do not agree with the physical results in the area immediately downstream of the powerhouse. As with the upstream model, the flow in this zone is extremely turbulent, and three-dimensional. In fact, the flow leaving the draft tube is essentially a submersed jet. The numerical model attempts, with no success, to represent this complex flow with a depth-averaged, open surface flow. The physical and numerical models are in better agreement further downstream of this phenomenon, at a point where the flows are more uniform.

The other way to view the results is by comparing the water level differences for the various cofferdam removal alternatives. Figure 7.8 shows relatively small headlosses, for both physical and numerical models, across the upstream cofferdam for three inverts and varying bottom widths. These losses are for a discharge of 1100 m^3/s and an upstream water surface elevation of 257.56 m. The forebay in the physical model experienced some fluctuations thus making the comparison to the numerical results less consistent. Obviously, decreasing the forebay level while maintaining the flow would result in higher headlosses. This is an important consideration in designing the approach channel. The worst case for the scenarios tested shows a headloss of only 0.073 m. This information

can be used in a cost-benefit analysis to select an optimum design by comparing the cost of the various design alternatives to the savings associated with the minimizing the head-loss. The headloss, measured in the physical model and generated by the numerical model, over the downstream cofferdam remnant is shown in a slightly different format in Figure 7.9. Here, the net water level is compared for two bottom widths at various inverts. The value at an invert of 238 m represents the water level difference for complete removal of the cofferdam. Three cofferdam inverts were tested with the physical model, but the numerical model could only simulate the designs having inverts of 240 m and 242 m. The water level difference for invert 244 m could not be determined with the numerical model because the flow conditions through the cofferdam were near critical depth. According to the results from the physical model, the difference in head for this invert was approximately 1.49 m for the 113 m wide excavation, and 1.13 m for the 131 m alternative. The losses for the downstream cofferdam are significantly greater than the upstream cofferdam because of the different flow regimes in each reach.

7.3.4 Flow Patterns

The performance of the powerhouse is affected by the flow patterns in the approach channel. In order to achieve maximum power output, each of the turbine units would require equivalent, uniform, and parallel flows. Flows entering the powerhouse at oblique angles could cause undesireable headlosses at the intake trash racks. The formation of significant eddies in the approach channel are good indicators for potential vorticy formation that may lead to air entrainment. Air entrainment is undesirable as it can decrease the discharge capacity thereby reducing the powerhouse efficiency.

The physical modelling of vortices is complicated in that, fundamentally, they are a two-phase phenomena composed of water and air. In maintaining the criteria of similarity, both the Froude and Reynolds effects have impacts on the system. It has been stated that "apart from forces of gravity, viscous forces and, to a smaller extent, surface tension also affect the vortices" (Novak and Cábelka, 1981). Modelling vortices using a two-dimensional, depth-averaged computer model is not possible. Although the numerical model cannot simulate air entrainment, it can provide a qualitative indication, using velocity vector plots or flow trace animation, of whether or not such a phenomena might be initiated on a large scale. The value of ε_{ij} has a strong impact on how 'real' the flow patterns appear. High coefficients may converge to a solution, but yield flows that indicate a highly viscous fluid, whereas lower values of the coefficient yield flow patterns of a low viscosity fluid capable of eddies. The large scale circular flow patterns modelled by *FastTABS* give some indication of potential vortex formation, but the fact that vortices do not show up in the numerical model does not mean that vortices cannot occur in the prototype.

A qualitative analysis of the flow patterns for both the physical and numerical models reveal no serious problems for air entrainment at the turbine intakes. Observations of the physical model, under the range of flow conditions tested, show outward spiraling eddies on either side of the channel center, between the upstream cofferdam remnant and the powerhouse. The flow patterns generated by *FastTABS* display a strong agreement with respect to the major eddies observed in the physical model. The velocity vector plot in Figure 7.10 provides an illustration of these eddies in the upstream river section. In both

the physical and the numerical model, the center of these circulating flows are off to the sides of the powerhouse intakes, well out of range for air entrainment problems. The numerical model, as it is defined, does not capture the return currents that occur along the inside faces of the removal area. Figure 5.14 shows the separation and slight return current occurring along the side slope of the cofferdam excavation in the physical model. The results, from Figure 7.10, also indicate that a higher velocity occurs slightly to the right of the centerline. In other words, the right-hand turbine unit consistently receives more of the flow than the left-hand turbine unit. Widening the upstream cofferdam opening towards the right side of the river bend only serves to heighten the difference between the turbine units. The velocity vector plots in Appendix H also show that the flow lines entering the powerhouse are parallel to one another and perpendicular to the powerhouse axis.

7.4 Comparison with 1-D Models

A simplified way of getting hydraulic information for hydrodynamic problems is by using one-dimensional computer models. There are advantages as well as disadvantages when comparing the usage and results of a two-dimensional model like *FastTABS* to a one-dimensional model. The time constraints of this project did not permit a thorough calibration and verification process to be undertaken for a one-dimension model and therefore, only a qualitative comparison can be offered.

Typical one-dimensional or backwater programs are capable of computing water surface profiles in non-prismatic irregular channels under steady-state, subcritical flow conditions. Such programs apply the Standard Step Backwater Method to evaluate the

average velocity, water surface elevation, and the energy losses for each cross-section. The parameters requiring calibration include the Manning's *n*, and expansion, contraction and bend losses. One advantage of a one-dimensional model over the two-dimensional model is that it can provide reasonable results using a relatively simple mathematical process that takes a short computational time. *FastTABS* applies finite-element analysis to calculate the hydraulic solution, and depending on the size and detail of the mesh, it can require a relatively longer computational time. One-dimensional backwater programs also use significantly fewer data to define the model's cross sections. The proximity of the applied boundary conditions to areas of concern can taint the results in the two-dimensional model, whereas a one-dimensional model does not show such sensitivity. Even though both types of models are limited to subcritical flow, the one-dimensional program can assume critical depth in reaches where supercritical flow conditions exist, while *FastTABS* will not converge for such conditions.

There are several areas in which a one-dimensional model is not as attractive as *Fast-TABS*. Although one-dimensional models requires fewer data, more assumptions are necessary to calculate the results. The two-dimensional model offers a plan view of the velocity, water level and Froude number distribution while a one-dimensional model would only provide an average value at each section. The two programs are comparable in that they both require, as well as produce, similar types of information. For example, they both require geometry data and boundary conditions, and they both provide velocity and water surface elevation estimates. One significant difference is that *FastTABS* uses more data in the geometry of the mesh, but it consequently yields a solution with that

much more detail. For the purpose of designing the approach and tailrace channels of a power generating station, *FastTABS* offers greater versatility and usefulness through the detail and distribution of the solution.

The exercise of calibrating, verifying, and executing a one-dimensional backwater model for comparison with the two-dimensional model is supplementary to the goals of this project and can be performed at a future date. It should be noted that there are other one-, two-, and three-dimensional models available that may produce similar and additional information, but many of these may also have significantly more data requirements.

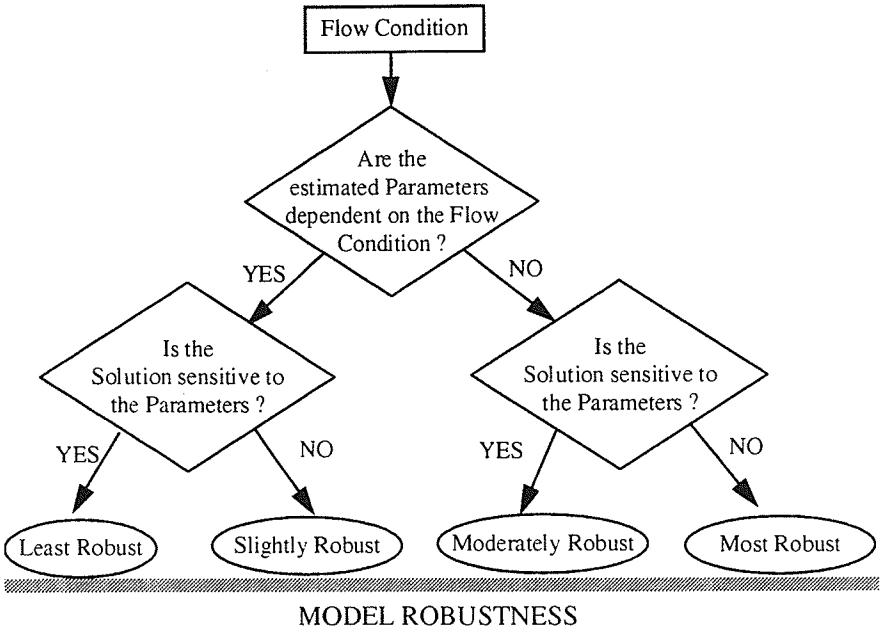

Figure 7.1 *Numerical model robustness as a function of sensitivity to the parameters*

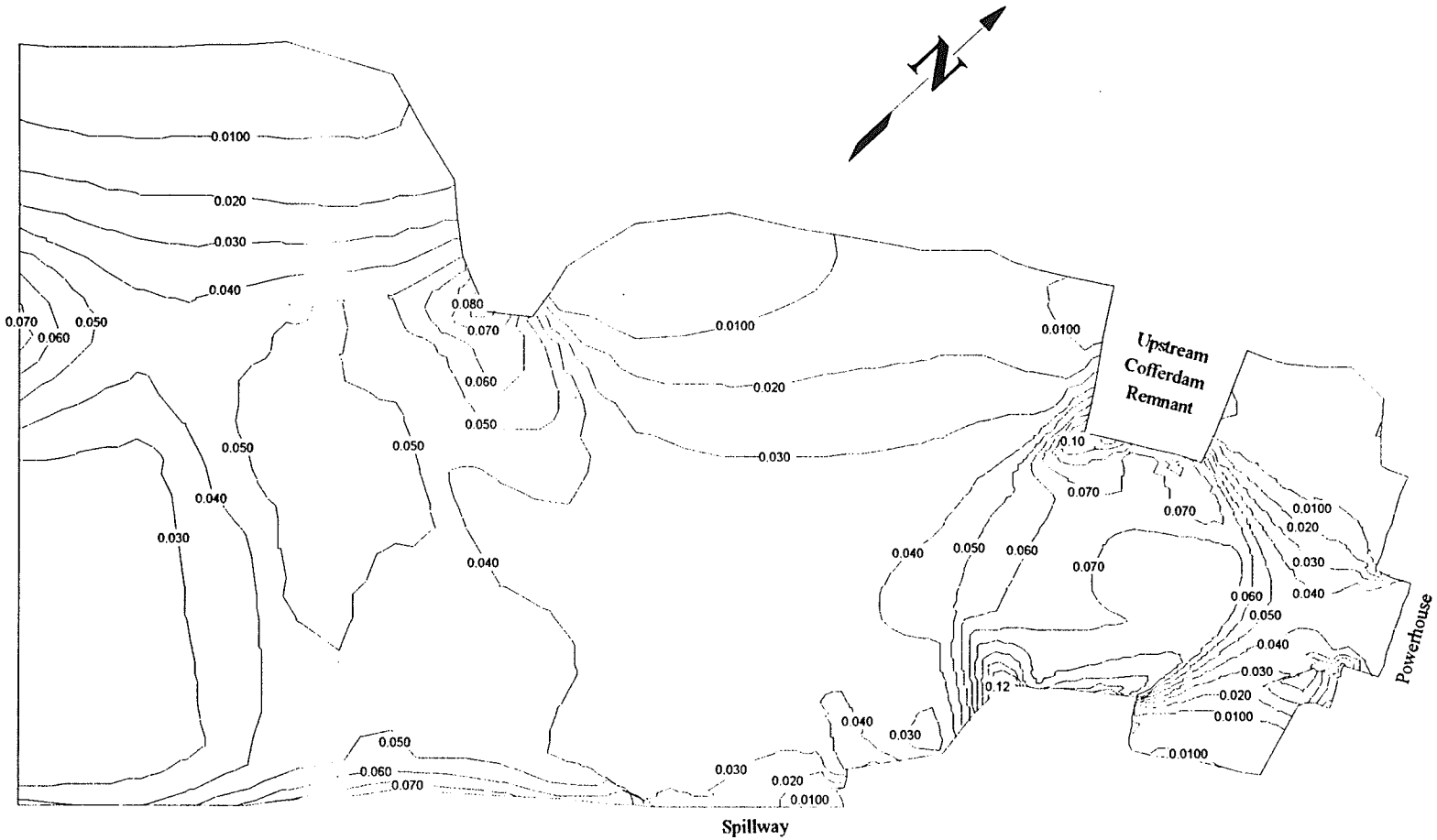

Figure 7.2 Froude Number Contour Plot for Upstream Cofferdam Removal Scheme UC1c

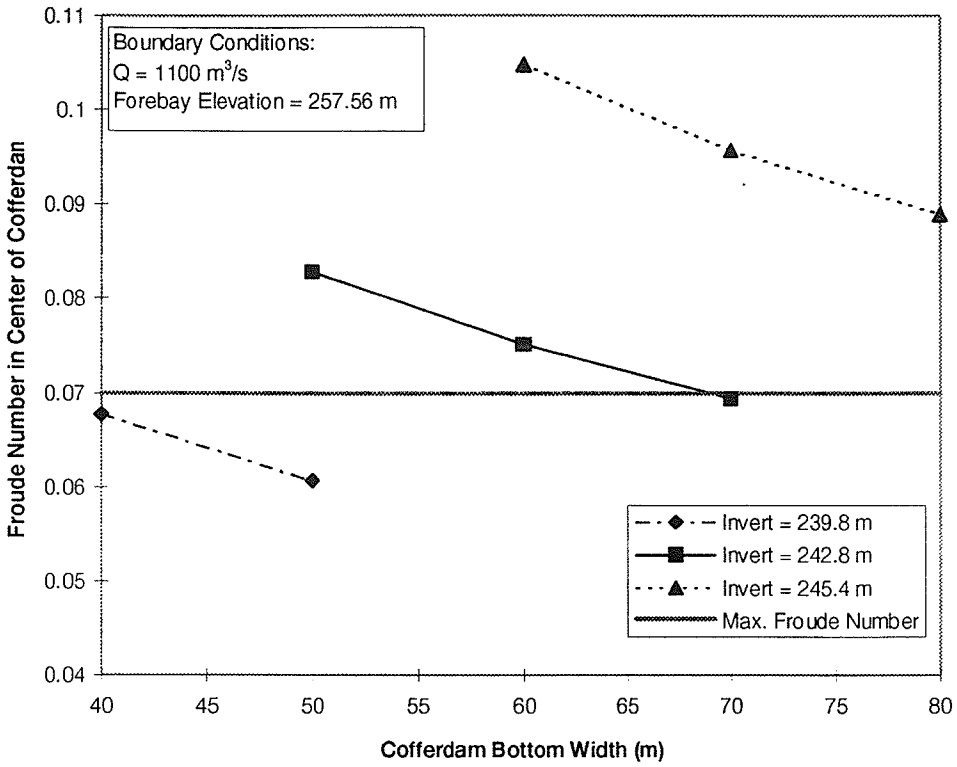

Figure 7.3 *Comparison of Froude number in the upstream cofferdam for various design alternatives, as generated by the numerical model*

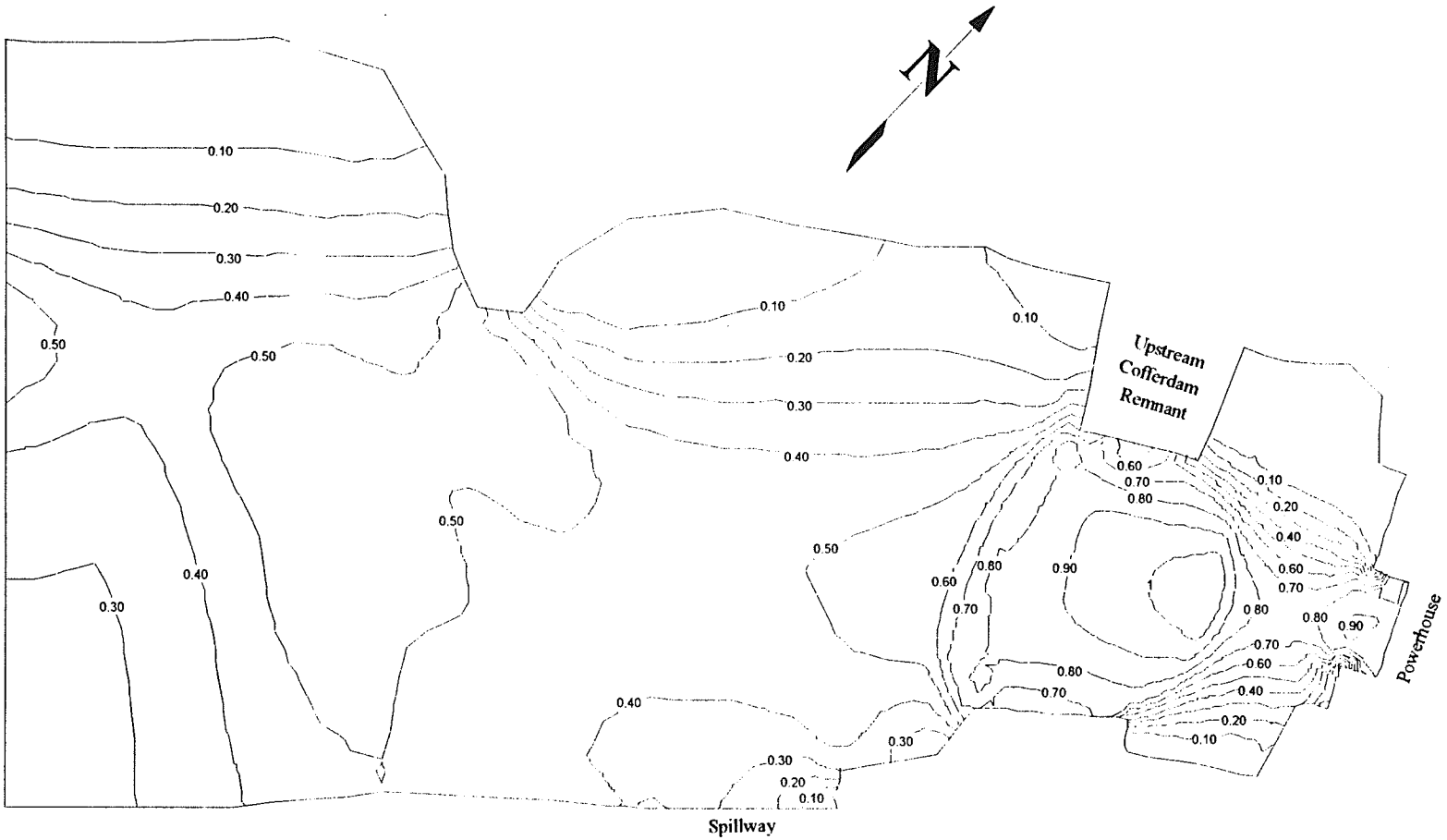

***Figure 7.4** Velocity Contour Plot for Upstream Cofferdam Removal Scheme UC2b*

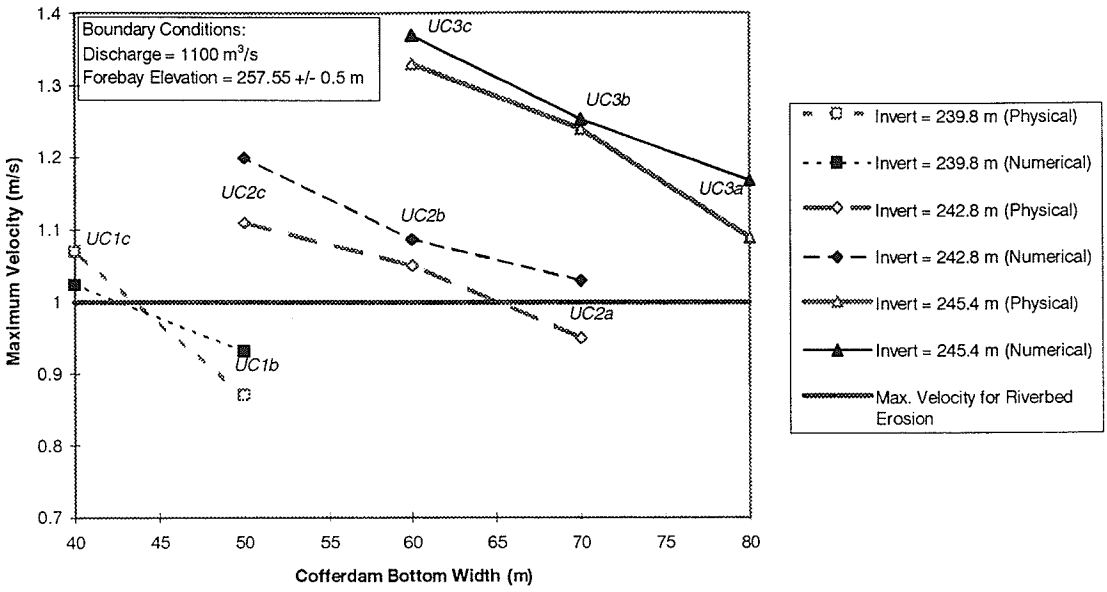

Figure 7.5 *Comparison of the physical and numerical maximum velocity through the upstream cofferdam for various design alternatives*

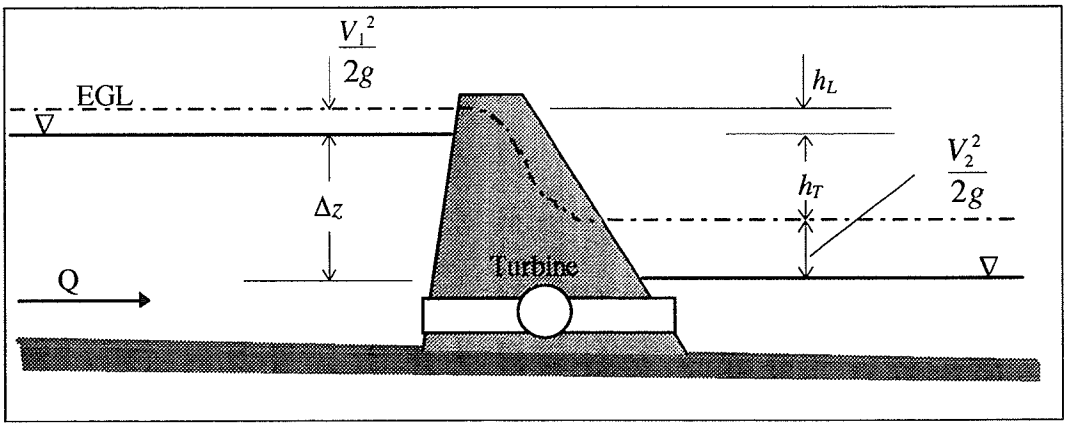

Figure 7.6 *Energy available for a turbine*

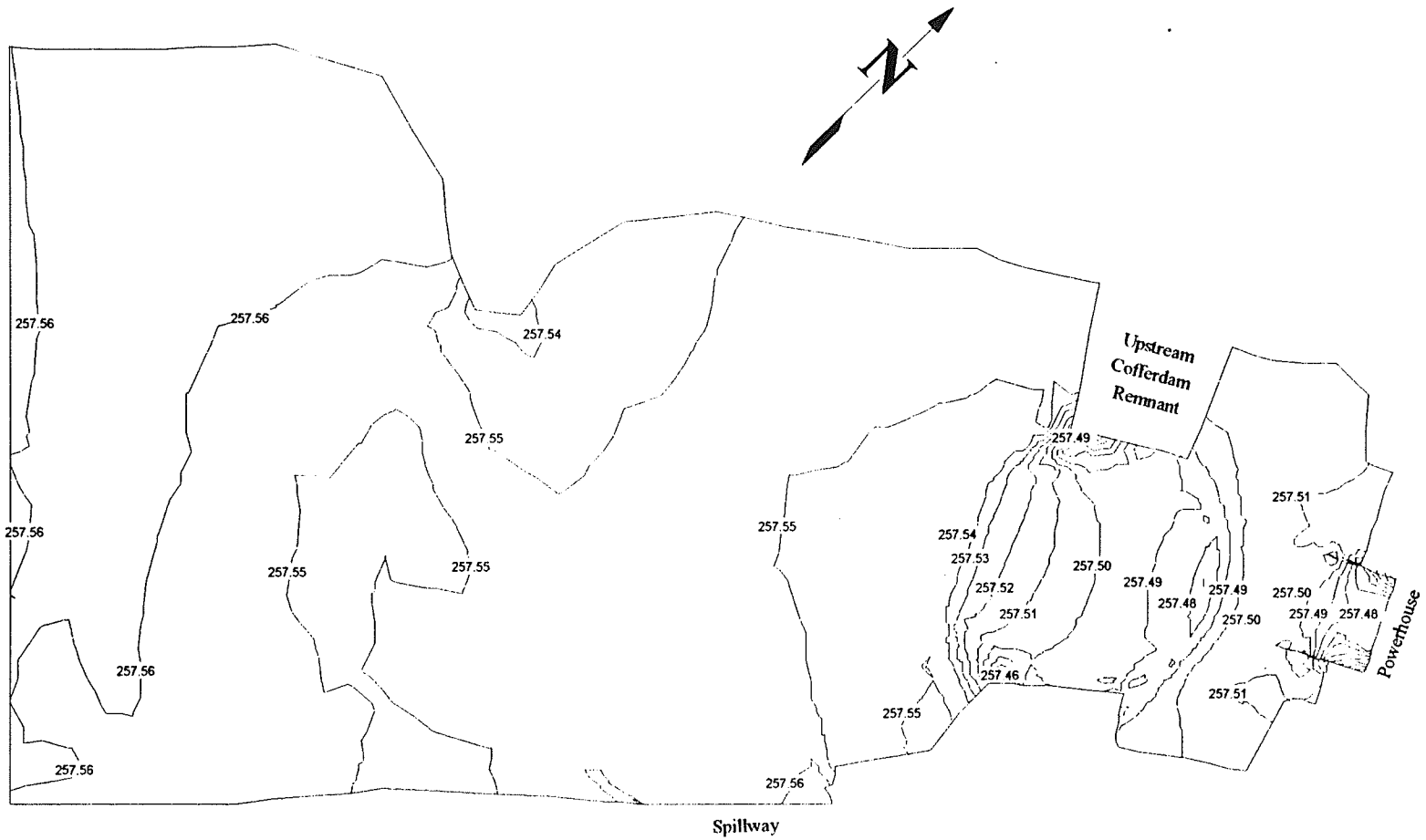

***Figure 7.7** Water Level Contour Plot for Upstream Cofferdam Removal Scheme UC2c*

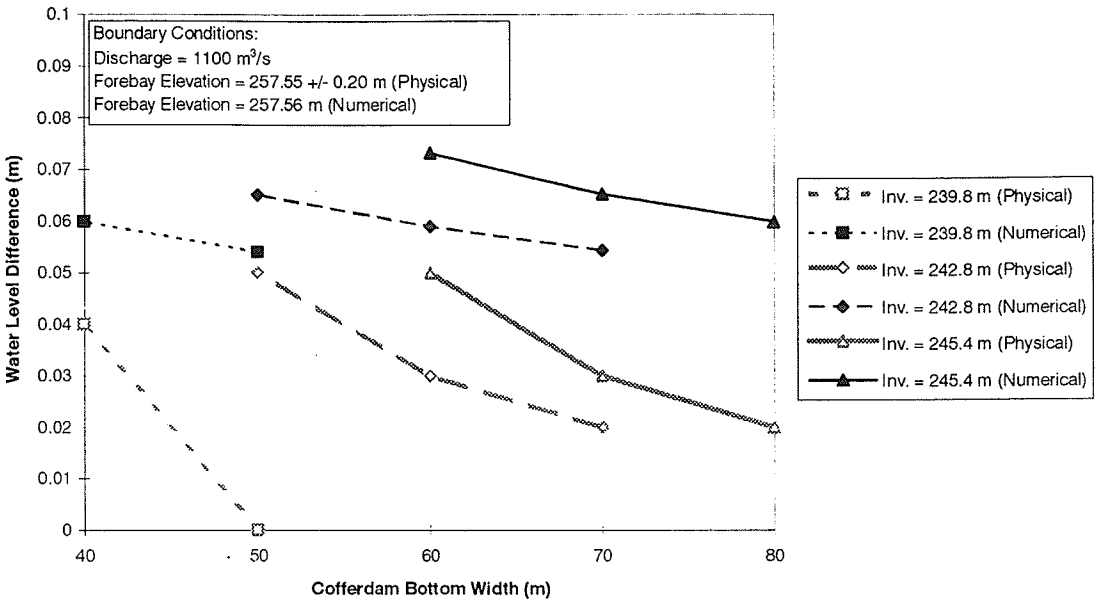

Figure 7.8 Physical and numerical water level difference across the upstream cofferdam for various design alternatives

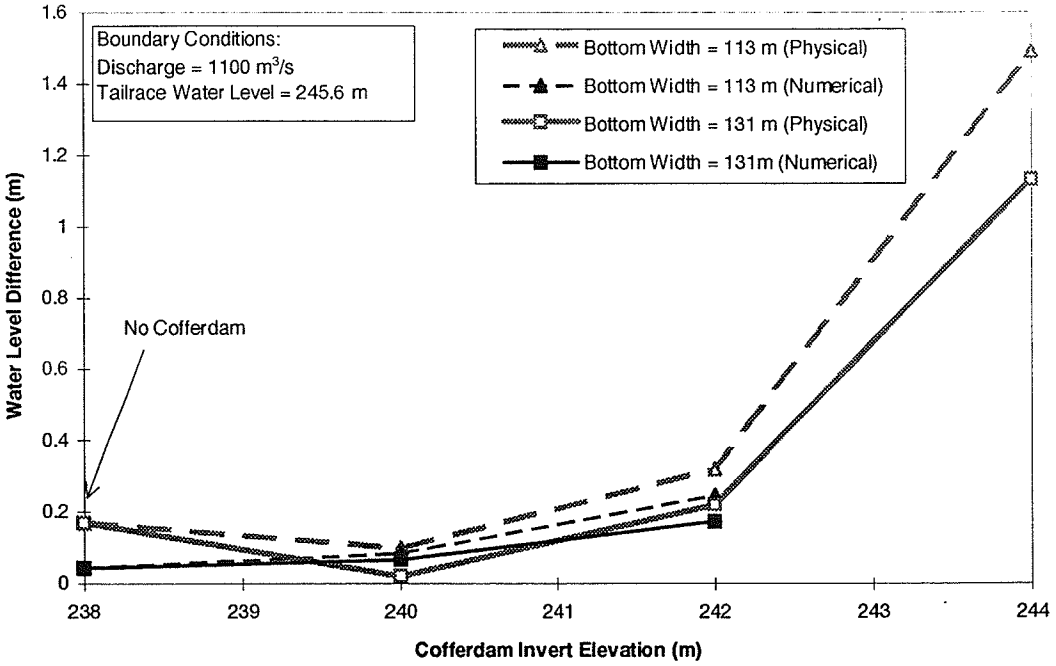

Figure 7.9 Physical and numerical water level difference across the downstream cofferdam for various design alternatives

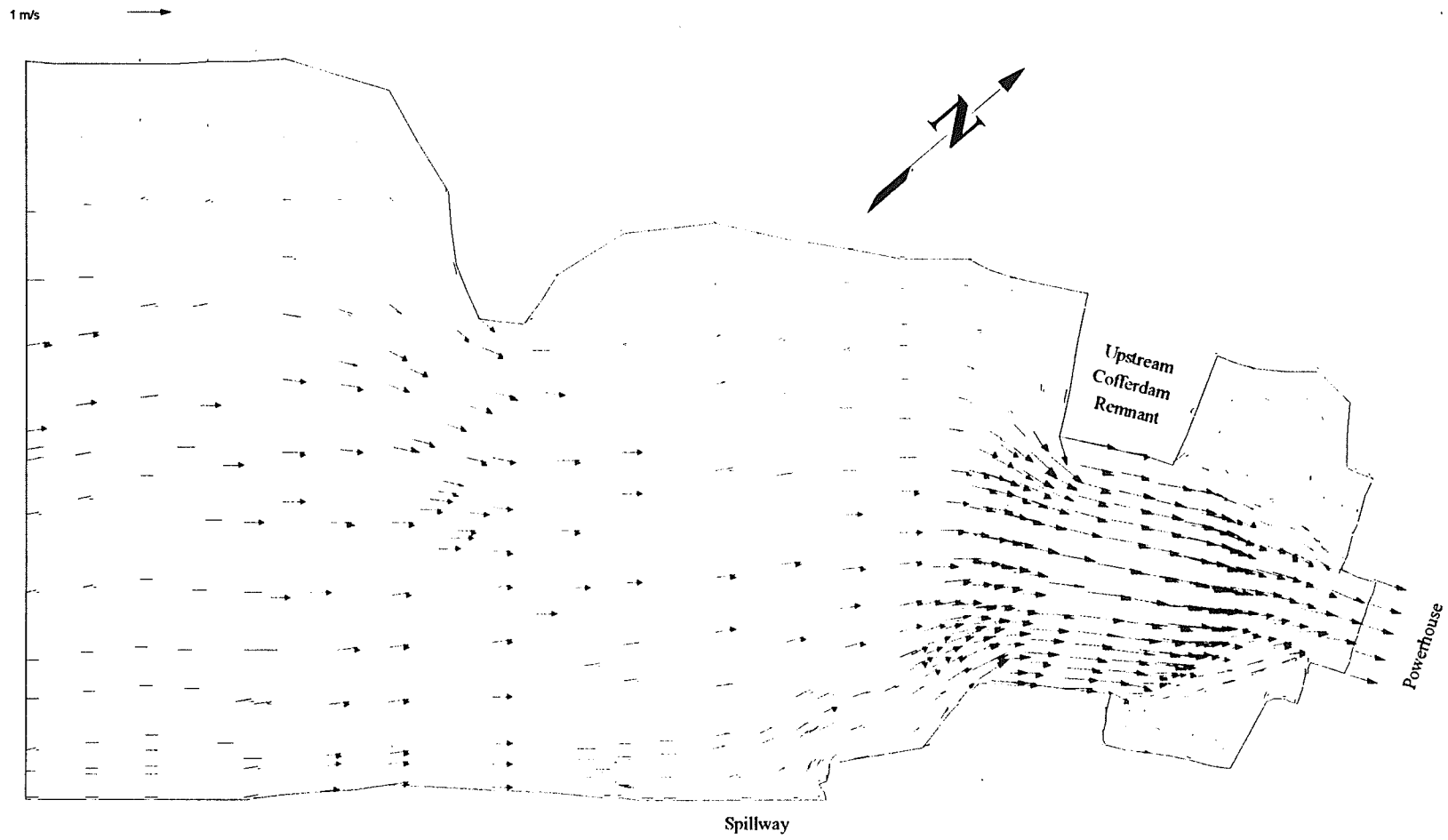

Figure 7.10 *Velocity Vector Plot for Upstream Cofferdam Removal Scheme UC2c*

8. CONCLUSIONS AND RECOMMENDATIONS

8.1 Conclusions

The numerical models of both the upstream and downstream river sections have been developed and calibrated for a range of flow and water level conditions. The use of a physical model provided the basic and necessary information for the development and verification of the numerical model. The numerical model offers greater consistency and precision than could be attained in the physical model, making it useful in the comparison of various design alternatives. Several design alternatives for the approach and tailrace channels were studied and compared with the results from physical modelling. The design alternatives included cofferdam removal alternatives, downstream overburden removal schemes, as well as intake and draft tube transitions. It was also demonstrated that the numerical model could be used to address various issues in the design of powerhouse approach and tailrace channels including ice formation, erosion, head optimization for power production, and flow patterns.

The level of agreement between the two models depended on a number of factors. In the numerical model, the design and construction of the mesh is extremely important for ensuring the viability of the solution. The assignment of appropriate values for the Manning's n and the ε_{ij} coefficient to produce a model capable of a handling a variety of flow and design conditions was achieved with limited success. The assumption of a single ε_{ij} value over the entire model, in order to simplify the calibration and verification process, was part of the reason for some of the discrepancy between the physical and numerical

data. It was shown that, although small changes in the boundary conditions may require potentially different values for the exchange coefficient, using the calibrated model under a specified range of flow conditions would still yield reasonable results. The numerical model offered only limited agreement in zones that were extremely turbulent and characteristically three-dimensional. Furthermore, the model verified the expected result that it would not be able to simulate critical flow scenarios, as was demonstrated for the downstream cofferdam case having an invert of 244 m. The level of agreement between the physical and numerical models is also affected by several limitations within the physical model. The conditions in some portions of the physical model were such that accurate measurements, with the instrumentation available, were not possible. Some approximations were also necessary in terms of the steady-state assumption due to some minor fluctuations in the boundary conditions. The physical model, based on a Froude model scale, could only yield approximate similitude to reality in some zones of the model. In spite of these limitations, the physical and numerical models produced reasonable agreement.

The calibrated numerical model was shown to be applicable for only a small range of boundary conditions. On the other hand, the calibration process did reveal that by using the spinning up technique referred to in Chapter 6, reasonable flow simulations could be obtained for various boundary conditions and design alternatives without requiring a fixed set of calibrated parameters for all scenarios. Thus, the numerical model can be applied to a wider range of flow and water level conditions as well as to study other approach and

tailrace channel design alternatives. Development and usage of such a model requires some expertise and engineering judgment.

8.2 Recommendations

In conducting the tests on both the physical and numerical models, several concerns arose, which the following recommendations address. Although the *FastTABS* program has interactive graphical tools that produce visual plots, there is still some effort and expertise required to produce a quality mesh that not only has sufficient resolution to define the physical surface being modelled, but also has enough resolution to solve for the velocity and water depth gradients on the interior of the mesh. This task is perhaps the most important aspect in the construction of numerical models. It is acknowledged that the meshes used in this project do not meet every quality criterion and also have not been evaluated as to whether or not the level of refinement is sufficient, thereby limiting the accuracy of the solutions in some portions of the mesh. For this reason, the results from these tests should only be considered as good predictions of the general tendencies in the flow hydraulics, and should not be used as exact for specific design applications. It is recommended that there be further investigation into the sensitivity of grid refinement for possible improvements in the results. In using the calibrated numerical model, the values of the calibrated parameters are only applicable within the boundary conditions and design alternatives for which the model was calibrated, for while solutions ranging beyond these limits may be realized, there is no way to verify their validity. As was previously mentioned, boundary conditions and design alternatives beyond the limits tested in this project

can still be investigated experimentally using the spinning up approach, provided that this approach complies with the general guidelines specified for the *FastTABS* program.

Another recommendation, in terms of future physical model studies of a similar nature and purpose as in this project, is to ensure that the geometric scales used to construct the physical model are such that scale effects and instrument limitations are reduced.

Applying the *FastTABS* program to the design of powerhouse approach and tailrace channels is possible, provided that there is a recognition and understanding of the limitations of the numerical model. The program offers efficient and precise estimates of hydraulic flow characteristics that are useful in comparing the relative impact of various design alternatives. In the design of powerhouse approach and tailrace channels, differences in head of as little as 0.01 m can mean significant loss of potential profits. Although the numerical model showed reasonable agreement in the comparison of velocity magnitudes and water level profiles of both the upstream and downstream sections, further mesh refinement and fine-tuning of the parameters would be required to achieve this level of accuracy.

The *FastTABS* program is still a relatively new product to the market of hydraulic computer programs, and as such it is still being upgraded and improved on an ongoing basis. Other hydraulic computational programs are also being developed and it may be beneficial to investigate and compare the capabilities and limitations of such programs to the *FastTABS* program.

LIST OF REFERENCES

Abbott, M.B., and D.R. Bosco (1989). Computational Fluid Dynamics: An Introduction for Engineers, New York, John Wiley and Sons, Inc., 414 p.

BOSS Corporation (1993). BOSS *FastTABS* User's Manual, Brigham Young University Engineering Computer Graphics, Madison, WI.

Cheng, R.T. (1981). "Modeling of tidal and residual circulation in San Francisco Bay, California," Proceedings of the First National U.S. Army Corps of Engineers-Sponsored Seminar on Two-Dimensional Flow Modeling, Davis, California, pp. 172-185.

Chow, Ven Te (1959). Open-Channel Hydraulics, New York, McGraw-Hill Book Company, Inc., 680 p.

Fread, D.L. (1981). "Two-dimensional flow modeling for riverine forecasting by the National Weather Service," Proceedings of the First National U.S. Army Corps of Engineers-Sponsored Seminar on Two-Dimensional Flow Modeling, Davis, California, pp. 9-17.

Grover, P.R. (1989). "Conawapa generating station: intake approach area," Memorandum to M.H. Boase, July 21, 1989, File H10003.37.

Gurule, J.E. (1981). "An approach to hydraulic simulation of complex floodplains," Proceedings of the First National U.S. Army Corps of Engineers-Sponsered Seminar on Two-Dimensional Flow Modeling, Davis, California, pp. 147-155.

Henderson, F.M. (1966). Open Channel Flow, New York, The MacMillan Company, 522 p.

Kells, James A., and C.D. Smith (1988). "Head recovery at submerged abrupt conduit outlets," Canadian Journal of Civil Engineering, 15:272-274.

Lai, C., R.A. Baltzer, and R.W Schaffranek (1980). "Techniques and experiences in the utilization of unsteady open-channel flow models," Proceedings of the Specialty Conference on Computer and Physical Modeling in Hydraulic Engineering, Chicago, Illinios, pp.177-191.

Larock, B.E. (1981). "Two-dimensional turbulent flow simulation," Proceedings of the First National U.S. Army Corps of Engineers-Sponsored Seminar on Two-Dimensional Flow Modeling, Davis, California, pp. 83-91.

Lee, J.K., and D.C. Froehlich (1986). "Review of literature on the finite-element solution of the equations of two-dimensional surface-water flow in the horizontal plane," U.S. Geological Survey Circular 1009, Denver. CO, 60 p.

Lesleighter, E.J. (1983) "Flood plain flow using a two-dimensional numerical simulation," paper presented at the International Conference on the Hydraulic Aspects of Flood and Flood Control, London, England, pp. 207-213.

Liggett, J.A. (1994). Fluid Mechanics, New York, McGraw-Hill, Inc., 495 p.

Manitoba Hydro (1978). Burntwood River Study, Appendix 6 of Report No. SPD-78-14, System Planning Division, Hydro Development Department.

Noble, C., and R.E. Narum (1981). "A two-dimensional flood routing calculation," Proceedings of the First National U.S. Army Corps of Engineers-Sponsored Seminar on Two-Dimensional Flow Modeling, Davis, California, pp. 41-55.

Novak, P., and J. Cábelka (1981). Models in Hydraulic Engineering, London, Pitman Advanced Publishing Program, 459 p.

Östberg, J., and N. Johansson (1992). "Mathematical modelling of flow patterns," paper presented at the 4th International Conference on Hydraulic Engineering Software (*HYDROSOFT '92*), Valencia, Spain. Published in Computer Techniques and Applications, edited by W.R. Blain and E. Cabera, pp. 153-164.

Pariset, E., and R. Hausser (1961). "Formation and evolution of ice covers on rivers," Transactions of the Engineering Institute of Canada, 5(1):41-49.

Patankar, S.V. (1980). Numerical Heat Transfer and Fluid Flow, New York, McGraw-Hill, Inc., 197 p.

Perham, R.E. (1983). "Ice sheet retention structures," CRREL Report 83-30 for the U.S. Army Cold Regions Research and Engineering Laboratory, Hanover, New Hampshire, 33 p.

Pinder. G.F., and W.G. Gray (1977) Finite Element Simulation in Surface and Subsurface Hydrology, New York. Academic Press, 295 p.

Robertson, J.A., and C.T. Crowe (1985). Engineering Fluid Mechanics, 3rd Edition, Boston, Houghton Mifflin Company, 712 p.

Schlichting, H. (1968). Boundary Layer Theory, 6th Edition, New York, McGraw-Hill, 748 p.

Staubli, T., and S. Deniz (1994). "Analyzing draft tube flow kinetics," International Water Power and Dam Construction, 46(12):38-42.

Thomann, R., and J. Mueller (1987). Principles of Surface Water Quality Modeling and Control, New York, Harper & Row, Publishers, 644 p.

United States Department of the Interior, Bureau of Reclamation (1975). Water Measurement Manual, Second edition, Washington.

United States Department of the Interior, Water and Power Resources Service (1980). Hydraulic Laboratory Techniques, Published by U.S. Government Printing Office, Denver, Colorado.

Williams, D.T. (1993). 2-Dimensional Modeling Short Course, presented by WEST Consultants, Inc., sponsored by ASCE Water Resources Planning and Management Division, Seattle, WA.

Yalin, M.S. (1971). Theory of Hydraulic Models, London, The MacMillan Press Ltd., 266 p.

APPENDIX A: COMPARISON OF NUMERICAL MODELS

2-D SURFACE WATER MODELS

CHARACTERISTIC	*FESWMS-2DH*	*FastTABS*
Distributor	WEST Consultants, Inc. 2111 Palomar Airport Rd., Suite 180 Carlsbad, California 92009-1419 (619)-431-8813	Boss Corporation 6612 Mineral Point Rd. Madison, Wisconsin 53705-4220 (800)-488-4775
Contact Person	David T. Williams, Pres.	Patrick Brenzel
Version of Software	Extended System (4000 elements)	Professional (3000 elements) (unlimited available)
Cost (U.S. $)	$995.00	$2500.00 (15% discount for each additional copy)
Computer Requirements	IBM PC 386 MS-DOS (PC-DOS) 2.1 Math coprocessor at least 6 Mbytes RAM	IBM PC 386 (or Macintosh) also available for UNIX MS-WINDOWS 3.1 Math coprocessor at least 6 Mbytes RAM
Programs	*DINMOD* -data input module preprocessor *FLOMOD* -depth averaged flow module *ANOMOD* -analysis of output Also: Menu system, Data input program, full-screen editor, plotting, support utilities	*GEFGEN* -geometrical pre-processor *RMA-2* 2-D depth averaged finite-element program *RMA-4* -contaminant transport *FastTABS* -graphical pre- and post-processor

CHARACTERISTIC	*FESWMS-2DH*	*FastTABS*
Applications:		
River, harbour, estuary	x	x
Irregular floodplains	x	x
Split flows	x	x
Multi-opening bridge crossings	x	x
Weir flow	x	N.A.[1]
Culverts (source,sink)	x	N.A.
Contaminant transport	N.A.	x
Tidal cycles (wet/dry)	x	x
Sediment Transport	N.A.	N.A.
Unit System:		
English	x	x
Metric	x	x
Hydrology:		
Steady-state	x	x
Transient (dynamic)	x	x
Flow conditions:		
Subcritical	x	x
Supercritical	x	N.A.
Weir flow	x	N.A.
Pressure flow	x	N.A.
Weir + Pressure flow	x	N.A.
Element configuration:		
Linear triangles	x	x
Quadratic (6 node) triangles	x	x
Linear Quadrilaterals	x	x
Quadratic (8 node) quad's	x	x
Lagrangian (9) quadrilaterals	x	N.A.
Curved sided elements	x	N.A.
Methodology:		
Galerkin Finite Element	x	x
Integration by Gaussian Quadrature	x	x
Newton iteration	x	x
Method of Weighted Residuals	x	x
Depth-avg momentum + mass eqn's	x	x
Resequencing:		
Minimum Frontgrowth Method	x	x
Level Structure Method	x	x

[1] N.A. = not available.

CHARACTERISTIC	*FESWMS-2DH*	*FastTABS*
Material Properties, Coefficients, Parameters:		
Manning's *n*	x	x
Chezy *C*	x	N.A.
Eddy viscosity or turbulent exchange coefficient	x	x
Coriolis Parameter , Ω	x	optional
Fluid density,ρ	x	optional
Bed and surface shear stresses	x	x
Momentum correction coefficient	x	N.A.
Wind velocity, direction	x	optional
Water Temperature	N.A.	x
Output or Results:		
Depth averaged velocities	x	x
Flow depth	x	x
Water surface elevation	x	x
Flow checks	x	optional
Froude number	x	N.A.
Energy head	x	N.A.
Continuity norms	x	N.A.
Residual error	N.A.	N.A.
Concentration (pollutant or sediment)	N.A.	x
Deposition rate	N.A.	N.A.
Time-history report (vel.,flow,stage)	x	x
Graphical Output:		
Finite Element mesh	x	x
Vector Plots:		
Velocity	x	x
Unit flow	x	N.A.
Vector Size options	N.A.	x
Contour (Isoline) Plots:		
Ground elevation	x	x
Water surface elevation	x	x
Velocity magnitude	x	x
Total energy head	x	N.A.
Froude number	x	x
Differences in 2 simulations	x	N.A.
Time-history plots	x	x
Contour (colour fill)	N.A.	x
Animation	N.A.	x

COMMENTS

FESWMS-2DH

BENEFITS:

able to handle a wider variety of factors and conditions; and

uses elements with nodes in the centre which provide a much more accurate interpolation of values within an element.

DISADVANTAGES:

poor graphical interaction and manipulation;

difficult to execute because all the information needs to be typed in;

when program fails, it is difficult to determine why failure occurred (poor error tracing); and

may import *FastTABS* data but not easily done.

FUTURE POSSIBILITES:

possibly contaminant and sediment transport modelling.

COMMENTS

FastTABS

BENEFITS:

easy to set up element mesh using a graphical display rather than a table of node points;

a variety of mesh generation and interactive editing tools available;

excellent interaction and use of graphical display;

easy to use because it is based on a *WINDOWS* application;

can import *FESWMS-2DH* data; and

excellent support staff at BOSS Corporation.

DISADVANTAGES:

limited application (cannot model supercritical flow conditions, some weirs, or pressure flow problems);

bottom slope in direction parallel to flow needs to be less than 1:10 for mild slope assumption; and

RMA-4 does not model temperature or salinity (for estuary studies).

FUTURE POSSIBILITIES:

3-D sediment transport model is being developed. This model is a separate module that uses the *FastTABS* interface. It may also be able to model temperature and salinity;

boundary conditions will be dialogue driven;

interaction with Autocad software; and

improved meshing algorythm.

NOTE: *FastTABS* is constantly being improved and any upgrades released during the first year after purchase are sent to the user.

APPENDIX B: TABLES OF THE OVERBURDEN

1.) Manning's Roughness Coefficients, *n*

2.) Grainsize Distribution of Overburden and Riprap Material in the Physical Model

TABLE B-1 VALUES FOR THE COMPUTATION OF THE ROUGHNESS COEFFICIENT BY EQ. $n = (n_0 + n_1 + n_2 + n_3 + n_4)m_5$ (Chow, 1959)

Channel conditions		Values	
Material involved	Earth	n_0	0.020
	Rock cut		0.025
	Fine gravel		0.024
	Coarse gravel		0.028
Degree of irregularity	Smooth	n_1	0.000
	Minor		0.005
	Moderate		0.010
	Severe		0.020
Variations of channel cross section	Gradual	n_2	0.000
	Alternating occasionally		0.005
	Alternating frequently		0.010–0.015
Relative effect of obstructions	Negligible	n_3	0.000
	Minor		0.010–0.015
	Appreciable		0.020–0.030
	Severe		0.040–0.060
Vegetation	Low	n_4	0.005–0.010
	Medium		0.010–0.025
	High		0.025–0.050
	Very high		0.050–0.100
Degree of meandering	Minor	m_5	1.000
	Appreciable		1.150
	Severe		1.300

TABLE B-1 VALUES OF THE ROUGHNESS COEFFICIENT n
(Boldface figures are values generally recommended in design)

Type of channel and description	Minimum	Normal	Maximum
A. CLOSED CONDUITS FLOWING PARTLY FULL			
A-1. Metal			
a. Brass, smooth	0.009	**0.010**	0.013
b. Steel			
1. Lockbar and welded	0.010	0.012	0.014
2. Riveted and spiral	0.013	0.016	0.017
c. Cast iron			
1. Coated	0.010	0.013	0.014
2. Uncoated	0.011	0.014	0.016
d. Wrought iron			
1. Black	0.012	0.014	0.015
2. Galvanized	0.013	0.016	0.017
e. Corrugated metal			
1. Subdrain	0.017	0.019	0.021
2. Storm drain	0.021	**0.024**	0.030
A-2. Nonmetal			
a. Lucite	0.008	0.009	0.010
b. Glass	0.009	**0.010**	0.013
c. Cement			
1. Neat, surface	0.010	0.011	0.013
2. Mortar	0.011	0.013	0.015
d. Concrete			
1. Culvert, straight and free of debris	0.010	0.011	0.013
2. Culvert with bends, connections, and some debris	0.011	**0.013**	0.014
3. Finished	0.011	0.012	0.014
4. Sewer with manholes, inlet, etc., straight	0.013	0.015	0.017
5. Unfinished, steel form	0.012	0.013	0.014
6. Unfinished, smooth wood form	0.012	**0.014**	0.016
7. Unfinished, rough wood form	0.015	0.017	0.020
e. Wood			
1. Stave	0.010	0.012	0.014
2. Laminated, treated	0.015	0.017	0.020
f. Clay			
1. Common drainage tile	0.011	**0.013**	0.017
2. Vitrified sewer	0.011	0.014	0.017
3. Vitrified sewer with manholes, inlet, etc.	0.013	0.015	0.017
4. Vitrified subdrain with open joint	0.014	0.016	0.018
g. Brickwork			
1. Glazed	0.011	0.013	0.015
2. Lined with cement mortar	0.012	0.015	0.017
h. Sanitary sewers coated with sewage slimes, with bends and connections	0.012	0.013	0.016
i. Paved invert, sewer, smooth bottom	0.016	0.019	0.020
j. Rubble masonry, cemented	0.018	0.025	0.030

TABLE B-1 VALUES OF THE ROUGHNESS COEFFICIENT n (*continued*)

Type of channel and description	Minimum	Normal	Maximum
B. LINED OR BUILT-UP CHANNELS			
B-1. Metal			
a. Smooth steel surface			
1. Unpainted	0.011	**0.012**	0.014
2. Painted	0.012	0.013	0.017
b. Corrugated	0.021	0.025	0.030
B-2. Nonmetal			
a. Cement			
1. Neat, surface	0.010	0.011	0.013
2. Mortar	0.011	0.013	0.015
b. Wood			
1. Planed, untreated	0.010	0.012	0.014
2. Planed, creosoted	0.011	0.012	0.015
3. Unplaned	0.011	0.013	0.015
4. Plank with battens	0.012	0.015	0.018
5. Lined with roofing paper	0.010	0.014	0.017
c. Concrete			
1. Trowel finish	0.011	**0.013**	0.015
2. Float finish	0.013	0.015	0.016
3. Finished, with gravel on bottom	0.015	0.017	0.020
4. Unfinished	0.014	0.017	0.020
5. Gunite, good section	0.016	0.019	0.023
6. Gunite, wavy section	0.018	0.022	0.025
7. On good excavated rock	0.017	0.020	
8. On irregular excavated rock	0.022	0.027	
d. Concrete bottom float finished with sides of			
1. Dressed stone in mortar	0.015	0.017	0.020
2. Random stone in mortar	0.017	0.020	0.024
3. Cement rubble masonry, plastered	0.016	0.020	0.024
4. Cement rubble masonry	0.020	0.025	0.030
5. Dry rubble or riprap	0.020	0.030	0.035
e. Gravel bottom with sides of			
1. Formed concrete	0.017	0.020	0.025
2. Random stone in mortar	0.020	0.023	0.026
3. Dry rubble or riprap	0.023	0.033	0.036
f. Brick			
1. Glazed	0.011	**0.013**	0.015
2. In cement mortar	0.012	**0.015**	0.018
g. Masonry			
1. Cemented rubble	0.017	0.025	0.030
2. Dry rubble	0.023	0.032	0.035
h. Dressed ashlar	0.013	0.015	0.017
i. Asphalt			
1. Smooth	0.013	0.013	
2. Rough	0.016	0.016	
j. Vegetal lining	0.030	.....	0.500

TABLE B-1 VALUES OF THE ROUGHNESS COEFFICIENT n (*continued*)

Type of channel and description	Minimum	Normal	Maximum
C. EXCAVATED OR DREDGED			
a. Earth, straight and uniform			
1. Clean, recently completed	0.016	0.018	0.020
2. Clean, after weathering	0.018	**0.022**	0.025
3. Gravel, uniform section, clean	0.022	0.025	0.030
4. With short grass, few weeds	0.022	0.027	0.033
b. Earth, winding and sluggish			
1. No vegetation	0.023	0.025	0.030
2. Grass, some weeds	0.025	0.030	0.033
3. Dense weeds or aquatic plants in deep channels	0.030	0.035	0.040
4. Earth bottom and rubble sides	0.028	0.030	0.035
5. Stony bottom and weedy banks	0.025	0.035	0.040
6. Cobble bottom and clean sides	0.030	0.040	0.050
c. Dragline-excavated or dredged			
1. No vegetation	0.025	0.028	0.033
2. Light brush on banks	0.035	0.050	0.060
d. Rock cuts			
1. Smooth and uniform	0.025	0.035	0.040
2. Jagged and irregular	0.035	0.040	0.050
e. Channels not maintained, weeds and brush uncut			
1. Dense weeds, high as flow depth	0.050	0.080	0.120
2. Clean bottom, brush on sides	0.040	0.050	0.080
3. Same, highest stage of flow	0.045	0.070	0.110
4. Dense brush, high stage	0.080	0.100	0.140
D. NATURAL STREAMS			
D-1. Minor streams (top width at flood stage <100 ft)			
a. Streams on plain			
1. Clean, straight, full stage, no rifts or deep pools	0.025	**0.030**	0.033
2. Same as above, but more stones and weeds	0.030	0.035	0.040
3. Clean, winding, some pools and shoals	0.033	0.040	0.045
4. Same as above, but some weeds and stones	0.035	0.045	0.050
5. Same as above, lower stages, more ineffective slopes and sections	0.040	0.048	0.055
6. Same as 4, but more stones	0.045	0.050	0.060
7. Sluggish reaches, weedy, deep pools	0.050	0.070	0.080
8. Very weedy reaches, deep pools, or floodways with heavy stand of timber and underbrush	0.075	0.100	0.150

TABLE B-1 VALUES OF THE ROUGHNESS COEFFICIENT n (*continued*)

Type of channel and description	Minimum	Normal	Maximum
b. Mountain streams, no vegetation in channel, banks usually steep, trees and brush along banks submerged at high stages			
1. Bottom: gravels, cobbles, and few boulders	0.030	0.040	0.050
2. Bottom: cobbles with large boulders	0.040	0.050	0.070
D-2. Flood plains			
a. Pasture, no brush			
1. Short grass	0.025	0.030	0.035
2. High grass	0.030	0.035	0.050
b. Cultivated areas			
1. No crop	0.020	0.030	0.040
2. Mature row crops	0.025	0.035	0.045
3. Mature field crops	0.030	0.040	0.050
c. Brush			
1. Scattered brush, heavy weeds	0.035	0.050	0.070
2. Light brush and trees, in winter	0.035	0.050	0.060
3. Light brush and trees, in summer	0.040	0.060	0.080
4. Medium to dense brush, in winter	0.045	0.070	0.110
5. Medium to dense brush, in summer	0.070	0.100	0.160
d. Trees			
1. Dense willows, summer, straight	0.110	0.150	0.200
2. Cleared land with tree stumps, no sprouts	0.030	0.040	0.050
3. Same as above, but with heavy growth of sprouts	0.050	0.060	0.080
4. Heavy stand of timber, a few down trees, little undergrowth, flood stage below branches	0.080	0.100	0.120
5. Same as above, but with flood stage reaching branches	0.100	0.120	0.160
D-3. Major streams (top width at flood stage >100 ft). The n value is less than that for minor streams of similar description, because banks offer less effective resistance.			
a. Regular section with no boulders or brush	0.025	.....	0.060
b. Irregular and rough section	0.035	.....	0.100

FIGURE B-1 NOTIGI G.S. MODEL GRAIN SIZE DISTRIBUTION CONVERTED TO PROTOTYPE VALUES

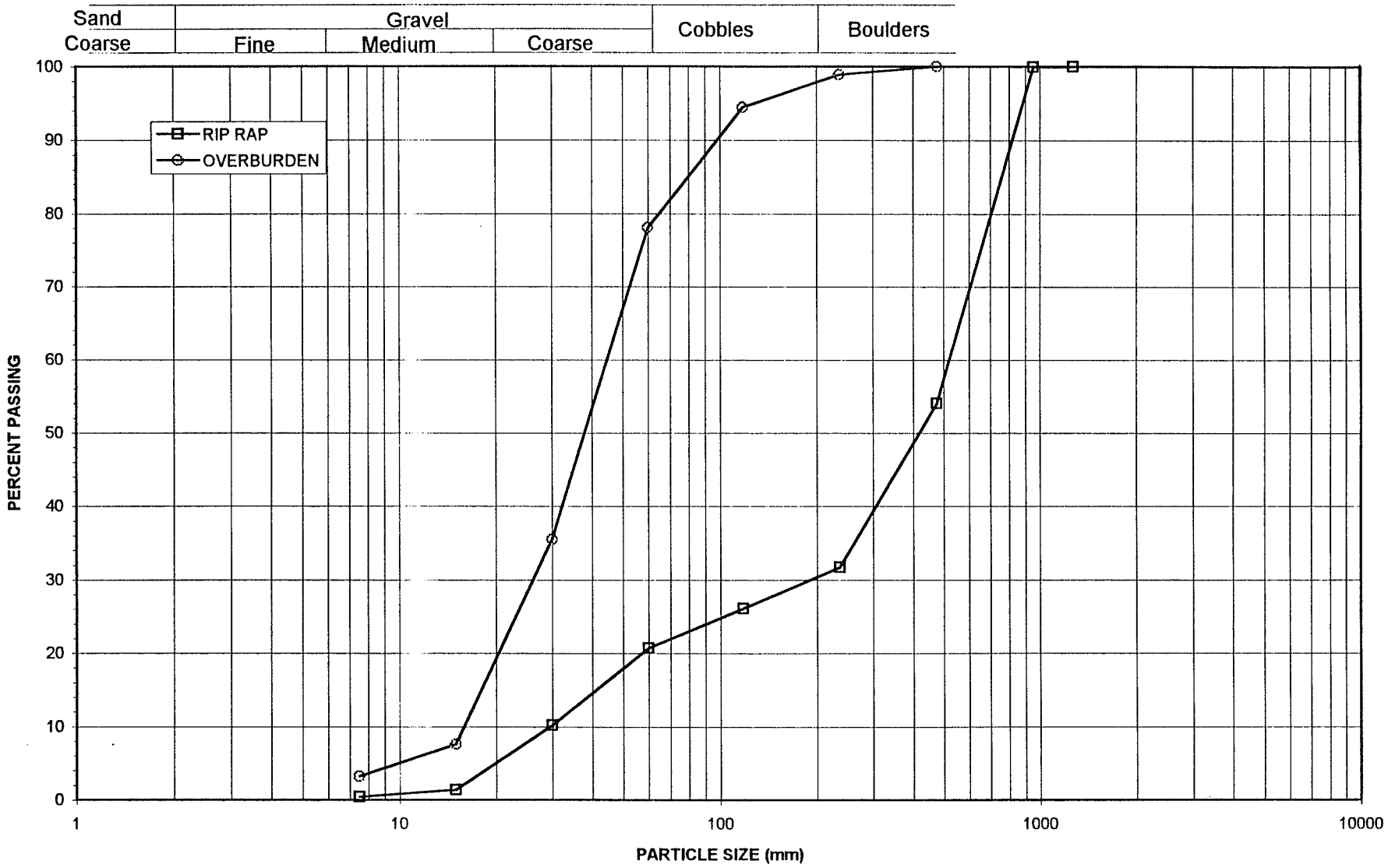

APPENDIX C: DOWNSTREAM PHYSICAL MODEL TEST RESULTS

The downstream tests are each summarized on a separate sheet identifying the particular design alternative and the boundary conditions.
All measurements are in prototype scale.
Included in each test summary are the following:

1. Date and time of test.
2. Boundary conditions: flow and water levels at model boundaries.
3. Comments.
4. Data measurements
   a) columns 1 and 2 give *x* and *y* reference coordinates for the data measurements
   b) columns 3 and 4 give velocities at 0.2 depth and 0.8 depth when depths are greater than 8 m.
   c) column 5 is the velocity at 0.6 depth for depths less than 8 m.
   d) column 6 shows the depth-averaged velocity at that point
   e) column 7 gives an approximate measurement of the direction of flow, measured counter clockwise to the longitudinal x-axis.
   f) columns 8 and 9 provide the calculated *x* and *y* velocities.
   g) column 10 gives an approximate measurement of the depth used to determine the depth for velocity measurements
   h) column 11 shows the water surface elevation measurements taken with the mobile point gauge at several different points. The measurements were conducted AFTER the velocity measurements.

TEST	DESIGN DESCRIPTION		BOUNDARY CONDITION	
	Invert (m)	Bottom width (m)	Flow	d/s WSEL
DOB	no cofferdam		FGD	245.5
DOB1	"		"	"
DOB2	"		"	"
DC1a	244	121 (113)	"	"
DC2a	242	112.5 (113)	"	"
DC3a	240	105.5 (113)	"	"
DC1b	244	139.1 (131)	"	"
DC2b	242	131 (131)	"	"
DC3b	240	123.5 (131)	"	"
DC3a	240	105.5 (113)	867	244.5
TR0 vs. TR3:1	240	105.5 (113)	FGD	245.5

where: FGD = 1100 m^3/s

Downstream Physical Model Tests

FULL TEST

Date: Sep 23/94
Time (start / finish): 8:15 am - 6:45 pm

Flow (cms): 1100.00
Upstream WSEL (m): 259.77
Downstream WSEL (m): 245.5
PH 1,2 WSEL (m): 245.47, 245.45

No Cofferdam

Description/Comments: - 3rd test with DOB, TR3:1, no riprap along leading edge of overburden
- overburden fixed by applying cement coating to prevent erosion
- no wsel data other than boundary conditions given above
- test used for numerical model calibration

*** Units are converted to proto type scale ***

Velocity - mini probe readings

Coordinates X	Y	0.2 d (m/s)	0.8 d (m/s)	0.6 d (m/s)	Average (m/s)	Angle (ccw-x) (degrees)	X-vel (m/s)	Y-vel (m/s)	Depth, d (m)
45	-110.5	0.918	1.996		**1.457**	28	1.287	0.684	14.5
47	-129	0.649	1.762		**1.205**	12	1.179	0.251	15.17
56	-93	0.579	0.681		**0.630**	26	0.566	0.276	9.44
57	-146	0.000	1.996		**0.998**	-2	0.998	-0.035	13.38
69	-109	1.053	1.862		**1.457**	15	1.408	0.377	9.32
70	-125	0.918	1.969		**1.444**	8	1.430	0.201	10.11
72	-160	0.729	1.902		**1.316**	-25	1.193	-0.556	8.3
77	-86			1.363	**1.363**	26	1.225	0.597	5.7
78	-142	0.864	1.835		**1.349**	-1	1.349	-0.024	9.36
80	-151.2	0.676	1.848		**1.262**	-8	1.250	-0.176	8.56
80	-160			1.727	**1.727**	-26	1.552	-0.757	5.67
80	-174			1.403	**1.403**	-38	1.106	-0.864	shallow
92	-163			2.185	**2.185**	-26	1.964	-0.958	4.32
93	-74	0.720	0.436		**0.578**	23	0.532	0.226	6.68
94.4	-192			0.783	**0.783**	-35	0.642	-0.449	shallow
98.4	-148.8			1.821	**1.821**	-16	1.751	-0.502	5.76
101	-101	1.320	1.277		**1.298**	10	1.279	0.225	7.52
101	-120	1.943	1.867		**1.905**	0	1.905	0.000	7.25
103	-132	1.654	1.743		**1.699**	-1	1.698	-0.030	7.35
110	-170			1.794	**1.794**	-25	1.626	-0.758	4.52
116	-146.4			1.549	**1.549**	-11	1.520	-0.296	5.82
120	-72	0.000	0.000		**0.000**	16	0.000	0.000	7.14
125	-91	1.242	0.738		**0.990**	2	0.989	0.035	7.89
127	-110	1.584	1.525		**1.554**	-5	1.548	-0.135	8.08
128	-212.83			0.956	**0.956**	-36	0.773	-0.562	2.46
132	-130	1.597	1.339		**1.468**	-7	1.457	-0.179	7.7
146	-185			1.708	**1.708**	-28	1.508	-0.802	3.56
161	-25			0.000	**0.000**	0	0.000	0.000	
167.6	-36			0.000	**0.000**	0	0.000	0.000	
171.2	-153.6			1.306	**1.306**	-18	1.242	-0.404	5.98
176	-56.4			0.000	**0.000**	0	0.000	0.000	
182	-130			1.538	**1.538**	-13	1.499	-0.346	7.38
182.2255	-261.299			0.496	**0.496**	-57	0.270	-0.416	shallow
184	-104			1.069	**1.069**	-17	1.022	-0.313	7.57
184.5	-209			1.457	**1.457**	-40	1.116	-0.937	3.74
186	-79			0.000	**0.000**	0	0.000	0.000	7.4
189.6	-277.2			0.000	**0.000**	0	0.000	0.000	shallow
194	-178			1.250	**1.250**	-36	1.011	-0.735	4.68
194	-211			1.560	**1.560**	-34	1.293	-0.872	3.02
196	-160			1.341	**1.341**	-21	1.252	-0.481	6.52
197	-136			1.463	**1.463**	-24	1.336	-0.595	7.37
201.2	-282			0.494	**0.494**	-65	0.209	-0.448	shallow
202	-112			1.177	**1.177**	-16	1.131	-0.324	7.96
205	-181			1.320	**1.320**	-37	1.054	-0.794	4.63
210	-163			1.347	**1.347**	-22	1.249	-0.505	6.53
214	-84			0.000	**0.000**	0	0.000	0.000	7.1
220	-223			1.215	**1.215**	-38	0.957	-0.748	4.55
222	-144			1.385	**1.385**	-28	1.222	-0.650	7.3
228	-55			0.000	**0.000**	0	0.000	0.000	
233	-124			1.199	**1.199**	-25	1.086	-0.507	7.88

Downstream Physical Model Tests

Velocity - mini probe readings									
Coordinates		0.2 d	0.8 d	0.6 d	Average	Angle (ccw-x)	X-vel	Y-vel	Depth, d
X	Y	(m/s)	(m/s)	(m/s)	(m/s)	(degrees)	(m/s)	(m/s)	(m)
240	-240			1.331	**1.331**	-48	0.890	-0.989	4.48
244	-91			0.000	**0.000**	0	0.000	0.000	
244.3907	-355.109			0.402	**0.402**	-63	0.182	-0.358	shallow
247.2	-183.6			1.339	**1.339**	-38	1.055	-0.824	6.38
252	-60			0.000	**0.000**	0	0.000	0.000	
252	-269			1.390	**1.390**	-54	0.817	-1.124	3.73
260	-154			1.317	**1.317**	-43	0.963	-0.898	7.42
273.6	-217.2			1.201	**1.201**	-48	0.804	-0.893	5.55
274	-125			0.796	**0.796**	-39	0.619	-0.501	7.39
288	-96			0.000	**0.000**	0	0.000	0.000	
291.9213	-206.013			1.252	**1.252**	-50	0.805	-0.959	7.08
296	-62.4			0.000	**0.000**	0	0.000	0.000	
298.4	-255.2			1.204	**1.204**	-53	0.725	-0.961	5.58
312	-185			1.177	**1.177**	-54	0.692	-0.952	7.66
319.2	-355.2			1.147	**1.147**	-87	0.060	-1.146	6.1
331	-246			1.155	**1.155**	-54	0.679	-0.935	7.95
336	-163			0.341	**0.341**	-54	0.201	-0.276	7.78
355	-355.2			1.174	**1.174**	-90	0.000	-1.174	8.52
360	-140			0.000	**0.000**	0	0.000	0.000	
367	-235			0.845	**0.845**	-67	0.330	-0.778	7.94
382	-120			0.000	**0.000**	0	0.000	0.000	
386	-355.2			1.064	**1.064**	-99	-0.166	-1.051	8.22
406.4	-94.8			0.000	**0.000**	0	0.000	0.000	
408	-223			0.000	**0.000**	0	0.000	0.000	
408	-355.2			0.837	**0.837**	-112	-0.314	-0.776	7.74
450	-215			0.000	**0.000**	0	0.000	0.000	
476	-204			0.000	**0.000**	0	0.000	0.000	

Downstream Physical Model Tests

PARTIAL TEST

Date: Sep 29/94
Time (start / finish): 8:45 am -

Flow (cms): 1100.00
Upstream WSEL (m): 259.6
Downstream WSEL (m): 245.5
PH 1,2 WSEL (m): 245.47, 245.41

No Cofferdam

Description/Comments: - test with DOB1, overburden removed to 1/3 the distance to the d/s cofferdam, down to invert 231 m
- overburden in the removal area fixed by applying cement coating to prevent erosion
- test used for numerical model verification

*** Units are converted to proto type scale ***

Coordinates X	Coordinates Y	Velocity - mini probe readings 0.2 d (m/s)	0.8 d (m/s)	0.6 d (m/s)	Average (m/s)	Angle (ccw-x) (degrees)	X-vel (m/s)	Y-vel (m/s)	Depth, d (m)	Water Surface Elevation (m)
45	-110.5	0.632	1.573		**1.103**	25	1.000	0.466	14.74	
47	-129	1.250	2.428		**1.839**	6	1.829	0.192	15.16	
57	-146	0.461	2.005		**1.233**	-5	1.228	-0.107	14.14	
69	-109	0.851	1.155		**1.003**	13	0.977	0.226	14.39	
70	-125	1.282	2.441		**1.862**	3	1.859	0.097	14.72	
78	-142	0.880	1.552		**1.216**	-26.5	1.088	-0.543	11.03	
92	-163			2.185	**2.185**	-33	1.833	-1.190	4.34	
101	-101	1.355	1.452		**1.403**	8	1.390	0.195	7.2	
101	-120	2.172	2.271		**2.221**	2	2.220	0.078	7	
103	-132	2.166	2.422		**2.294**	-6	2.282	-0.240	6.96	
110	-170			1.829	**1.829**	-30	1.584	-0.915	4.27	
116	-146.4			1.668	**1.668**	-17	1.595	-0.488	5.62	
125	-91	1.142	0.891		**1.017**	0	1.017	0.000	7.68	
127	-110	1.870	1.681		**1.775**	-2	1.774	-0.062	7.43	
182	-130			1.471	**1.471**	-20	1.382	-0.503	7.1	
Water Surface ElevationTest										
20	*-134.5*									**245.37**
42	*-130*									**245.46**
52	*-129*									**245.51**
72	*-125*									**245.56**
182	*-130*									**245.62**
184	*-104*									**245.63**
260	*-154*									**245.69**
336	*-163*									**245.67**
367	*-235*									**245.67**
386	*-355.2*									**245.67**
d/s wsel										**245.54**

Downstream Physical Model Tests

PARTIAL TEST

Date: Oct 5/94
Time (start / finish): 8:45 am - 7:30 pm

Flow (cms): 1100.00
Upstream WSEL (m): 260.23
Downstream WSEL (m): 245.5
PH 1,2 WSEL (m): 245.51, 245.46

No Cofferdam

Description/Comments: - test with DOB2, overburden removed to 2/3 the distance to the d/s cofferdam, down to invert 231 m
- overburden in the removal area fixed by applying cement coating to prevent erosion
- test used for numerical model verification

*** Units are converted to proto type scale ***

Coordinates X	Coordinates Y	Velocity - mini probe readings 0.2 d (m/s)	0.8 d (m/s)	0.6 d (m/s)	Average (m/s)	Angle (ccw-x) (degrees)	X-vel (m/s)	Y-vel (m/s)	Depth, d (m)	Water Surface Elevation (m)
45	-110.5	0.472	2.091		**1.281**	25	1.161	0.541	14.8	
47	-129	0.593	2.104		**1.333**	13	1.298	0.300	15.2	
56	-93	0.740	0.791		**0.766**	16	0.736	0.211	9.66	
57	-146	0.352	1.840		**1.096**	-8	1.085	-0.153	14	
69	-109	0.361	1.638		**1.000**	15	0.966	0.259	14.2	
70	-125	0.815	1.994		**1.328**	10	1.308	0.231	14.7	
72	-160	0.562	1.948		**1.255**	-20	1.179	-0.429	8.2	
77	-86			1.134	**1.134**	14	1.100	0.274	6.53	
78	-142	0.363	1.681		**1.022**	-2	1.021	-0.036	11	
80	-151.2	0.509	1.843		**1.176**	-4	1.173	-0.082	8.12	
80	-160			1.646	**1.646**	-27	1.467	-0.747	5.85	
80	-174			1.137	**1.137**	-37	0.908	-0.684	shallow	
101	-101	0.662	0.999		**0.831**	17	0.794	0.243	14.86	
101	-120	0.953	1.403		**1.178**	8	1.167	0.164	14.22	
103	-132	0.678	1.161		**0.920**	3	0.918	0.048	10.4	
110	-170			1.425	**1.425**	-33	1.195	-0.776	4.28	
120	-72	0.864	0.000		**0.432**	30	0.374	0.216	10.7	
125	-91	0.851	0.456		**0.653**	24	0.597	0.266	14.54	
127	-110	1.101	0.915		**1.008**	0	1.008	0.000	14.4	
132	-130	0.872	0.872		**0.872**	-15	0.843	-0.226	10.66	
146	-185			1.546	**1.546**	-39	1.202	-0.973	shallow	
182	-130			1.209	**1.209**	-17	1.156	-0.354	7.13	
184	-104			1.050	**1.050**	-13	1.023	-0.236	7.43	
260	-154			0.953	**0.953**	-41	0.719	-0.625	7.24	

Water Surface Elevation Test		
20	*-134.5*	**245.45**
42	*-130*	**245.53**
52	*-129*	**245.54**
72	*-125*	**245.57**
182	*-130*	**245.66**
184	*-104*	**245.68**
260	*-154*	**245.65**
336	*-163*	**245.68**
367	*-235*	**245.69**
386	*-355.2*	**245.67**
d/s wsel		**245.5**

Downstream Physical Model Tests

PARTIAL TEST

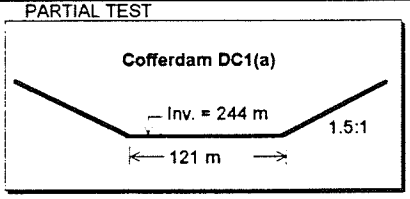

Date: Oct 24/94
Time (start / finish): 8:35 am - 11:00 pm

Flow (cms): 1100.00
Upstream WSEL (m): 261.52
Downstream WSEL (m): 245.5
PH 1,2 WSEL (m): 246.9, 246.9

Description/Comments: - test with DC1a, invert 244 m and bottom width = 121 m
- with overburden removed to 2/3 the distance to the cofferdam; cemented
- test used for numerical model verification

*** Units are converted to proto type scale ***

Coordinates X	Coordinates Y	Velocity - mini probe readings 0.2 d (m/s)	0.8 d (m/s)	0.6 d (m/s)	Average (m/s)	Angle (ccw-x) (degrees)	X-vel (m/s)	Y-vel (m/s)	Depth, d (m)	Water Surface Elevation (m)
205	-155				**3.50**					
215	-120				**3.91**					
230	-75				**3.70**					
Water Surface ElevationTest										
20	*-134.5*									**246.87**
42	*-130*									**246.88**
52	*-129*									**246.9**
72	*-125*									**246.93**
182	*-130*									**247.01**
184	*-104*									**247.01**
215	*-127*									**245.9**
260	*-154*									**245.43**
336	*-163*									**245.49**
367	*-235*									**245.48**
386	*-355.2*									**245.52**
d/s wsel										**245.5**

Downstream Physical Model Tests

PARTIAL TEST

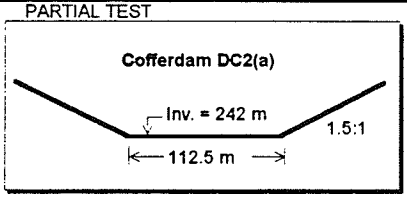

Date: Oct 24/94
Time (start / finish): 11:00 am - 1:00 pm

Flow (cms): 1100.00
Upstream WSEL (m): 260.91
Downstream WSEL (m): 245.5
PH 1,2 WSEL (m): 245.77, 245.78

Description/Comments: - test with DC2a, invert 242 m and bottom width = 112.5 m
- with overburden removed to 2/3 the distance to the cofferdam, cemented
- test used for numerical model verification

*** Units are converted to proto type scale ***

Coordinates X	Coordinates Y	Velocity - mini probe readings 0.2 d (m/s)	0.8 d (m/s)	0.6 d (m/s)	Average (m/s)	Angle (ccw-x) (degrees)	X-vel (m/s)	Y-vel (m/s)	Depth, d (m)	Water Surface Elevation (m)
205	-155				**2.50**					
215	-120				**2.52**					
230	-75				**2.45**					
Water Surface ElevationTest										
20	*-134.5*									**245.73**
42	*-130*									**245.76**
52	*-129*									**245.8**
72	*-125*									**245.81**
182	*-130*									**245.9**
184	*-104*									**245.9**
215	*-127*									**245.53**
260	*-154*									**245.57**
336	*-163*									**245.56**
367	*-235*									**245.51**
386	*-355.2*									**245.58**
d/s wsel										**245.5**

Date: Oct 25/94
Time (start / finish) 8:15 am - 4:15 pm

Flow (cms): 1100.00
Upstream WSEL (m): 261.3
Downstream WSEL (m): 245.5
PH 1,2 WSEL (m): 245.61, 245.63

FULL TEST

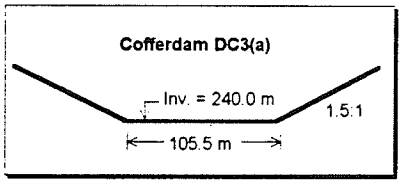

Description/Comments: - test with DC3a, invert 240 m and bottom width = 105.5 m
- with overburden removed to 2/3 the distance to the cofferdam, cemented
- test used for numerical model calibration and verification

*** Units are converted to proto type scale ***

Coordinates X	Coordinates Y	Velocity - mini probe readings 0.2 d (m/s)	0.8 d (m/s)	0.6 d (m/s)	Average (m/s)	Angle (ccw-x) (degrees)	X-vel (m/s)	Y-vel (m/s)	Depth, d (m)	Water Surface Elevation (m)
45	-110.5	0.000	1.813		**0.907**	24	0.828	0.369	14.76	
47	-129	0.576	2.250		**1.413**	13	1.377	0.318	15.26	
56	-93	0.729	1.018		**0.874**	17	0.836	0.255	10.65	
57	-146	0.354	2.018		**1.186**	2	1.185	0.041	13.98	
69	-109	0.422	1.519		**0.971**	20	0.912	0.332	14.42	
70	-125	0.708	2.085		**1.397**	11	1.371	0.266	14.74	
72	-160	0.402	1.344		**0.873**	-10	0.860	-0.152	8.08	
77	-86			1.053	**1.053**	19	0.996	0.343	6.18	
78	-142	0.000	1.943		**0.971**	-2	0.971	-0.034	11	
80	-151.2	0.791	1.980		**1.386**	-6	1.378	-0.145	8.16	
80	-160			1.592	**1.592**	-32	1.350	-0.844	5.82	
80	-174			0.000	**0.000**	0	0.000	0.000	shallow	
92	-163			1.668	**1.668**	-27	1.486	-0.757	4.16	
93	-74			0.329	**0.329**	28	0.291	0.154	5.48	
94.4	-192			0.000	**0.000**				shallow	
98.4	-148.8			1.409	**1.409**	-14	1.367	-0.341	5.33	
101	-101	0.670	0.783		**0.727**	24	0.664	0.296	14.87	
101	-120	0.697	1.571		**1.134**	10	1.117	0.197	14.64	
103	-132	0.832	0.862		**0.847**	-5	0.844	-0.074	10.24	
110	-170			0.579	**0.579**	-10	0.571	-0.101	4.15	
116	-146.4			1.269	**1.269**	-5	1.264	-0.111	5.29	
120	-72	0.875	0.514		**0.694**	30	0.601	0.347	10.83	
125	-91	0.523	0.423		**0.473**	35	0.387	0.271	14.6	
127	-110	0.818	0.907		**0.863**	15	0.834	0.223	14.98	
128	-212.83			0.000	**0.000**				shallow	
132	-130	0.959	0.864		**0.911**	-5	0.908	-0.079	9.72	
146	-185			0.000	**0.000**		0.000	0.000		
161	-25				**0.000**					
167.6	-36				**0.000**	25				
171.2	-153.6			1.312	**1.312**	5	1.307	0.114	5.84	
176	-56.4			0.705	**0.705**	3	0.704	0.037	7.06	
182	-130			1.296	**1.296**	0	1.296	0.000	6.92	
182.2255	-261.299				**0.000**	75			shallow	
184	-104			1.285	**1.285**	-5	1.280	-0.112	7.38	
186	-79			0.969	**0.969**	-7	0.962	-0.118	7.02	
189.6	-277.2			0.000	**0.000**	100	0.000	0.000	shallow	
196	-160			1.854	**1.854**	7	1.840	0.226	5.64	
197	-136			1.619	**1.619**	-2	1.618	-0.057	5.74	
200	-161			1.808	**1.808**	5	1.801	0.158	5.56	
201.2	-282			0.608	**0.608**	97	-0.074	0.603	shallow	
202	-112			1.476	**1.476**	-12	1.444	-0.307	7.02	
208	-139			1.781	**1.781**	-7	1.767	-0.217	5.66	
210	-163			1.118	**1.118**	3	1.116	0.058	shallow	
214	-84			1.597	**1.597**	-8	1.582	-0.222	5.63	
216	-115			1.705	**1.705**	-9	1.684	-0.267	5.7	
220	-223			0.369	**0.369**	83	0.045	0.366	3.54	
222	-144			2.026	**2.026**	-7	2.011	-0.247	5.66	
225.5	-86			1.538	**1.538**	-14	1.492	-0.372	5.75	
228	-55			0.905	**0.905**	-30	0.783	-0.452	shallow	
233	-124			1.705	**1.705**	-17	1.631	-0.499	shallow	
240	-240			0.000	**0.000**	102	0.000	0.000	3.55	
244	-91			1.646	**1.646**	-20	1.547	-0.563	6.83	
244.3907	-355.109			0.381	**0.381**	-170	-0.375	-0.066	shallow	
247.2	-183.6			0.000	**0.000**	10	0.000	0.000	5.87	
252	-60			0.000	**0.000**		0.000	0.000		
252	-269			0.000	**0.000**		0.000	0.000	shallow	
260	-154			1.810	**1.810**	-20	1.701	-0.619	7.4	
273.6	-217.2			0.000	**0.000**	0	0.000	0.000		
274	-125			1.503	**1.503**	-27	1.339	-0.682	7.72	

Downstream Physical Model Tests

Velocity - mini probe readings										Water Surface
Coordinates		0.2 d	0.8 d	0.6 d	Average	Angle (ccw-x)	X-vel	Y-vel	Depth, d	Elevation
X	Y	(m/s)	(m/s)	(m/s)	(m/s)	(degrees)	(m/s)	(m/s)	(m)	(m)
288	-96			1.293	**1.293**	-29	1.131	-0 627	7.52	
291.9213	-206.013			0.000	**0.000**	-40	0.000	0.000	6.66	
296	-62.4			0.000	**0.000**		0.000	0.000		
298.4	-255.2			0.000	**0.000**		0.000	0.000		
312	-185			1.743	**1.743**	-40	1.335	-1.120	7.26	
319.2	-355.2			1.145	**1.145**	-132	-0.766	-0.851	5.36	
331	-246			0.897	**0.897**	-70	0.307	-0.843	7.59	
336	-163			1.560	**1.560**	-47	1.064	-1.141	7.5	
355	-355.2			1.554	**1.554**	-124	-0.869	-1.289	7.66	
360	-140			1.325	**1.325**	-41	1.000	-0.869	7.33	
367	-235			1.581	**1.581**	-75	0.409	-1.527	7.88	
382	-120			0.000	**0.000**		0.000	0.000		
386	-355.2			1.584	**1.584**	-116	-0.694	-1.424	7.78	
406.4	-94.8			0.000	**0.000**	165	0.000	0.000		
408	-223			1.258	**1.258**	-73	0.368	-1.203	7.58	
408	-355.2			1.325	**1.325**	-130	-0.852	-1.015	6.98	
450	-215			0.000	**0.000**		0.000	0.000		
476	-204			0.000	**0.000**		0.000	0.000		
Water Surface ElevationTest										
20	*-134.5*									**245.56**
42	*-130*									**245.61**
52	*-129*									**245.62**
72	*-125*									**245.69**
182	*-130*									**245.7**
184	*-104*									**245.7**
215	*-127*									**245.6**
260	*-154*									**245.59**
336	*-163*									**245.6**
367	*-235*									**245.6**
386	*-355.2*									**245.6**
d/s wsel										**245.5**
205	-155			1.94	**1.94**					
215	-120			1.69	**1.69**	Velocity through the d/s cofferdam				
230	-75			1.38	**1.38**					

Downstream Physical Model Tests

PARTIAL TEST

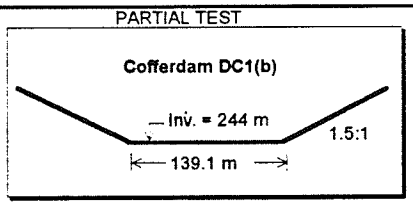

Date: Oct 13/94
Time (start / finish): 8:20 am - 10:30 pm

Flow (cms): 1100.00
Upstream WSEL (m): 260.69
Downstream WSEL (m): 245.5
PH 1,2 WSEL (m): 246.59, 246.6

Description/Comments: - test with DC1b, invert 244 m and bottom width = 139.1 m
- with overburden removed to 2/3 the distance to the cofferdam
- test used for numerical model verification
- significant erosion just d/s of the cofferdam

*** Units are converted to proto type scale ***

Coordinates X	Coordinates Y	Velocity - mini probe readings 0.2 d (m/s)	0.8 d (m/s)	0.6 d (m/s)	Average (m/s)	Angle (ccw-x) (degrees)	X-vel (m/s)	Y-vel (m/s)	Depth, d (m)	Water Surface Elevation (m)
max. velocity through cofferdam					**3.32**					
Water Surface ElevationTest										
20	*-134.5*									**246.52**
42	*-130*									**246.56**
52	*-129*									**246.59**
72	*-125*									**246.66**
182	*-130*									**246.71**
184	*-104*									**246.71**
215	*-127*									**na**
260	*-154*									**245.56**
336	*-163*									**245.61**
367	*-235*									**245.58**
386	*-355.2*									**245.58**
d/s wsel										**245.5**

FULL TEST

Date: Oct 18/94
Time (start / finish): 8.30 am - 7:00 pm

Flow (cms): 1100.00
Upstream WSEL (m): 260.92
Downstream WSEL (m): 245.5
PH 1,2 WSEL (m): 245.67, 245.64

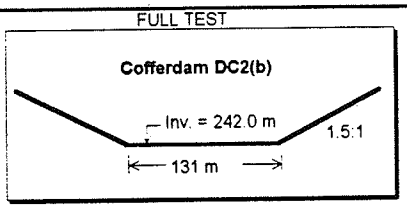

Description/Comments: - test with DC2b, invert 242 m and bottom width = 131 m
- with overburden removed to 2/3 the distance to the cofferdam, cemented
- test used for numerical model calibration and verification

*** Units are converted to proto type scale ***

Coordinates X	Coordinates Y	Velocity - mini probe readings 0.2 d (m/s)	0.8 d (m/s)	0.6 d (m/s)	Average (m/s)	Angle (ccw-x) (degrees)	X-vel (m/s)	Y-vel (m/s)	Depth, d (m)	Water Surface Elevation (m)
45	-110.5	0.000	1.743		**0.872**	25	0.790	0.368	14.8	
47	-129	0.000	2.172		**1.086**	13	1.058	0.244	15.33	
56	-93	0.764	0.967		**0.865**	16	0.832	0.238	9.58	
57	-146	0.000	1.894		**0.947**	2	0.946	0.033	14.1	
69	-109	0.843	1.638		**1.240**	10	1.221	0.215	11	
70	-125	0.670	1.991		**1.331**	26	1.196	0.583	14.84	
72	-160	0.522	1.851		**1.186**	-18	1.128	-0.367	8.32	
77	-86			1.026	**1.026**	30	0.889	0.513	6.6	
78	-142	0.000	1.651		**0.826**	3	0.825	0.043	10.94	
80	-151.2	0.000	1.767		**0.884**	-1	0.884	-0.015	8.45	
80	-160			1.576	**1.576**	-13	1.536	-0.355	5.84	
80	-174			0.000	**0.000**	-45	0.000	0.000	shallow	
92	-163			1.654	**1.654**	-7	1.642	-0.202	4.36	
93	-74			0.000	**0.000**		0.000	0.000		
98.4	-148.8			1.449	**1.449**	-3	1.447	-0.076	5.66	
101	-101	0.533	0.845		**0.689**	23	0.634	0.269	14.75	
101	-120	0.859	1.452		**1.155**	19	1.092	0.376	14.6	
103	-132	0.721	1.042		**0.882**	1	0.882	0.015	10.27	
110	-170			1.091	**1.091**	-12	1.067	-0.227	4.2	
116	-146.4			1.169	**1.169**	-5	1.164	-0.102	5.32	
120	-72	0.832	0.000		**0.416**	30	0.360	0.208	10.83	
125	-91	0.572	0.384		**0.478**	29	0.418	0.232	14.78	
127	-110	0.964	0.848		**0.906**	8	0.897	0.126	14.8	
132	-130	0.800	0.781		**0.790**	-3	0.789	-0.041	10.7	
146	-185			0.765	**0.765**	0	0.765	0.000	3.42	
161	-25			0.000	**0.000**					
167.6	-36			0.000	**0.000**					
171.2	-153.6			1.212	**1.212**	-10	1.194	-0.210	5.54	
176	-56.4			0.751	**0.751**	-2	0.751	-0.026	7.02	
182	-130			1.134	**1.134**	-6	1.128	-0.119	7.16	
184	-104	1.223	1.161		**1.192**	-4	1.189	-0.083	7.5	
186	-79	0.980	0.886		**0.933**	-8	0.924	-0.130	7.14	
189.6	-277.2			0.711	**0.711**	88	0.025	0.710	shallow	
194	-178			0.940	**0.940**	-11	0.922	-0.179	3.54	
196	-160			2.347	**2.347**	-11	2.304	-0.448	3.55	
197	-136			1.802	**1.802**	-17	1.724	-0.527	4.24	
200	-161			2.355	**2.355**	-11	2.312	-0.449	3.56	
201.2	-282			0.756	**0.756**	88	0.026	0.756	shallow	
202	-112			1.336	**1.336**	-16	1.284	-0.368	6.56	
205	-181			2.412	**2.412**	-6	2.398	-0.252	3.46	
208	-139			2.269	**2.269**	-12	2.219	-0.472	3.5	
210	-163			2.465	**2.465**	-7	2.447	-0.300	3.38	
214	-84			1.290	**1.290**	-14	1.252	-0.312	5.8	
216	-115			2.398	**2.398**	-9	2.369	-0.375	3.7	
220	-223			0.000	**0.000**	80	0.000	0.000	3.86	
222	-144			2.288	**2.288**	-15	2.210	-0.592	4.14	
225.5	-86			2.209	**2.209**	-16	2.124	-0.609	3.5	
228	-55			1.390	**1.390**	-37	1.110	-0.836	shallow	
233	-124			0.937	**0.937**	-27	0.835	-0.425	7.22	
240	-240			0.000	**0.000**	76	0.000	0.000	shallow	
244	-91			1.875	**1.875**	-37	1.498	-1.128	5.64	
244.3907	-355.109			0.000	**0.000**	160	0.000	0.000	shallow	
247.2	-183.6			1.730	**1.730**	-25	1.568	-0.731	6.16	
252	-60			0.000	**0.000**		0.000	0.000		
252	-269			0.000	**0.000**		0.000	0.000		
260	-154			1.201	**1.201**	-28	1.061	-0.564	7.23	
273.6	-217.2			0.000	**0.000**	-40	0.000	0.000	5.06	
274	-125			1.403	**1.403**	-32	1.190	-0.744	7.1	
288	-96			1.018	**1.018**	-30	0.882	-0.509	7.04	

Downstream Physical Model Tests

Coordinates		Velocity - mini probe readings								Water Surface Elevation
X	Y	0.2 d (m/s)	0.8 d (m/s)	0.6 d (m/s)	Average (m/s)	Angle (ccw-x) (degrees)	X-vel (m/s)	Y-vel (m/s)	Depth, d (m)	(m)
291.9213	-206.013			1.837	**1.837**	-38	1.448	-1.131	6.71	
296	-62.4			0.000	**0.000**	170	0.000	0.000		
298.4	-255.2			0.000	**0.000**		0.000	0.000		
312	-185			1.565	**1.565**	-44	1.126	-1.087	7.4	
319.2	-355.2			1.161	**1.161**	-130	-0.746	-0.889	5.38	
331	-246			1.560	**1.560**	-57	0.849	-1.308	7.64	
336	-163			1.579	**1.579**	-43	1.155	-1.077	7.28	
355	-355.2			1.616	**1.616**	-110	-0.553	-1.519	8.06	
360	-140			0.622	**0.622**	-50	0.400	-0.476	7.4	
367	-235			1.519	**1.519**	-63	0.690	-1.354	7.8	
382	-120			0.000	**0.000**		0.000	0.000		
386	-355.2			1.449	**1.449**	-110	-0.496	-1.362	7.74	
406.4	-94.8			0.000	**0.000**	165	0.000	0.000		
408	-223			1.174	**1.174**	-65	0.496	-1.064	7.66	
408	-355.2			1.296	**1.296**	-112	-0.485	-1.201		
450	-215			0.000	**0.000**		0.000	0.000		
476	-204			0.000	**0.000**	120	0.000	0.000		
Water Surface ElevationTest										
20	*-134.5*									**245.61**
42	*-130*									**245.69**
52	*-129*									**245.7**
72	*-125*									**245.76**
182	*-130*									**245.81**
184	*-104*									**245.82**
215	*-127*									**245.58**
260	*-154*									**245.65**
336	*-163*									**245.63**
367	*-235*									**245.62**
386	*-355.2*									**245.6**
d/s wsel										**245.5**
205	-155			2.13	**2.13**					
215	-120			2.24	**2.24**	Velocity through the d/s cofferdam				
230	-75			2.32	**2.32**					

Downstream Physical Model Tests

PARTIAL TEST

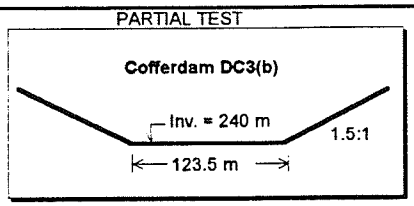

Date: Oct 14/94
Time (start / finish): 12:00 am - 2:15 pm

Flow (cms): 1100.00
Upstream WSEL (m): 259.77
Downstream WSEL (m): 245.5
PH 1,2 WSEL (m): 245.57, 245.54

Description/Comments: - test with DC3b, invert 240 m and bottom width = 123.5 m
- with overburden removed to 2/3 the distance to the cofferdam, cemented
- test used for numerical model verification
- no erosion at the cofferdam

*** Units are converted to proto type scale ***

Coordinates X	Coordinates Y	Velocity - mini probe readings 0.2 d (m/s)	0.8 d (m/s)	0.6 d (m/s)	Average (m/s)	Angle (ccw-x) (degrees)	X-vel (m/s)	Y-vel (m/s)	Depth, d (m)	Water Surface Elevation (m)
					1.59					
average velocity through cofferdam					**1.40**					
					1.08					
Water Surface ElevationTest										
20	*-134.5*									**245.51**
42	*-130*									**245.59**
52	*-129*									**245.61**
72	*-125*									**245.69**
182	*-130*									**245.7**
184	*-104*									**245.68**
215	*-127*									**245.65**
260	*-154*									**245.67**
336	*-163*									**245.7**
367	*-235*									**245.68**
386	*-355.2*									**245.67**
d/s wsel										**245.5**

FULL TEST

Date: Jan 23/95
Time (start / finish): 7:45 am - 6:00 pm

Flow (cms): 867.00
Upstream WSEL (m): 254.08
Downstream WSEL (m): 244.5
PH 1,2 WSEL (m): na, 244.55

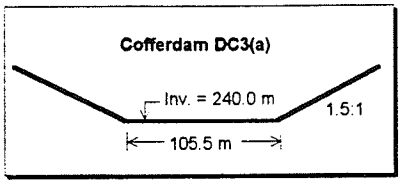

Description/Comments: - test with DC3a, invert 240 m and bottom width = 105.5 m
- test using different boundary condition, long term average summer flow, MSL in forebay
- with overburden removed to 2/3 the distance to the cofferdam
- test used for numerical model calibration and verification

*** Units are converted to proto type scale ***

Coordinates X	Coordinates Y	Velocity - mini probe readings 0.2 d (m/s)	0.8 d (m/s)	0.6 d (m/s)	Average (m/s)	Angle (ccw-x) (degrees)	X-vel (m/s)	Y-vel (m/s)	Depth, d (m)	Water Surface Elevation (m)
45	-110.5	0.810	2.158		**1.484**	15	1.434	0.384	13.85	
47	-129	1.619	2.293		**1.956**	10	1.926	0.340	14.39	
56	-93	0.810	0.810		**0.810**	23	0.746	0.317	8.76	
69	-109	1.080	1.619		**1.349**	10	1.329	0.234	13.15	
70	-125	1.484	1.349		**1.417**	4	1.413	0.099	13.49	
72	-160			0.810	**0.810**	-150	-0.702	-0.405	6.97	
77	-86			1.215	**1.215**	14	1.179	0.294	5.4	
78	-142	0.810	0.810		**0.810**	-30	0.702	-0.405	9.47	
80	-151.2			0.676	**0.676**	-120	-0.338	-0.585	6.5	
80	-160			0.676	**0.676**	-130	-0.434	-0.518	4.06	
92	-163			0.445	**0.445**	-70	0.152	-0.418	2.54	
94.4	-192			0.000	**0.000**		0.000	0.000	shallow	
98.4	-148.8			0.810	**0.810**	-40	0.621	-0.521	4.26	
101	-101	1.080	1.080		**1.080**	13	1.052	0.243	13.1	
101	-120	1.080	0.810		**0.945**	7	0.938	0.115	12.82	
103	-132	1.080	0.945		**1.013**	0	1.013	0.000	8.63	
110	-170			0.445	**0.445**	-30	0.385	-0.222	2.92	
116	-146.4			1.080	**1.080**	-22	1.001	-0.405	3.88	
120	-72	0.810	0.391		**0.601**	30	0.520	0.300	9.38	
125	-91	1.215	0.810		**1.013**	20	0.951	0.346	13.06	
127	-110	1.080	0.676		**0.878**	5	0.874	0.077	13.21	
128	-212.8			0.000	**0.000**		0.000	0.000	shallow	
132	-130	1.080	0.810		**0.945**	-10	0.931	-0.164	8.82	
146	-185			0.391	**0.391**	0	0.391	0.000		
161	-25			0.000	**0.000**		0.000	0.000	shallow	
167.6	-36			0.000	**0.000**		0.000	0.000		
171.2	-153.6			1.035	**1.035**	2	1.034	0.036	4.63	
176	-56.4			0.713	**0.713**	0	0.713	0.000	5.97	
182	-130			1.249	**1.249**	0	1.249	0.000	6.43	
181	-255			0.000	**0.000**		0.000	0.000		
184	-104			1.249	**1.249**	-2	1.248	-0.044	6.54	
186	-79			1.195	**1.195**	-2	1.195	-0.042	6.16	
189.6	-277.2			0.000	**0.000**		0.000	0.000	shallow	
193.5	-214.6			0.000	**0.000**		0.000	0.000		
196.9	-135.9			1.678	**1.678**	-3	1.675	-0.088	4.8	
201.2	-282			0.000	**0.000**		0.000	0.000		
201.9	-109.4			1.329	**1.329**	-5	1.324	-0.116	6.53	
210.4	-140.2			1.731	**1.731**	-5	1.725	-0.151	4.62	
214.8	-84.1			1.597	**1.597**	-10	1.573	-0.277	4.93	
219.3	-114.6			1.678	**1.678**	-8	1.661	-0.234	4.93	
220	-223			0.000	**0.000**	120	0.000	0.000		
221.5	-143.8			1.839	**1.839**	-12	1.798	-0.382	4.61	
228.4	-88.1			1.705	**1.705**	-11	1.673	-0.325	4.8	
227.5	-56.3			1.249	**1.249**	-25	1.132	-0.528	2.42	
235.3	-119.4			1.624	**1.624**	-24	1.484	-0.661	6.2	
240	-240			0.472	**0.472**	125	-0.271	0.386		
244.2	-92.9			1.544	**1.544**	-16	1.484	-0.426	6.18	
244.4	-355.1			0.445	**0.445**	-140	-0.341	-0.286		
251.6	-61.9			0.391	**0.391**	-16	0.376	-0.108	3.83	
252	-269			0.552	**0.552**	120	-0.276	0.478		
260	-154			1.571	**1.571**	-20	1.476	-0.537	5.86	
273.6	-217.2			0.000	**0.000**		0.000	0.000		
274	-125			1.490	**1.490**	-24	1.361	-0.606	5.8	
288	-96			1.356	**1.356**	-26	1.219	-0.595	5.8	
291.9	-206			0.767	**0.767**	-40	0.587	-0.493	5.42	
296	-62.4			0.364	**0.364**	170	-0.359	0.063		

Downstream Physical Model Tests

Coordinates X	Coordinates Y	Velocity - mini probe readings 0.2 d (m/s)	0.8 d (m/s)	0.6 d (m/s)	Average (m/s)	Angle (ccw-x) (degrees)	X-vel (m/s)	Y-vel (m/s)	Depth, d (m)	Water Surface Elevation (m)
298.4	-255.2			0.000	**0.000**		0.000	0.000	3.87	
312	-185			1.597	**1.597**	-45	1.130	-1.130	5.95	
319.2	-355.2			1.088	**1.088**	-120	-0.544	-0.942	4.48	
331	-246			1.035	**1.035**	-70	0.354	-0.972	6.21	
336	-163			1.383	**1.383**	-45	0.978	-0.978	6.08	
355	-355.2			1.356	**1.356**	-110	-0 464	-1.274	6 5	
360	-140			1.142	**1.142**	-40	0.875	-0.734	5.92	
367	-235			1.276	**1.276**	-75	0.330	-1.232	6.58	
386	-355.2			1.356	**1.356**	-115	-0.573	-1.229	6.87	
406 4	-97.8			0.552	**0.552**	165	-0.533	0.143		
408	-223			0.927	**0.927**	-70	0.317	-0 871	6.4	
408	-355.2			1.142	**1.142**	-120	-0.571	-0 989	6.59	
450	-215			0.000	**0.000**		0.000	0.000		
476	-204			0.000	**0.000**		0.000	0.000		
Water Surface ElevationTest										
20	*-134.5*									**244.6**
42	*-130*									**244.72**
52	*-129*									**244.65**
72	*-125*									**244.72**
182	*-130*									**244.75**
184	*-104*									**244.75**
215	*-127*									**244.69**
260	*-154*									**244.65**
336	*-163*									**244.65**
367	*-235*									**244.65**
386	*-355.2*									**244.67**
d/s wsel										**244.5**

PARTIAL TEST

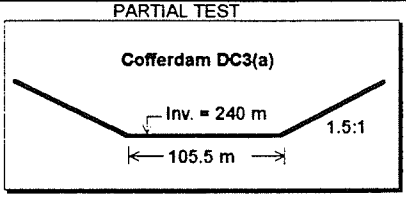

Date: Oct 27/94
Time (start / finish): 9:20 am - 12:15 pm

Flow (cms): 1100.00
Upstream WSEL (m): 260.88
Downstream WSEL (m): 245.5
PH 1,2 WSEL (m): 245.57, 245.52

Description/Comments: - test with Tailrace Expansion TR0, no expansion
- with overburden removed to 2/3 the distance to the cofferdam, cemented; Cofferdam DC3a
- test used for numerical model verification

*** Units are converted to proto type scale ***

Coordinates X	Coordinates Y	Velocity - mini probe readings 0.2 d (m/s)	0.8 d (m/s)	0.6 d (m/s)	Average (m/s)	Angle (ccw-x) (degrees)	X-vel (m/s)	Y-vel (m/s)	Depth, d (m)	Water Surface Elevation (m)
47	-129	0.446	2.320		**1.383**					
70	-125	0.694	2.288		**1.491**					
101	-101	0.654	1.136		**0.895**					
127	-110	1.020	1.023		**1.022**					
205	-155			1.662	**1.662**					
215	-120			1.773	**1.773**					
230	-75			1.242	**1.242**					
Water Surface ElevationTest										
20	*-134.5*									**245.54**
42	*-130*									**245.58**
52	*-129*									**245.59**
72	*-125*									**245.61**
182	*-130*									**245.7**
184	*-104*									**245.72**
215	*-127*									**245.63**
260	*-154*									**245.6**
336	*-163*									**245.63**
367	*-235*									**245.62**
386	*-355.2*									**245.62**
d/s wsel										**245.5**

Date: Oct 27/94
Time (start / finish): 2:15 am - 4:00 pm

Flow (cms): 1100.00
Upstream WSEL (m):
Downstream WSEL (m): 245.5
PH 1,2 WSEL (m): 245.62, 245.58

Description/Comments: - test with Tailrace Expansion TR3:1, 3:1 expansion
- with overburden removed to 2/3 the distance to the cofferdam, cemented; cofferdam DC3a
- test used for numerical model verification

*** Units are converted to proto type scale ***

Coordinates X	Coordinates Y	Velocity - mini probe readings 0.2 d (m/s)	0.8 d (m/s)	0.6 d (m/s)	Average (m/s)	Angle (ccw-x) (degrees)	X-vel (m/s)	Y-vel (m/s)	Depth, d (m)	Water Surface Elevation (m)
Water Surface ElevationTest										
20	*-134.5*									**245.6**
42	*-130*									**245.61**
52	*-129*									**245.64**
72	*-125*									**245.71**
182	*-130*									**245.7**
184	*-104*									**245.7**
215	*-127*									**245.62**
260	*-154*									**245.6**
336	*-163*									**245.63**
367	*-235*									**245.61**
386	*-355.2*									**245.62**
d/s wsel										**245.5**

APPENDIX D: UPSTREAM PHYSICAL MODEL TEST RESULTS

The upstream tests are each summarized on a separate sheet identifying the particular design alternative and the boundary conditions.
All measurements are in prototype scale.
Included in each test summary are the following:

1. Date and time of test.
2. Boundary conditions: flow and water levels at model boundaries.
3. Comments.
4. Data measurements
   a) columns 1 and 2 give *x* and *y* reference coordinates for the data measurements
   b) columns 3 and 4 give velocities at 0.2 depth and 0.8 depth when depths are greater than 8 m.
   c) column 5 is the velocity at 0.6 depth for depths less than 8 m.
   d) column 6 shows the depth-averaged velocity at that point
   e) column 7 gives an approximate measurement of the direction of flow, measured counter clockwise to the longitudinal x-axis.
   f) columns 8 and 9 provide the calculated *x* and *y* velocities.
   g) column 10 gives an approximate measurement of the depth used to determine the depth for velocity measurements
   h) column 11 shows the water surface elevation measurements taken with the mobile point gauge at several different points. The measurements were conducted AFTER the velocity measurements.

TEST	DESIGN DESCRIPTION		BOUNDARY CONDITION	
	Invert (m)	Bottom width (m)	Flow	u/s WSEL
UOB	No cofferdam		FGD	FSL
UC1b	239.8	50	FGD	FSL
UC1c	239.8	40	FGD	FSL
UC2a	242.8	70	FGD	FSL
UC2b	242.8	60	FGD	FSL
UC2c	242.8	50	FGD	FSL
UC3a	245.4	80	FGD	FSL
UC3b	245.4	70	FGD	FSL
UC3c	245.4	60	FGD	FSL
UC3c	245.4	60	867	MSL

Desired BC's: FGD = 1100 m^3/s
FSL = 257.4 m
MSL = 254.2 m

Velocity Test of Notigi G.S. Physical Model

Date: November 25/94
Time (start / finish): 8:30 - 4:45 pm

Test **UOB** F1100 AP1.5:1
no cofferdam

Flow (cms): 1100
Upstream WSEL (m): 257.84
Downstream WSEL (m): 254.5
u/s PH WSEL (m): 257.97

Description/Comments: - powerhouse opening initially required closing to achieve the upstream head, but by the afternoon, opening was increased (back to calibrated setting) in order to maintain upstream WSEL.
- water surface increased with time for measurements taken in the upstream direction.

Coordinates		Velocity - mini probe readings								Water Surface Elevation
X	Y	0.2 d (m/s)	0.8 d (m/s)	0.6 d (m/s)	Average (m/s)	Angle (ccw-x) (degrees)	X-vel (m/s)	Y-vel (m/s)	Depth, d (m)	(m)
41	60	0.42	0.36		**0.39**	9	0.386	0.061	19.3	
41	100	0.42	0.39		**0.40**	6	0.402	0.042	20.23	257.92
41	245			0.47	**0.47**	-5	0.470	-0.041	6.4	
131	79	0.53	0.53		**0.53**	0	0.525	0.000	13.05	
140	207	0.00	0.00		**0.00**	-30	0.000	0.000	7.8	
140	250	0.00	0.36		**0.18**	-8	0.180	-0.025	8.09	
158	127	0.61	0.55		**0.58**	0	0.579	0.000	10.47	257.88
220	82	0.53	0.55		**0.54**	10	0.530	0.094	12.53	
220	133.5	0.47	0.34		**0.40**	-8	0.401	-0.056	18.85	257.86
220	207			0.47	**0.47**	-25	0.427	-0.199	3.72	
305	86	0.47	0.42		**0.44**	2	0.445	0.016	16.26	
305	147.5	0.44	0.44		**0.44**	-1	0.445	-0.008	20.58	257.84
305	197.5			0.00	**0.00**		0.000	0.000	14.65	
376	75.5	0.47	0.47		**0.47**	1	0.472	0.008	16.15	
376	123.5	0.47	0.55		**0.51**	-1	0.512	-0.009	20.22	257.84
376	167	0.39	0.44		**0.42**	-3	0.417	-0.022	16.86	
376	203			0.00	**0.00**		0.000	0.000	8.57	
438	156	0.47	0.44		**0.46**	-12	0.448	-0.095	12.18	
445.602	117.1537	0.53	0.53		**0.53**	-8	0.520	-0.073	20.03	257.79
452.5	81	0.58	0.61		**0.59**	5	0.590	0.052	17.24	
484.3074	89.2957	0.55	0.42		**0.49**	-2	0.485	-0.017	27.5	
489.0531	107.2925	0.50	0.50		**0.50**	-10	0.491	-0.087	28.38	257.77
493.8605	125.4125	0.34	0.36		**0.35**	-15	0.339	-0.091	27.9	
527	86	0.36	0.87		**0.62**	-8	0.613	-0.086	36.25	
530	95									257.75
532.5	103.75	0.36	0.85		**0.61**	-13	0.590	-0.136	36.24	

Velocity Test of Notigi G.S. Physical Model

FULL TEST

Date: Dec 12/94
Time (start / finish): 2:10 pm - 4:35 pm

Flow (cms): 973.77
Upstream WSEL (m): 257.58
Downstream WSEL (m): 245.45
u/s PH WSEL (m): 257.6

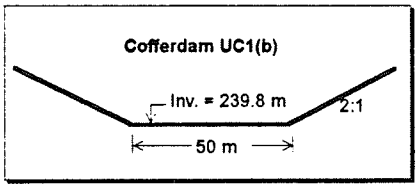

Description/Comments: - flow decreased with time, but head stayed fairly constant.

*** Units are converted to proto type scale ***

Coordinates X	Coordinates Y	Velocity - mini probe readings 0.2 d (m/s)	0.8 d (m/s)	0.6 d (m/s)	Average (m/s)	Angle (ccw-x) (degrees)	X-vel (m/s)	Y-vel (m/s)	Depth, d (m)	Water Surface Elevation (m)
41	60	0.39	0.39		**0.39**	2	0.391	0.014	18.71	
41	*100*	0.42	0.39		**0.40**	2	0.404	0.014	19.93	257.56
41	245			0.42	**0.42**	-12	0.409	-0.087	5.9	
131	79	0.50	0.53		**0.51**	4	0.511	0.036	12.37	
140	207			0.00	**0.00**	-18	0.000	0.000	7.26	
140	250			0.39	**0.39**	-20	0.368	-0.134	7.64	
158	*127*	0.58	0.63		**0.61**	9	0.598	0.095	9.95	257.56
220	82	0.55	0.53		**0.54**	10	0.530	0.094	12.03	
220	*133.5*	0.55	0.39		**0.47**	-9	0.466	-0.074	18.39	257.55
220	207			0.44	**0.44**	-23	0.410	-0.174	3.12	
305	86	0.53	0.47		**0.50**	0	0.498	0.000	15.78	
305	*147.5*	0.44	0.42		**0.43**	-3	0.431	-0.023	20.08	257.56
305	197.5			0.00	**0.00**		0.000	0.000		
340.5	80.75	0.50	0.47		**0.49**	10	0.478	0.084	15.12	
376	75.5	0.53	0.47		**0.50**	17	0.477	0.146	15.92	
376	*123.5*	0.58	0.47		**0.53**	-6	0.522	-0.055	20.14	257.56
376	167	0.00	0.00		**0.00**	-2	0.000	0.000	16.53	
376	195			0.00	**0.00**					
376	203			0.00	**0.00**					
422.53	*119.62*	0.63	0.74		**0.69**	-7	0.681	-0.084	17.71	257.56
438	156			0.71	**0.71**	-35	0.584	-0.409	5.73	
445.602	*117.1537*	0.74	0.79		**0.77**	-8	0.759	-0.107	17.72	257.57
452.5	81	0.77	0.82		**0.79**	-2	0.793	-0.028	17.67	
468.28	*109.5*	0.77	0.85		**0.81**	-8	0.799	-0.112	17.98	257.56
484.3074	89.2957	0.85	0.90		**0.87**	-2	0.873	-0.030	17.98	
489.0531	*107.2925*	0.82	0.87		**0.85**	-7	0.841	-0.103	18.06	257.56
493.8605	125.4125	0.69	0.85		**0.77**	-5	0.764	-0.067	14.43	
509.75	*101.5*	0.82	0.34		**0.58**	-2	0.579	-0.020	27.83	257.56
527	86	0.66	0.85		**0.75**	-10	0.742	-0.131	36.22	
530	*95*									257.56
532.5	103.75	0.63	0.66		**0.65**	-9	0.638	-0.101	36.21	
TEST 2	(Supplementary Check)									
41	*100*									257.56
530	*95*									257.56

Velocity Test of Notigi G.S. Physical Model

PARTIAL TEST

Date: Dec 12/94
Time (start / finish): 8:15 am - 2:10 pm

Flow (cms): 1100
Upstream WSEL (m): 257.26
Downstream WSEL (m): 245.5
u/s PH WSEL (m): 257.31

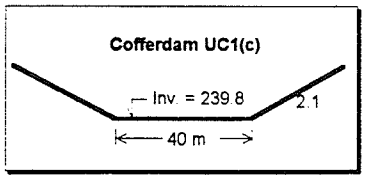

Description/Comments:
- partial test
- WSEL varied +/- 5 mm during test of velocities
- large fluctuation of velocity near powerhouse, +/- 0.6 m/s, low fluctuation at cofferdam +/- 0.4 m/s
- noted a 0.1 m increase in water level over 15 minutes
- test (2) shows water levels at upstream end of model and at powerhouse intake using mobile point gauge

*** Units are converted to proto type scale ***

Coordinates X	Coordinates Y	Velocity - mini probe readings 0.2 d (m/s)	0.8 d (m/s)	0.6 d (m/s)	Average (m/s)	Angle (ccw-x) (degrees)	X-vel (m/s)	Y-vel (m/s)	Depth, d (m)	Water Surface Elevation (m)
41	60									
41	*100*									257.26
41	245									
131	79									
140	207									
140	250									
158	*127*									257.26
220	82									
220	*133.5*									257.25
220	207									
305	86									
305	*147.5*									257.25
305	197.5									
340.5	80.75									
376	75.5	0.53	0.47		**0.50**	10	0.491	0.087	15.21	
376	*123.5*	0.58	0.55		**0.57**	4	0.564	0.039	19	257.24
376	167	0.34	0.44		**0.39**	5	0.390	0.034	15.72	
376	195	0.00	0.00	0.00	**0.00**					
376	203									
422.53	*119.62*	0.82	0.79		**0.81**	-6	0.802	-0.084	16.8	257.19
438	156									
445.602	*117.1537*	0.93	0.95		**0.94**	-8	0.932	-0.131	16.81	257.18
452.5	81									
468.28	*109.5*									257.17
484.3074	89.2957	1.06	1.09		**1.07**	-9	1.061	-0.168	17.09	
489.0531	*107.2925*	1.06	1.09		**1.07**	-11	1.055	-0.205	17.01	257.17
493.8605	125.4125									
509.75	*101.5*	1.01	0.39	1.06	**0.70**	-10	0.689	-0.121	26.91	257.17
527	86	0.61	0.69		**0.65**	-12	0.632	-0.134	36.43	
530	*95*									257.18
532.5	103.75	0.63	0.63		**0.63**	-10	0.623	-0.110	36.12	
TEST 2	(Supplementary Check)									
41	*100*									257.34
530	*95*									257.3

Velocity Test of Notigi G.S. Physical Model

PARTIAL TEST

Date: Dec 14/94
Time (start / finish): 6:15 PM

Flow (cms): 1100
Upstream WSEL (m): 257.56
Downstream WSEL (m): 245.49
u/s PH WSEL (m): 257.66

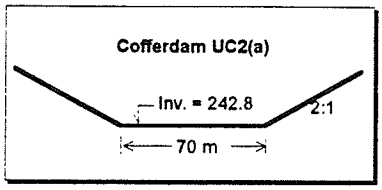

Description/Comments: -Cofferdam UC2a (invert = 242.8 m, inside bottom width = 70 m)

*** Units are converted to proto type scale ***

Coordinates X	Coordinates Y	Velocity - mini probe readings 0.2 d (m/s)	0.8 d (m/s)	0.6 d (m/s)	Average (m/s)	Angle (ccw-x) (degrees)	X-vel (m/s)	Y-vel (m/s)	Depth, d (m)	Water Surface Elevation (m)
41	60									
41	*100*									257.61
41	245									
131	79									
140	207									
140	250									
158	*127*									257.6
220	82									
220	*133.5*									257.59
220	207									
305	86									
305	*147.5*									257.59
305	197.5									
340.5	80.75									
376	75.5									
376	*123.5*	0.53	0.58		**0.55**	-4	0.551	-0.039	20.11	257.58
376	167									
376	195									
376	203									
422.53	*119.62*	0.71	0.74		**0.73**	-11	0.713	-0.139	15.6	257.57
438	156									
445.602	*117.1537*	0.79	0.85		**0.82**	-8	0.812	-0.114	15.12	257.56
452.5	81	0.82	0.82		**0.82**	-4	0.818	-0.057	14.63	
468.28	*109.5*	0.85	0.87		**0.86**	-9	0.850	-0.135	15.14	257.56
484.3074	89.2957									
489.0531	*107.2925*	0.93	0.98		**0.95**	-12	0.933	-0.198	15.17	257.57
493.8605	125.4125									
509.75	*101.5*	0.87	0.39		**0.63**	-13	0.616	-0.142	27.36	257.58
527	86	0.61	0.90		**0.75**	-6	0.749	-0.079	36.32	
530	*95*									257.57
532.5	103.75	0.53	0.69		**0.61**	-13	0.590	-0.136	36.36	
		In "dead" zone to the right of PH between the coffer dam and the PH the WSEL is								257.59

Velocity Test of Notigi G.S. Physical Model

PARTIAL TEST

Date: Dec 14/94
Time (start / finish): 5:15 PM

Flow (cms): 1100
Upstream WSEL (m): 257.57
Downstream WSEL (m): 245.51
u/s PH WSEL (m): 257.6

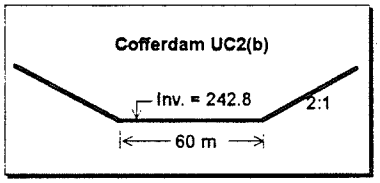

Description/Comments: -Cofferdam UC2b (invert = 242.8 m, inside bottom width = 60 m)
- less separation at cofferdam corners
- much more stable conditions than earlier tests

*** Units are converted to proto type scale ***

Coordinates X	Coordinates Y	Velocity - mini probe readings 0.2 d (m/s)	0.8 d (m/s)	0.6 d (m/s)	Average (m/s)	Angle (ccw-x) (degrees)	X-vel (m/s)	Y-vel (m/s)	Depth, d (m)	Water Surface Elevation (m)
41	60									
41	*100*									257.56
41	245									
131	79									
140	207									
140	250									
158	*127*									257.56
220	82									
220	*133.5*									257.56
220	207									
305	86									
305	*147.5*									257.56
305	197.5									
340.5	80.75									
376	75.5									
376	*123.5*	0.58	0.58		**0.58**	-2	0.579	-0.020	19.93	257.55
376	167									
376	195									
376	203									
422.53	*119.62*	0.82	0.79		**0.81**	-10	0.794	-0.140	15.05	257.53
438	156									
445.602	*117.1537*	0.87	0.93		**0.90**	-11	0.884	-0.172	15.08	257.53
452.5	81	0.90	0.90		**0.90**	-7	0.894	-0.110	14.59	
468.28	*109.5*	0.98	1.01		**0.99**	-10	0.979	-0.173	15.11	257.54
484.3074	89.2957									
489.0531	*107.2925*	0.98	1.11		**1.05**	-10	1.032	-0.182	15.2	257.53
493.8605	125.4125									
509.75	*101.5*	0.95	0.36		**0.66**	-12	0.645	-0.137	26.94	257.49
527	86	0.71	0.90		**0.81**	-10	0.794	-0.140	36.13	
530	*95*									257.5
532.5	103.75	0.71	0.69		**0.70**	-15	0.676	-0.181	36.35	
			In "dead" zone to the right of PH between the cofferdam and the PH the WSEL is							257.53

Velocity Test of Notigi G.S. Physical Model

FULL TEST

Date: Dec 14/94
Time (start / finish): 8:00 am - 4:20 pm

Flow (cms): 1100
Upstream WSEL (m): 257.94
Downstream WSEL (m): 245.5
u/s PH WSEL (m): 257.91

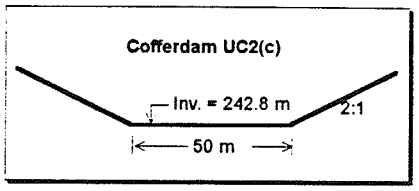

Description/Comments: -Cofferdam UC2c (invert = 242.8 m, inside bottom width = 50 m)
- with model saturated from Wednesdays test, the upstream head quickly reached and surpassed the 257.4 m elev. In attempt to maintain the upstream wsel near 257.4 m we lowered the d.s. wsel. Not very successful and therefore removed a screen from PH units and tested again (later).

*** Units are converted to proto type scale ***

Coordinates X	Coordinates Y	Velocity - mini probe readings 0.2 d (m/s)	0.8 d (m/s)	0.6 d (m/s)	Average (m/s)	Angle (ccw-x) (degrees)	X-vel (m/s)	Y-vel (m/s)	Depth, d (m)	Water Surface Elevation (m)
41	60	0.34	0.36		**0.35**	3	0.351	0.018	19.27	
41	*100*	0.34	0.34		**0.34**	0	0.338	0.000	20.2	257.97
41	245			0.34	**0.34**	-1	0.338	-0.006	6.18	
131	79	0.47	0.42		**0.44**	3	0.444	0.023	12.71	
140	207			0.00	**0.00**	-23	0.000	0.000	7.47	
140	250			0.34	**0.34**	-20	0.317	-0.115	7.86	
158	*127*	0.58	0.50		**0.54**	5	0.537	0.047	10.21	257.94
220	82	0.47	0.42		**0.44**	14	0.432	0.108	12.25	
220	*133.5*	0.44	0.00		**0.22**	-3	0.222	-0.012	18.96	257.95
220	207			0.44	**0.44**	-35	0.364	-0.255	3.38	
305	86	0.50	0.47		**0.49**	2	0.485	0.017	15.96	
305	*147.5*	0.42	0.44		**0.43**	0	0.431	0.000	20.62	257.95
305	197.5			0.00	**0.00**		0.000	0.000		
340.5	80.75	0.50	0.42		**0.46**	2	0.458	0.016	15.55	
376	75.5	0.47	0.44		**0.46**	22	0.425	0.172	16.32	
376	*123.5*	0.47	0.42		**0.44**	-1	0.445	-0.008	20.32	257.94
376	167	0.00	0.36		**0.18**	1	0.182	0.003	16.72	
376	195			0.00	**0.00**					
376	203			0.00	**0.00**					
422.53	*119.62*	0.71	0.74		**0.73**	-5	0.724	-0.063	15.26	257.94
438	156			0.90	**0.90**	-40	0.690	-0.579	5.8	
445.602	*117.1537*	0.85	0.87		**0.86**	-9	0.850	-0.135	15.24	257.87
452.5	81	0.87	0.87		**0.87**	-4	0.872	-0.061	13.22	
468.28	*109.5*	0.95	0.95		**0.95**	-11	0.937	-0.182	15.24	257.87
484.3074	89.2957	1.06	1.09		**1.07**	-5	1.071	-0.094	16.34	
489.0531	*107.2925*	0.95	1.06		**1.01**	-10	0.992	-0.175	15.25	257.86
493.8605	125.4125	0.77	0.93		**0.85**	-15	0.818	-0.219	14.27	
509.75	*101.5*	0.93	0.34		**0.63**	-8	0.626	-0.088	26.98	257.86
527	86	0.55	0.66	0.74	**0.61**	-13	0.590	-0.136	36.16	
530	*95*									257.86
532.5	103.75	0.55	0.50	0.66	**0.53**	-12	0.514	-0.109	35.98	
TEST 2										
41	*100*									257.93
530	*95*									257.86

Velocity Test of Notigi G.S. Physical Model

PARTIAL TEST

Date: Dec 19/94
Time (start / finish): 4:10 - 5:25 PM

Flow (cms): 1100
Upstream WSEL (m): 257.61
Downstream WSEL (m): 245.51
u/s PH WSEL (m): 257.73

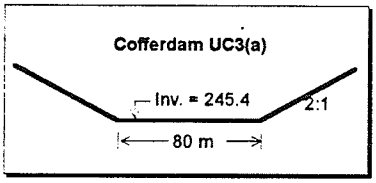

Description/Comments: -Cofferdam UC3a (invert = 245.4 m, inside bottom width = 80 m)
- head still increasing vary gradually
- during WSEL readings, head increased by 0.04 m ; during velocity test, head increased by 0.22 m.

*** Units are converted to proto type scale ***

Coordinates X	Coordinates Y	Velocity - mini probe readings 0.2 d (m/s)	0.8 d (m/s)	0.6 d (m/s)	Average (m/s)	Angle (ccw-x) (degrees)	X-vel (m/s)	Y-vel (m/s)	Depth, d (m)	Water Surface Elevation (m)
41	60									
41	*100*									257.75
41	245									
131	79									
140	207									
140	250									
158	*127*									257.72
220	82									
220	*133.5*									257.73
220	207									
305	86									
305	*147.5*									257.75
305	197.5									
340.5	80.75									
376	75.5									
376	*123.5*	0.55	0.47		**0.51**	-10	0.504	-0.089	20.17	257.74
376	167									
376	195									
376	203									
422.53	*119.62*	0.85	0.82		**0.83**	-12	0.815	-0.173	12.25	257.71
438	156									
445.602	*117.1537*	0.93	0.87		**0.90**	-15	0.870	-0.233	12.37	257.71
452.5	81	0.93	0.93		**0.93**	-7	0.920	-0.113	12.02	
468.28	*109.5*	1.01	1.01		**1.01**	-15	0.973	-0.261	12.13	257.69
484.3074	89.2957	1.09	1.09		**1.09**	-15	1.051	-0.282	13.99	
489.0531	*107.2925*	1.09	1.03		**1.06**	-19	1.004	-0.346	14.17	257.69
493.8605	125.4125	0.87	0.98		**0.93**	-8	0.918	-0.129	14.12	
509.75	*101.5*	0.95	0.36	0.63	**0.66**	-8	0.653	-0.092	27.04	257.68
527	86	0.61	0.93	0.93	**0.77**	-6	0.762	-0.080	36.14	
530	*95*									257.69
532.5	103.75	0.66	0.66	0.61	**0.66**	-17	0.630	-0.193	36.11	
TEST 2										
41	*100*									257.74
530	*95*									257.72

Velocity Test of Notigi G.S. Physical Model

PARTIAL TEST

Date: Dec 19/94
Time (start / finish): 2:45 - 3:45 PM

Flow (cms): 1100
Upstream WSEL (m): 257.54
Downstream WSEL (m): 245.51
u/s PH WSEL (m): 257.56

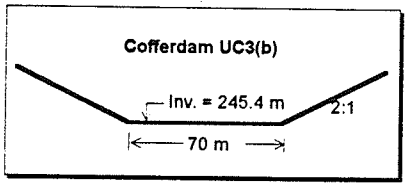

Description/Comments: -Cofferdam UC3b (invert = 245.4 m, inside bottom width = 70 m)
- head increase of 0.04m during velocity test

*** Units are converted to proto type scale ***

Coordinates X	Coordinates Y	Velocity - mini probe readings 0.2 d (m/s)	0.8 d (m/s)	0.6 d (m/s)	Average (m/s)	Angle (ccw-x) (degrees)	X-vel (m/s)	Y-vel (m/s)	Depth, d (m)	Water Surface Elevation (m)
41	60									
41	*100*									257.52
41	245									
131	79									
140	207									
140	250									
158	*127*									257.5
220	82									
220	*133.5*									257.49
220	207									
305	86									
305	*147.5*									257.5
305	197.5									
340.5	80.75									
376	75.5									
376	*123.5*	0.53	0.50		**0.51**	-7	0.508	-0.062	20.1	257.51
376	167									
376	195									
376	203									
422.53	*119.62*	0.90	0.87		**0.89**	-12	0.868	-0.184	12.1	257.51
438	156									
445.602	*117.1537*	1.01	1.03		**1.02**	-12	0.999	-0.212	12.24	257.47
452.5	81	1.09	1.03		**1.06**	-8	1.051	-0.148	11.86	
468.28	*109.5*	1.11	1.11		**1.11**	-13	1.086	-0.251	12.09	257.46
484.3074	89.2957	1.22	1.25		**1.24**	-15	1.193	-0.320	14.06	
489.0531	*107.2925*	1.22	0.98		**1.10**	-18	1.048	-0.340	14.59	257.48
493.8605	125.4125	1.01	1.01		**1.01**	-15	0.973	-0.261	14.61	
509.75	*101.5*	1.14	0.00	0.50	**0.57**	-14	0.554	-0.138	26.93	257.48
527	86	0.66	0.90	1.01	**0.78**	-6	0.776	-0.082	36.29	
530	*95*									257.48
532.5	103.75	0.82	0.71	0.82	**0.77**	-11	0.752	-0.146	36.18	
TEST 2	(Supplementary Check)									
41	*100*									257.51
530	*95*									257.5
		In "dead" zone to the right of PH between the coffer dam and the PH the WSEL is								257.48

Velocity Test of Notigi G.S. Physical Model

FULL TEST

Date: Dec 19/94
Time (start / finish): 8:05 am - 2:20 pm

Flow (cms): 1100
Upstream WSEL (m): 257.585
Downstream WSEL (m): 245.5
u/s PH WSEL (m): 257.46

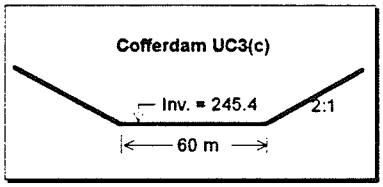

Description/Comments: -Cofferdam UC3c (invert = 245.4 m, inside bottom width = 60 m)
- head increase of 0.37 m during velocity test

*** Units are converted to proto type scale ***

Coordinates X	Coordinates Y	Velocity - mini probe readings 0.2 d (m/s)	0.8 d (m/s)	0.6 d (m/s)	Average (m/s)	Angle (ccw-x) (degrees)	X-vel (m/s)	Y-vel (m/s)	Depth, d (m)	Water Surface Elevation (m)
41	60	0.42	0.39		**0.40**	8	0.401	0.056	19.08	
41	*100*	0.42	0.36		**0.39**	0	0.391	0.000	20.34	257.45
41	245			0.44	**0.44**	-12	0.435	-0.092	5.84	
131	79	0.55	0.53		**0.54**	1	0.539	0.009	12.07	
140	207			0.00	**0.00**				7.15	
140	250			0.00	**0.00**				7.56	
158	*127*	0.61	0.55		**0.58**	5	0.577	0.050	10.15	257.43
220	82	0.53	0.50		**0.51**	8	0.507	0.071	11.91	
220	*133.5*	0.58	0.36		**0.47**	-12	0.461	-0.098	18.76	257.44
220	207			0.50	**0.50**	-28	0.440	-0.234	2.97	
305	86	0.55	0.39		**0.47**	2	0.471	0.016	15.65	
305	*147.5*	0.53	0.42		**0.47**	-5	0.470	-0.041	20.34	257.43
305	197.5			0.00	**0.00**		0.000	0.000		
340.5	80.75	0.47	0.44		**0.46**	2	0.458	0.016	14.82	
376	75.5	0.58	0.53		**0.55**	17.5	0.527	0.166	15.92	
376	*123.5*	0.55	0.50		**0.53**	-2	0.525	-0.018	19.96	257.45
376	167	0.00	0.00		**0.00**	-12.5	0.000	0.000	16.47	
376	195			0.00	**0.00**					
376	203			0.00	**0.00**					
422.53	*119.62*	1.06	0.98		**1.02**	-9	1.009	-0.160	12.03	257.41
438	156			1.09	**1.09**	-40	0.834	-0.699	5.52	
445.602	*117.1537*	1.11	1.17		**1.14**	-13	1.112	-0.257	12.08	257.39
452.5	81	1.25	1.28		**1.26**	-4	1.259	-0.088	11.74	
468.28	*109.5*	1.30	1.33		**1.32**	-13	1.282	-0.296	11.88	257.39
484.3074	89.2957	1.41	1.25	1.44	**1.33**	-13.5	1.293	-0.310	14.05	
489.0531	*107.2925*	1.38	1.14	1.41	**1.26**	-15	1.219	-0.327	14.24	257.39
493.8605	125.4125	1.22	1.36		**1.29**	-15	1.245	-0.334	13.4	
509.75	*101.5*	1.33	0.00	0.44	**0.66**	-10	0.655	-0.115	27.13	257.41
527	86	0.77	0.66	0.93	**0.71**	-7	0.708	-0.087	36.03	
530	*95*									257.43
532.5	103.75	0.87	0.42	0.71	**0.65**	-12	0.632	-0.134	36.06	
TEST 2	(Supplementary Check)									
41	*100*									257.48
530	*95*									257.43
	In "dead" zone to the right of PH between the coffer dam and the PH the WSEL is									257.43

Velocity Test of Notigi G.S. Physical Model

FULL TEST

Date: Jan 23/95
Time (start / finish): 7:45 AM

Flow (cms): **867**
Upstream WSEL (m): 254.12
Downstream WSEL (m):
u/s PH WSEL (m): 254.04

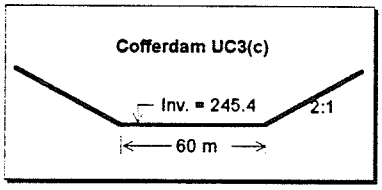

Description/Comments: -Cofferdam UC3c (invert = 245.4 m, inside bottom width = 60 m)
- changed screens in the power house and openings

*** Units are converted to proto type scale ***

Coordinates X	Coordinates Y	Velocity - mini probe readings 0.2 d (m/s)	0.8 d (m/s)	0.6 d (m/s)	Average (m/s)	Angle (ccw-x) (degrees)	X-vel (m/s)	Y-vel (m/s)	Depth, d (m)	Water Surface Elevation (m)
41	60	0.36	0.34		**0.35**	0	0.351	0.000	15.2	
41	*100*	0.36	0.28		**0.32**	0	0.324	0.000	16.38	254.02
41	245					-55	0.000	0.000	0	
131	79	0.61	0.55		**0.58**	0	0.579	0.000	8.58	
140	207			0.00	**0.00**				3.14	
140	250			0.00	**0.00**				0	
158	*127*			0.82	**0.82**	3	0.000	0.000	5.95	254.01
220	82			0.66	**0.66**	5	0.000	0.000	7.99	
220	*133.5*	0.63	0.34		**0.49**	-20	0.456	-0.166	15.13	254.02
220	207					0	0.000	0.000	0	
305	86	0.61	0.34		**0.47**	0	0.472	0.000	11.81	
305	*147.5*	0.58	0.50		**0.54**	-2	0.538	-0.019	16.73	254.02
305	197.5			0.00	**0.00**		0.000	0.000		
340.5	80.75	0.61	0.42		**0.51**	6	0.509	0.054	11.11	
376	75.5	0.50	0.28		**0.39**	28	0.345	0.184	12.37	
376	*123.5*	0.47	0.34		**0.40**	-5	0.403	-0.035	16.38	254.03
376	167	0.00	0.00		**0.00**	12	0.000	0.000	12.78	
376	195									
376	203									
422.53	*119.62*	1.14	1.09		**1.11**	-14	1.082	-0.270	8.46	253.98
438	156			1.14	**1.14**	-52	0.703	-0.900	2.32	
445.602	*117.1537*	1.28	1.25		**1.26**	-13	1.230	-0.284	8.7	253.97
452.5	81	1.36	1.30		**1.33**	-10	1.309	-0.231	8.18	
468.28	*109.5*	1.36	1.30		**1.33**	-13	1.295	-0.299	8.26	253.95
484.3074	89.2957	1.52	0.87		**1.20**	-11	1.173	-0.228	9.84	
489.0531	*107.2925*	1.52	0.87		**1.20**	-11	1.173	-0.228	9.91	253.92
493.8605	125.4125	1.41	1.52		**1.46**	-18	1.392	-0.452	9.55	
509.75	*101.5*	1.25	0.00		**0.62**	0	0.624	0.000	22.98	253.99
527	86	0.77	0.28		**0.53**	-12	0.514	-0.109	32.68	
530	*95*									254
532.5	103.75	0.66	0.50		**0.58**	-17	0.554	-0.169	32.8	

APPENDIX E: DOWNSTREAM CALIBRATION AND VERIFICATION SUMMARY

Table E-1 Summary of Calibation and Verification of Parameters for the downstream Notigi G.S. Model

Task	Design Alternative	Boundary Conditions		Parameters		Velocity Magnitude Criteria			WSEL Criteria
		Flow [cms]	d/s wsel [m]	Turbulent Exchange Coefficient	Manning's *n*	Regression of Phys. vs. Num.. r^2	intercept	slope	Root Mean Square Error
Calibration	DOB*	1100	245.5	425	0.025	0.9002	0.1814	0.8391	na
Calibration	DC3a	1100	245.5	800	0.025	0.7594	0.2139	0.7680	0.06486
Verification	DC3a	867	244.5	"	"	0.7900	0.1530	0.7690	0.07863
Verification	DC2b	1100	245.5	"	"	0.6130	0.2520	0.8020	0.10790
Average						0.7208	0.2063	0.7797	0.08380
Calibration	DC3a	867	244.5	650	0.03	0.7912	0.1514	0.7665	0.08039
Verification	DC3a	1100	245.5	"	"	0.7580	0.2190	0.7610	0.06653
Verification	DC2b	1100	245.5	"	"	0.6052	0.2438	0.7975	na
Average						0.7181	0.2047	0.7750	0.07346
Calibration	DC2b	1100	245.5	**850**	**0.035**	0.6838	0.1361	0.8645	0.09843
Verification	DC3a	1100	245.5	"	"	0.7710	0.2490	0.7320	0.06606
Verification	DC3a	867	244.5	"	"	0.8030	0.1590	0.7530	0.07919
Average				**850**	**0.035**	**0.7526**	**0.1814**	**0.7832**	0.08123

* Not included in the verification process.

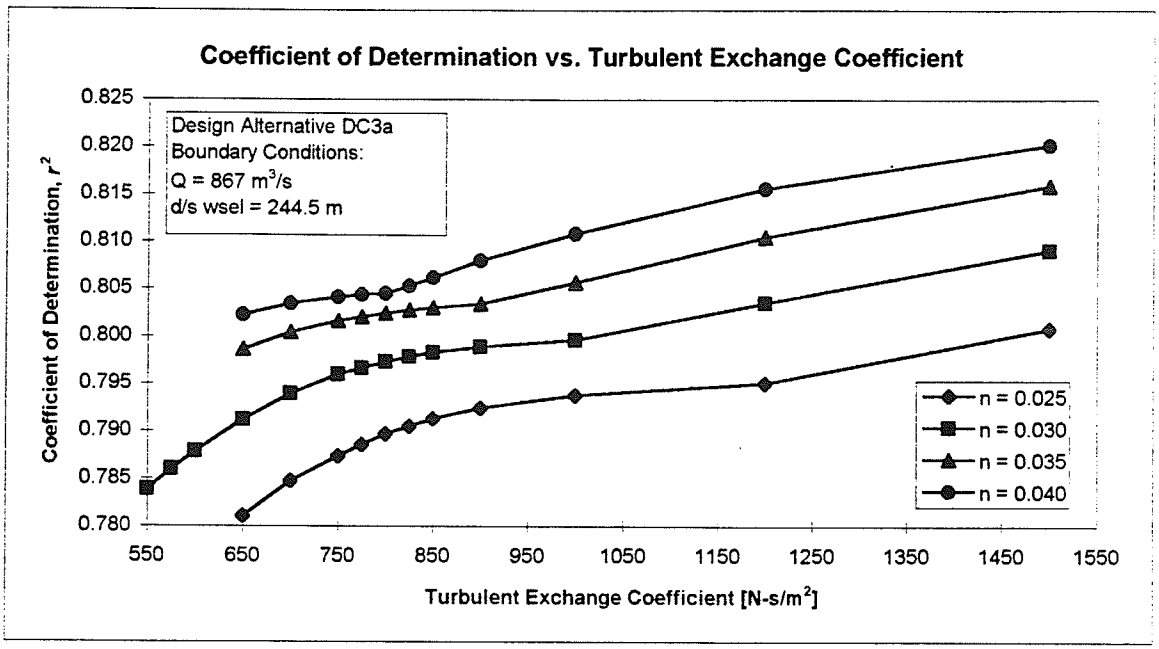

Figure E-1 *Regression Criterion of Coefficient of Determination vs. the Turbulent Exchange Coefficient and Manning's n for the comparison of velocity magnitudes between the physical and numerical data from test scenario DC3a with a flow of 867 m^3/s and a downstream water level at 244.5 m.*

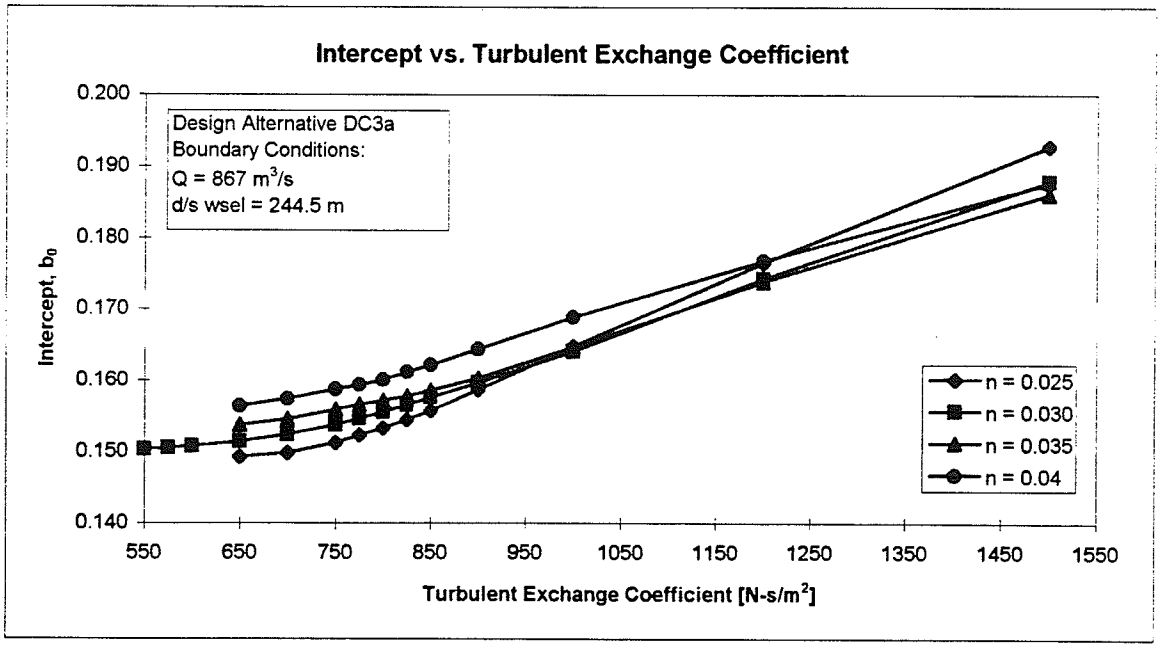

Figure E-2 *Regression Criterion of Intercept vs. the Turbulent Exchange Coefficient and Manning's n for the comparison of velocity magnitudes between the physical and numerical data from test scenario DC3a with a flow of 867 m3/s and a downstream water level at 244.5 m.*

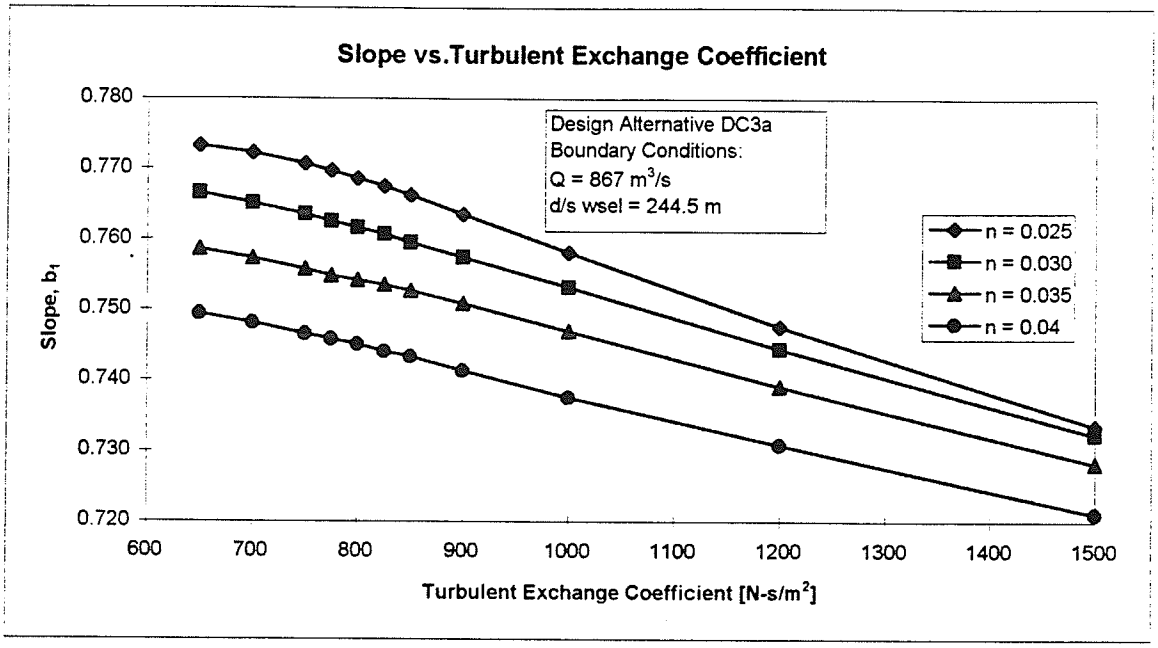

Figure E-3 *Regression Criterion of Slope vs. the Turbulent Exchange Coefficient and Manning's n for the comparison of velocity magnitudes between the physical and numerical data from test scenario DC3a with a flow of 867 m3 s and a downstream water level at 244.5 m.*

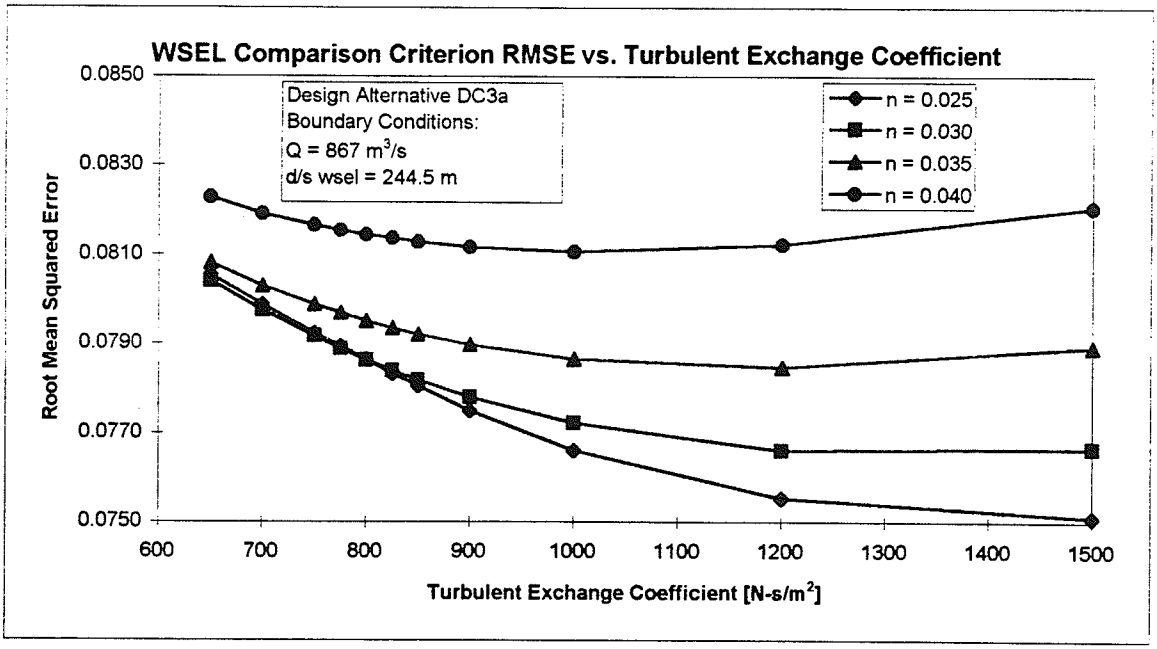

Figure E-4 *Root Mean Squared Error vs. the Turbulent Exchange Coefficient and Manning's n for the comparison of water surface elevations between the physical and numerical data from test scenario DC3a with a flow of 867 m3/s and a downstream water level at 244.5 m.*

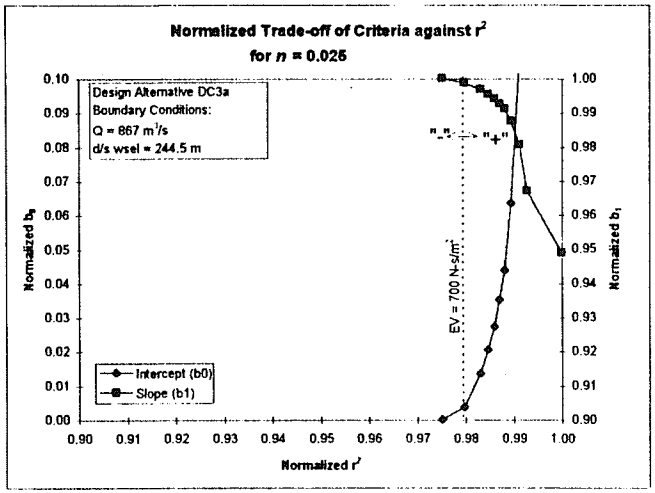

Figure E-5 Trade-off between Regression Statistics for Manning's n = 0.025 for the comparison of velocity magnitudes between the physical and numerical data from test scenario DC3a with a flow of 867 m³/s and a downstream water level at 244.5 m.

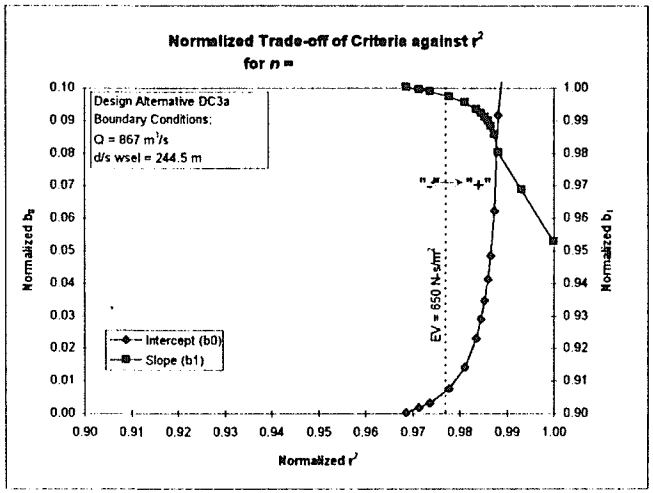

Figure E-6 Trade-off between Regression Statistics for Manning's n = 0.030 for the comparison of velocity ma nitudes between the physical and numerical data from test scenario DC3a with a flow of 867 m³/s and a downstream water level at 244.5 m.

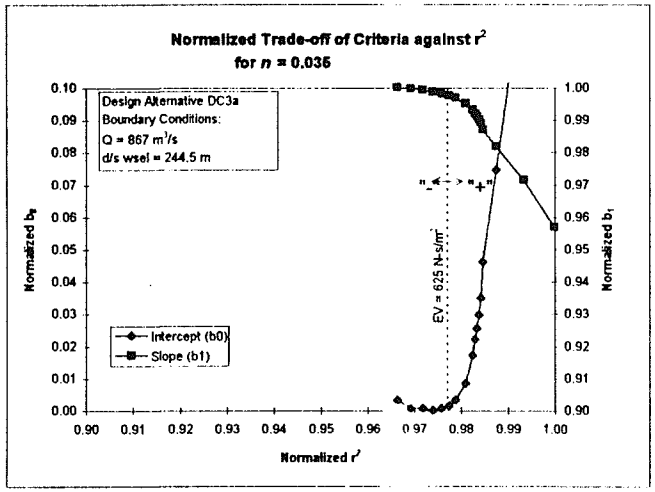

Figure E-7 Trade-off between Regression Statistics for Manning's n = 0.035 for the comparison of velocity magnitudes between the physical and numerical data from test scenario DC3a with a flow of 867 m³/s and a downstream water level at 244.5 m.

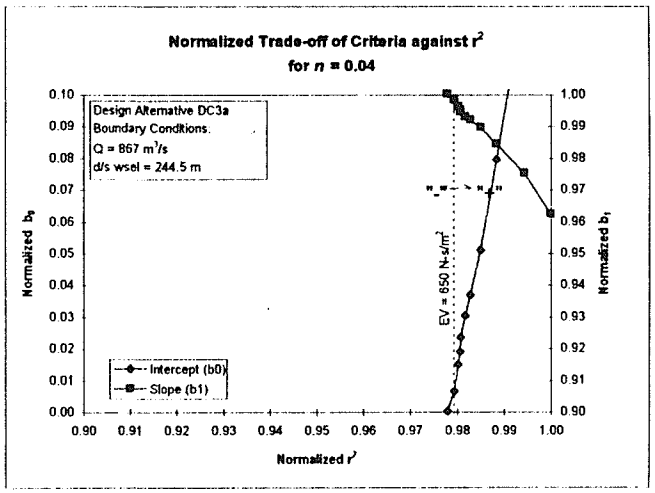

Figure E-8 Trade-off between Regression Statistics for Manning's n = 0.040 for the comparison of velocity magnitudes between the physical and numerical data from test scenario DC3a with a flow of 867 m³/s and a downstream water level at 244.5 m.

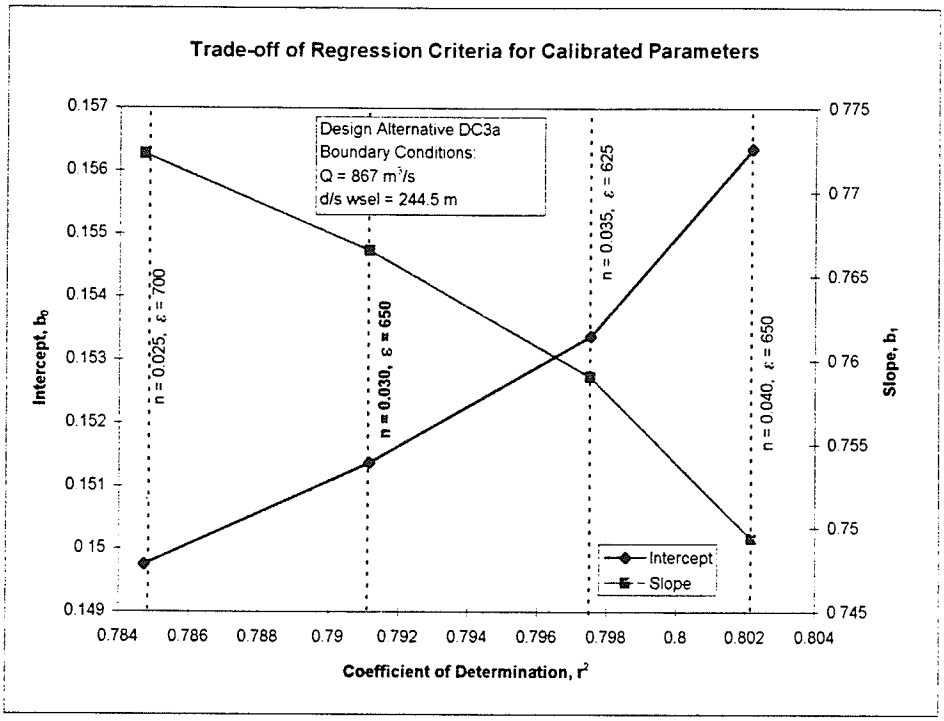

Figure E-9 *Trade-off between Regression Criteria for the Calibrated Parameters of scenario DC3a with a flow of 867 m^3/s and a downstream water level at 244.5 m. The best trade-off occurs for n=0.030 and $\varepsilon = 650$ N-s/m^2.*

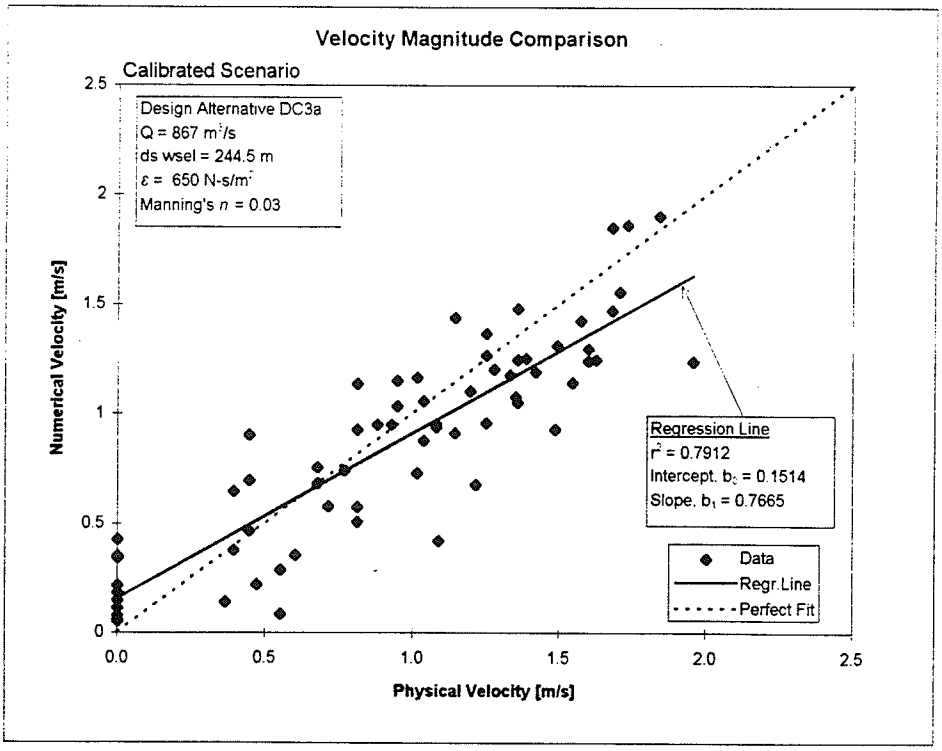

Figure E-10 *Scatter plot comparing numerical and physical velocity magnitudes for scenario DC3a with a flow of 867 m^3/s and a downstream water level at 244.5 m. The calibrated parameters for this scenario are n=0.030 and $\varepsilon = 650$ N-s/m^2.*

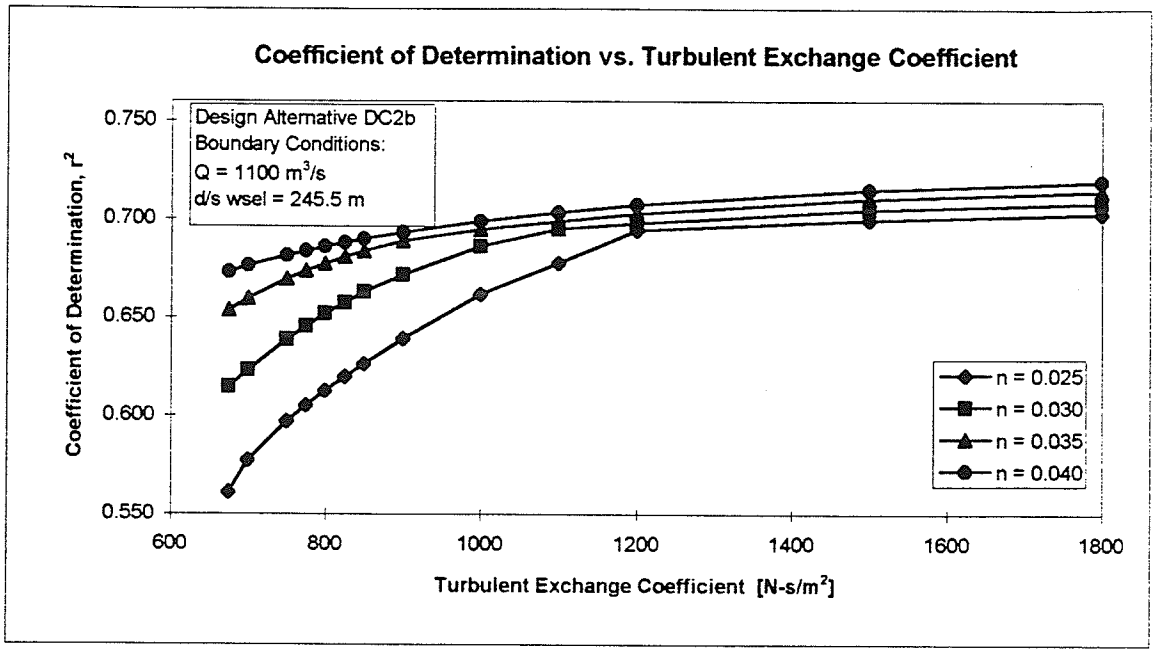

Figure E-11 *Regression Criterion of Coefficient of Determination vs. the Turbulent Exchange Coefficient and Manning's n for the comparison of velocity magnitudes between the physical and numerical data from test scenario DC2b with a flow of 1100 m^3/s and a downstream water level at 245.5 m.*

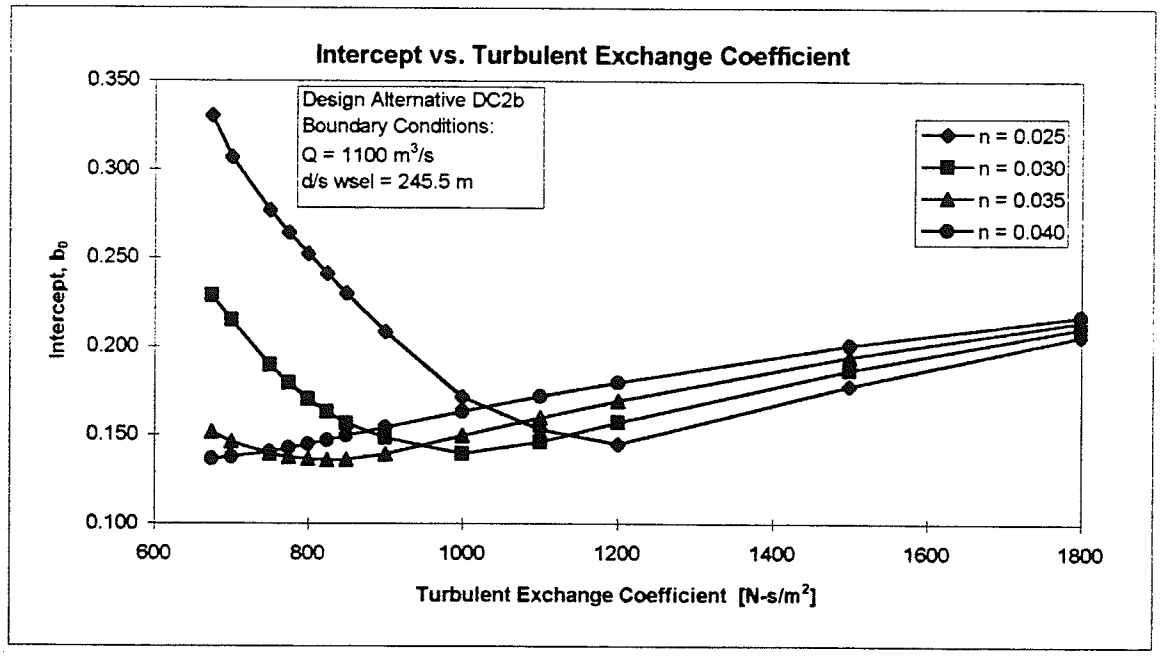

Figure E-12 *Regression Criterion of Intercept vs. the Turbulent Exchange Coefficient and Manning's n for the comparison of velocity magnitudes between the physical and numerical data from test scenario DC2b with a flow of 1100 m^3/s and a downstream water level at 245.5 m.*

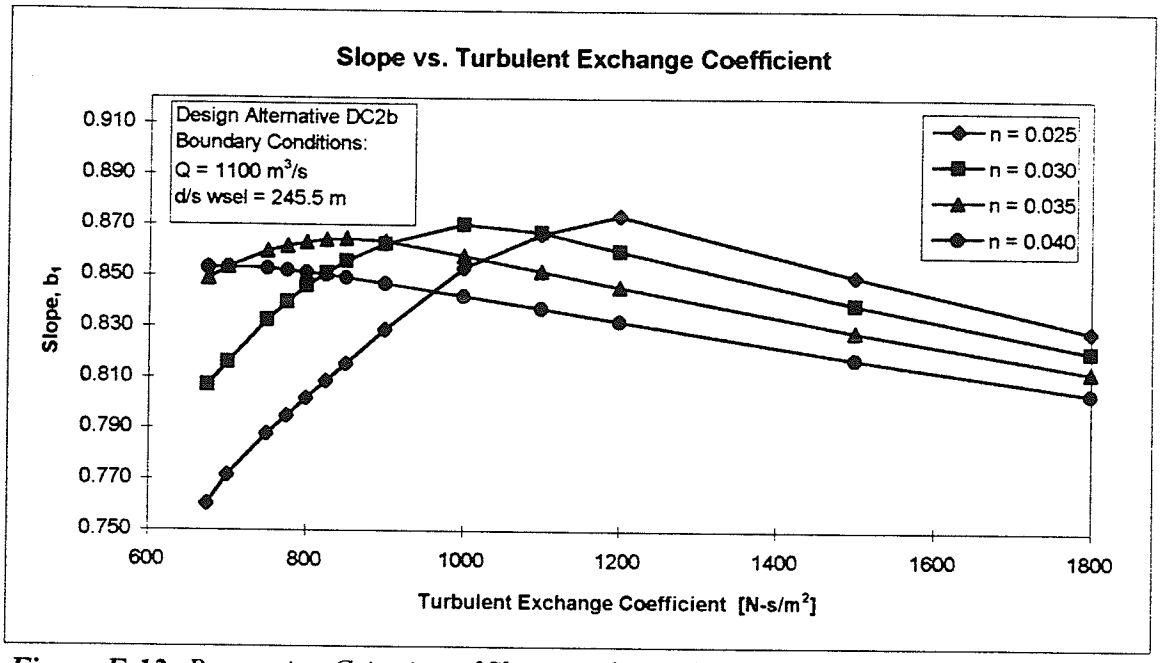

Figure E-13 *Regression Criterion of Slope vs. the Turbulent Exchange Coefficient and Manning's n for the comparison of velocity magnitudes between the physical and numerical data from test scenario DC2b with a flow of 1100 m ^{3}/s and a downstream water level at 245.5 m.*

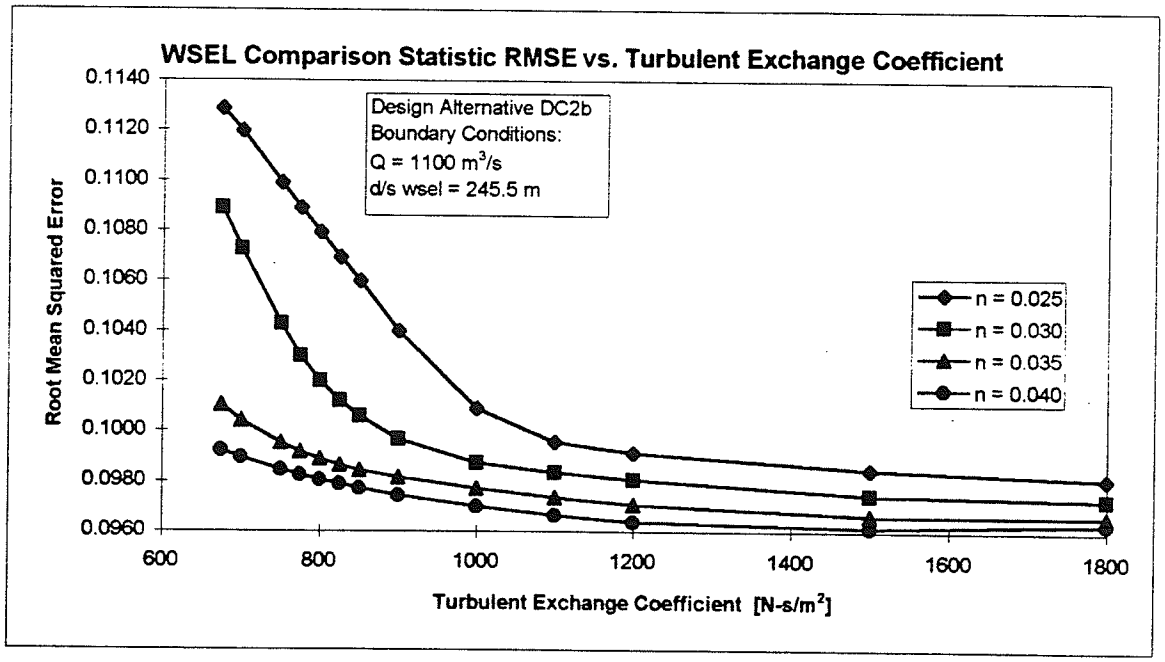

Figure E-14 *Root Means Squared Error vs. the Turbulent Exchange Coefficient and Manning's n for the comparison of water surface elevations between the physical and numerical data from test scenario DC2b with a flow of 1100 m ^{3}/s and a downstream water level at 245.5 m.*

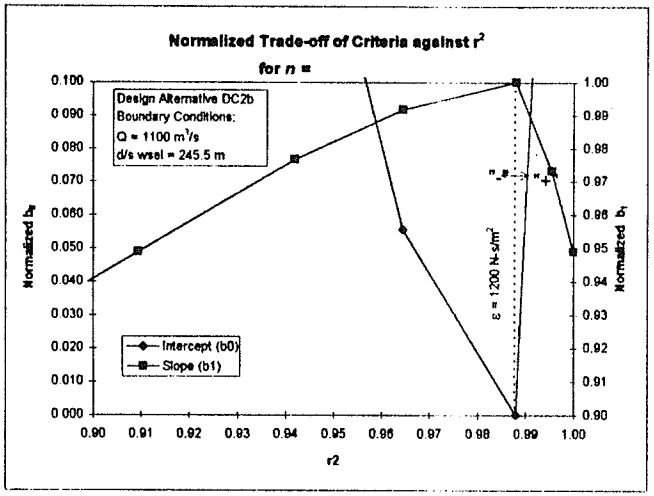

Figure E-15 Trade-off between Regression Statistics for Manning's n = 0.025 for the comparison of velocity magnitudes between the physical and numerical data from test scenario DC2b with a flow of 1100 m³/s and a downstream water level at 245.5 m.

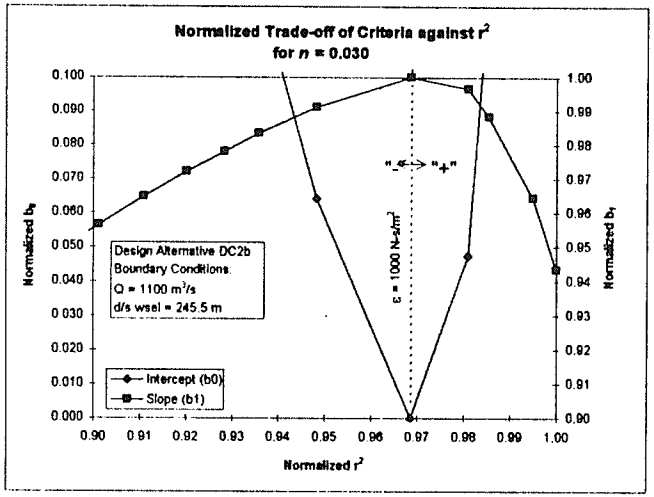

Figure E-16 Trade-off between Regression Statistics for Manning's n = 0.030 for the comparison of velocity magnitudes between the physical and numerical data from test scenario DC2b with a flow of 1100 m³/s and a downstream water level at 245.5 m.

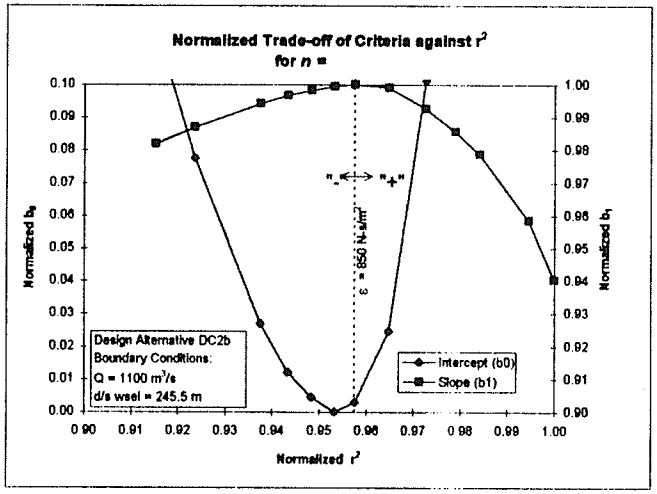

Figure E-17 Trade-off between Regression Statistics for Manning's n = 0.035 for the comparison of velocity magnitudes between the physical and numerical data from test scenario DC2b with a flow of 1100 m³/s and a downstream water level at 245.5 m.

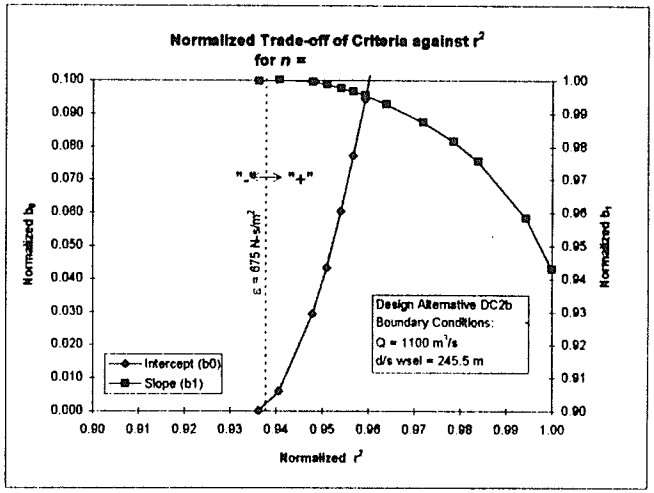

Figure E-18 Trade-off between Regression Statistics for Manning's n = 0.040 for the comparison of velocity magnitudes between the physical and numerical data from test scenario DC2b with a flow of 1100 m³/s and a downstream water level at 245.5 m.

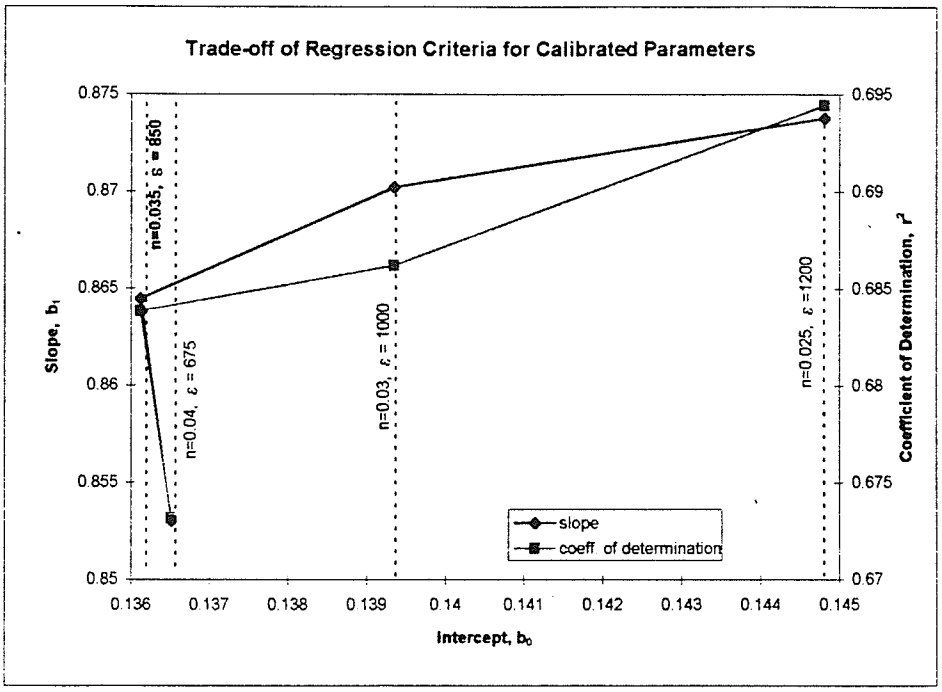

Figure E-19 *Trade-off between Regression Criteria for the Calibrated Parameters of scenario DC2b with a flow of 1100 m^3/s and a downstream water level at 245.5 m. The best trade-off occurs for n=0.035 and ε = 850 N-s/m^2.*

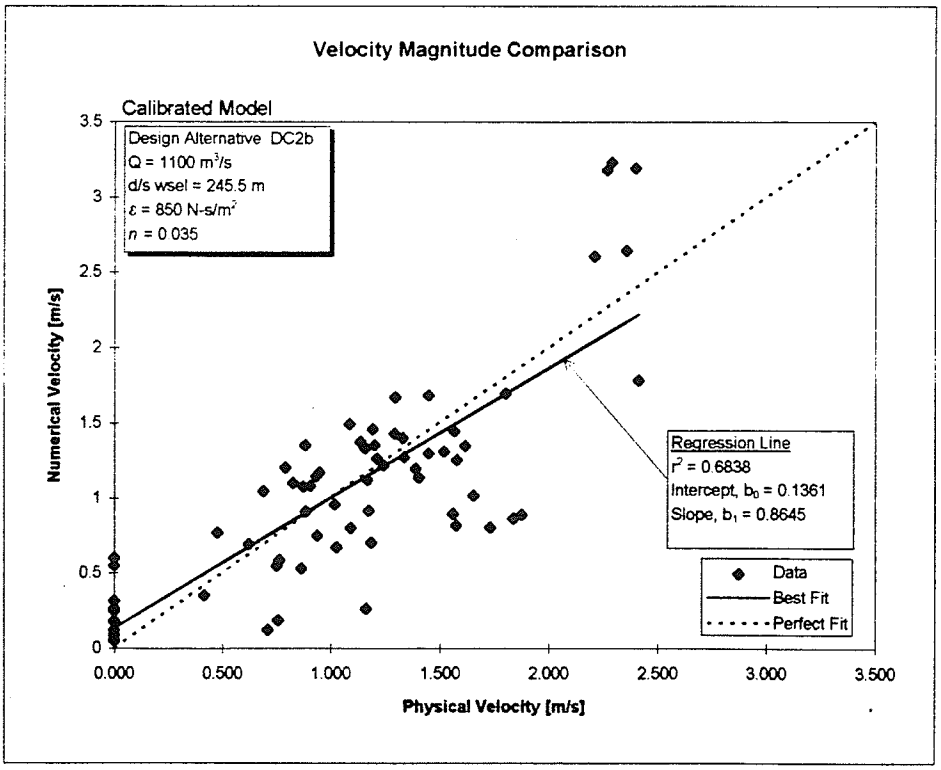

Figure E-20 *Scatter plot comparing numerical and physical velocity magnitudes for scenario DC2b with a flow of 1100 m^3/s and a downstream water level at 245.5 m. The calibrated parameters for this scenario are n=0.035 and ε = 850 N-s/m^2.*

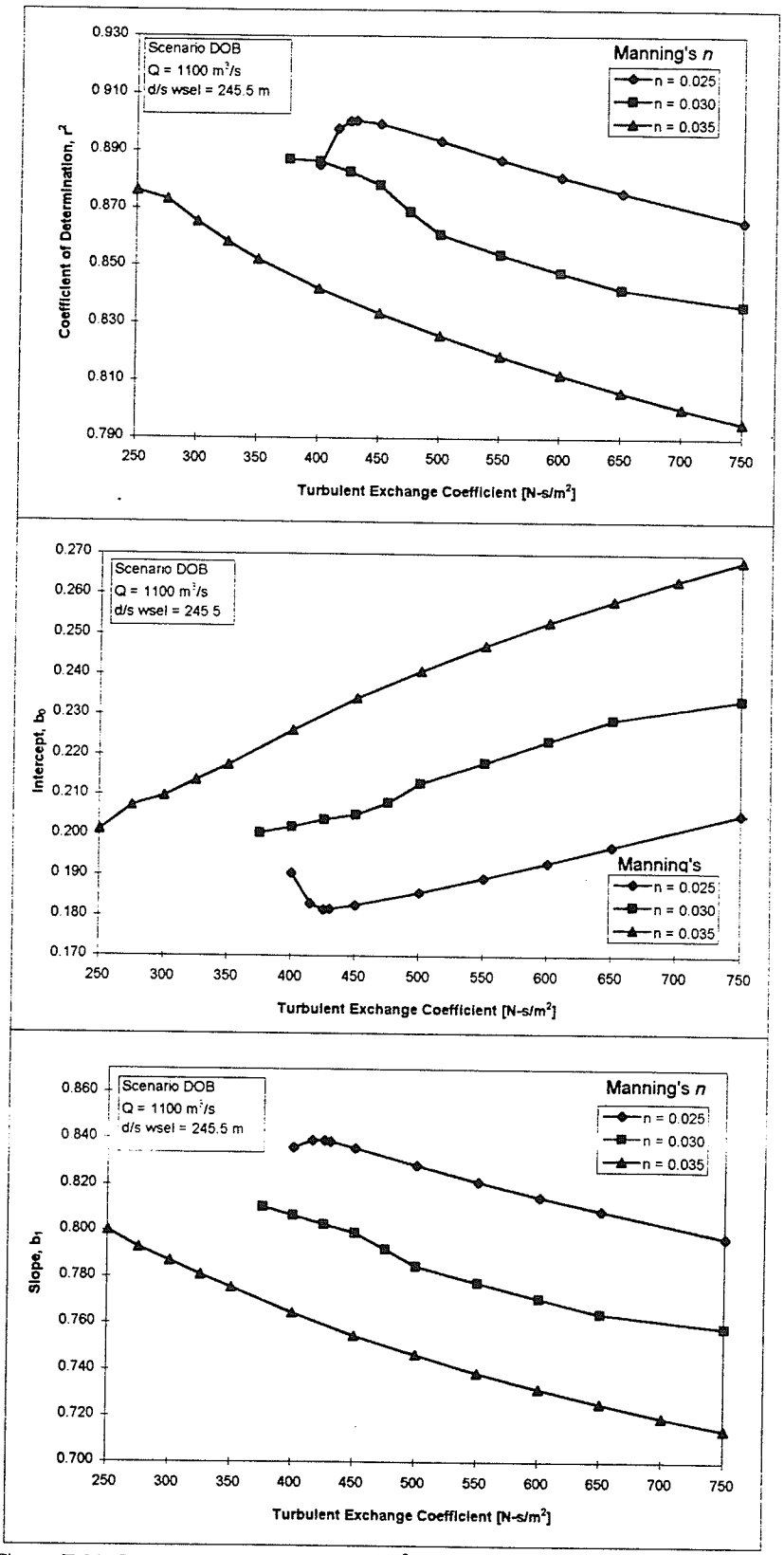

Figure E-21 Regression Statistics Criteria, r^2, b_0 and b_1, versus Turbulent Exchange Coefficients for various Manning's n for the DOB scenario with no cofferdam.

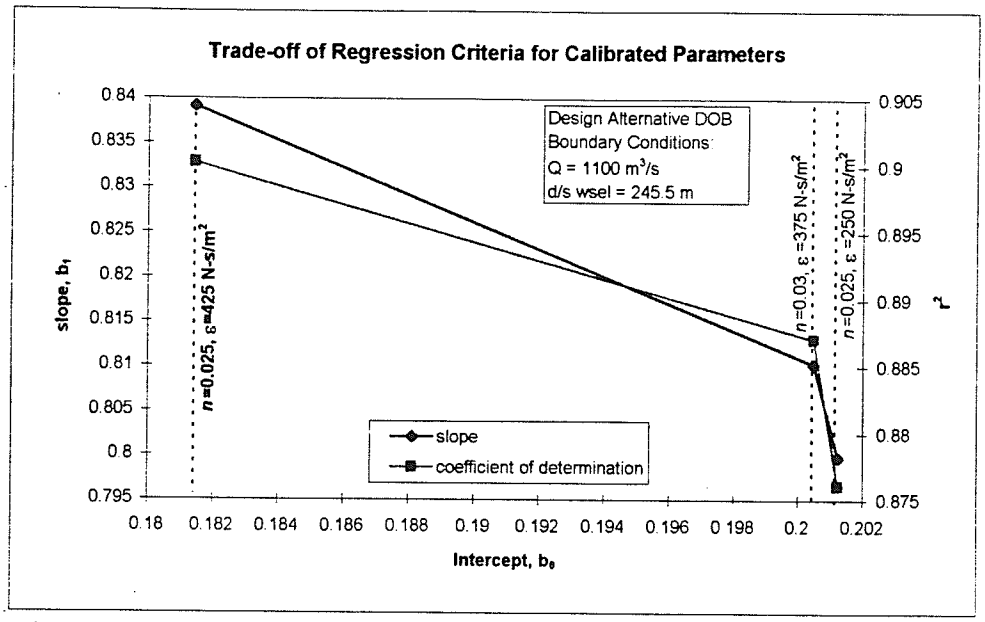

Figure E-22 *Trade-off between Regression Criteria for the Calibrated Parameters of Scenario DOB with a flow of 1100 m /s² and a downstream watersurface elevation at 245.5 m. The best trade-off occurs for n = 0.025 and ε =425 N-s/m².*

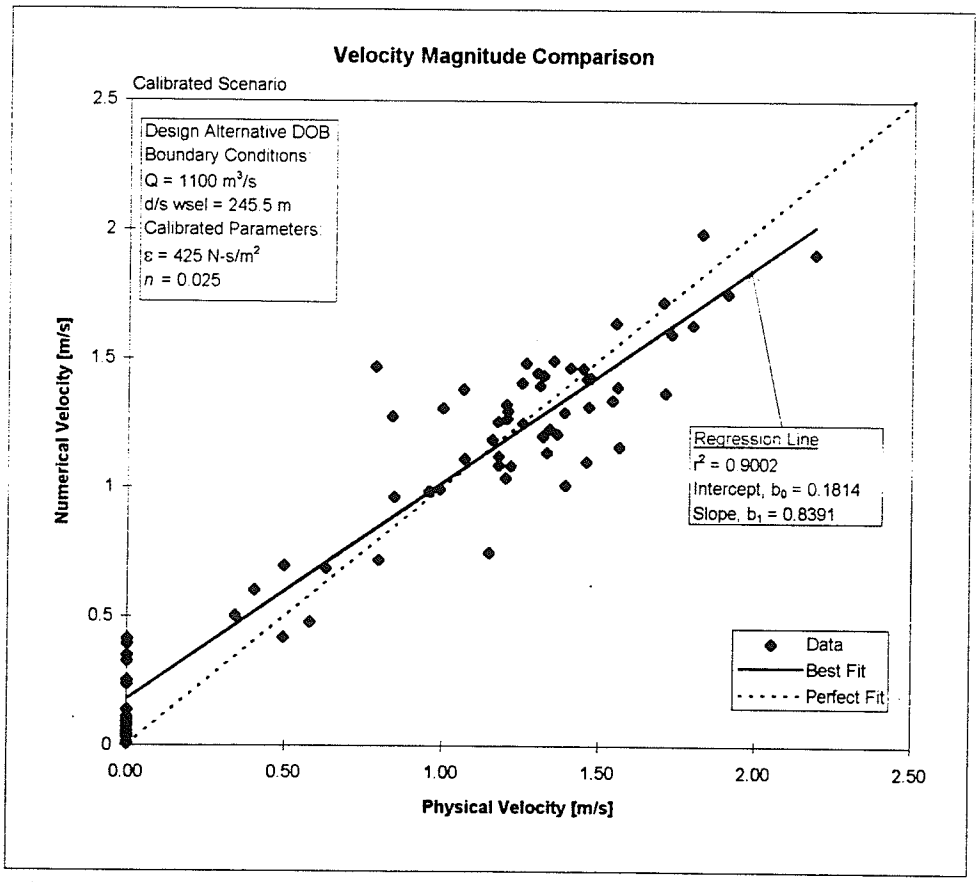

Figure E-23 *Scatter plot comparing numerical and physical velocity magnitudes for scenario DOB with a flow of 1100 m /s² and a downstream watersurface elevation at 245.5 m. The calibrated parameters for this scenario are for n = 0.025 and ε =425 N-s/m².*

Physical and Numerical Velocity Magnitudes

Removal Scheme:	DC3a		
Flow (m^3/s):	1100	Avg. Difference (m/s):	-0.023
d/s wsel (m):	245.5	Avg. Abs. Diff. (m/s):	0.270
ε_{ij} (N-s/m^2):	800	Standard Dev.(diff):	0.335
Manning's n:	0.025	Max. (diff):	0.819
Number of data:	72	Min. (diff.):	-0.518

Node Coordinate		Physical	Calibrated Numerical		Absolute
X	Y	Velocity (m/s)	Velocity (m/s)	Difference	Difference
45	-110.5	0.907	1.1	-0.193	0.193
47	-129	1.413	1.495	-0.082	0.082
56	-93	0.874	0.547	0.327	0.327
57	-146	1.186	1.171	0.015	0.015
69	-109	0.971	1.253	-0.282	0.282
70	-125	1.397	1.416	-0.019	0.019
72	-160	0.873	0.672	0.201	0.201
77	-86	1.053	0.701	0.352	0.352
78	-142	0.971	1.106	-0.135	0.135
80	-151.2	1.386	0.89	0.496	0.496
80	-160	1.592	0.773	0.819	0.819
80	-174	0.000	0.518	-0.518	0.518
92	-163	1.668	0.978	0.690	0.690
93	-74	0.329	0.26	0.069	0.069
94.4	-192	0.000	0.315	-0.315	0.315
98.4	-148.8	1.409	1.28	0.129	0.129
101	-101	0.727	1.091	-0.364	0.364
101	-120	1.134	1.354	-0.220	0.220
103	-132	0.847	1.364	-0.517	0.517
110	-170	0.579	0.742	-0.163	0.163
116	-146.4	1.269	1.099	0.170	0.170
120	-72	0.694	0.372	0.322	0.322
125	-91	0.473	0.819	-0.346	0.346
127	-110	0.863	1.122	-0.259	0.259
128	-212.8	0.000	0.066	-0.066	0.066
132	-130	0.911	1.215	-0.304	0.304
146	-185	0.000	0.377	-0.377	0.377
161	-25	0.000	0.057	-0.057	0.057
167.6	-36	0.000	0.18	-0.180	0.180
171.2	-153.6	1.312	1.196	0.116	0.116
176	-56.4	0.705	0.569	0.136	0.136
182	-130	1.296	1.435	-0.139	0.139
184	-104	1.285	1.5	-0.215	0.215
186	-79	0.969	1.157	-0.188	0.188
189.6	-277.2	0.000	0.071	-0.071	0.071
197	-136	1.619	1.636	-0.017	0.017
201.2	-282	0.608	0.123	0.485	0.485
202	-112	1.476	1.332	0.144	0.144

Physical and Numerical Velocity Magnitudes

Node Coordinate X	Y	Physical Velocity (m/s)	Calibrated Numerical Velocity (m/s)	Difference	Absolute Difference
208	-139	1.781	1.996	-0.215	0.215
214	-84	1.597	1.291	0.306	0.306
216	-115	1.705	1.949	-0.244	0.244
220	-223	0.369	0.085	0.284	0.284
222	-144	2.026	2.018	0.008	0.008
225.5	-86	1.538	1.57	-0.032	0.032
228	-55	0.905	0.905	0.000	0.000
233	-124	1.705	1.43	0.275	0.275
240	-240	0.000	0.186	-0.186	0.186
244	-91	1.646	1.232	0.414	0.414
244.4	-355.1	0.381	0.292	0.089	0.089
247.2	-183.6	0.000	0.547	-0.547	0.547
252	-269	0.000	0.243	-0.243	0.243
260	-154	1.810	1.582	0.228	0.228
273.6	-217.2	0.000	0.081	-0.081	0.081
274	-125	1.503	1.456	0.047	0.047
288	-96	1.293	1.073	0.220	0.220
291.9	-206	0.000	0.86	-0.860	0.860
296	-62.4	0.000	0.141	-0.141	0.141
298.4	-255.2	0.000	0.125	-0.125	0.125
312	-185	1.743	1.49	0.253	0.253
319.2	-355.2	1.145	0.246	0.899	0.899
331	-246	0.897	0.956	-0.059	0.059
336	-163	1.560	1.405	0.155	0.155
355	-355.2	1.554	1.36	0.194	0.194
360	-140	1.325	0.933	0.392	0.392
367	-235	1.581	1.393	0.188	0.188
382	-120	0.000	0.247	-0.247	0.247
386	-355.2	1.584	1.69	-0.106	0.106
406.4	-97.8	0.000	0.092	-0.092	0.092
408	-223	1.258	1.059	0.199	0.199
408	-355.2	1.325	1.666	-0.341	0.341
450	-215	0.000	0.327	-0.327	0.327
476	-204	0.000	0.057	-0.057	0.057

Physical and Numerical Velocity Magnitudes

Removal Scheme:	DC3a(Q2)		
Flow (m^3/s):	867	Avg. Difference (m/s):	0.039
d/s wsel (m):	244.5	Avg. Abs. Diff. (m/s):	0.215
ε_{ij} (N-s/m^2):	650	Standard Dev.(diff):	0.279
Manning's n:	0.03	Max. (diff):	0.718
Number of data:	68	Min. (diff.):	-0.457

Node Coordinate		Physical	Calibrated Numerical		Absolute
X	Y	Velocity (m/s)	Velocity (m/s)	Difference	Difference
45	-110.5	1.484	0.929	0.555	0.555
47	-129	1.956	1.238	0.718	0.718
56	-93	0.810	0.506	0.304	0.304
69	-109	1.349	1.075	0.274	0.274
70	-125	1.417	1.19	0.227	0.227
72	-160	0.810	0.571	0.239	0.239
77	-86	1.215	0.675	0.540	0.540
78	-142	0.810	0.924	-0.114	0.114
80	-151.2	0.676	0.753	-0.077	0.077
80	-160	0.676	0.68	-0.004	0.004
92	-163	0.445	0.902	-0.457	0.457
94.4	-192	0.000	0.427	-0.427	0.427
98.4	-148.8	0.810	1.135	-0.325	0.325
101	-101	1.080	0.951	0.129	0.129
101	-120	0.945	1.149	-0.204	0.204
103	-132	1.013	1.165	-0.152	0.152
110	-170	0.445	0.695	-0.250	0.250
116	-146.4	1.080	0.936	0.144	0.144
120	-72	0.601	0.354	0.247	0.247
125	-91	1.013	0.726	0.287	0.287
127	-110	0.878	0.949	-0.071	0.071
128	-212.8	0.000	0.078	-0.078	0.078
132	-130	0.945	1.032	-0.087	0.087
146	-185	0.391	0.375	0.016	0.016
161	-25	0.000	0.052	-0.052	0.052
167.6	-36	0.000	0.185	-0.185	0.185
171.2	-153.6	1.035	1.057	-0.022	0.022
176	-56.4	0.713	0.576	0.137	0.137
182	-130	1.249	1.267	-0.018	0.018
184	-104	1.249	1.366	-0.117	0.117
186	-79	1.195	1.104	0.091	0.091
189.6	-277.2	0.000	0.216	-0.216	0.216
197	-136	1.678	1.47	0.208	0.208
201.2	-282	0.000	0.349	-0.349	0.349
202	-112	1.329	1.176	0.153	0.153
208	-139	1.731	1.862	-0.131	0.131
214	-84	1.597	1.239	0.358	0.358
216	-115	1.678	1.85	-0.172	0.172

Physical and Numerical Velocity Magnitudes

Node Coordinate X	Y	Physical Velocity (m/s)	Calibrated Numerical Velocity (m/s)	Difference	Absolute Difference
220	-223	0.000	0.15	-0.150	0.150
222	-144	1.839	1.903	-0.064	0.064
225.5	-86	1.705	1.554	0.151	0.151
228	-55	1.249	0.956	0.293	0.293
233	-124	1.624	1.247	0.377	0.377
240	-240	0.472	0.22	0.252	0.252
244	-91	1.544	1.141	0.403	0.403
244.4	-355.1	0.445	0.465	-0.020	0.020
251.6	-61.9	0.391	0.645	-0.254	0.254
252	-269	0.552	0.287	0.265	0.265
260	-154	1.571	1.423	0.148	0.148
273.6	-217.2	0.000	0.115	-0.115	0.115
274	-125	1.490	1.311	0.179	0.179
288	-96	1.356	1.05	0.306	0.306
291.9	-206	0.767	0.737	0.030	0.030
296	-62.4	0.364	0.141	0.223	0.223
298.4	-255.2	0.000	0.149	-0.149	0.149
312	-185	1.597	1.295	0.302	0.302
319.2	-355.2	1.088	0.416	0.672	0.672
331	-246	1.035	0.874	0.161	0.161
336	-163	1.383	1.252	0.131	0.131
355	-355.2	1.356	1.246	0.110	0.110
360	-140	1.142	0.909	0.233	0.233
367	-235	1.276	1.201	0.075	0.075
386	-355.2	1.356	1.479	-0.123	0.123
406.4	-97.8	0.552	0.085	0.467	0.467
408	-223	0.927	0.947	-0.020	0.020
408	-355.2	1.142	1.439	-0.297	0.297
450	-215	0.000	0.34	-0.340	0.340
476	-204	0.000	0.059	-0.059	0.059

Physical and Numerical Velocity Magnitudes

Removal Scheme:	DC2b		
Flow (m^3/s):	1100	Avg. Difference (m/s):	-0.031
d/s wsel (m):	245.5	Avg. Abs. Diff. (m/s):	0.267
ε_{ij} ($N\text{-}s/m^2$):	850	Standard Dev.(diff):	0.329
Manning's n:	0.035	Max. (diff):	0.762
Number of data:	73	Min. (diff.):	-0.602

Node Coordinate X	Y	Physical Velocity (m/s)	Calibrated Numerical Velocity (m/s)	Difference	Absolute Difference
45	-110.5	0.872	1.075	-0.203	0.203
47	-129	1.086	1.491	-0.405	0.405
56	-93	0.865	0.531	0.334	0.334
57	-146	0.947	1.168	-0.221	0.221
69	-109	1.240	1.216	0.024	0.024
70	-125	1.331	1.399	-0.068	0.068
72	-160	1.186	0.7	0.486	0.486
77	-86	1.026	0.67	0.356	0.356
78	-142	0.826	1.102	-0.276	0.276
80	-151.2	0.884	0.909	-0.025	0.025
80	-160	1.576	0.814	0.762	0.762
80	-174	0.000	0.602	-0.602	0.602
92	-163	1.654	1.015	0.639	0.639
93	-74	0.000	0.258	-0.258	0.258
98.4	-148.8	1.449	1.296	0.153	0.153
101	-101	0.689	1.046	-0.357	0.357
101	-120	1.155	1.33	-0.175	0.175
103	-132	0.882	1.351	-0.469	0.469
110	-170	1.091	0.8	0.291	0.291
116	-146.4	1.169	1.116	0.053	0.053
120	-72	0.416	0.351	0.065	0.065
125	-91	0.478	0.77	-0.292	0.292
127	-110	0.906	1.081	-0.175	0.175
132	-130	0.790	1.2	-0.410	0.410
146	-185	0.765	0.588	0.177	0.177
161	-25	0.000	0.061	-0.061	0.061
167.6	-36	0.000	0.18	-0.180	0.180
171.2	-153.6	1.212	1.262	-0.050	0.050
176	-56.4	0.751	0.547	0.204	0.204
182	-130	1.134	1.374	-0.240	0.240
184	-104	1.192	1.458	-0.266	0.266
186	-79	0.933	1.141	-0.208	0.208
189.6	-277.2	0.711	0.123	0.588	0.588
197	-136	1.802	1.694	0.108	0.108
200	-161	2.355	2.647	-0.292	0.292
201.2	-282	0.756	0.186	0.570	0.570
202	-112	1.336	1.268	0.068	0.068
205	-181	2.412	1.783	0.629	0.629

Physical and Numerical Velocity Magnitudes

Node Coordinate X	Y	Physical Velocity (m/s)	Calibrated Numerical Velocity (m/s)	Difference	Absolute Difference
208	-139	2.269	3.18	-0.911	0.911
214	-84	1.290	1.427	-0.137	0.137
216	-115	2.398	3.195	-0.797	0.797
220	-223	0.000	0.183	-0.183	0.183
222	-144	2.288	3.231	-0.943	0.943
225.5	-86	2.209	2.608	-0.399	0.399
228	-55	1.390	1.195	0.195	0.195
233	-124	0.937	0.748	0.189	0.189
240	-240	0.000	0.185	-0.185	0.185
244	-91	1.875	0.888	0.987	0.987
244.3907	-355.109	0.000	0.319	-0.319	0.319
247.2	-183.6	1.730	0.804	0.926	0.926
252	-60	0.000	0.553	-0.553	0.553
252	-269	0.000	0.25	-0.250	0.250
260	-154	1.201	1.352	-0.151	0.151
273.6	-217.2	0.000	0.089	-0.089	0.089
274	-125	1.403	1.135	0.268	0.268
288	-96	1.018	0.957	0.061	0.061
291.9213	-206.013	1.837	0.862	0.975	0.975
296	-62.4	0.000	0.093	-0.093	0.093
298.4	-255.2	0.000	0.125	-0.125	0.125
312	-185	1.565	1.445	0.120	0.120
319.2	-355.2	1.161	0.263	0.898	0.898
331	-246	1.560	0.892	0.668	0.668
336	-163	1.579	1.251	0.328	0.328
355	-355.2	1.616	1.348	0.268	0.268
360	-140	0.622	0.691	-0.069	0.069
367	-235	1.519	1.31	0.209	0.209
382	-120	0.000	0.25	-0.250	0.250
386	-355.2	1.449	1.683	-0.234	0.234
406.4	-94.8	0.000	0.254	-0.254	0.254
408	-223	1.174	0.915	0.259	0.259
408	-355.2	1.296	1.669	-0.373	0.373
450	-215	0.000	0.267	-0.267	0.267
476	-204	0.000	0.049	-0.049	0.049

APPENDIX F: UPSTREAM CALIBRATION AND VERIFICATION SUMMARY

Table F-1 Summary of Calibated Parameters for the Upstream Notigi G.S. Model

Design Alternative	Parameters		Velocity Magnitude						WSEL			
				Boundary Conditions		Criteria				Boundary Conditions		Criteria
	Turbulent Exchange Coefficient	Manning's *n*	Number of Velocity Nodes	Flow [cms]	u/s wsel [m]	Regression of Phys. vs. Num. r^2	intercept	slope	Number of WSEL Nodes	Flow [cms]	u/s wsel [m]	RMSE
UC1b	2800	0.04	30	974	257.56	0.7872	0.1143	0.7089	11	974	257.56	0.0292
UC2c	2800	0.04	30	1100	257.66	0.8435	0.1132	0.9265	11	1100	257.97	0.0307
UC3c	2800	0.04	30	1100	257.59	0.8627	0.1532	0.7559	11	1100	257.45	0.0274
UC3c	5800 *	0.04	26	867	254.02	0.7908	0.1848	0.8134	11	867	254.02	0.0694
	2800	**0.04**										

* Using a reduced flow of 867 m^3/s and a reduced wsel of 254.02 m required a much higher Turbulent Exchange Coefficient for the model to converge. Therefore, flow conditions significantly different from those used to calibrate the model (Q = 1100 cms, and a FSL of 257.66 m) cannot be applied to the calibrated model. Calibration of all the full test cases revealed that there was very little difference in the criteria regardless of the Turbulent Exchange Coefficient and Manning's *n* selected.

Table F-2 Verification Summary using Calibated Parameters for the Upstream Notigi G.S. Model

Calibrated Parameters: Turbulent Exchange Coefficient[1] = 2800 N-s/m², Manning's *n* = 0.04											
Design Alternative	Number of Velocity Nodes	Velocity Magnitude						WSEL			
		Boundary Conditions		Criteria				Number of WSEL Nodes	Boundary Conditions		Criteria
		Flow [cms]	u/s wsel [m]	Regression of Phys. vs. Num. r^2	intercept	slope			Flow [cms]	u/s wsel [m]	RMSE
UOB	25	1100	257.84	0.5875	0.1623	0.6198		11	1100	257.56	0.0454
UC1c	11	1100	257.26	0.9162	0.1396	0.8428		11	1100	257.26	0.0216
UC2a	9	1100	257.56	0.8928	0.0218	1.0373		11	1100	257.61	0.0126
UC2b	9	1100	257.56	0.9409	-0.0050	1.0283		11	1100	257.56	0.0208
UC2c(ii)	9	1100	257.56	0.9170	0.1132	0.8780		11	1100	257.56	0.0200
UC3a	11	1100	257.61	0.6836	0.1399	0.8461		11	1100	257.75	0.0120
UC3b	11	1100	257.52	0.6773	0.2300	0.7486		11	1100	257.52	0.0240

1. The calibrated value of ε is 2800 N-s/m², and for Manning's *n* is 0.04. It should be noted that in the verification of some of the scenarios, the ε is not be able to be reduced to the calibrated value. If it comes within 500 N-s/m² it should be reasonable. The cases and their respective lowest ε are as follows:

Case	Turbulent Exchange Coefficient
UC1c	3000
UC3b	2850
UOB	3000

In other cases, the Turbulent Exchange Coefficient could have been reduced to values less than 2800 N-s/m², but not to any significant improvement in accuracy.

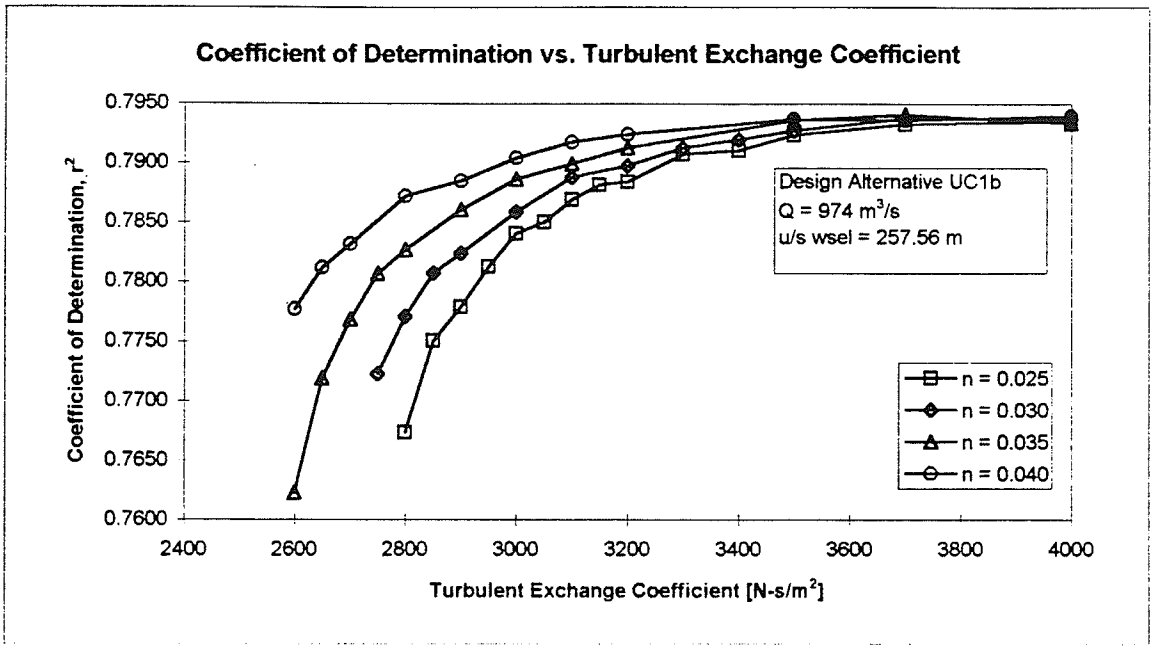

Figure F-1 *Regression Criterion of Coefficient of Determination vs. the Turbulent Exchange Coefficient and Manning's n for the comparison of velocity magnitudes between the physical and numerical data from test scenario UC1b with a flow of 974 m^3/s and a upstream water level at 257.56 m.*

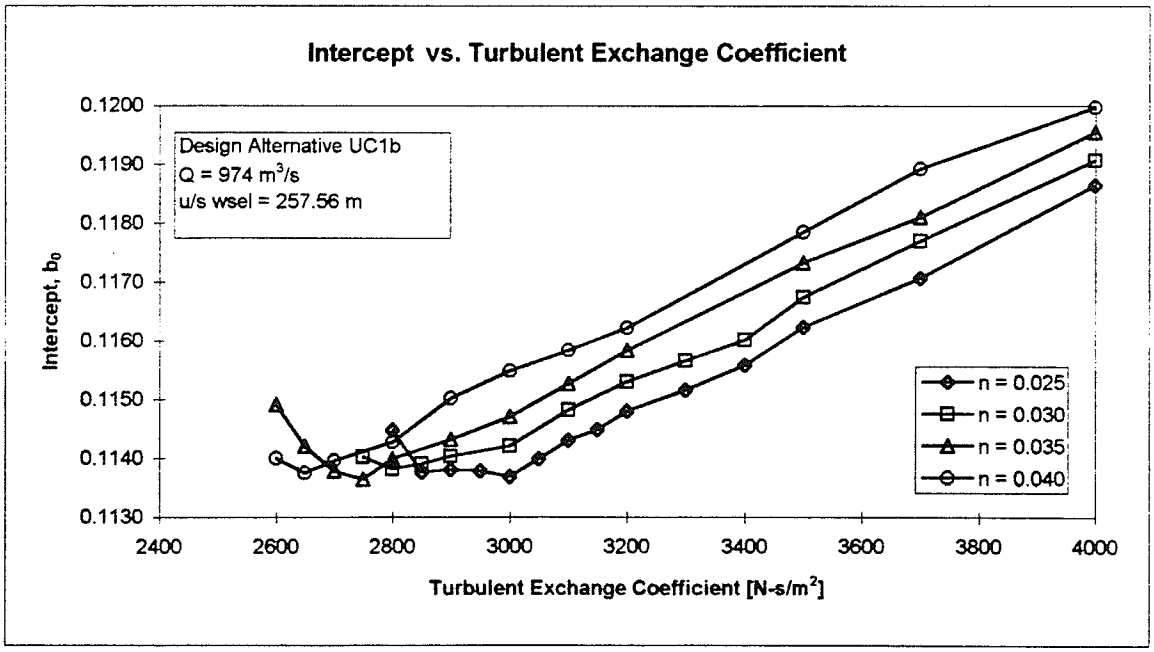

Figure F-2 *Regression Criterion of Intercept vs. the Turbulent Exchange Coefficient and Manning's n for the comparison of velocity magnitudes between the physical and numerical data from test scenario UC1b with a flow of 974 m^3/s and a upstream water level at 257.56 m.*

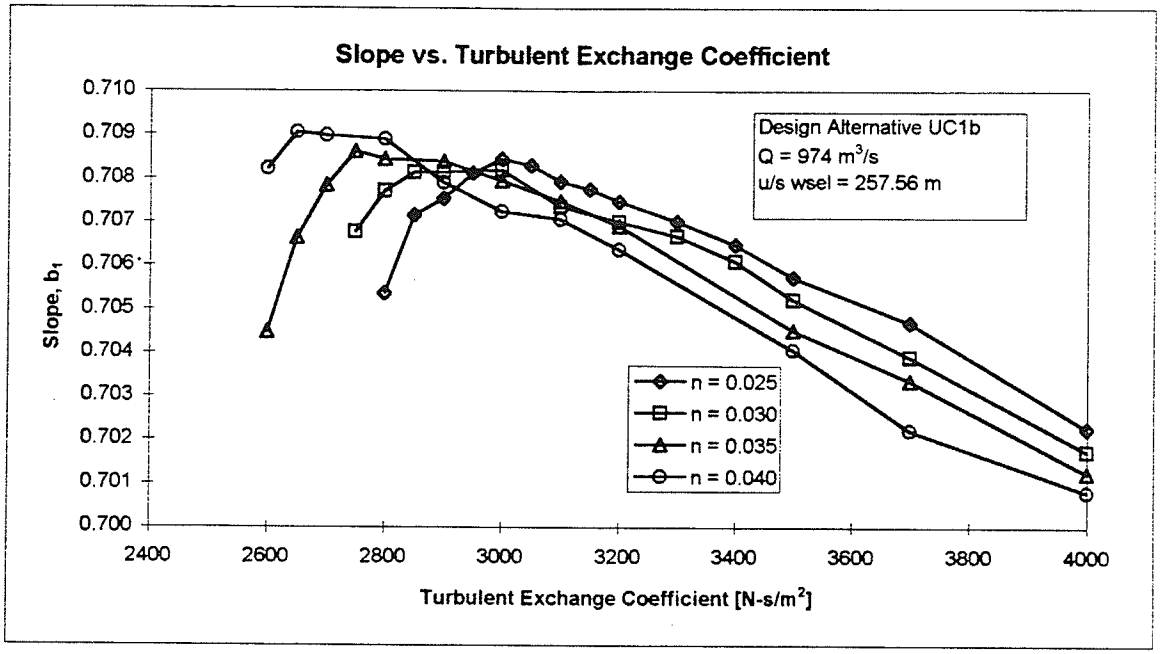

Figure F-3 Regression Criterion of Slope vs. the Turbulent Exchange Coefficient and Manning's n for the comparison of velocity magnitudes between the physical and numerical data from test scenario UC1b with a flow of 974 m^3/s and a upstream water level at 257.56 m.

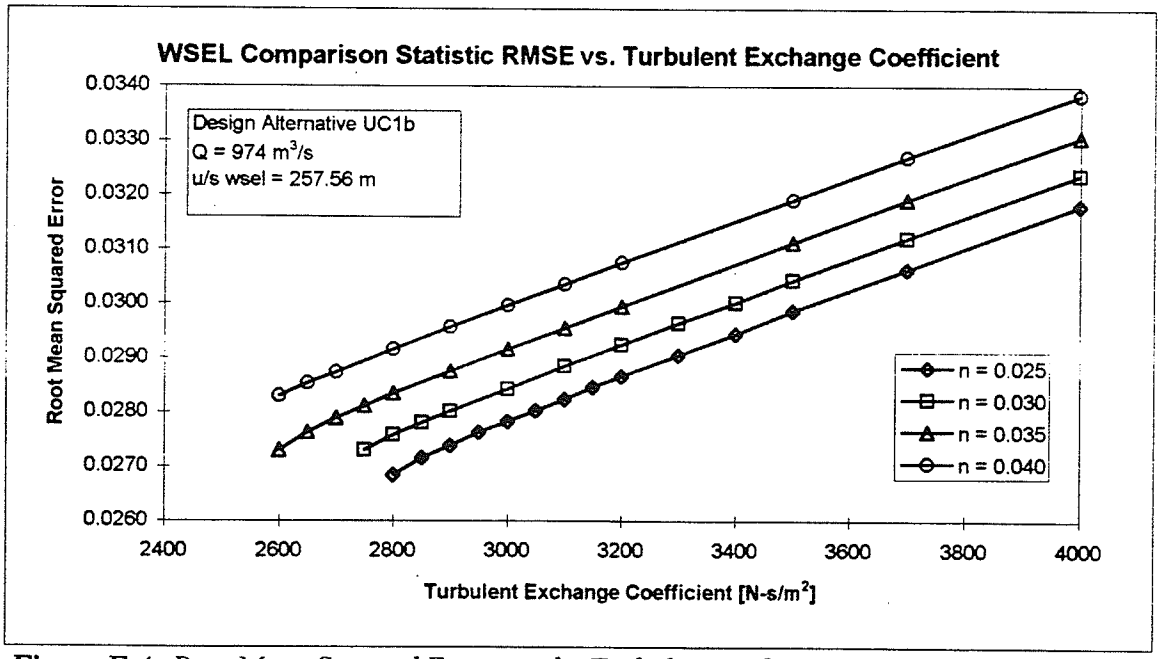

Figure F-4 Root Mean Squared Error vs. the Turbulent Exchange Coefficient and Manning's n for the comparison of water surface elevations between the physical and numerical data from test scenario UC1b with a flow of 974 m3/s and a upstream water level at 257.56 m.

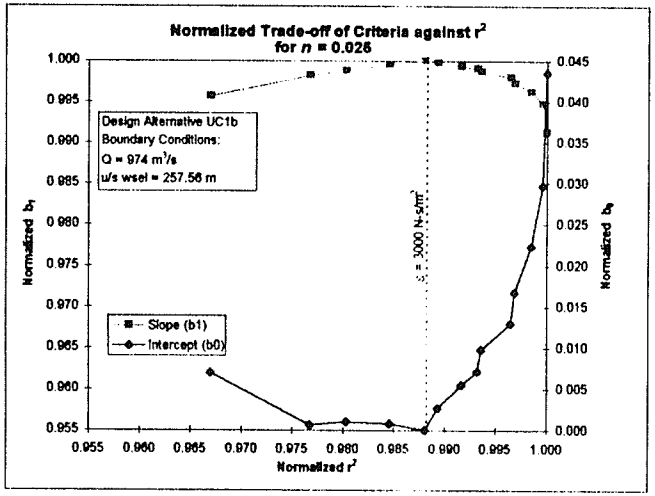

Figure F-5 Trade-off between Regression Statistics for Manning's n = 0.025 for the comparison of velocity magnitudes between the physical and numerical data from test scenario UC1b with a flow of 974 m³/s and a upstream water level at 257.56 m.

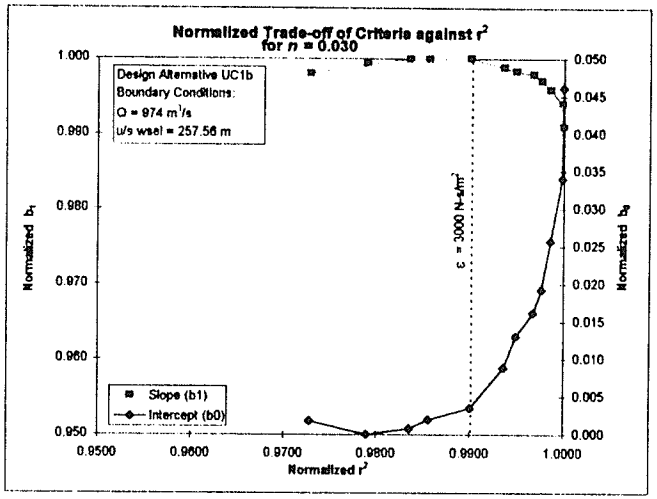

Figure F-6 Trade-off between Regression Statistics for Manning's n = 0.030 for the comparison of velocity magnitudes between the physical and numerical data from test scenario UC1b with a flow of 974 m³/s and a upstream water level at 257.56 m.

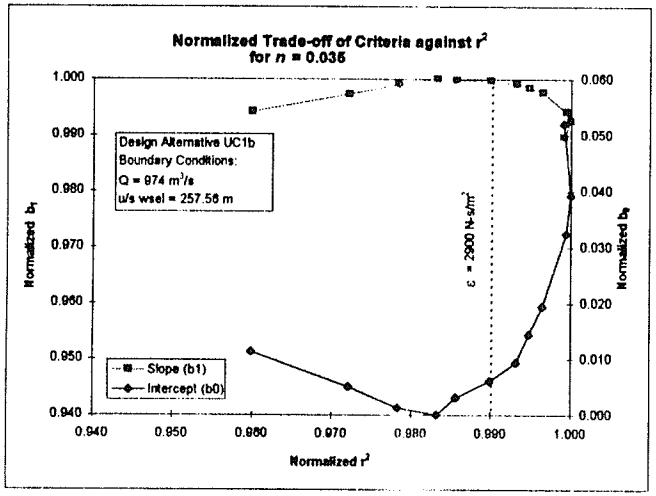

Figure F-7 Trade-off between Regression Statistics for Manning's n = 0.035 for the comparison of velocity magnitudes between the physical and numerical data from test scenario UC1b with a flow of 974 m³/s and a upstream water level at 257.56 m.

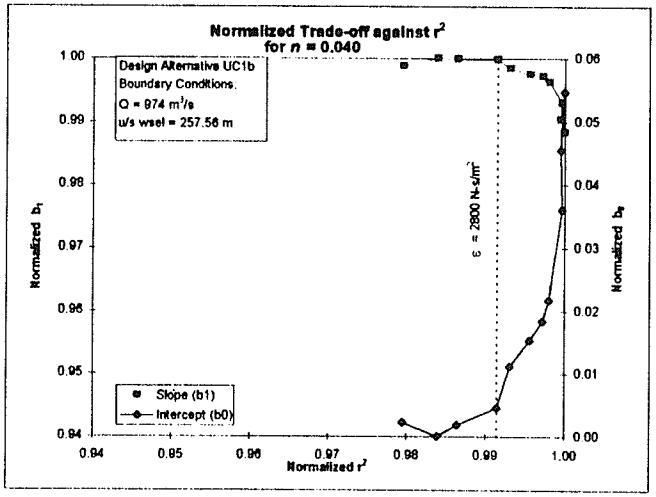

Figure F-8 Trade-off between Regression Statistics for Manning's n = 0.040 for the comparison of velocity magnitudes between the physical and numerical data from test scenario UC1b with a flow of 974 m³/s and a upstream water level at 257.56 m.

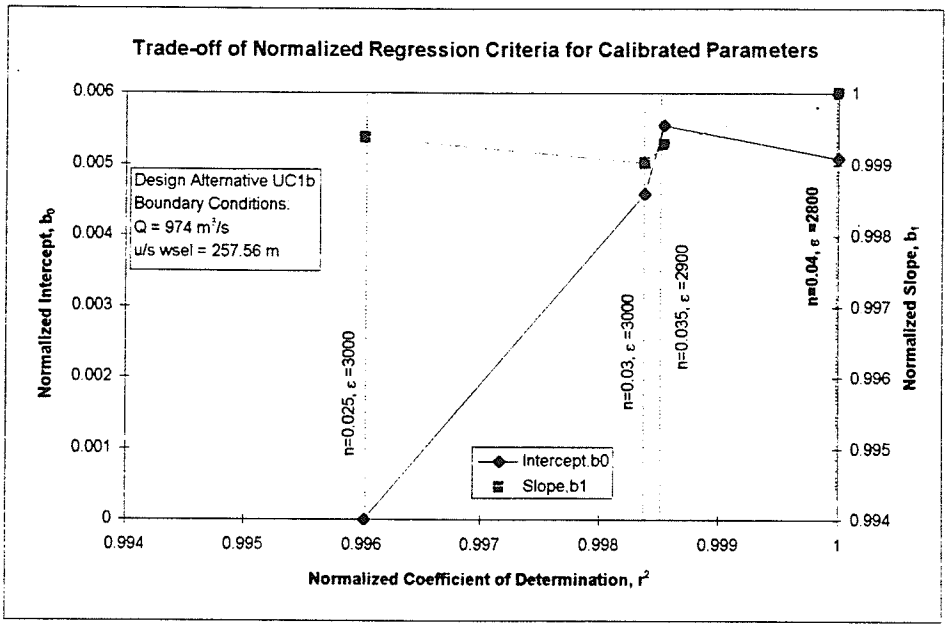

Figure F-9 *Trade-off between the Normalized Regression Criteria for the Calibrated Parameters of scenario UC1b with a flow of 974 m^3/s and a upstream water level at 257.56 m. The best trade-off occurs for n=0.04 and $\varepsilon = 2800$ N-s m^2.*

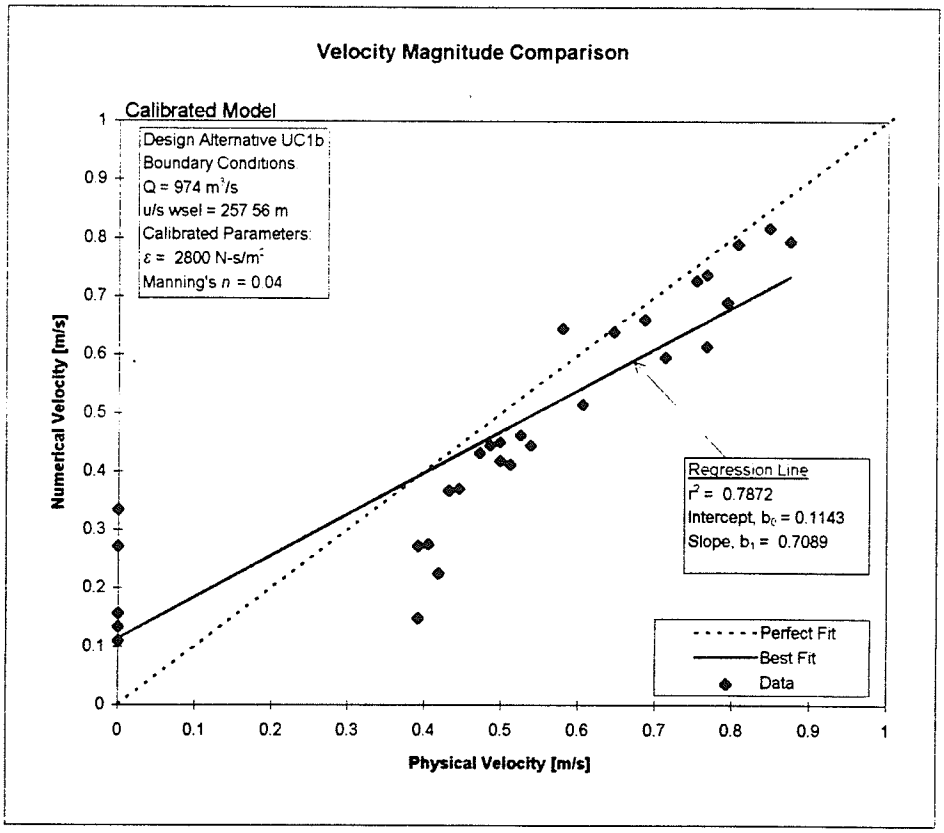

Figure F-10 *Scatter plot comparing numerical and physical velocity magnitudes for scenario UC1b with a flow of 974 m^3/s and a upstream water level at 257.56 m. The calibrated parameters for this scenario are n=0.04 and $\varepsilon = 2800$ N-s/m^2.*

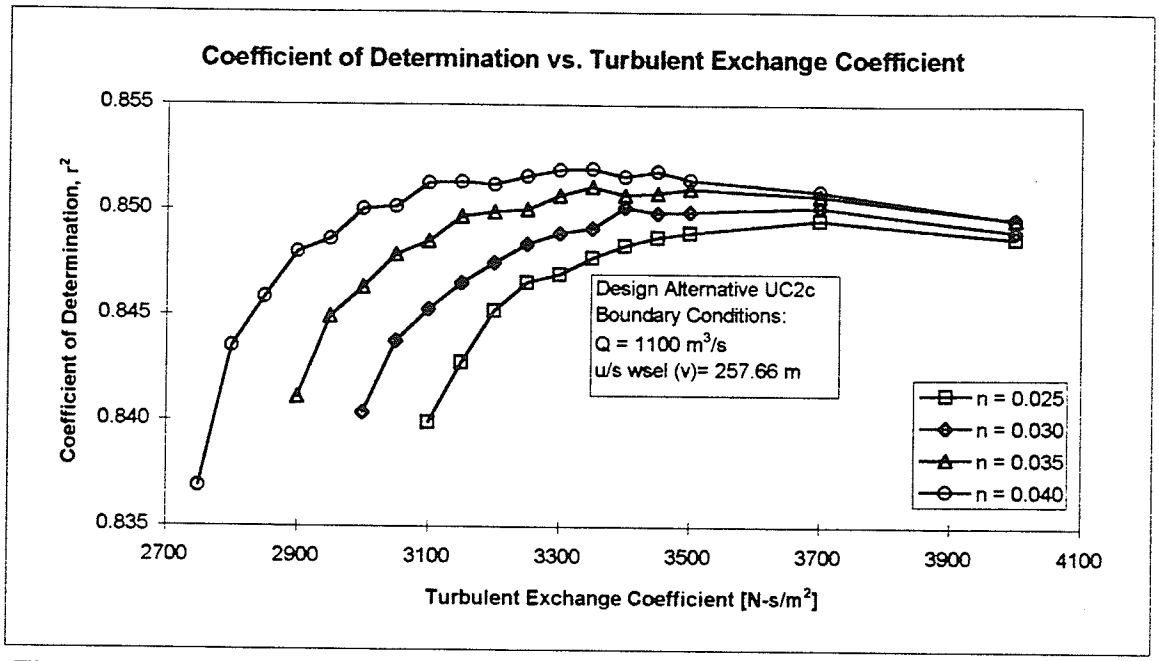

Figure F-11 *Regression Criterion of Coefficient of Determination vs. the Turbulent Exchange Coefficient and Manning's n for the comparison of velocity magnitudes between the physical and numerical data from test scenario UC2c with a flow of 1100 m³/s and a upstream water level at 257.66 m.*

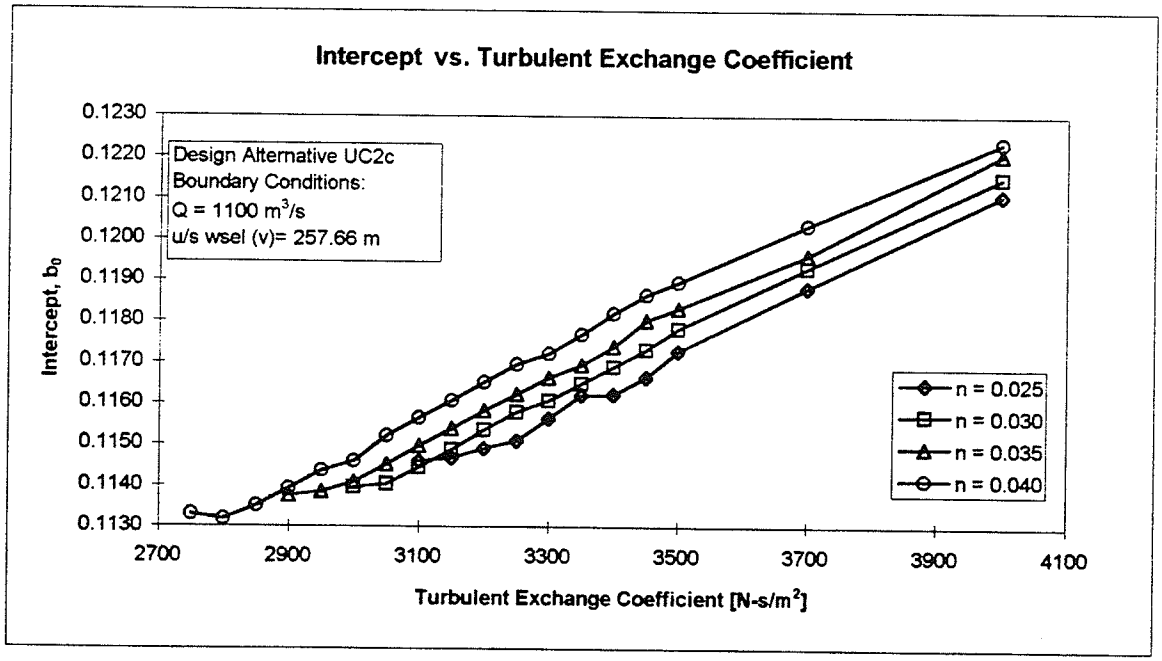

Figure F-12 *Regression Criterion of Intercept vs. the Turbulent Exchange Coefficient and Manning's n for the comparison of velocity magnitudes between the physical and numerical data from test scenario UC2c with a flow of 1100 m³/s and a upstream water level at 257.66 m.*

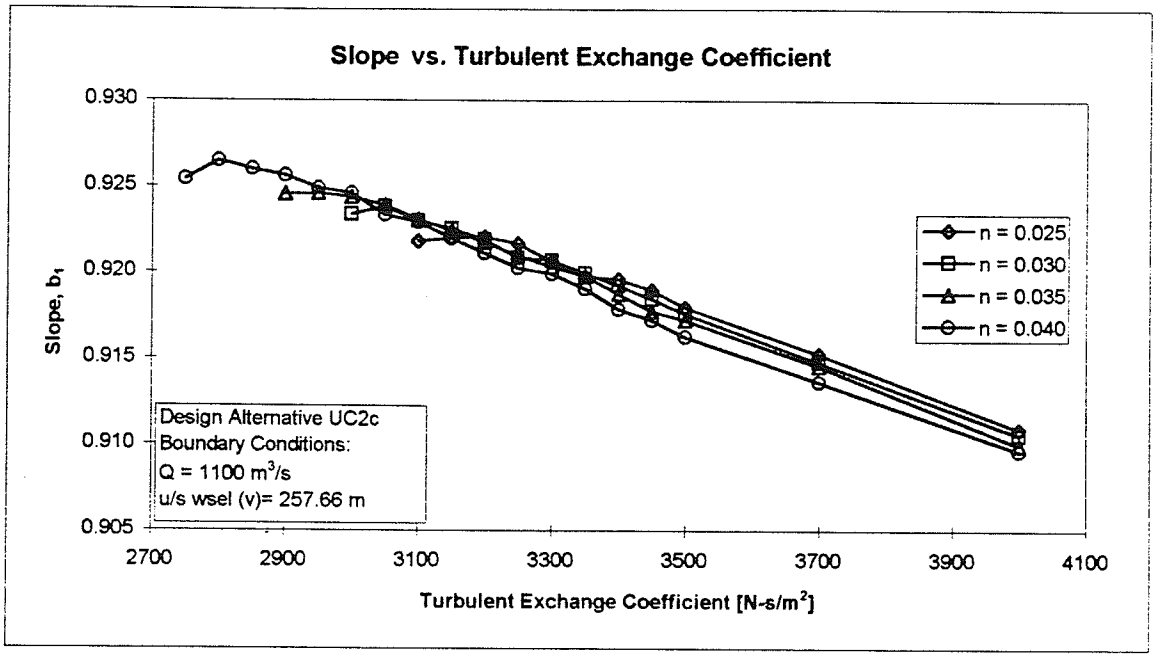

Figure F-13 *Regression Criterion of Slope vs. the Turbulent Exchange Coefficient and Manning's n for the comparison of velocity magnitudes between the physical and numerical data from test scenario UC2c with a flow of 1100 m^3/s and a upstream water level at 257.66 m.*

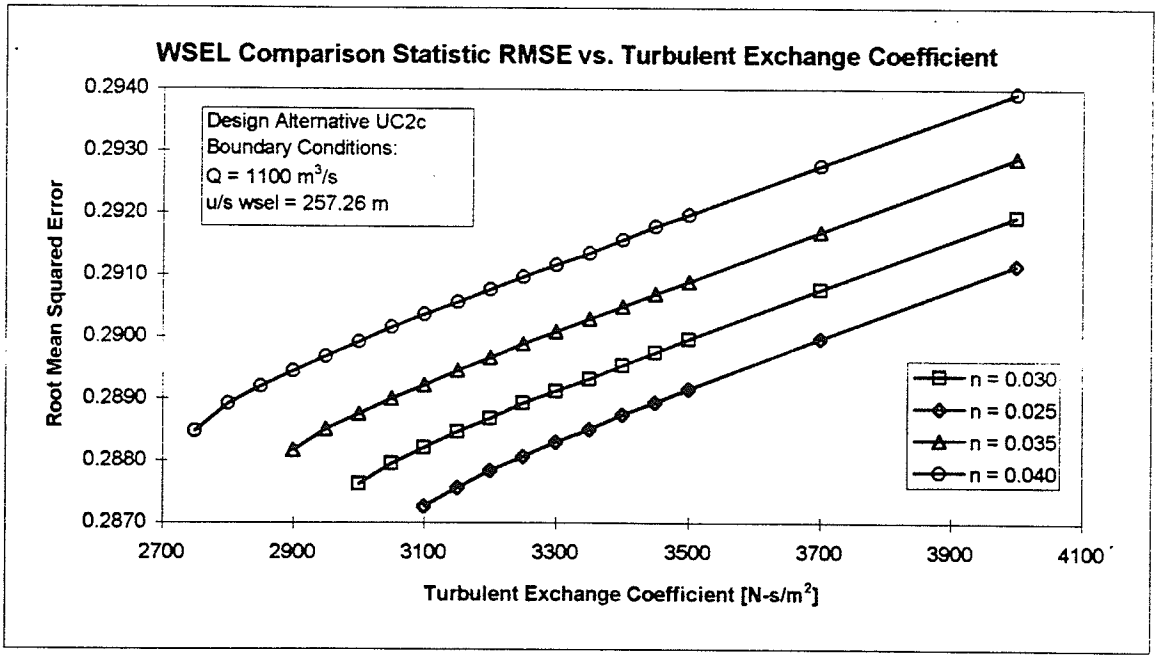

Figure F-14 *Root Mean Squared Error vs. the Turbulent Exchange Coefficient and Manning's n for the comparison of water surface elevations between the physical and numerical data from test scenario UC2c with a flow of 1100 m^3/s and a upstream water level at 257.66 m.*

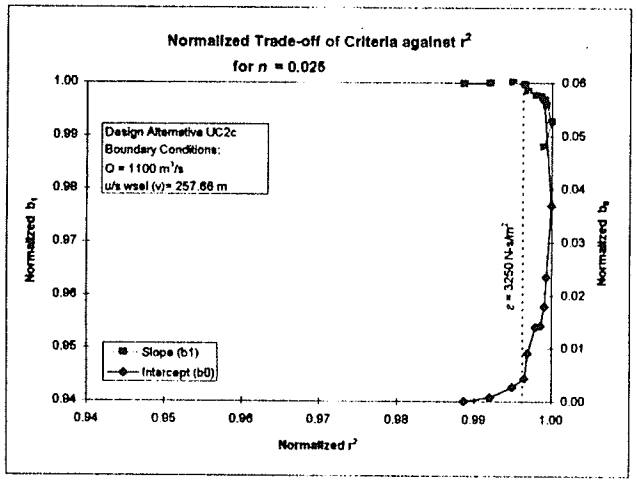

Figure F-15 *Trade-off between Regression Statistics for Manning's n = 0.025 for the comparison of velocity magnitudes between the physical and numerical data from test scenario UC2c with a flow of 1100 m³/s and an upstream water level at 257.66 m.*

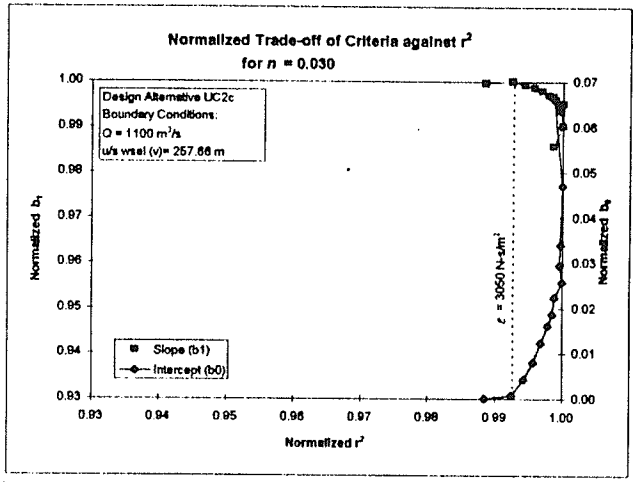

Figure F-16 *Trade-off between Regression Statistics for Manning's n = 0.030 for the comparison of velocit magnitudes between the physical and numerical data from test scenario UC2c with a flow of 1100 m³/s and an upstream water level at 257.66 m.*

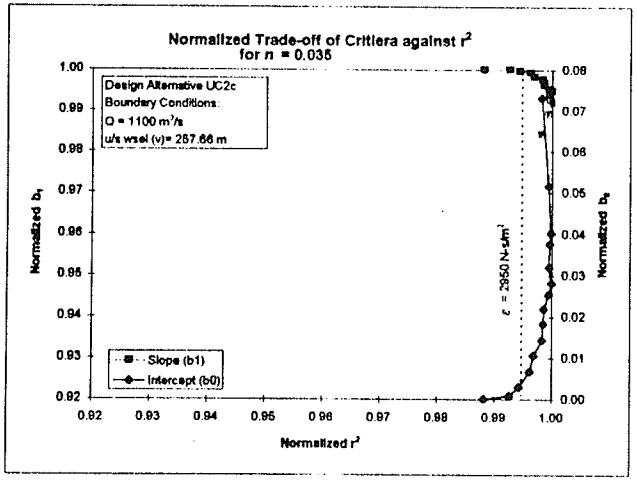

Figure F-17 *Trade-off between Regression Statistics for Manning's n = 0.035 for the comparison of velocity magnitudes between the physical and numerical data from test scenario UC2c with a flow of 1100 m³/s and an upstream water level at 257.66 m.*

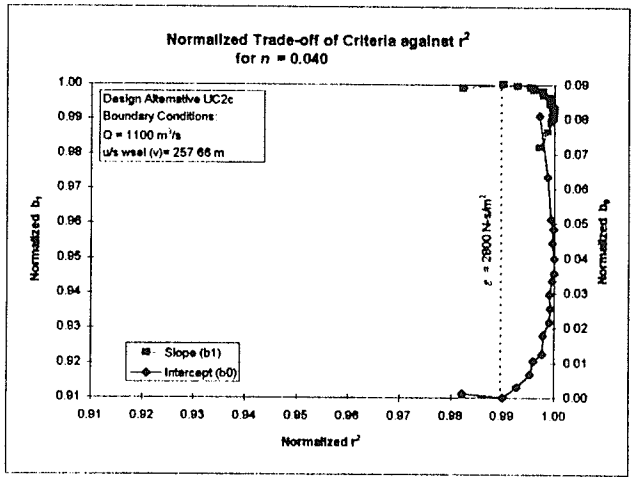

Figure F-18 *Trade-off between Regression Statistics for Manning's n = 0.040 for the comparison of velocity magnitudes between the physical and numerical data from test scenario UC2c with a flow of 1100 m³/s and an upstream water level at 257.66 m.*

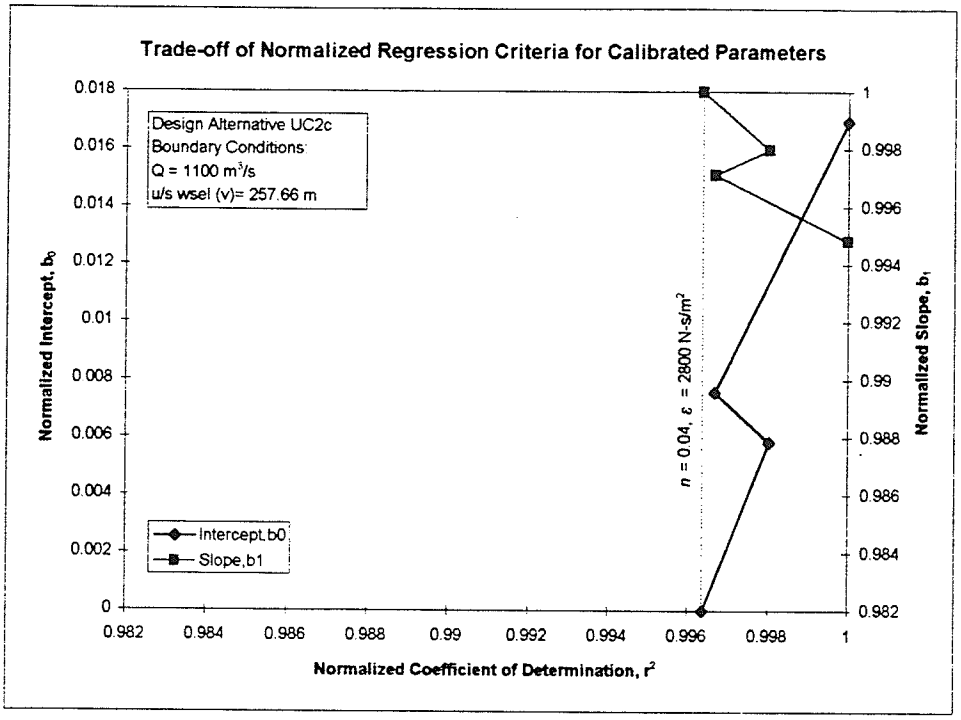

Figure F-19 *Trade-off between Normalized Regression Criteria for the Calibrated Parameters of scenario UC2c with a flow of 1100 m^3/s and an upstream water level at 257.66 m. The best trade-off occurs for n=0.040 and ε = 2800 N-s/m^2.*

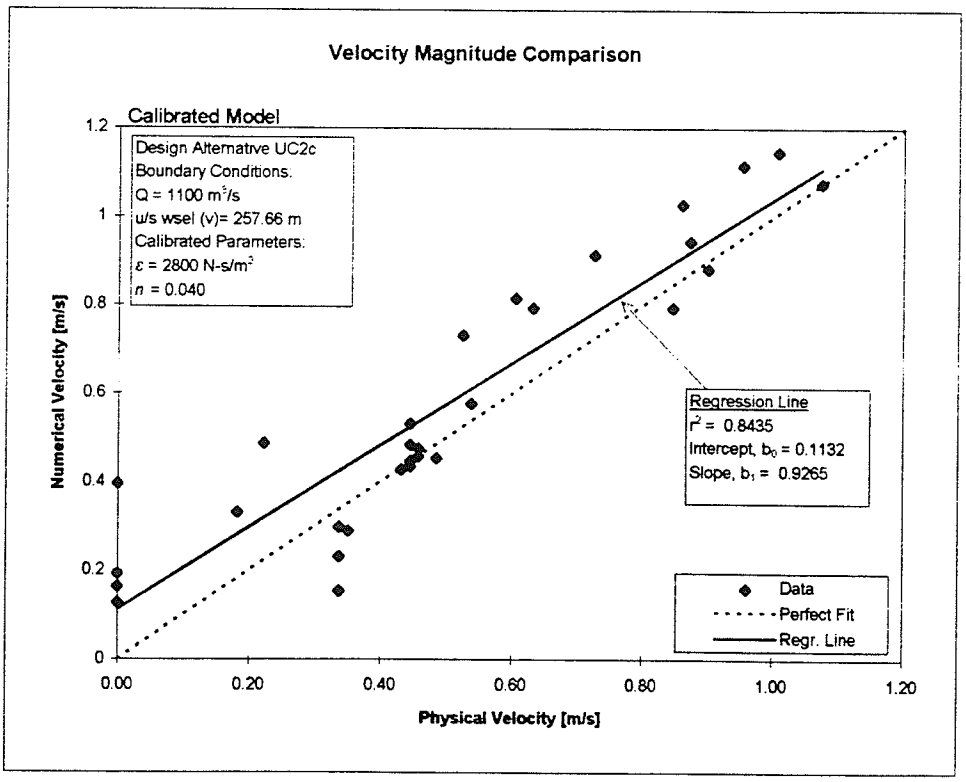

Figure F-20 *Scatter plot comparing numerical and physical velocity magnitudes for scenario UC2c with a flow of 1100 m^3/s and an upstream water level at 257.66 m. The calibrated parameters for this scenario are n=0.040 and ε = 2800 N-s/m^2.*

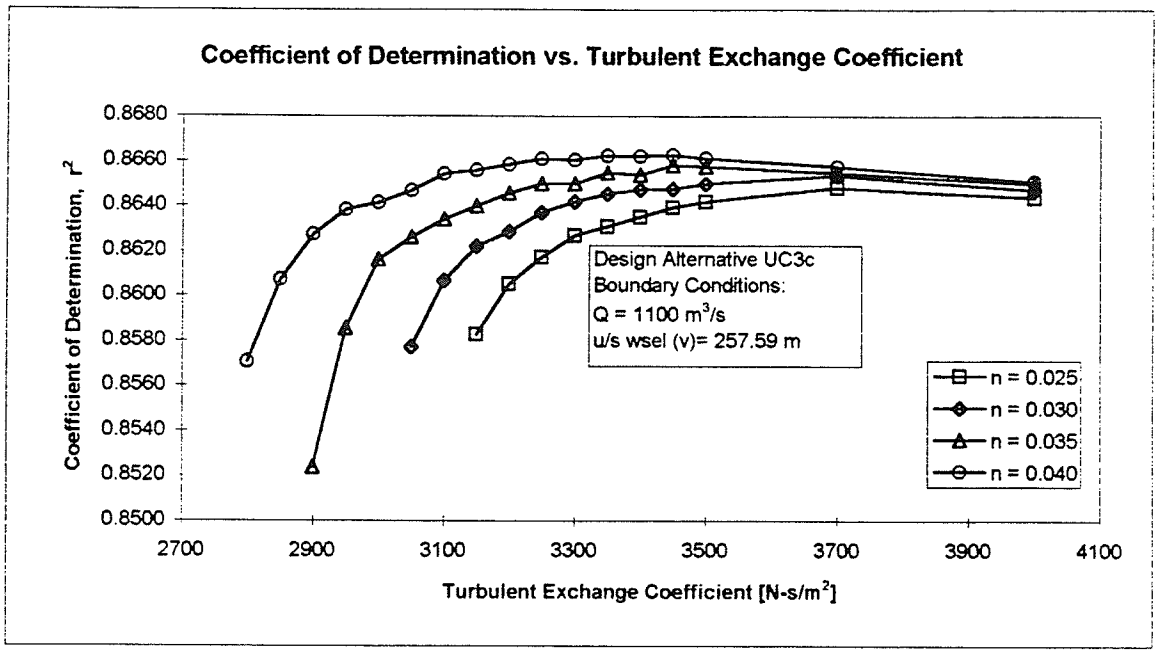

Figure F-21 Regression Criterion of Coefficient of Determination vs. the Turbulent Exchange Coefficient and Manning's n for the comparison of velocity magnitudes between the physical and numerical data from test scenario UC3c with a flow of 1100 m^3/s and a upstream water level at 257.59 m.

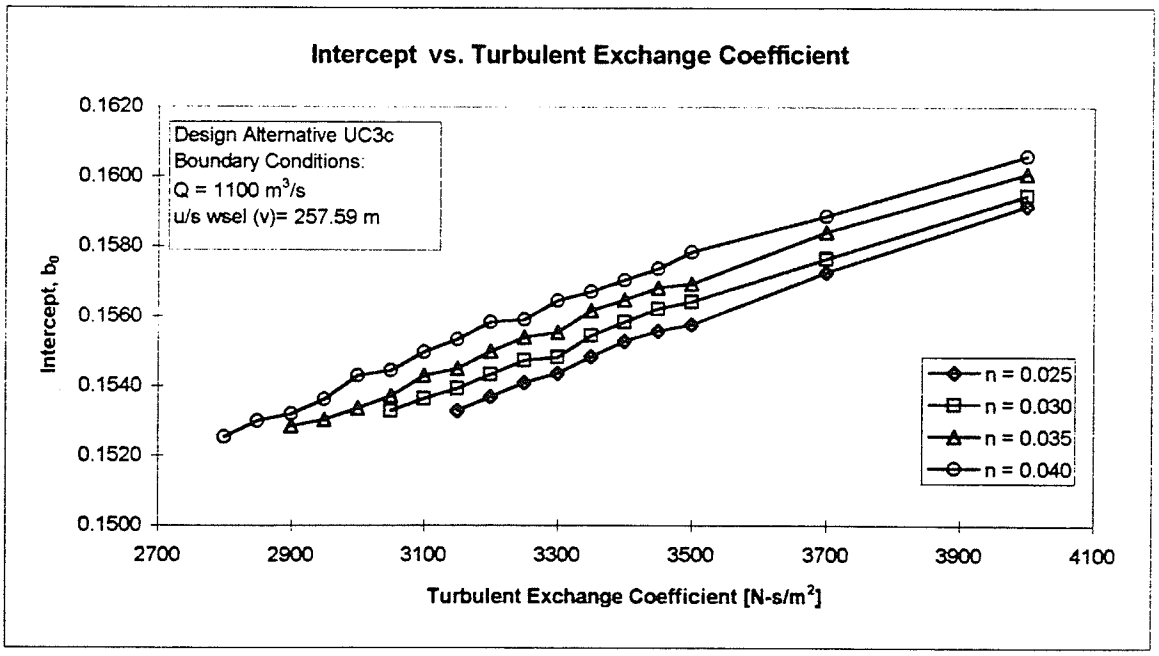

Figure F-22 Regression Criterion of Intercept vs. the Turbulent Exchange Coefficient and Manning's n for the comparison of velocity magnitudes between the physical and numerical data from test scenario UC3c with a flow of 1100 m^3/s and a upstream water level at 257.59 m.

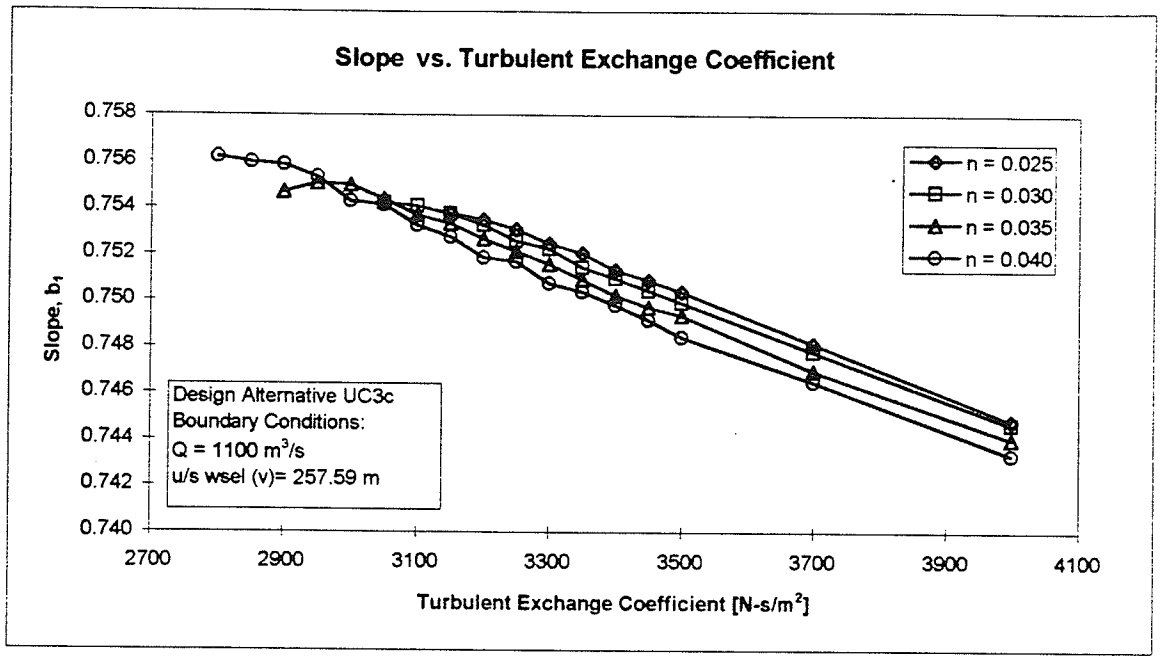

Figure F-23 *Regression Criterion of Slope vs. the Turbulent Exchange Coefficient and Manning's n for the comparison of velocity magnitudes between the physical and numerical data from test scenario UC3c with a flow of 1100 m^3/s and a upstream water level at 257.59 m.*

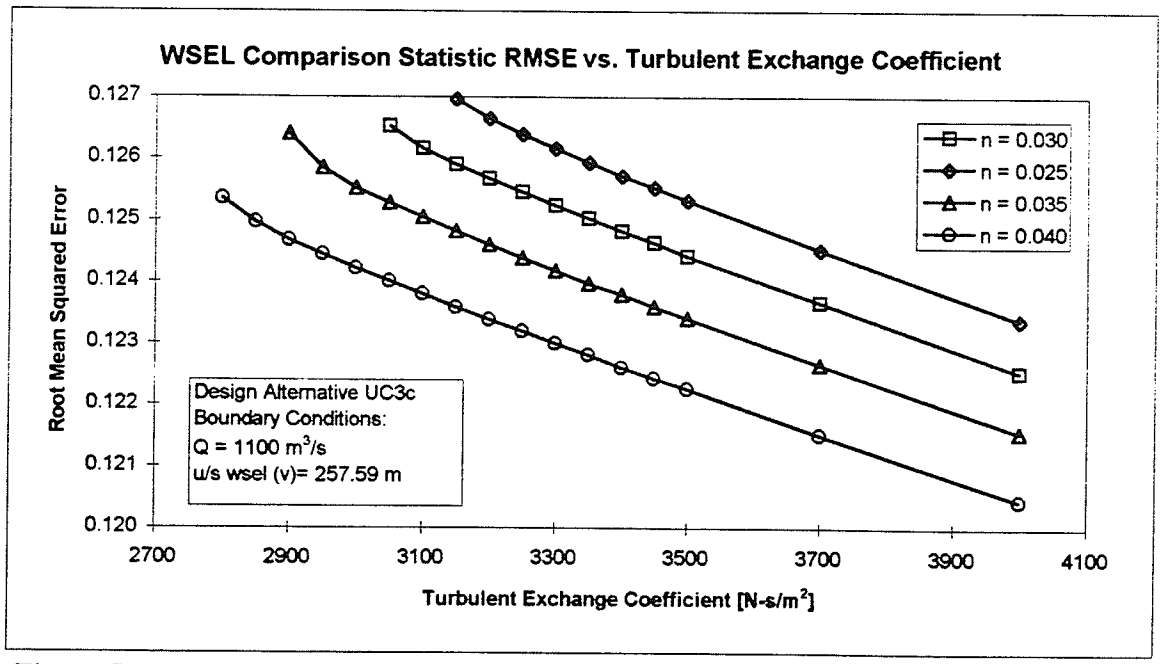

Figure F-24 *Root Mean Squared Error vs. the Turbulent Exchange Coefficient and Manning's n for the comparison of water surface elevations between the physical and numerical data from test scenario UC3c with a flow of 1100 m^3/s and a upstream water level at 257.59 m.*

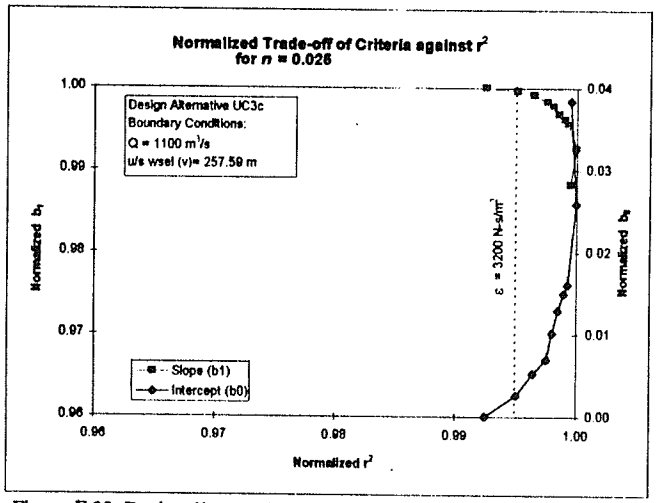

Figure F-25 *Trade-off between Regression Statistics for Manning's n = 0.025 for the comparison of velocity magnitudes between the physical and numerical data from test scenario UC3c with a flow of 1100 m^3/s and an upstream water level at 257.59 m.*

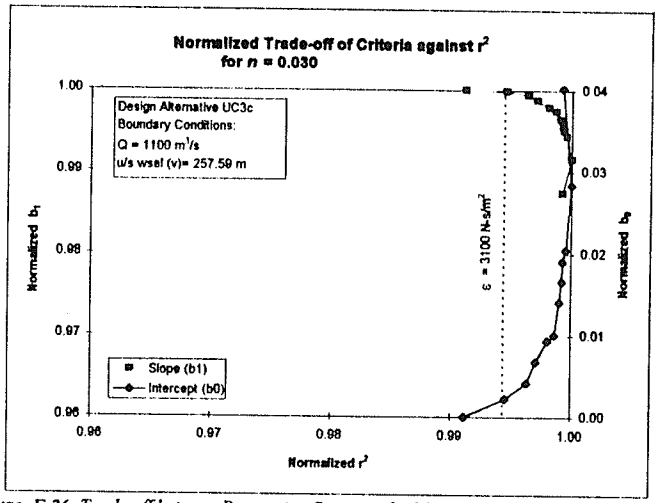

Figure F-26 *Trade-off between Regression Statistics for Manning's n = 0.030 for the comparison of velocity magnitudes between the physical and numerical data from test scenario UC3c with a flow of 1100 m^3/s and an upstream water level at 257.59 m.*

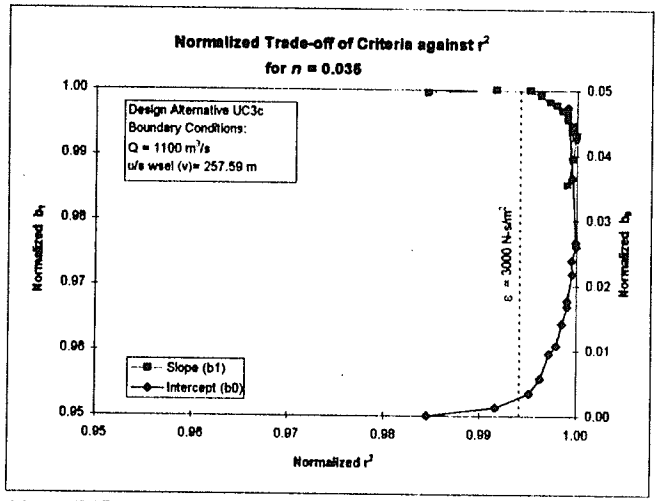

Figure F-27 *Trade-off between Regression Statistics for Manning's n = 0.035 for the comparison of velocity magnitudes between the physical and numerical data from test scenario UC3c with a flow of 1100 m^3/s and an upstream water level at 257.59 m.*

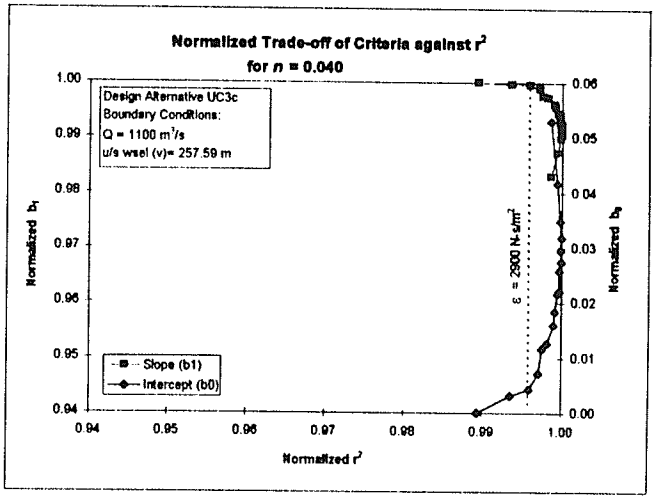

Figure F-28 *Trade-off between Regression Statistics for Manning's n = 0.040 for the comparison of velocity magnitudes between the physical and numerical data from test scenario UC3c with a flow of 1100 m^3/s and an upstream water level at 257.59 m.*

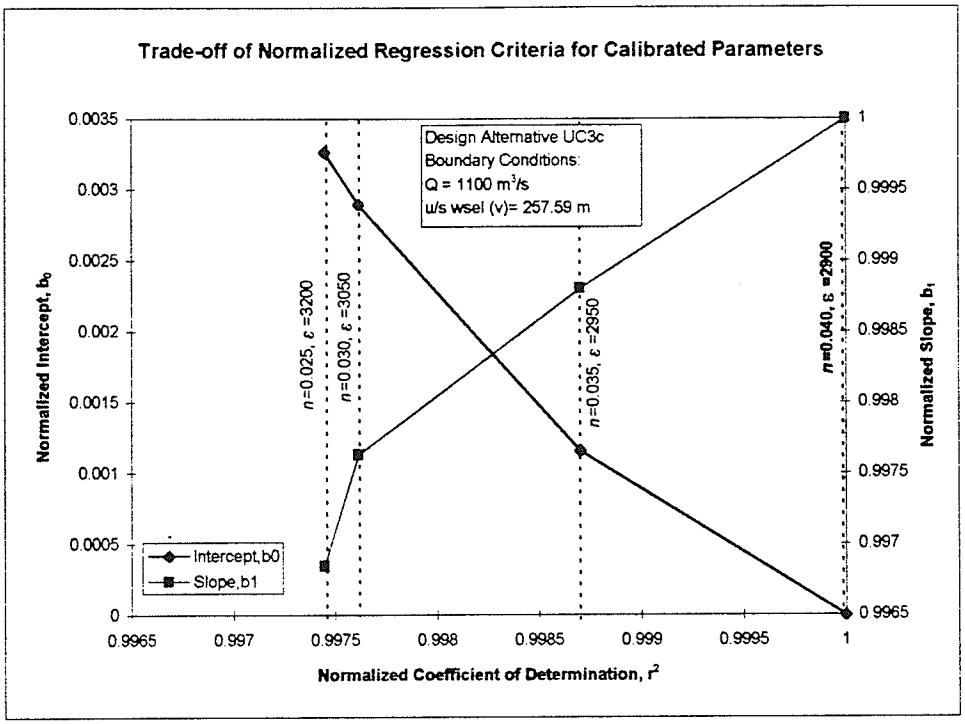

Figure F-29 *Trade-off between Normalized Regression Criteria for the Calibrated Parameters of scenario UC3c with a flow of 1100 m^3/s and an upstream water level at 257.59 m. The best trade-off occurs for n=0.040 and ε = 2900 $N\text{-}s/m^2$.*

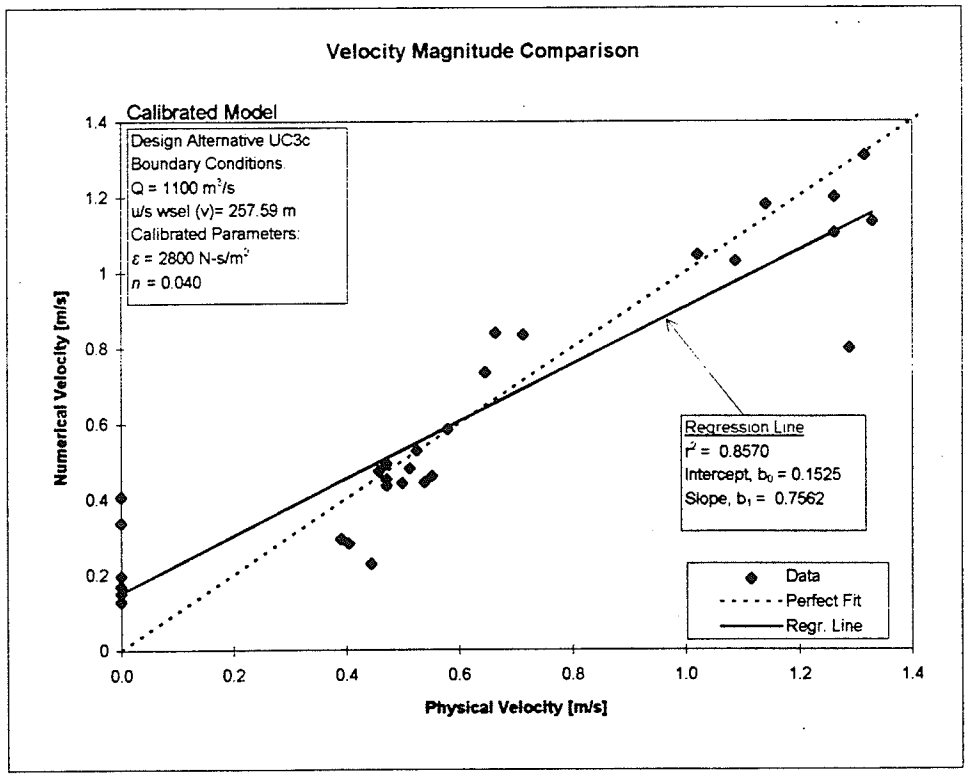

Figure F-30 *Scatter plot comparing numerical and physical velocity magnitudes for scenario UC3c with a flow of 1100 m^3/s and an upstream water level at 257.59 m. The calibrated parameters for this scenario are n=0.040 and ε = 2800 $N\text{-}s/m^2$.*

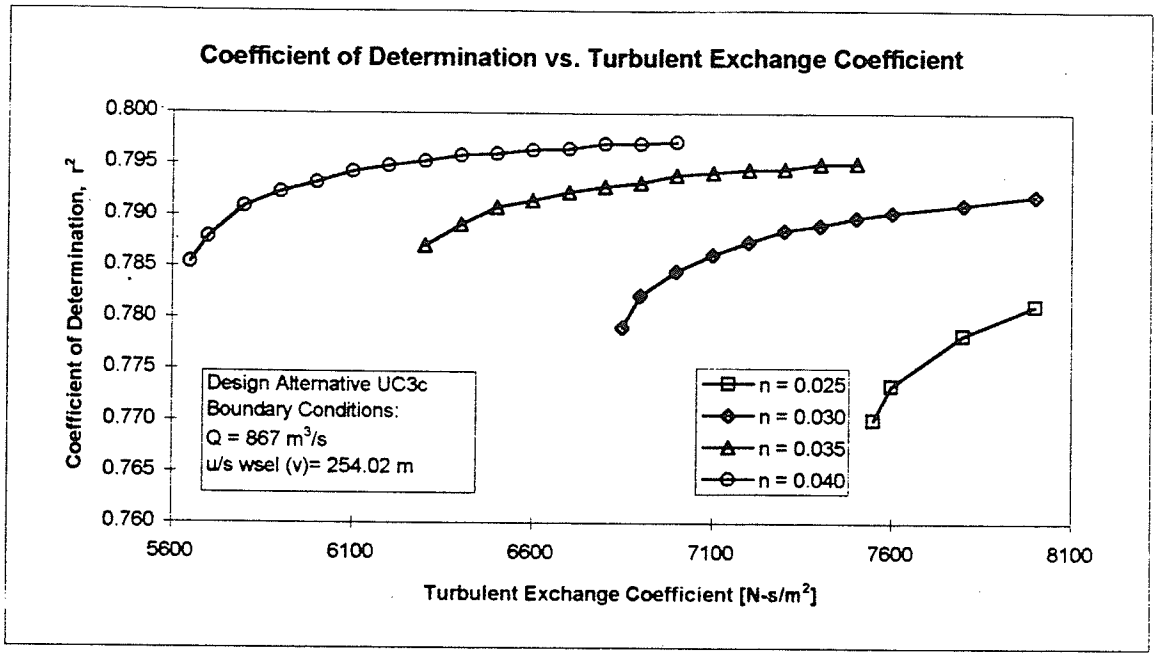

Figure F-31 Regression Criterion of Coefficient of Determination vs. the Turbulent Exchange Coefficient and Manning's n for the comparison of velocity magnitudes between the physical and numerical data from test scenario UC3c with a flow of 867 m^3/s and a upstream water level at 254.02 m.

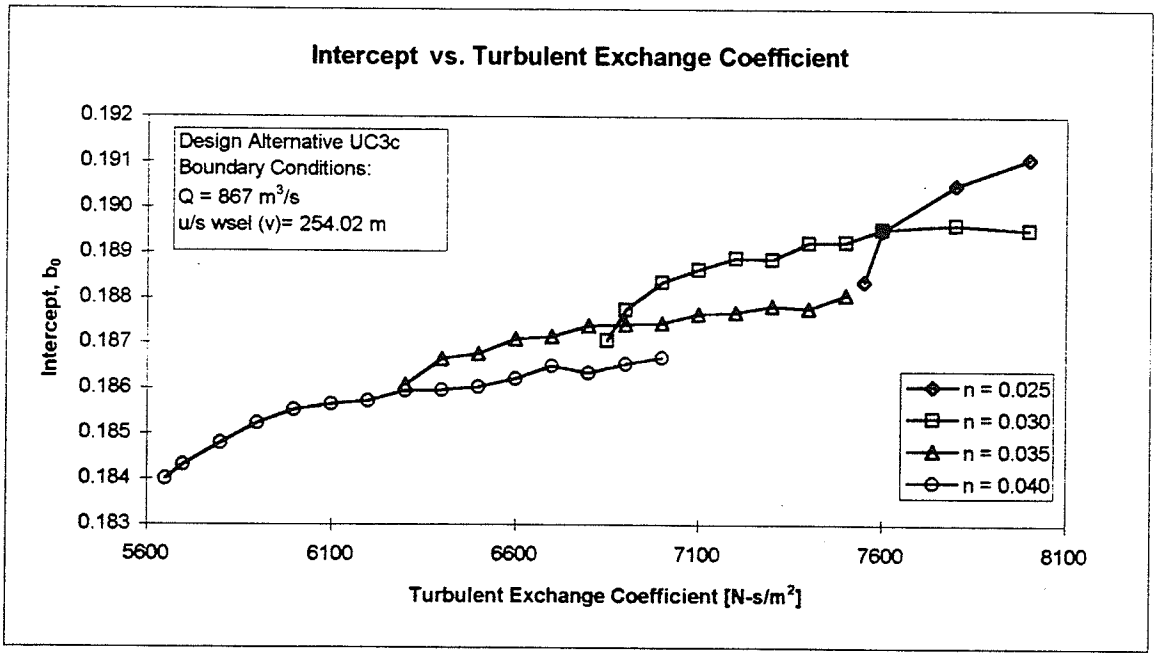

Figure F-32 Regression Criterion of Intercept vs. the Turbulent Exchange Coefficient and Manning's n for the comparison of velocity magnitudes between the physical and numerical data from test scenario UC3c with a flow of 867 m^3/s and a upstream water level at 254.02 m.

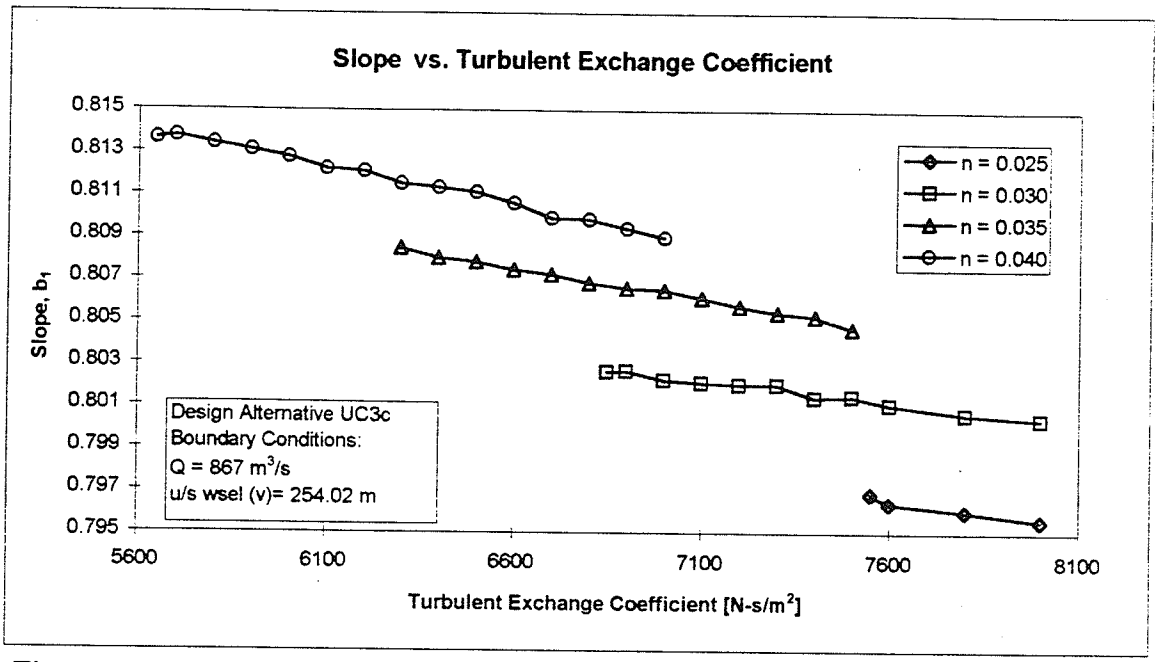

Figure F-33 *Regression Criterion of Slope vs. the Turbulent Exchange Coefficient and Manning's n for the comparison of velocity magnitudes between the physical and numerical data from test scenario UC3c with a flow of 867 m^3/s and a upstream water level at 254.02 m.*

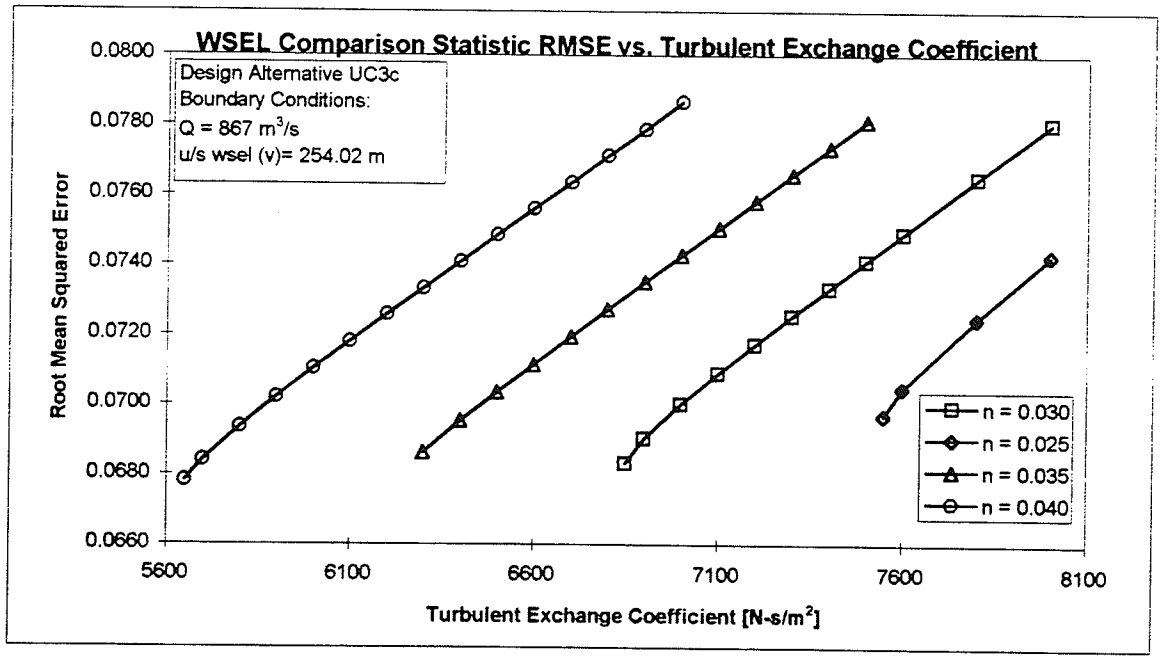

Figure F-34 *Root Mean Squared Error vs. the Turbulent Exchange Coefficient and Manning's n for the comparison of water surface elevations between the physical and numerical data from test scenario UC3c with a flow of 867 m^3/s and a upstream water level at 254.02 m.*

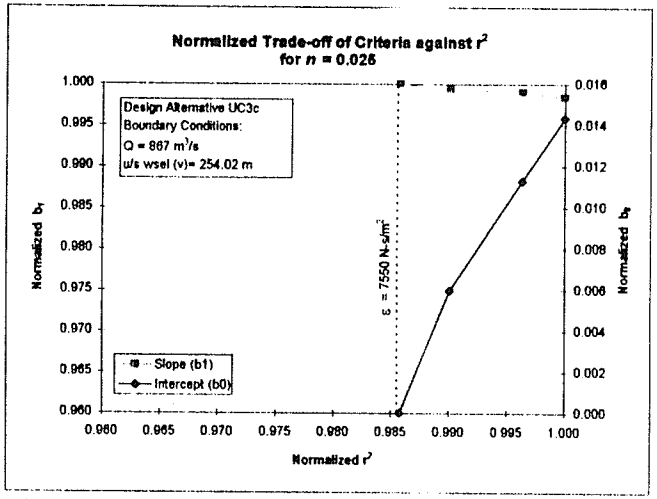

Figure F-35 *Trade-o f between Normalized Regression Statistics for Manning's n = 0.025 for the comparison of velocity magnitudes between the physical and numerical data from test scenario UC3c with a flow of 867 m³/s and an upstream water level at 254.02 m.*

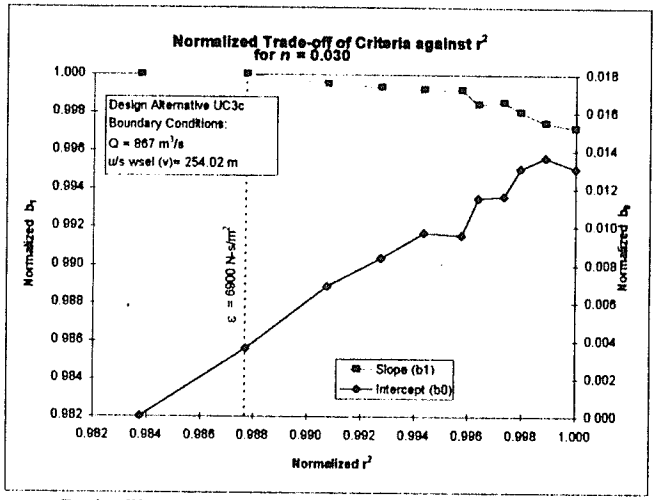

Figure F-36 *Trade-off between Normalized Regression Statistics for Manning's n = 0.030 for the comparison of velocity magnitudes between the physical and numerical data from test scenario UC3c with a flow of 867 m³/s and an upstream water level at 254.02 m.*

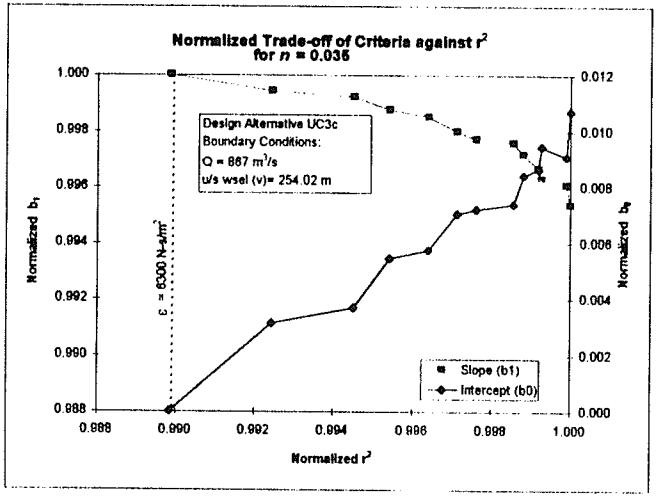

Figure F-37 *Trade-o f between Normalized Regression Statistics for Manning's n = 0.035 for the comparison of velocity magnitudes between the physical and numerical data from test scenario UC3c with a flow of 867 m³/s and an upstream water level at 254.02 m.*

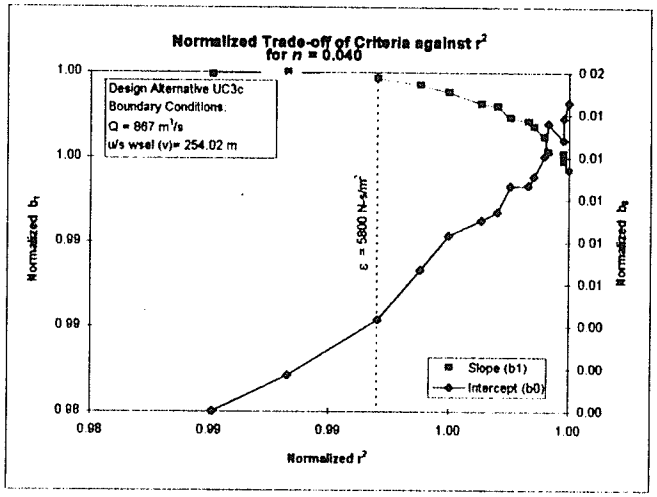

Figure F-38 *Trade-off between Normalized Regression Statistics for Manning's n = 0.040 for the comparison of velocity magnitudes between the physical and numerical data from test scenario UC3c with a flow of 867 m³/s and an upstream water level at 254.02 m.*

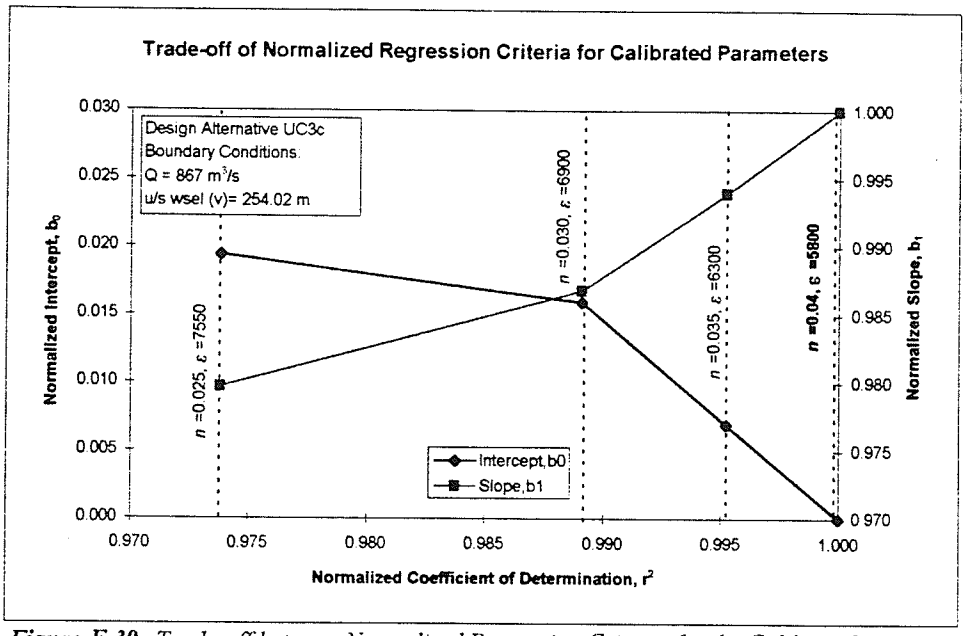

Figure F-39 *Trade-off between Normalized Regression Criteria for the Calibrated Parameters of scenario UC3c with a flow of 867 m^3/s and an upstream water level at 254.02 m. The best trade-off occurs for n=0.040 and ε = 5800 $N\text{-}s/m^2$.*

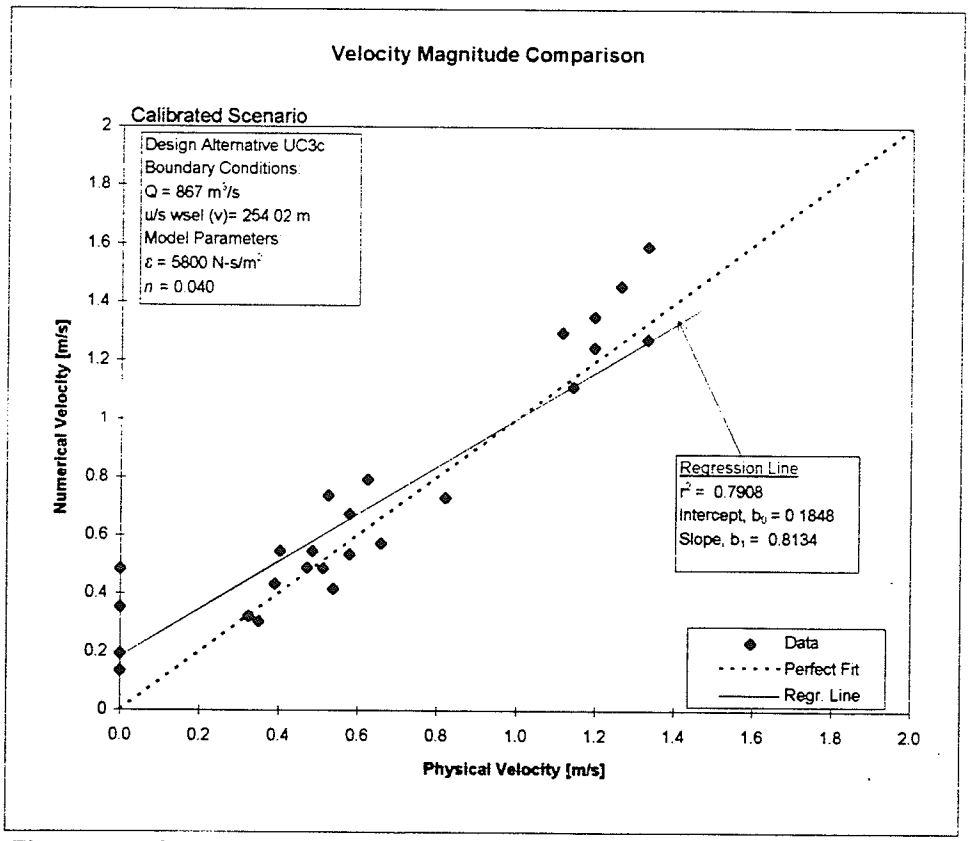

Figure F-40 *Scatter plot comparing numerical and physical velocity magnitudes for scenario UC3c with a flow of 867 m^3/s and an upstream water level at 254.02 m. The calibrated parameters for this scenario are n=0.040 and ε = 5800 $N\text{-}s/m^2$.*

Physical and Numerical Velocity Magnitudes

Removal Scheme:	*UOB*		
Flow (m^3/s):	1100	Avg. Difference (m/s):	-0.004
u/s wsel (m):	257.84	Avg. Abs. Diff. (m/s):	0.082
ε_{ij} ($N\text{-}s/m^2$):	5800	Standard Dev.(diff):	0.116
Manning's n:	0.04	Max. (diff):	0.229
Number of data:	25	Min. (diff.):	-0.367

Node Coordinate		Physical	Calibrated Numerical		Absolute
X	Y	Velocity (m/s)	Velocity (m/s)	Difference	Difference
41	60	0.391	0.301	0.090	0.090
41	100	0.405	0.304	0.101	0.101
41	245	0.472	0.243	0.229	0.229
131	79	0.525	0.453	0.072	0.072
140	207	0.000	0.367	-0.367	0.367
140	250	0.182	0.162	0.020	0.020
158	127	0.579	0.566	0.013	0.013
220	82	0.539	0.49	0.049	0.049
220	133.5	0.405	0.477	-0.072	0.072
220	207	0.472	0.415	0.057	0.057
305	86	0.445	0.458	-0.013	0.013
305	147.5	0.445	0.407	0.038	0.038
305	197.5	0.000	0.129	-0.129	0.129
376	75.5	0.472	0.488	-0.016	0.016
376	123.5	0.512	0.471	0.041	0.041
376	167	0.418	0.323	0.095	0.095
376	203	0.000	0.203	-0.203	0.203
438	156	0.458	0.438	0.020	0.020
445.602	117.1537	0.525	0.539	-0.014	0.014
452.5	81	0.592	0.516	0.076	0.076
484.3074	89.2957	0.485	0.456	0.029	0.029
489.0531	107.2925	0.498	0.458	0.040	0.040
493.8605	125.4125	0.351	0.4	-0.049	0.049
527	86	0.619	0.723	-0.104	0.104
532.5	103.75	0.606	0.714	-0.108	0.108

Physical and Numerical Velocity Magnitudes

Removal Scheme:	*UC1b*		
Flow (m^3/s):	974	Avg. Difference (m/s):	0.030
u/s wsel (m):	257.56	Avg. Abs. Diff. (m/s):	0.101
ε_{ij} (N-s/m^2):	2800	Standard Dev.(diff):	0.125
Manning's *n*:	0.04	Max. (diff):	0.243
Number of data:	30	Min. (diff.):	-0.334

Node Coordinate X	Y	Physical Velocity (m/s)	Calibrated Numerical Velocity (m/s)	Difference	Absolute Difference
41	60	0.391	0.272	0.119	0.119
41	100	0.405	0.275	0.130	0.130
41	245	0.418	0.224	0.194	0.194
131	79	0.512	0.412	0.100	0.100
140	207	0.000	0.334	-0.334	0.334
140	250	0.391	0.148	0.243	0.243
158	127	0.606	0.515	0.091	0.091
220	82	0.539	0.445	0.094	0.094
220	133.5	0.472	0.432	0.040	0.040
220	207	0.445	0.37	0.075	0.075
305	86	0.498	0.418	0.080	0.080
305	147.5	0.431	0.367	0.064	0.064
305	197.5	0.000	0.109	-0.109	0.109
340.5	80.75	0.485	0.445	0.040	0.040
376	75.5	0.498	0.45	0.048	0.048
376	123.5	0.525	0.462	0.063	0.063
376	167	0.000	0.272	-0.272	0.272
376	195	0.000	0.157	-0.157	0.157
376	203	0.000	0.134	-0.134	0.134
422.53	119.62	0.686	0.661	0.025	0.025
438	156	0.713	0.596	0.117	0.117
445.602	117.1537	0.767	0.737	0.030	0.030
452.5	81	0.793	0.69	0.103	0.103
468.28	109.5	0.807	0.79	0.017	0.017
484.3074	89.2957	0.874	0.794	0.080	0.080
489.0531	107.2925	0.847	0.817	0.030	0.030
493.8605	125.4125	0.767	0.615	0.152	0.152
509.75	101.5	0.579	0.645	-0.066	0.066
527	86	0.753	0.727	0.026	0.026
532.5	103.75	0.646	0.64	0.006	0.006

Physical and Numerical Velocity Magnitudes

Removal Scheme:	*UC1c*		
Flow (m^3/s):	1100	Avg. Difference (m/s):	-0.035
u/s wsel (m):	257.26	Avg. Abs. Diff. (m/s):	0.076
ε_{ij} ($N\text{-}s/m^2$):	3000	Standard Dev.(diff):	0.094
Manning's *n*:	0.04	Max. (diff):	0.091
Number of data:	11	Min. (diff.):	-0.194

Node Coordinate X	Y	Physical Velocity (m/s)	Calibrated Numerical Velocity (m/s)	Difference	Absolute Difference
376	75.5	0.498	0.464	0.034	0.034
376	123.5	0.565	0.554	0.011	0.011
376	167	0.391	0.337	0.054	0.054
376	195	0.000	0.194	-0.194	0.194
422.53	119.62	0.807	0.841	-0.034	0.034
445.602	117.1537	0.941	0.952	-0.011	0.011
484.3074	89.2957	1.075	0.984	0.091	0.091
489.0531	107.2925	1.075	1.039	0.036	0.036
509.75	101.5	0.699	0.787	-0.088	0.088
527	86	0.646	0.817	-0.171	0.171
532.5	103.75	0.632	0.744	-0.112	0.112

Physical and Numerical Velocity Magnitudes

Removal Scheme:	*UC2a*		
Flow (m^3/s):	1100	Avg. Difference (m/s):	-0.050
u/s wsel (m):	257.56	Avg. Abs. Diff. (m/s):	0.061
ε_{ij} ($N\text{-}s/m^2$):	2800	Standard Dev.(diff):	0.047
Manning's *n*:	0.04	Max. (diff):	0.049
Number of data:	9	Min. (diff.):	-0.096

Node Coordinate X	Node Coordinate Y	Physical Velocity (m/s)	Calibrated Numerical Velocity (m/s)	Difference	Absolute Difference
376	123.5	0.552	0.503	0.049	0.049
422.53	119.62	0.726	0.785	-0.059	0.059
445.602	117.1537	0.820	0.864	-0.044	0.044
452.5	81	0.820	0.832	-0.012	0.012
468.28	109.5	0.860	0.945	-0.085	0.085
489.0531	107.2925	0.954	0.981	-0.027	0.027
509.75	101.5	0.632	0.714	-0.082	0.082
527	86	0.753	0.845	-0.092	0.092
532.5	103.75	0.606	0.702	-0.096	0.096

Physical and Numerical Velocity Magnitudes

Removal Scheme:	*UC2b*		
Flow (m^3/s):	1100	Avg. Difference (m/s):	-0.019
u/s wsel (m):	257.56	Avg. Abs. Diff. (m/s):	0.034
ε_{ij} ($N\text{-}s/m^2$):	2800	Standard Dev.(diff):	0.040
Manning's *n*:	0.04	Max. (diff):	0.059
Number of data:	9	Min. (diff.):	-0.090

Node Coordinate X	Y	Physical Velocity (m/s)	Calibrated Numerical Velocity (m/s)	Difference	Absolute Difference
376	123.5	0.579	0.52	0.059	0.059
422.53	119.62	0.807	0.845	-0.038	0.038
445.602	117.1537	0.901	0.937	-0.036	0.036
452.5	81	0.901	0.891	0.010	0.010
468.28	109.5	0.994	1.02	-0.026	0.026
489.0531	107.2925	1.048	1.053	-0.005	0.005
509.75	101.5	0.659	0.749	-0.090	0.090
527	86	0.807	0.834	-0.027	0.027
532.5	103.75	0.699	0.715	-0.016	0.016

Physical and Numerical Velocity Magnitudes

Removal Scheme:	*UC2c(i)*		
Flow (m^3/s):	1100	Avg. Difference (m/s):	-0.077
u/s wsel (m):	257.66	Avg. Abs. Diff. (m/s):	0.110
ε_{ij} ($N\text{-}s/m^2$):	2800	Standard Dev.(diff):	0.124
Manning's *n*:	0.04	Max. (diff):	0.183
Number of data:	30	Min. (diff.):	-0.396

Node Coordinate X	Node Coordinate Y	Physical Velocity (m/s)	Calibrated Numerical Velocity (m/s)	Difference	Absolute Difference
41	60	0.35	0.29	0.061	0.061
41	100	0.34	0.299	0.039	0.039
41	245	0.34	0.232	0.106	0.106
131	79	0.44	0.447	-0.002	0.002
140	207	0.00	0.396	-0.396	0.396
140	250	0.34	0.155	0.183	0.183
158	127	0.54	0.579	-0.040	0.040
220	82	0.44	0.485	-0.040	0.040
220	133.5	0.22	0.488	-0.266	0.266
220	207	0.44	0.435	0.010	0.010
305	86	0.49	0.454	0.031	0.031
305	147.5	0.43	0.429	0.002	0.002
305	197.5	0.00	0.128	-0.128	0.128
340.5	80.75	0.46	0.476	-0.018	0.018
376	75.5	0.46	0.459	-0.001	0.001
376	123.5	0.44	0.532	-0.087	0.087
376	167	0.18	0.332	-0.150	0.150
376	195	0.00	0.193	-0.193	0.193
376	203	0.00	0.165	-0.165	0.165
422.53	119.62	0.73	0.915	-0.189	0.189
438	156	0.90	0.883	0.018	0.018
445.602	117.1537	0.86	1.029	-0.169	0.169
452.5	81	0.87	0.944	-0.070	0.070
468.28	109.5	0.95	1.117	-0.163	0.163
484.3074	89.2957	1.07	1.076	-0.001	0.001
489.0531	107.2925	1.01	1.147	-0.139	0.139
493.8605	125.4125	0.85	0.795	0.052	0.052
509.75	101.5	0.63	0.795	-0.163	0.163
527	86	0.61	0.817	-0.211	0.211
532.5	103.75	0.53	0.733	-0.208	0.208

Physical and Numerical Velocity Magnitudes

Removal Scheme:	*UC2c(ii)*		
Flow (m^3/s):	1100	Avg. Difference (m/s):	-0.004
u/s wsel (m):	257.56	Avg. Abs. Diff. (m/s):	0.054
ε_{ij} ($N\text{-}s/m^2$):	2800	Standard Dev.(diff):	0.063
Manning's *n*:	0.04	Max. (diff):	0.098
Number of data:	9	Min. (diff.):	-0.070

Node Coordinate		Physical	Calibrated Numerical		Absolute
X	Y	Velocity (m/s)	Velocity (m/s)	Difference	Difference
376	123.5	0.58	0.536	0.044	0.044
422.53	119.62	0.86	0.923	-0.063	0.063
445.602	117.1537	0.99	1.037	-0.047	0.047
452.5	81	1.05	0.952	0.098	0.098
468.28	109.5	1.11	1.126	-0.016	0.016
489.0531	107.2925	1.24	1.157	0.083	0.083
509.75	101.5	0.73	0.8	-0.070	0.070
527	86	0.79	0.82	-0.030	0.030
532.5	103.75	0.7	0.735	-0.035	0.035

Physical and Numerical Velocity Magnitudes

Removal Scheme:	*UC3a*		
Flow (m^3/s):	1100	Avg. Difference (m/s):	-0.009
u/s wsel (m):	257.61	Avg. Abs. Diff. (m/s):	0.083
ε_{ij} ($N\text{-}s/m^2$):	2800	Standard Dev.(diff):	0.109
Manning's *n*:	0.04	Max. (diff):	0.266
Number of data:	11	Min. (diff.):	-0.095

Node Coordinate X	Y	Physical Velocity (m/s)	Calibrated Numerical Velocity (m/s)	Difference	Absolute Difference
376	123.5	0.512	0.496	0.016	0.016
422.53	119.62	0.834	0.901	-0.067	0.067
445.602	117.1537	0.901	0.994	-0.093	0.093
452.5	81	0.927	0.971	-0.044	0.044
468.28	109.5	1.008	1.102	-0.094	0.094
484.3074	89.2957	1.088	1.015	0.073	0.073
489.0531	107.2925	1.061	1.009	0.052	0.052
493.8605	125.4125	0.927	0.661	0.266	0.266
509.75	101.5	0.659	0.737	-0.078	0.078
527	86	0.767	0.862	-0.095	0.095
532.5	103.75	0.659	0.696	-0.037	0.037

Physical and Numerical Velocity Magnitudes

Removal Scheme:	*UC3b*		
Flow (m^3/s):	1100	Avg. Difference (m/s):	0.000
u/s wsel (m):	257.52	Avg. Abs. Diff. (m/s):	0.094
ε_{ij} ($N\text{-}s/m^2$):	2850	Standard Dev.(diff):	0.134
Manning's *n*:	0.04	Max. (diff):	0.287
Number of data:	11	Min. (diff.):	-0.212

Node Coordinate		Physical	Calibrated Numerical		Absolute
X	Y	Velocity (m/s)	Velocity (m/s)	Difference	Difference
376	123.5	0.512	0.515	-0.003	0.003
422.53	119.62	0.887	0.973	-0.086	0.086
445.602	117.1537	1.021	1.082	-0.061	0.061
452.5	81	1.061	1.045	0.016	0.016
468.28	109.5	1.115	1.199	-0.084	0.084
484.3074	89.2957	1.236	1.078	0.158	0.158
489.0531	107.2925	1.102	1.096	0.006	0.006
493.8605	125.4125	1.008	0.721	0.287	0.287
509.75	101.5	0.571	0.783	-0.212	0.212
527	86	0.780	0.853	-0.073	0.073
532.5	103.75	0.767	0.714	0.053	0.053

Physical and Numerical Velocity Magnitudes

Removal Scheme:	*UC3c*		
Flow (m^3/s):	1100	Avg. Difference (m/s):	-0.006
u/s wsel (m):	257.59	Avg. Abs. Diff. (m/s):	0.121
ε_{ij} (N-s/m^2):	2800	Standard Dev.(diff):	0.171
Manning's n:	0.04	Max. (diff):	0.489
Number of data:	30	Min. (diff.):	-0.409

Node Coordinate X	Y	Physical Velocity (m/s)	Calibrated Numerical Velocity (m/s)	Difference	Absolute Difference
41	60	0.40	0.283	0.122	0.122
41	100	0.39	0.295	0.096	0.096
41	245	0.44	0.229	0.216	0.216
131	79	0.54	0.444	0.095	0.095
140	207	0.00	0.409	-0.409	0.409
140	250	0.00	0.153	-0.153	0.153
158	127	0.58	0.584	-0.005	0.005
220	82	0.51	0.482	0.030	0.030
220	133.5	0.47	0.494	-0.022	0.022
220	207	0.50	0.443	0.055	0.055
305	86	0.47	0.453	0.019	0.019
305	147.5	0.47	0.435	0.037	0.037
305	197.5	0.00	0.13	-0.130	0.130
340.5	80.75	0.46	0.474	-0.016	0.016
376	75.5	0.55	0.461	0.091	0.091
376	123.5	0.53	0.529	-0.004	0.004
376	167	0.00	0.339	-0.339	0.339
376	195	0.00	0.199	-0.199	0.199
376	203	0.00	0.171	-0.171	0.171
422.53	119.62	1.02	1.048	-0.027	0.027
438	156	1.09	1.03	0.058	0.058
445.602	117.1537	1.14	1.181	-0.039	0.039
452.5	81	1.26	1.105	0.157	0.157
468.28	109.5	1.32	1.31	0.006	0.006
484.3074	89.2957	1.33	1.135	0.194	0.194
489.0531	107.2925	1.26	1.2	0.062	0.062
493.8605	125.4125	1.29	0.8	0.489	0.489
509.75	101.5	0.66	0.841	-0.176	0.176
527	86	0.71	0.835	-0.122	0.122
532.5	103.75	0.65	0.735	-0.089	0.089

Physical and Numerical Velocity Magnitudes

Removal Scheme:	*UC3c(Q2)*		
Flow (m^3/s):	867	Avg. Difference (m/s):	-0.061
u/s wsel (m):	254.02	Avg. Abs. Diff. (m/s):	0.151
ε_{ij} ($N\text{-}s/m^2$):	5800	Standard Dev.(diff):	0.208
Manning's n:	0.04	Max. (diff):	0.669
Number of data:	26	Min. (diff.):	-0.487

Node Coordinate X	Y	Physical Velocity (m/s)	Calibrated Numerical Velocity (m/s)	Difference	Absolute Difference
41	60	0.351	0.305	0.046	0.046
41	100	0.324	0.322	0.002	0.002
131	79	0.579	0.535	0.044	0.044
140	207	0.000	0.487	-0.487	0.487
140	250	0.000	0.195	-0.195	0.195
158	127	0.820	0.73	0.090	0.090
220	82	0.659	0.571	0.088	0.088
220	133.5	0.485	0.545	-0.060	0.060
305	86	0.472	0.489	-0.017	0.017
305	147.5	0.539	0.417	0.122	0.122
305	197.5	0.000	0.136	-0.136	0.136
340.5	80.75	0.512	0.487	0.025	0.025
376	75.5	0.391	0.433	-0.042	0.042
376	123.5	0.405	0.545	-0.140	0.140
376	167	0.000	0.355	-0.355	0.355
422.53	119.62	1.115	1.297	-0.182	0.182
438	156	1.142	1.111	0.031	0.031
445.602	117.1537	1.262	1.457	-0.195	0.195
452.5	81	1.329	1.276	0.053	0.053
468.28	109.5	1.329	1.592	-0.263	0.263
484.3074	89.2957	1.195	1.247	-0.052	0.052
489.0531	107.2925	1.195	1.351	-0.156	0.156
493.8605	125.4125	1.463	0.794	0.669	0.669
509.75	101.5	0.624	0.79	-0.166	0.166
527	86	0.525	0.735	-0.210	0.210
532.5	103.75	0.579	0.672	-0.093	0.093

APPENDIX G: CONTOUR AND VECTOR PLOTS OF THE DOWNSTREAM RESULTS FROM NUMERICAL MODEL

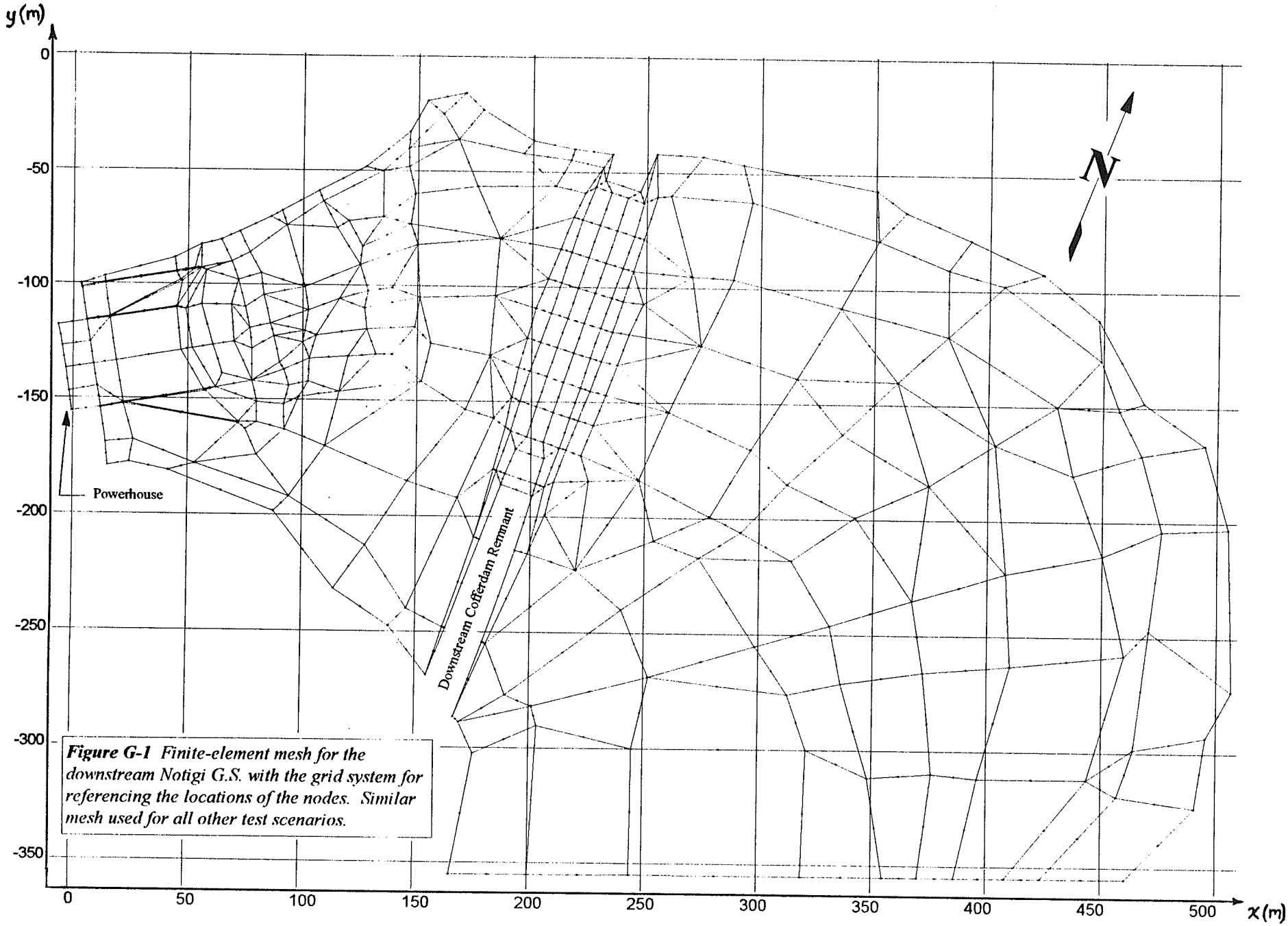

Figure G-1 *Finite-element mesh for the downstream Notigi G.S. with the grid system for referencing the locations of the nodes. Similar mesh used for all other test scenarios.*

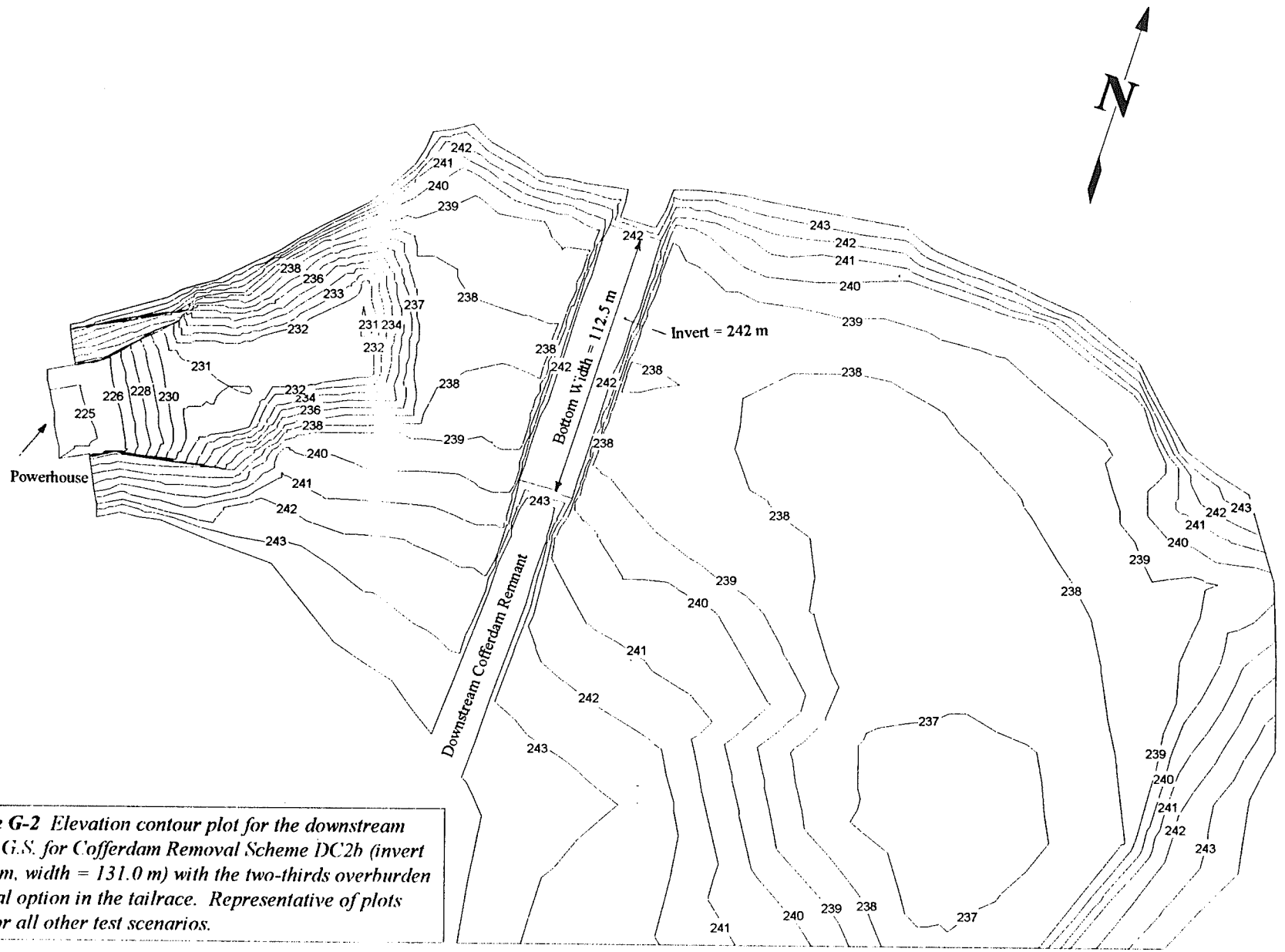

Figure G-2 *Elevation contour plot for the downstream Notigi G.S. for Cofferdam Removal Scheme DC2b (invert = 242 m, width = 131.0 m) with the two-thirds overburden removal option in the tailrace. Representative of plots used for all other test scenarios.*

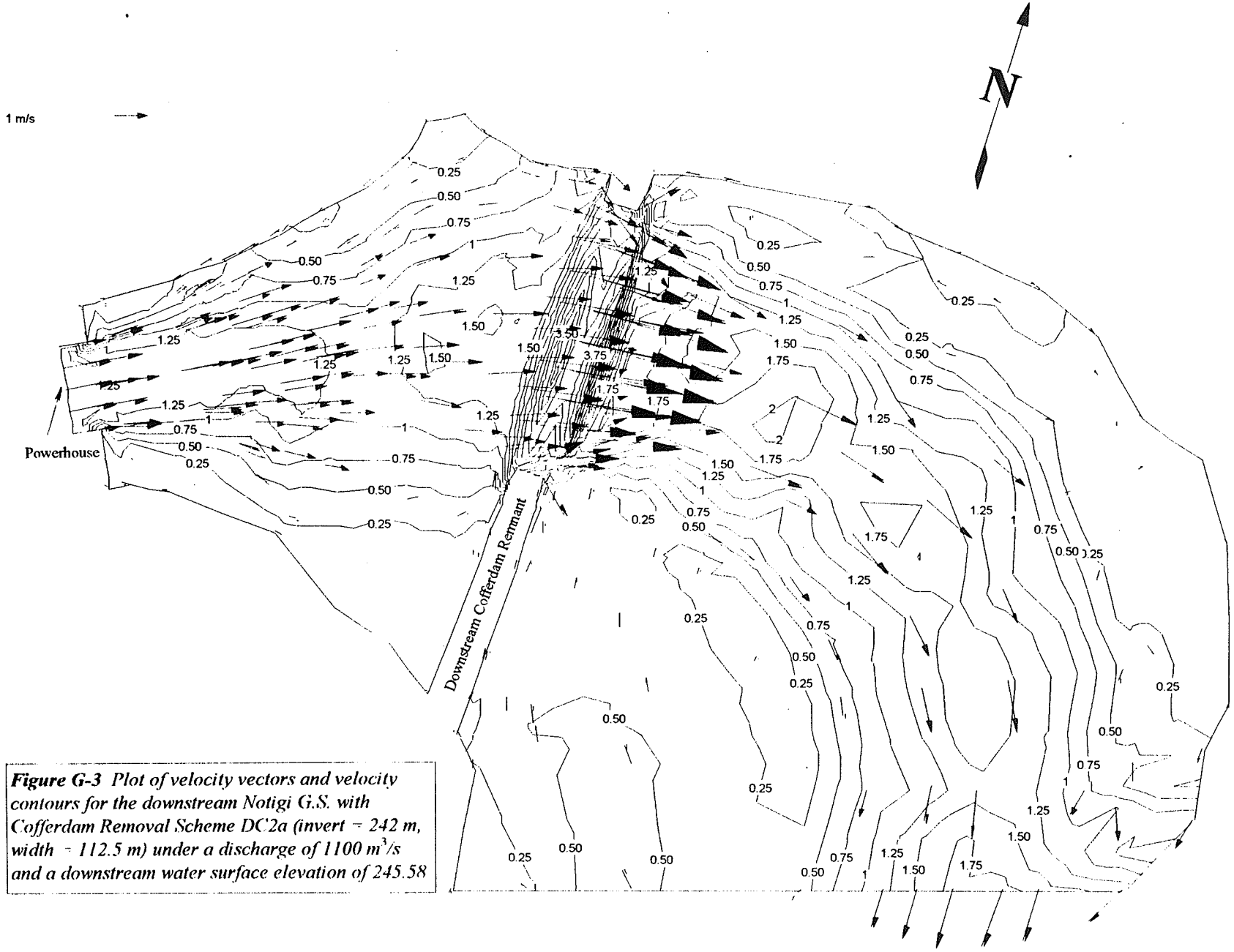

Figure G-3 *Plot of velocity vectors and velocity contours for the downstream Notigi G.S. with Cofferdam Removal Scheme DC2a (invert = 242 m, width = 112.5 m) under a discharge of 1100 m^3/s and a downstream water surface elevation of 245.58*

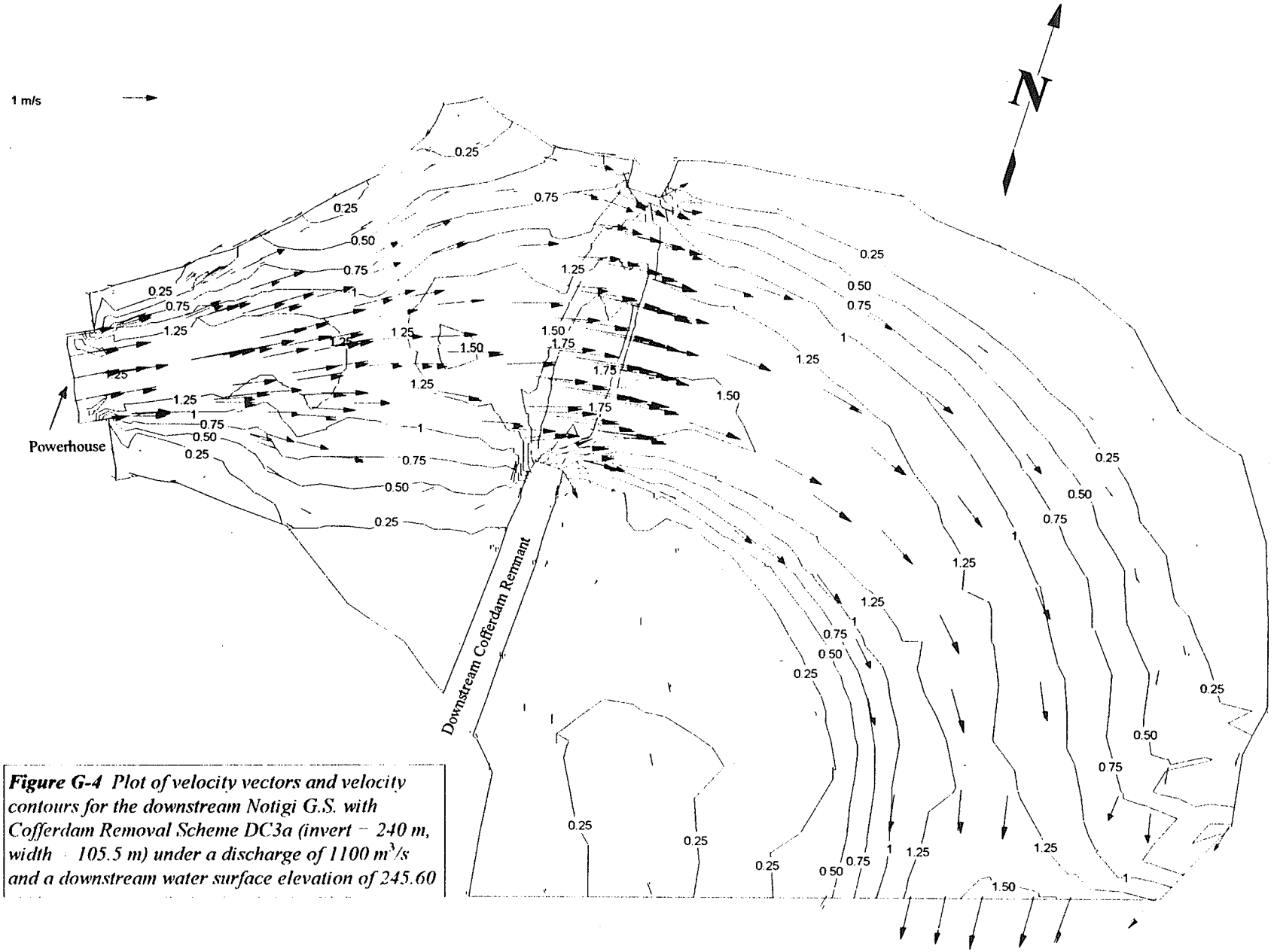

Figure G-4 *Plot of velocity vectors and velocity contours for the downstream Notigi G.S. with Cofferdam Removal Scheme DC3a (invert = 240 m, width = 105.5 m) under a discharge of 1100 m^3/s and a downstream water surface elevation of 245.60*

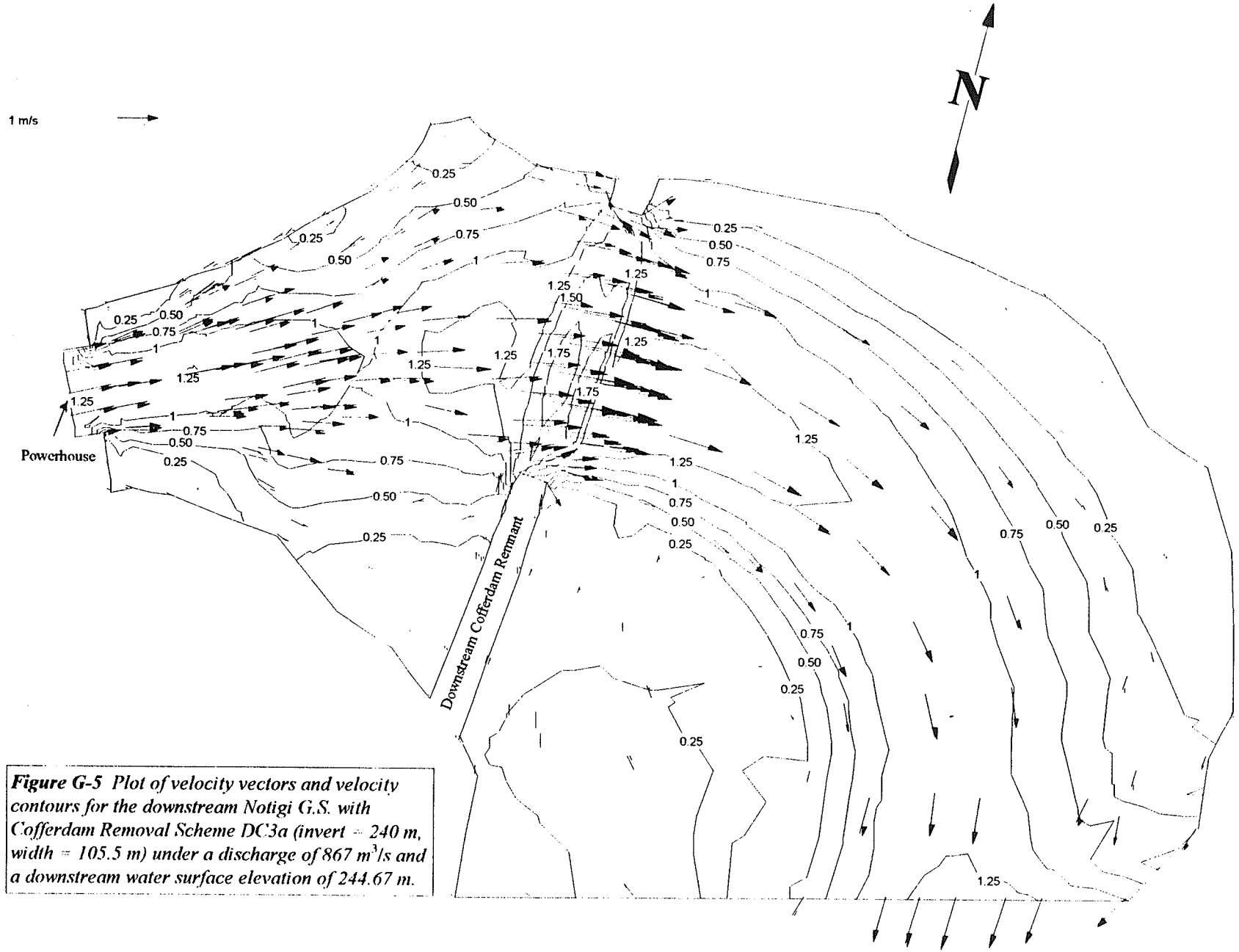

Figure G-5 *Plot of velocity vectors and velocity contours for the downstream Notigi G.S. with Cofferdam Removal Scheme DC3a (invert = 240 m, width = 105.5 m) under a discharge of 867 m^3/s and a downstream water surface elevation of 244.67 m.*

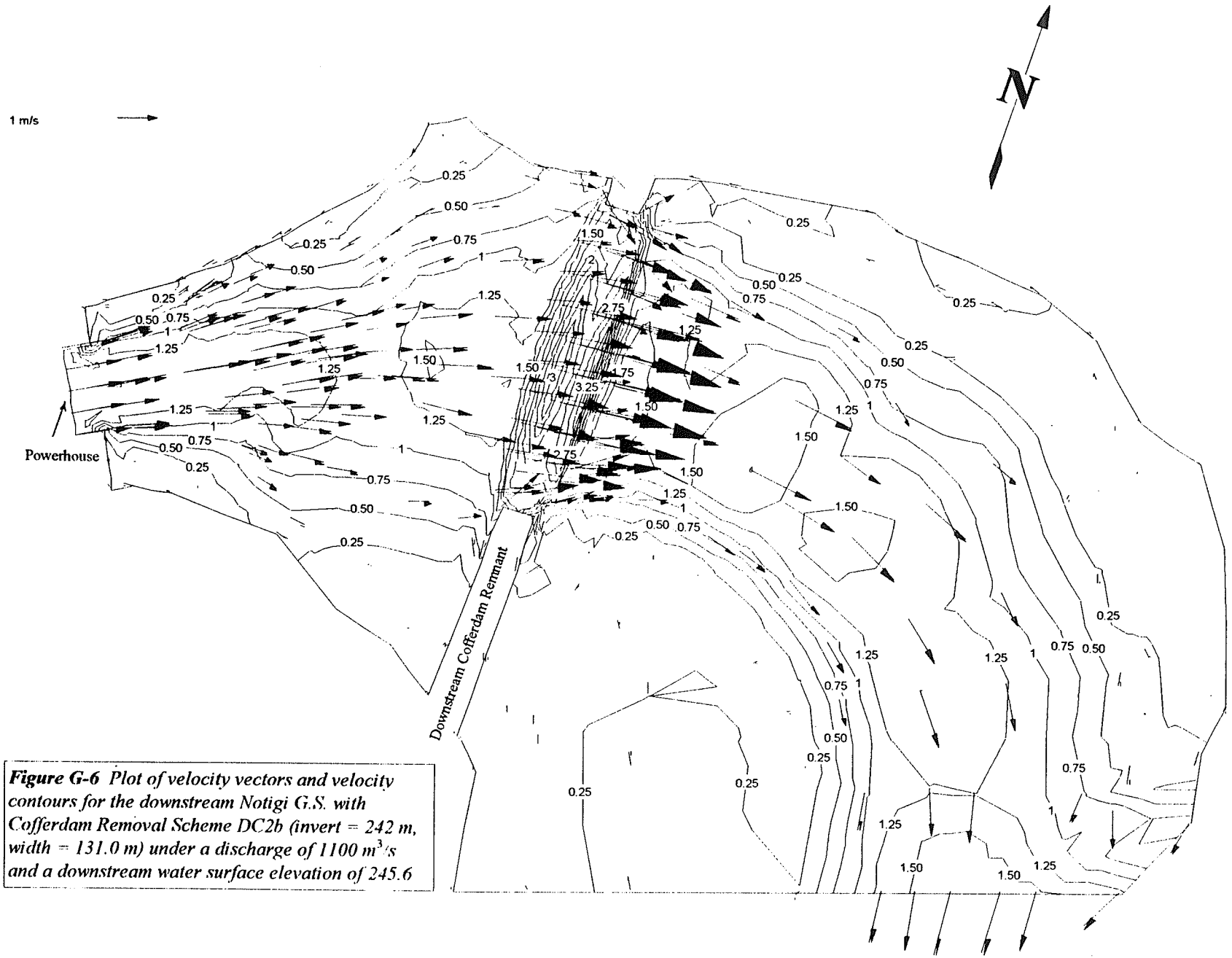

Figure G-6 *Plot of velocity vectors and velocity contours for the downstream Notigi G.S. with Cofferdam Removal Scheme DC2b (invert = 242 m, width = 131.0 m) under a discharge of 1100 m^3/s and a downstream water surface elevation of 245.6*

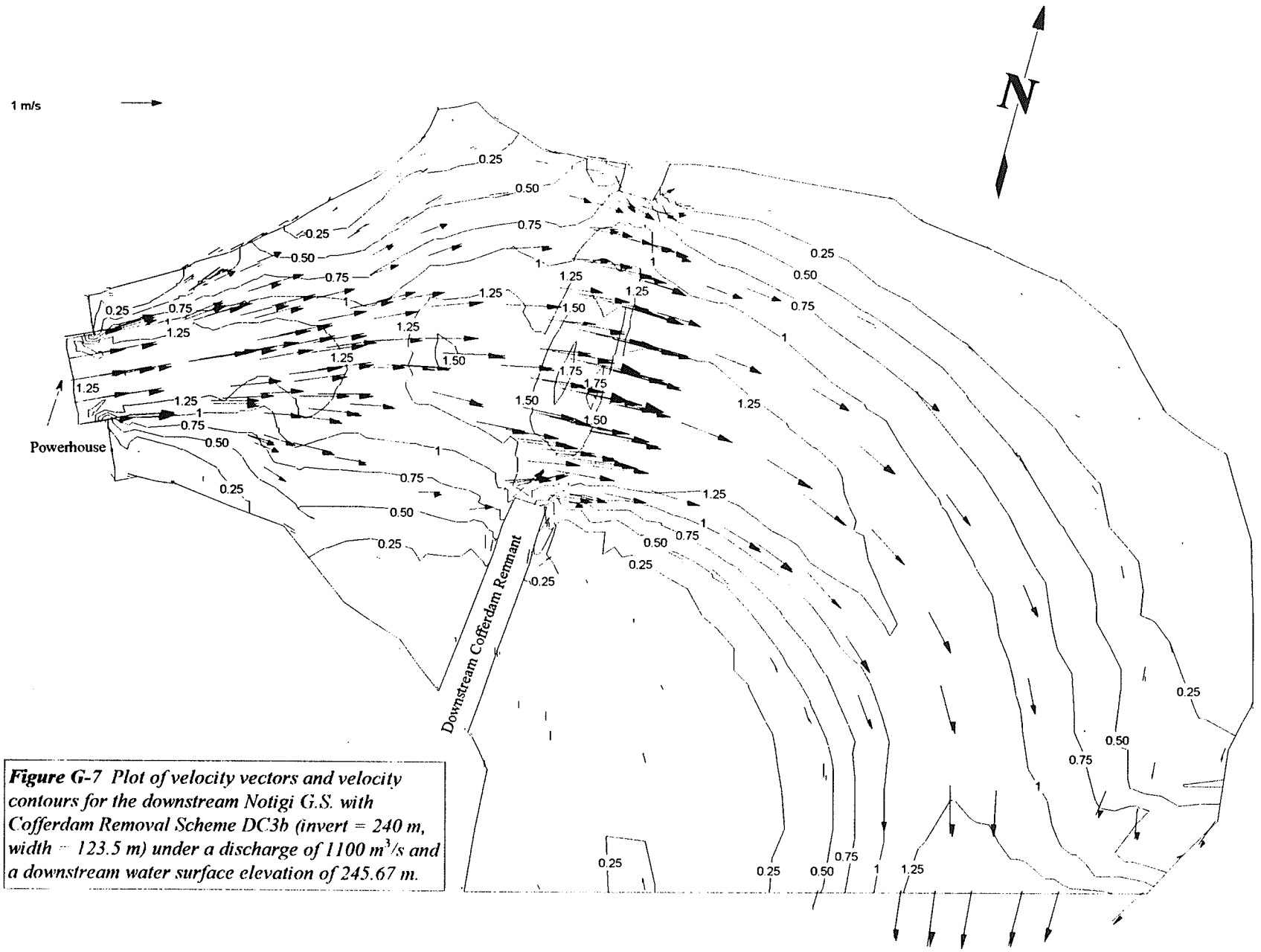

Figure G-7 *Plot of velocity vectors and velocity contours for the downstream Notigi G.S. with Cofferdam Removal Scheme DC3b (invert = 240 m, width = 123.5 m) under a discharge of 1100 m^3/s and a downstream water surface elevation of 245.67 m.*

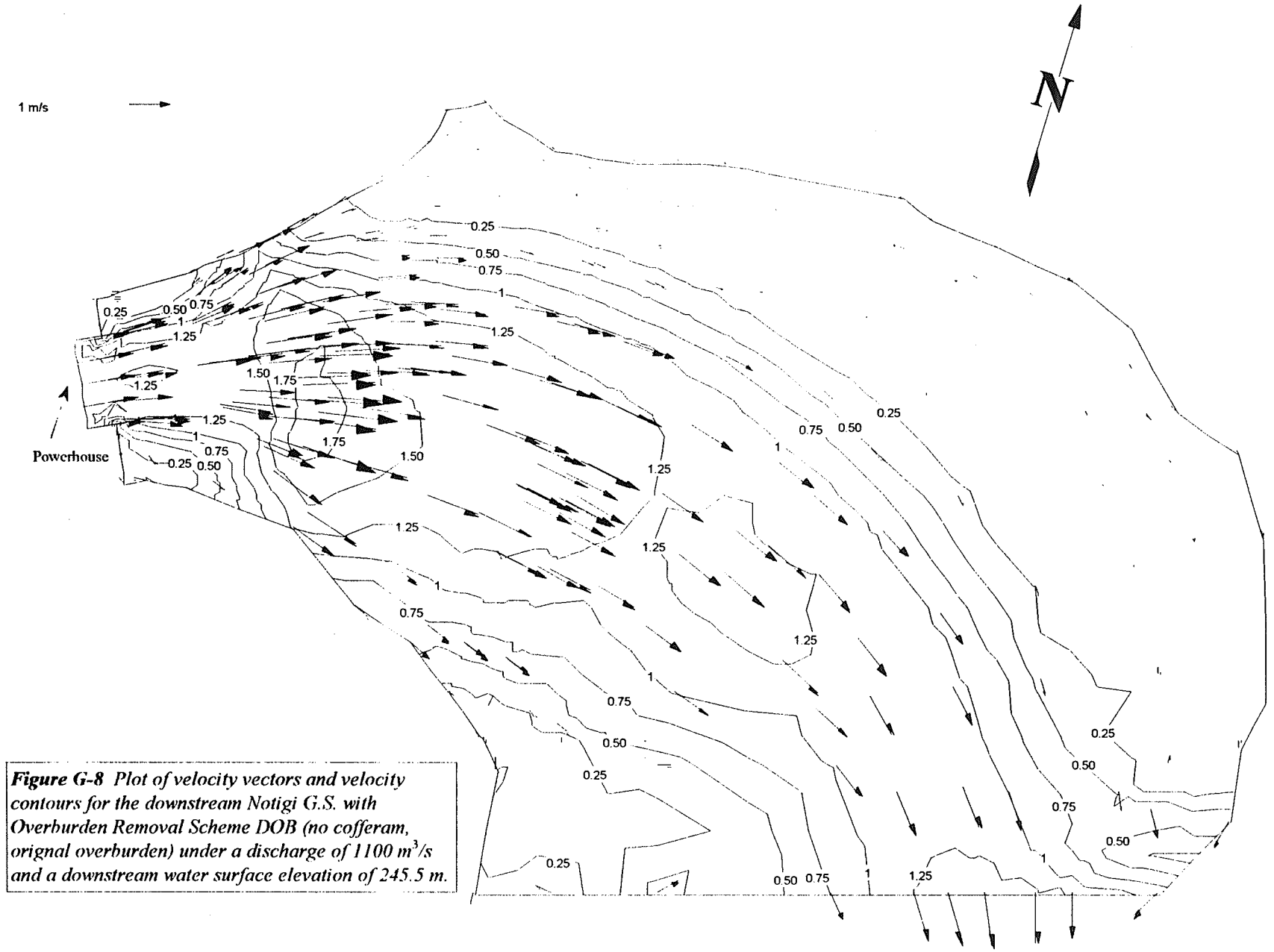

Figure G-8 *Plot of velocity vectors and velocity contours for the downstream Notigi G.S. with Overburden Removal Scheme DOB (no cofferam, orignal overburden) under a discharge of 1100 m^3/s and a downstream water surface elevation of 245.5 m.*

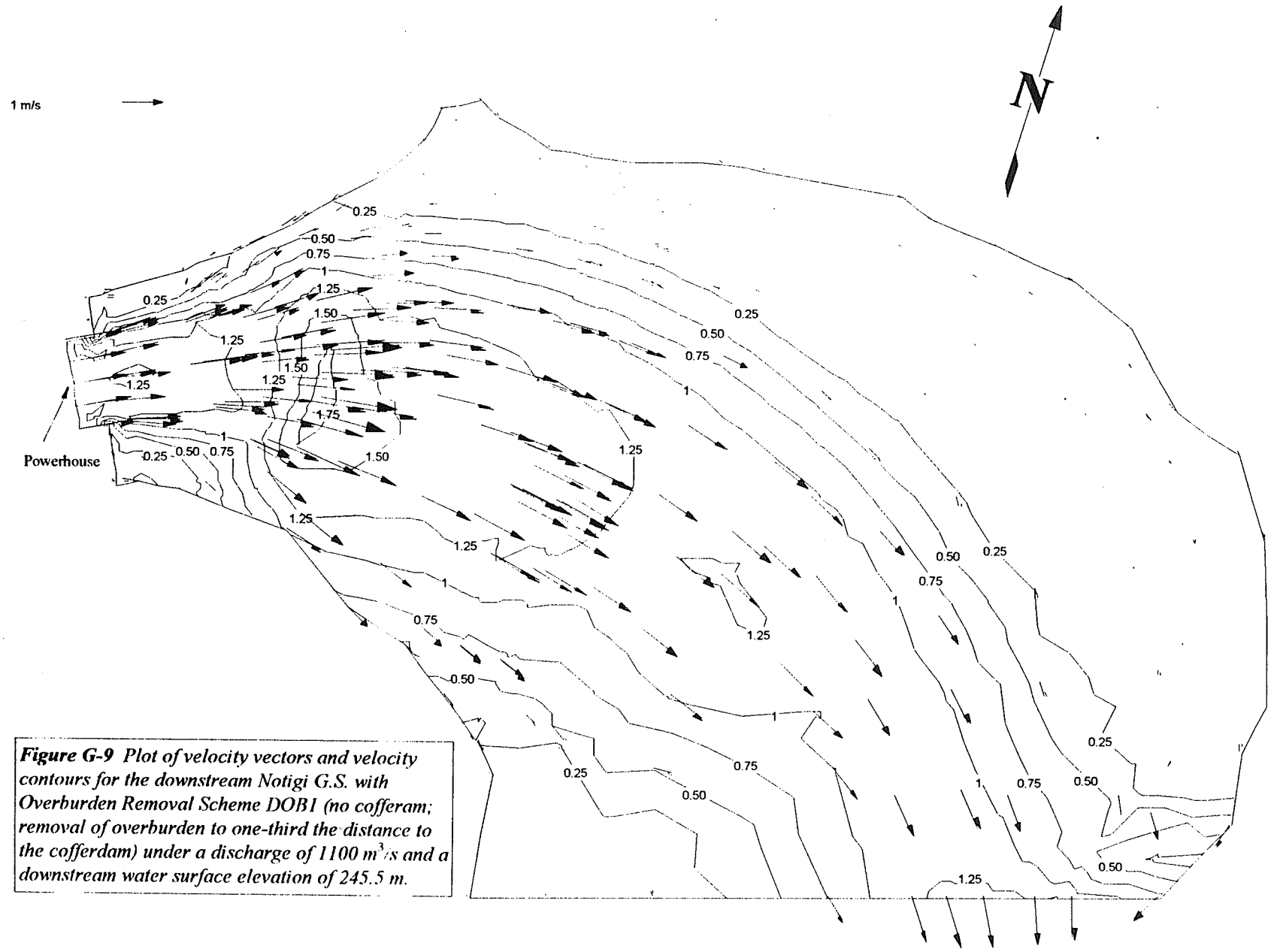

Figure G-9 *Plot of velocity vectors and velocity contours for the downstream Notigi G.S. with Overburden Removal Scheme DOB1 (no cofferam; removal of overburden to one-third the distance to the cofferdam) under a discharge of 1100 m^3/s and a downstream water surface elevation of 245.5 m.*

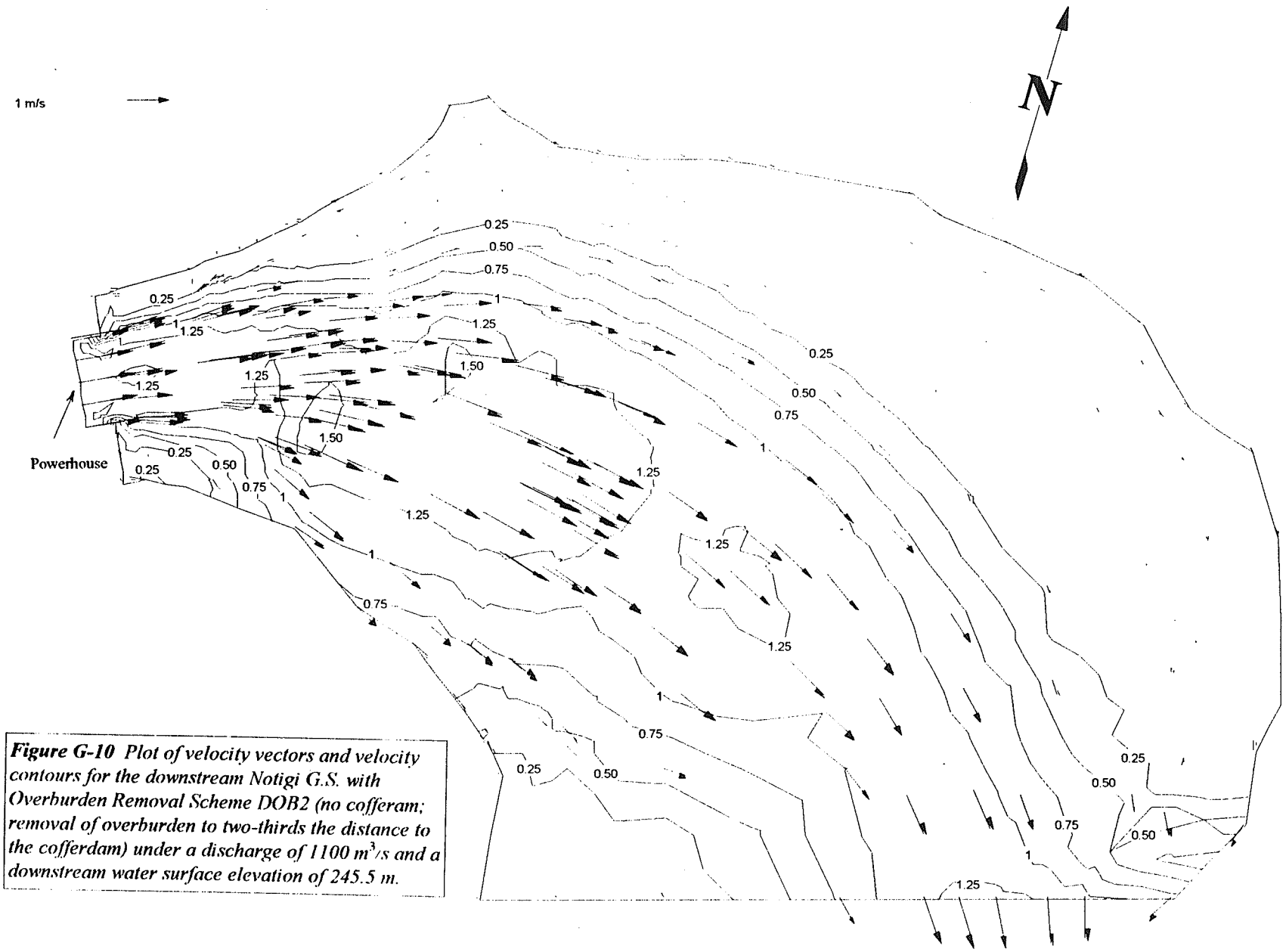

Figure G-10 *Plot of velocity vectors and velocity contours for the downstream Notigi G.S. with Overburden Removal Scheme DOB2 (no cofferam; removal of overburden to two-thirds the distance to the cofferdam) under a discharge of 1100 m^3/s and a downstream water surface elevation of 245.5 m.*

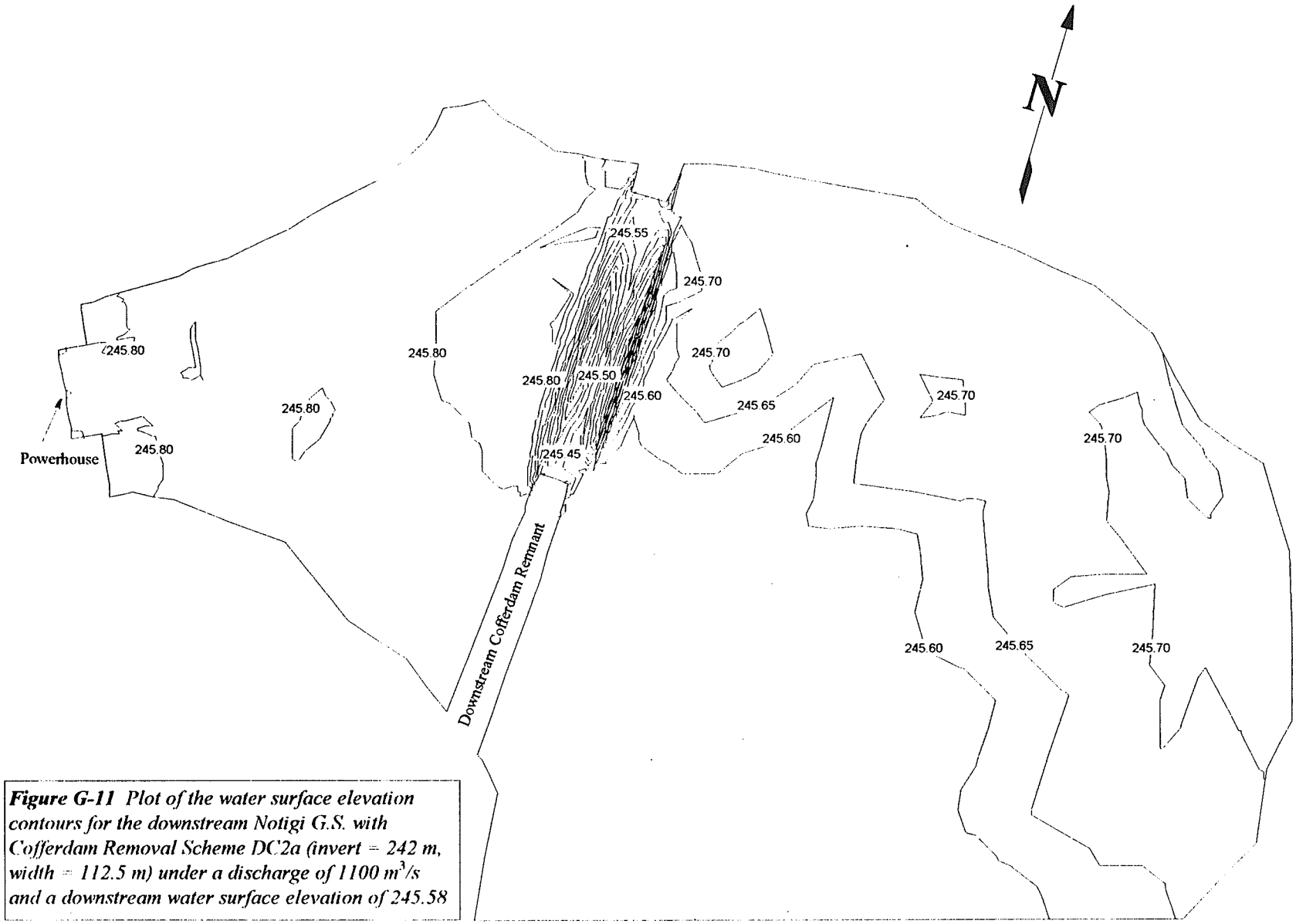

Figure G-11 *Plot of the water surface elevation contours for the downstream Notigi G.S. with Cofferdam Removal Scheme DC2a (invert = 242 m, width = 112.5 m) under a discharge of 1100 m^3/s and a downstream water surface elevation of 245.58*

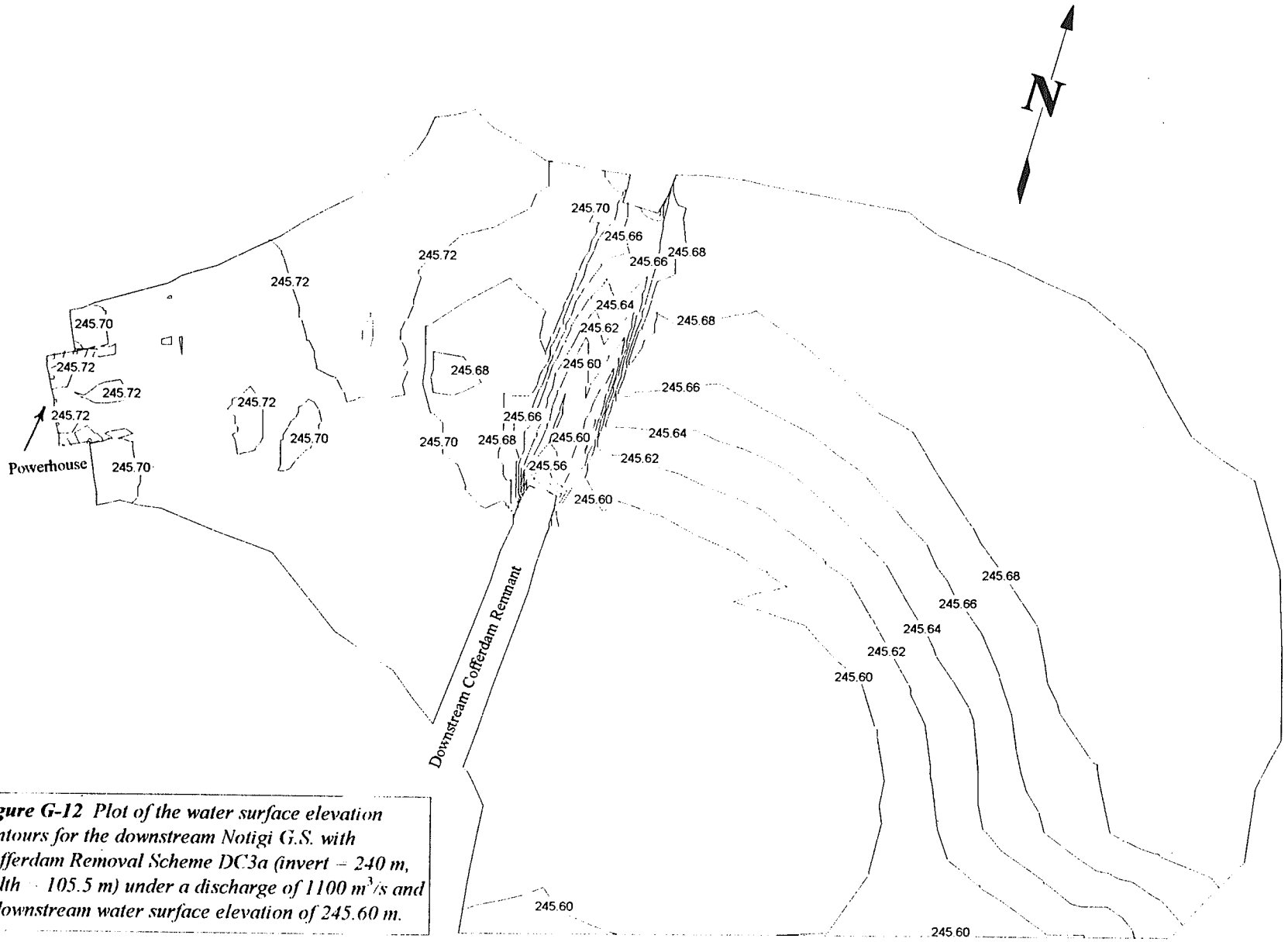

Figure G-12 *Plot of the water surface elevation contours for the downstream Notigi G.S. with Cofferdam Removal Scheme DC3a (invert = 240 m, width = 105.5 m) under a discharge of 1100 m^3/s and a downstream water surface elevation of 245.60 m.*

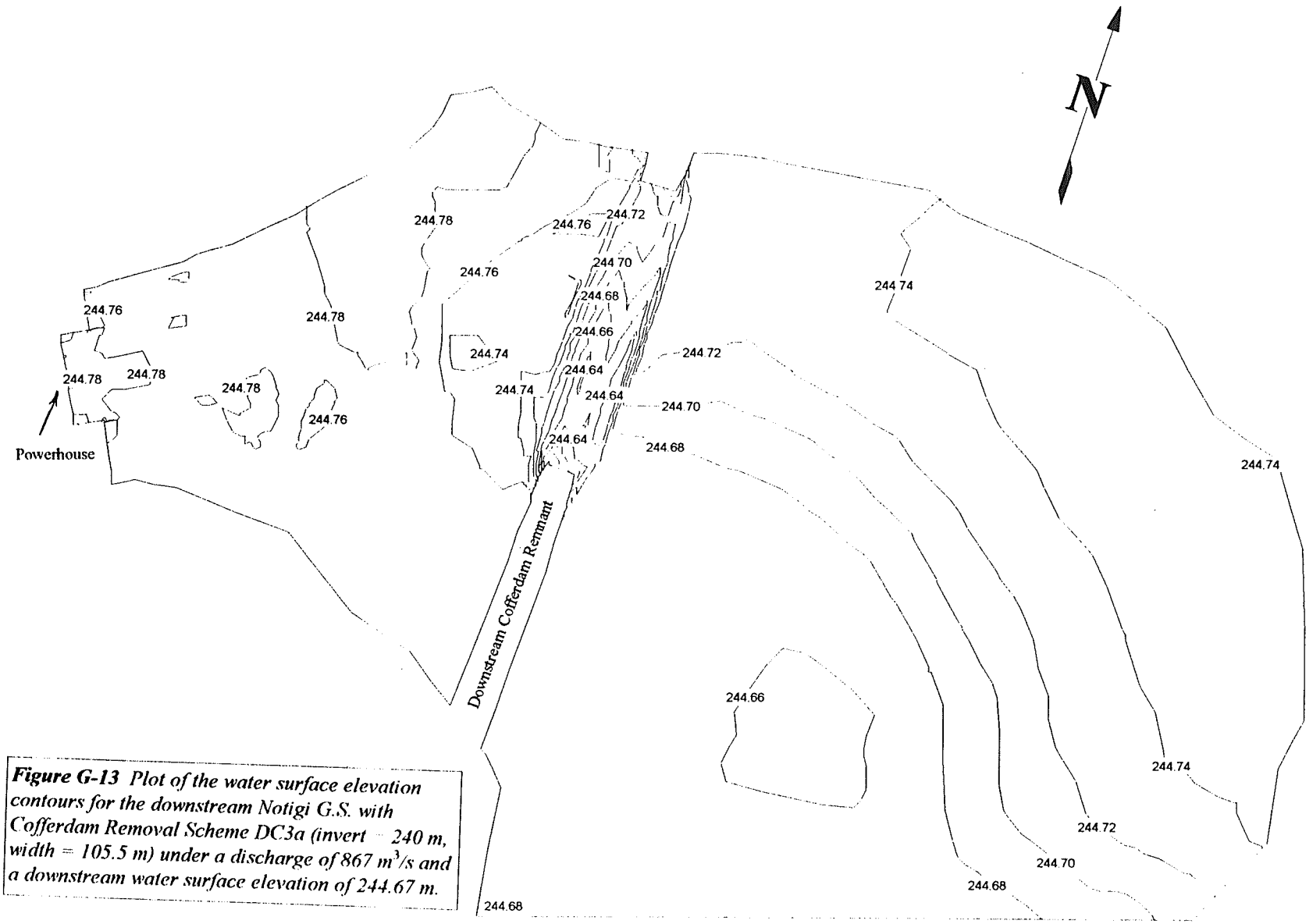

Figure G-13 *Plot of the water surface elevation contours for the downstream Notigi G.S. with Cofferdam Removal Scheme DC3a (invert = 240 m, width = 105.5 m) under a discharge of 867 m^3/s and a downstream water surface elevation of 244.67 m.*

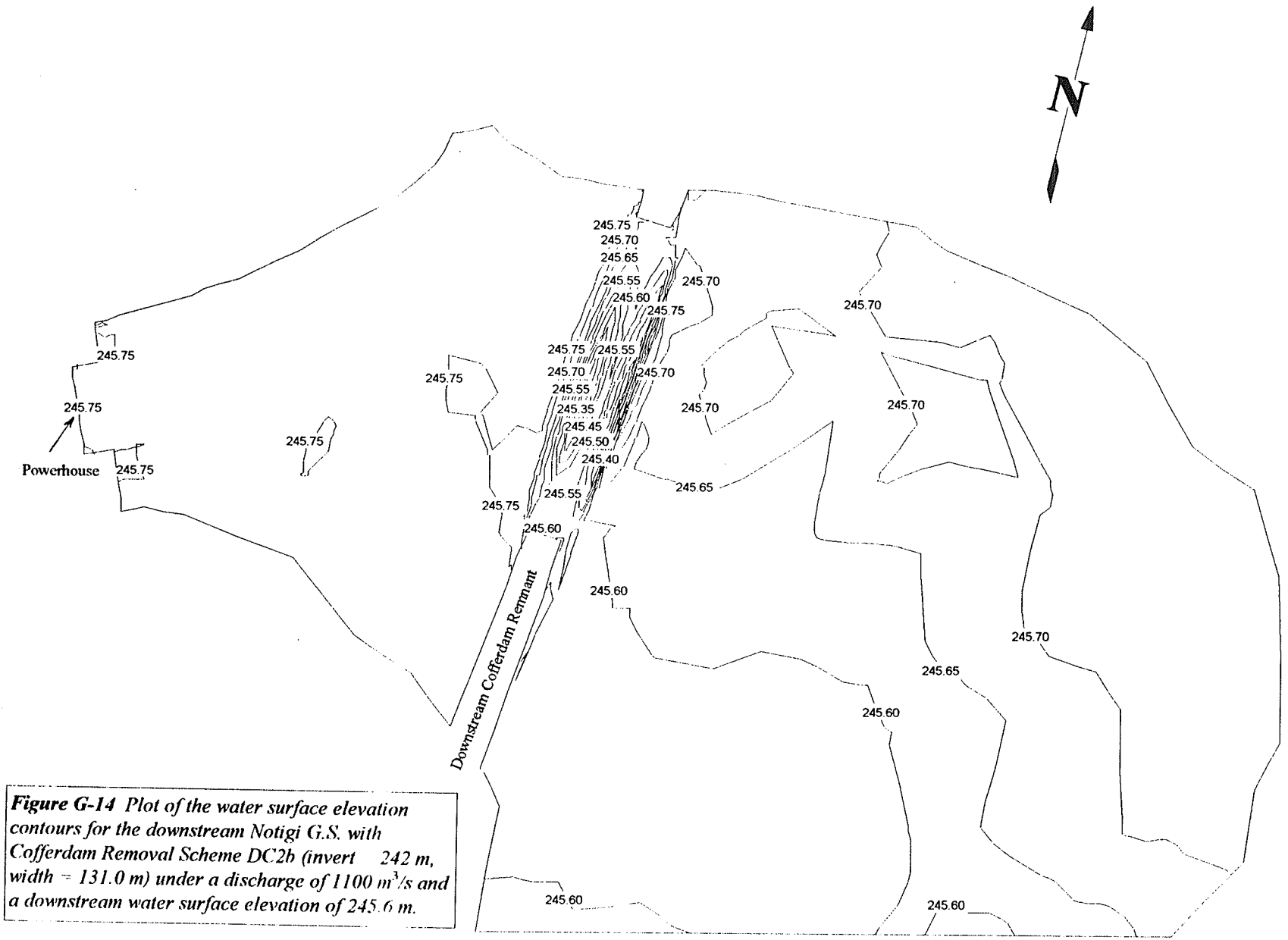

Figure G-14 *Plot of the water surface elevation contours for the downstream Notigi G.S. with Cofferdam Removal Scheme DC2b (invert 242 m, width = 131.0 m) under a discharge of 1100 m^3/s and a downstream water surface elevation of 245.6 m.*

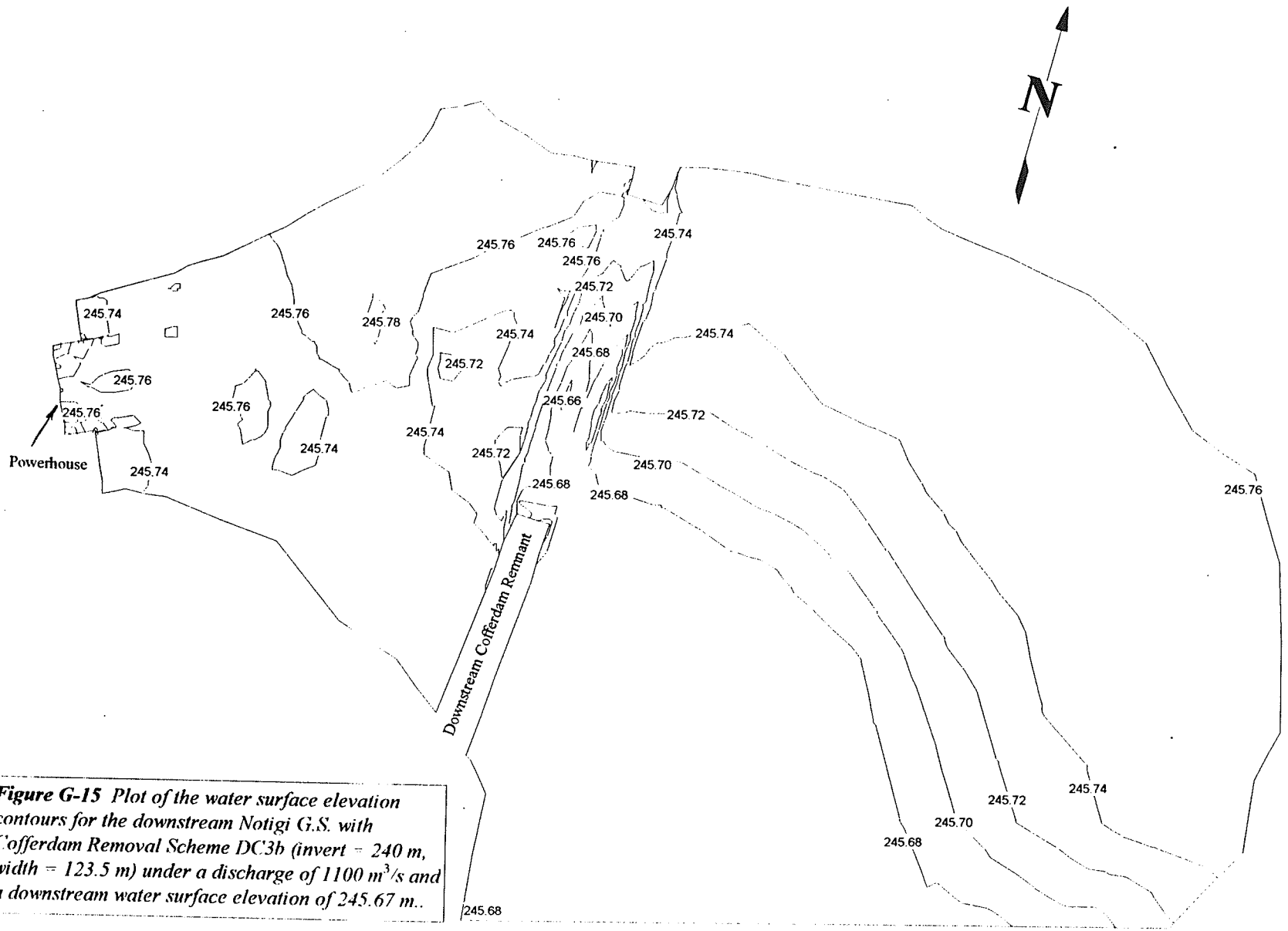

Figure G-15 *Plot of the water surface elevation contours for the downstream Notigi G.S. with Cofferdam Removal Scheme DC3b (invert = 240 m, width = 123.5 m) under a discharge of 1100 m^3/s and a downstream water surface elevation of 245.67 m..*

APPENDIX H: CONTOUR AND VECTOR PLOTS OF THE UPSTREAM RESULTS FROM NUMERICAL MODEL

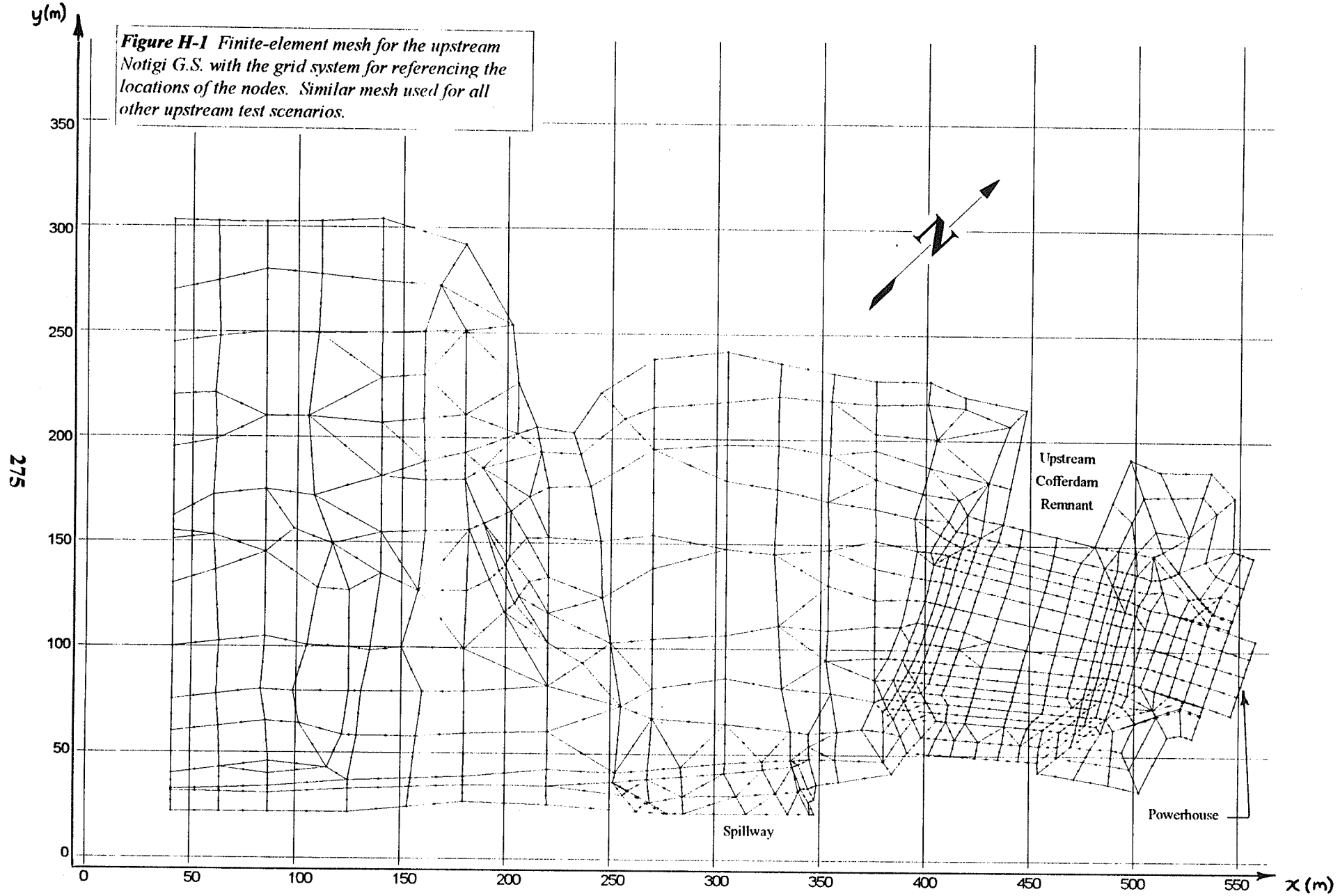

Figure H-1 *Finite-element mesh for the upstream Notigi G.S. with the grid system for referencing the locations of the nodes. Similar mesh used for all other upstream test scenarios.*

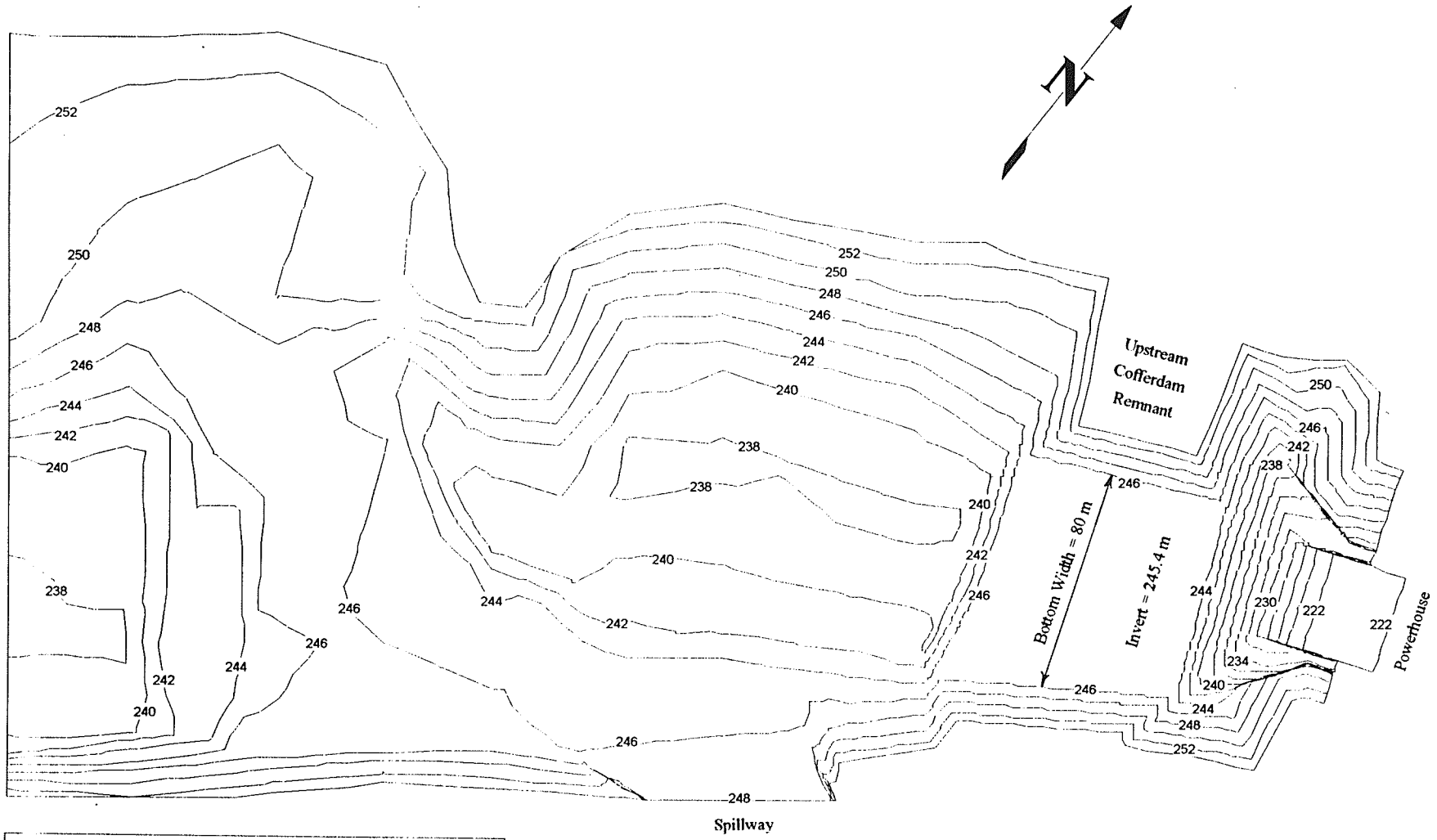

Figure H-2 *Elevation contour plot for the upstream Notigi G.S. for Cofferdam Removal Scheme UC3a (invert = 245.4 m, width = 80 m).*

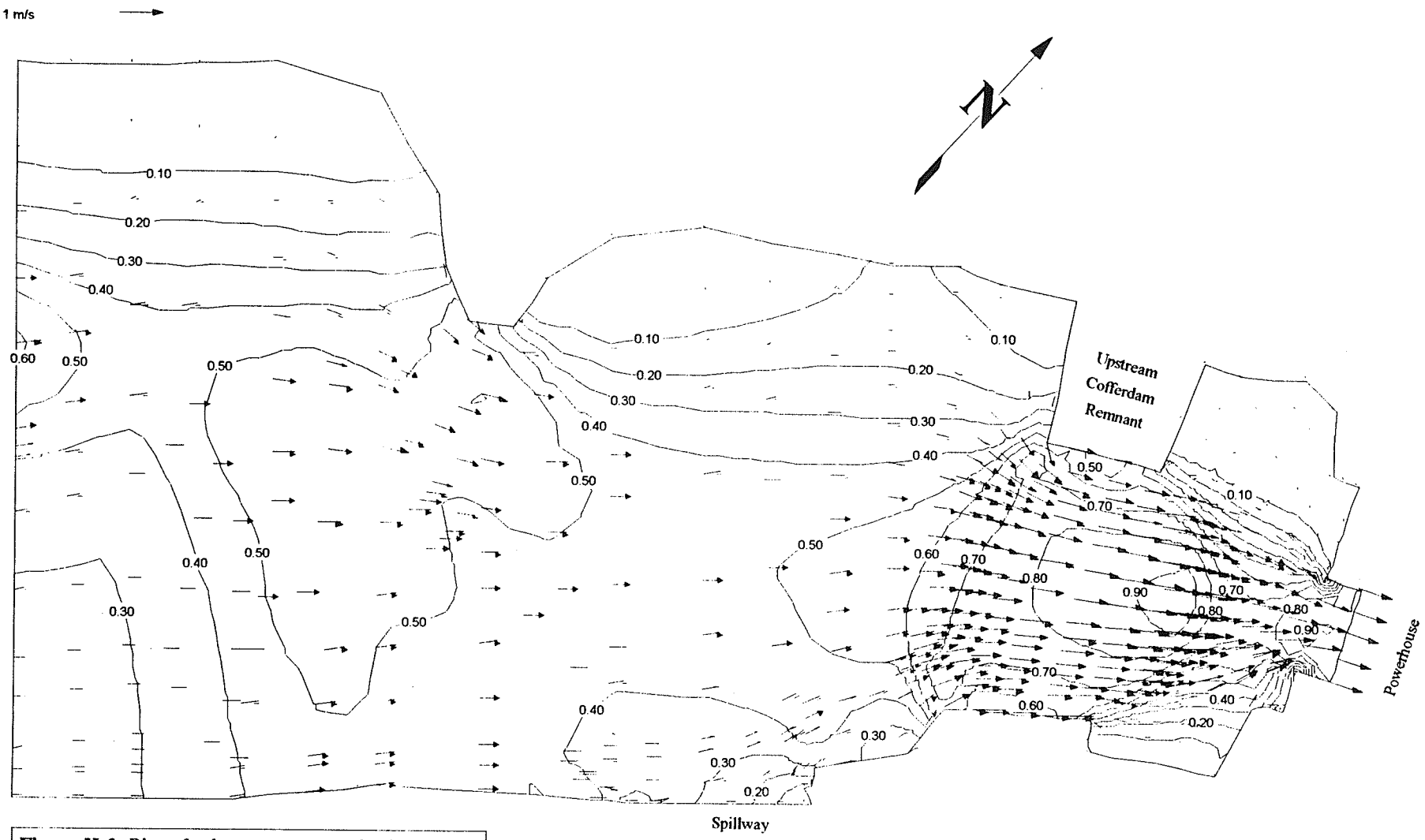

Figure H-3 *Plot of velocity vectors and velocity contours for the upstream Notigi G.S. with Cofferdam Removal Scheme UC1b (invert = 239.8 m, width = 50 m) under a discharge of 1100 m^3/s and an upstream water surface elevation of 257.56 m.*

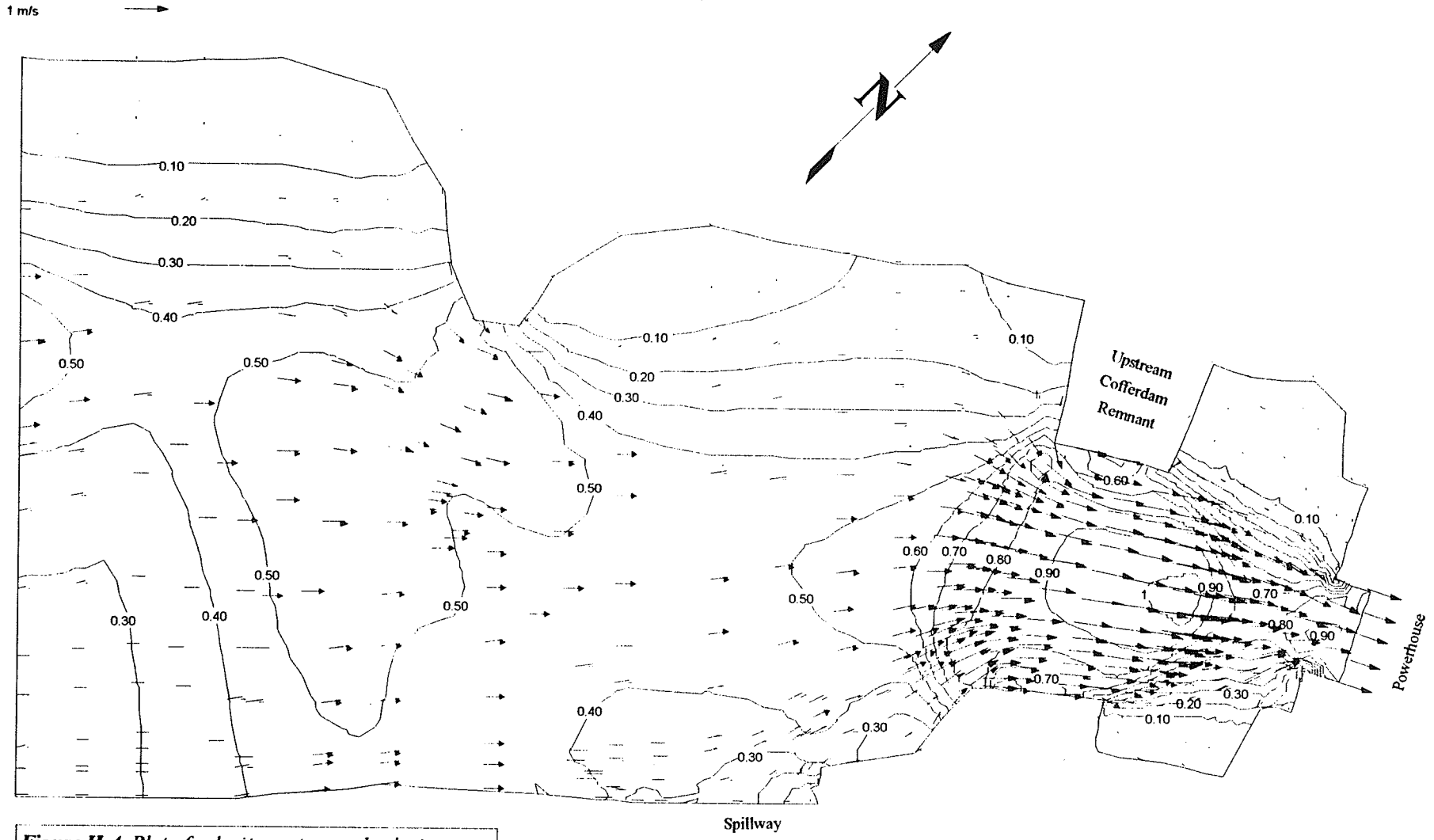

Figure H-4 *Plot of velocity vectors and velocity contours for the upstream Notigi G.S. with Cofferdam Removal Scheme UC1c (invert = 239.8 m, width = 40 m) under a discharge of 1100 m^3/s and an upstream water surface elevation of 257.56 m.*

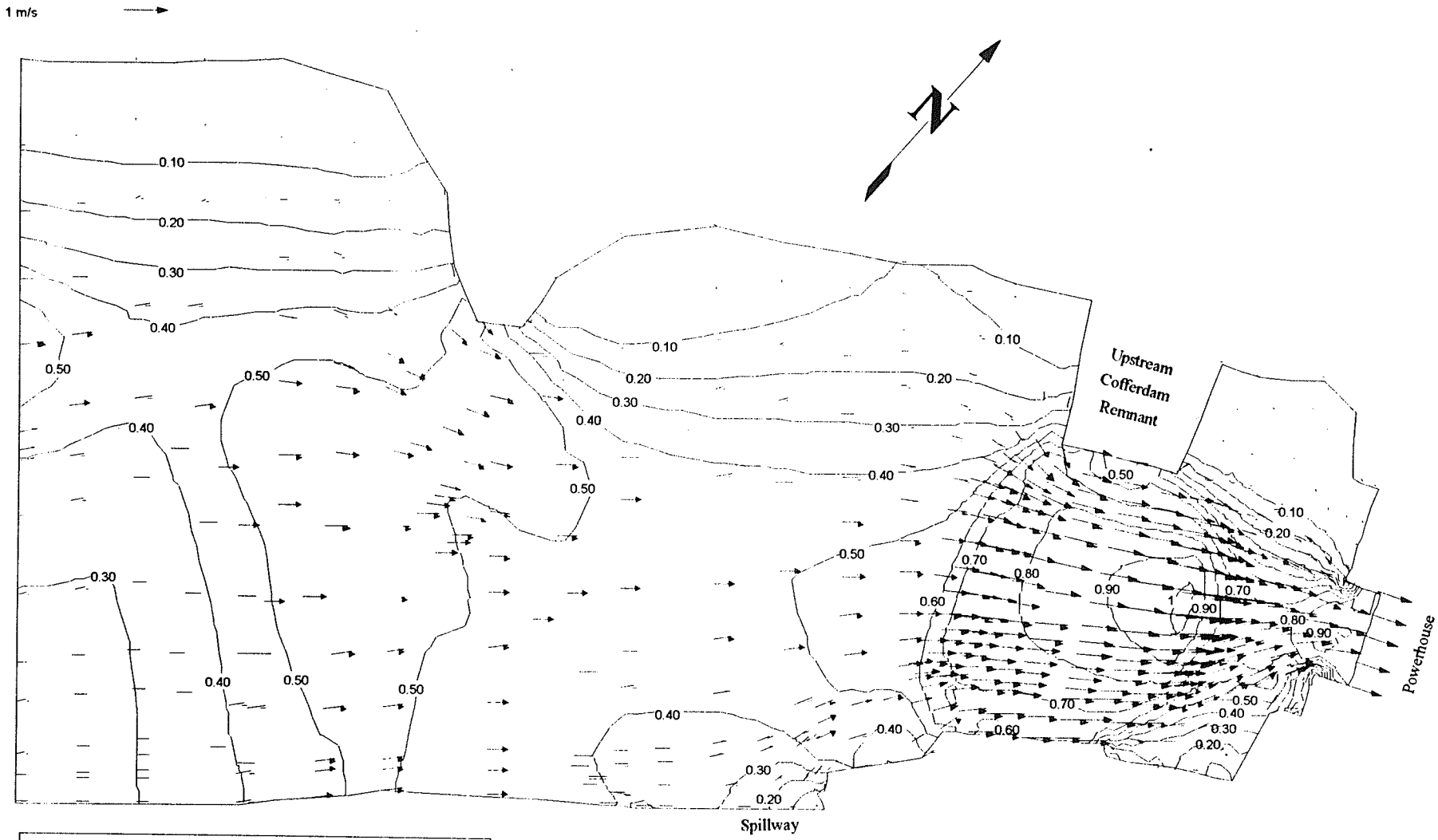

Figure H-5 *Plot of velocity vectors and velocity contours for the upstream Notigi G.S. with Cofferdam Removal Scheme UC2a (invert = 242.8 m, width = 70 m) under a discharge of 1100 m^3/s and an upstream water surface elevation of 257.56 m.*

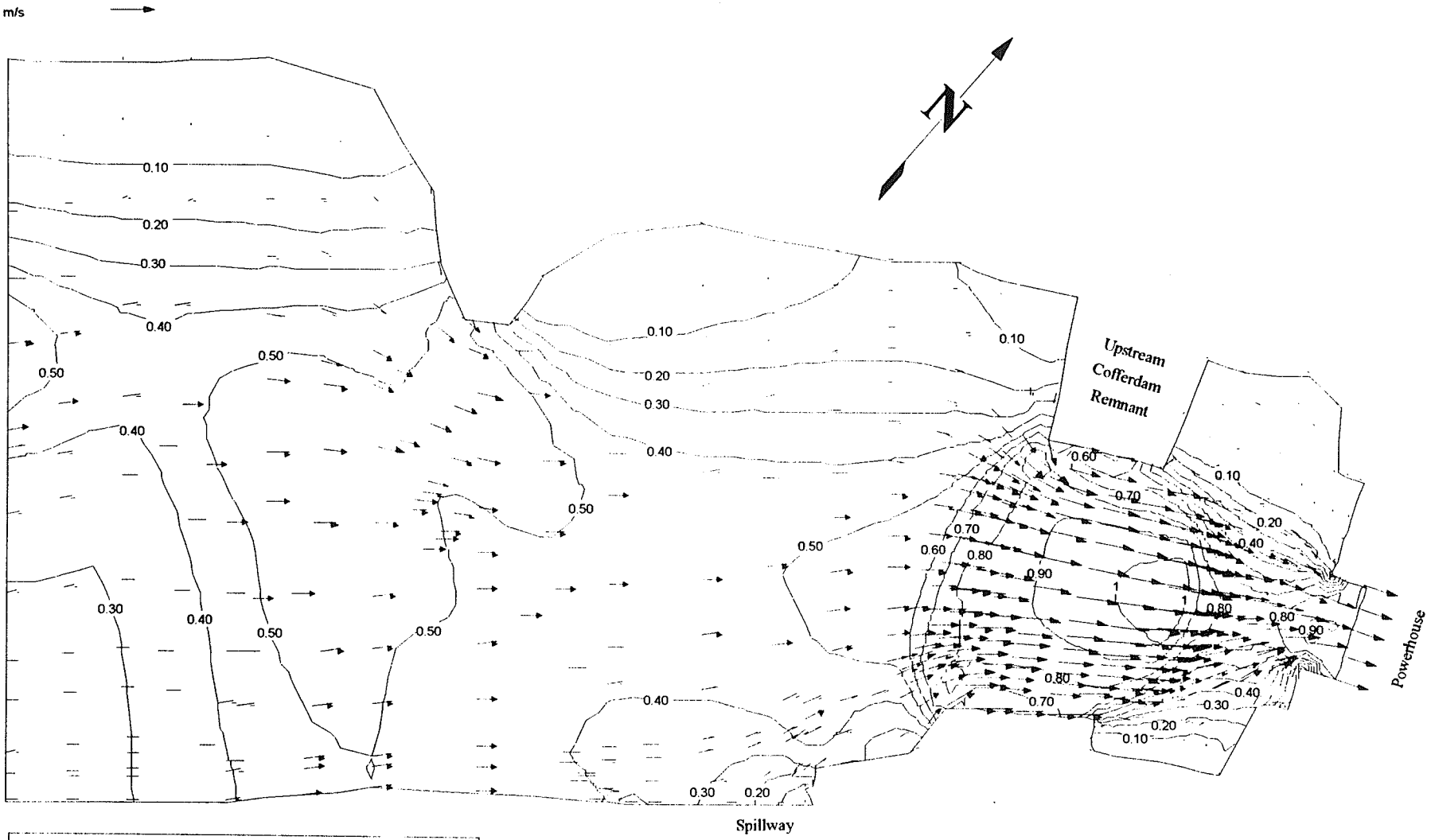

Figure H-6 *Plot of velocity vectors and velocity contours for the upstream Notigi G.S. with Cofferdam Removal Scheme UC2b (invert = 242.8 m, width = 60 m) under a discharge of 1100 m^3/s and an upstream water surface elevation of 257.56 m.*

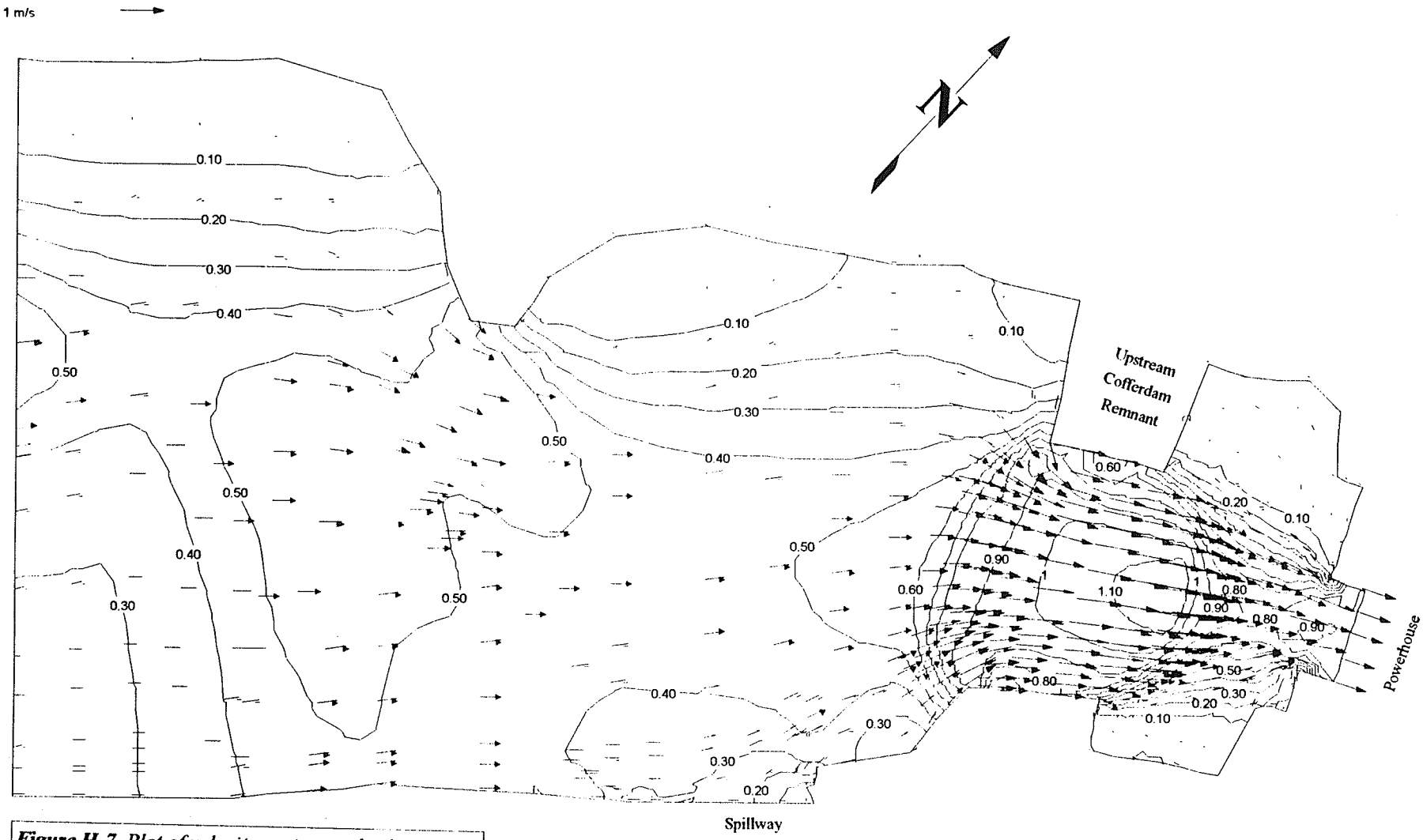

Figure H-7 *Plot of velocity vectors and velocity contours for the upstream Notigi G.S. with Cofferdam Removal Scheme UC2c (invert = 242.8 m, width = 50 m) under a discharge of 1100 m^3/s and an upstream water surface elevation of 257.56 m.*

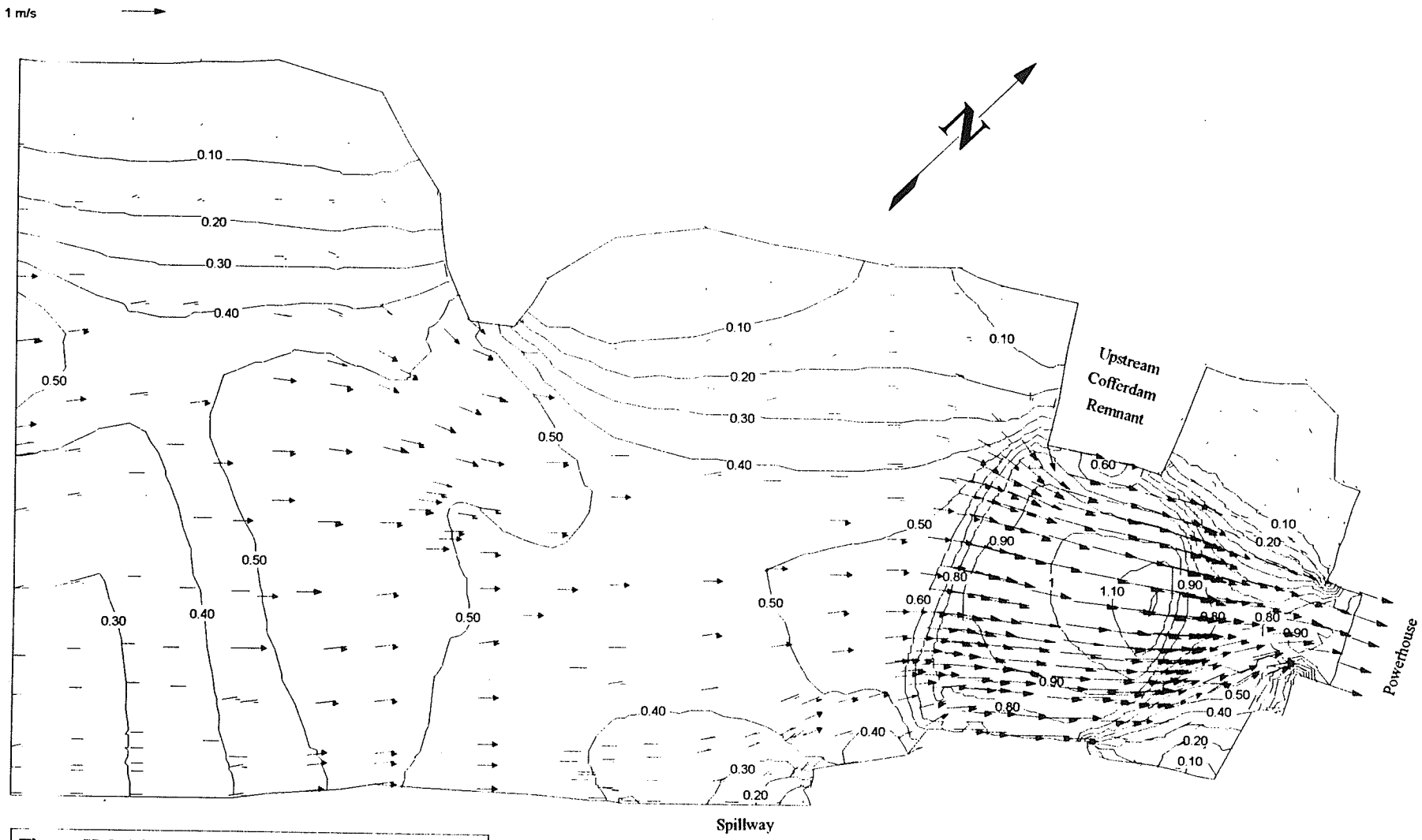

Figure H-8 *Plot of velocity vectors and velocity contours for the upstream Notigi G.S. with Cofferdam Removal Scheme UC3a (invert = 245.4 m, width = 80 m) under a discharge of 1100 m^3/s and an upstream water surface elevation of 257.4 m.*

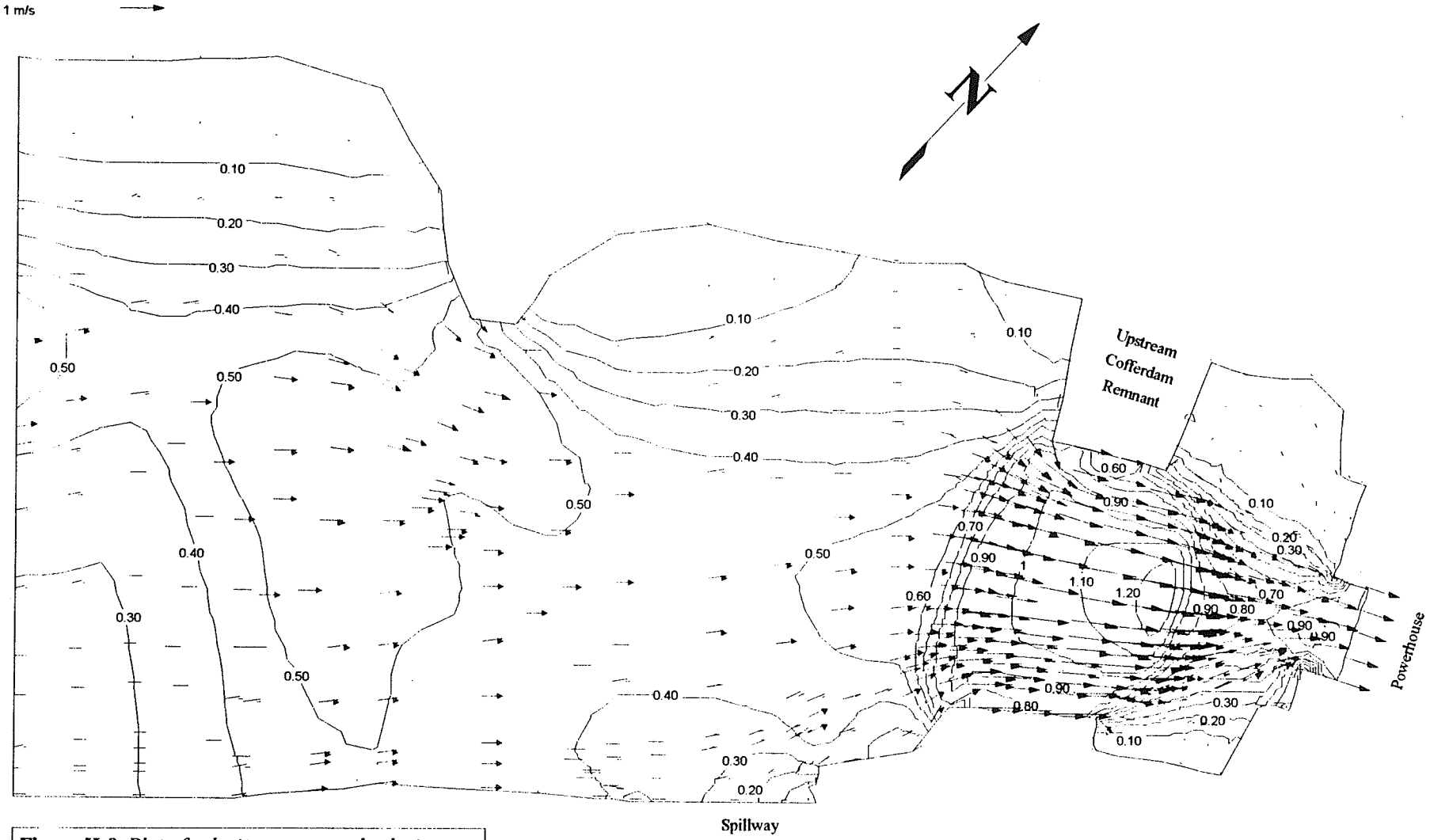

Figure H-9 *Plot of velocity vectors and velocity contours for the upstream Notigi G.S. with Cofferdam Removal Scheme UC3b (invert = 245.4 m, width = 70 m) under a discharge of 1100 m^3/s and an upstream water surface elevation of 257.56 m.*

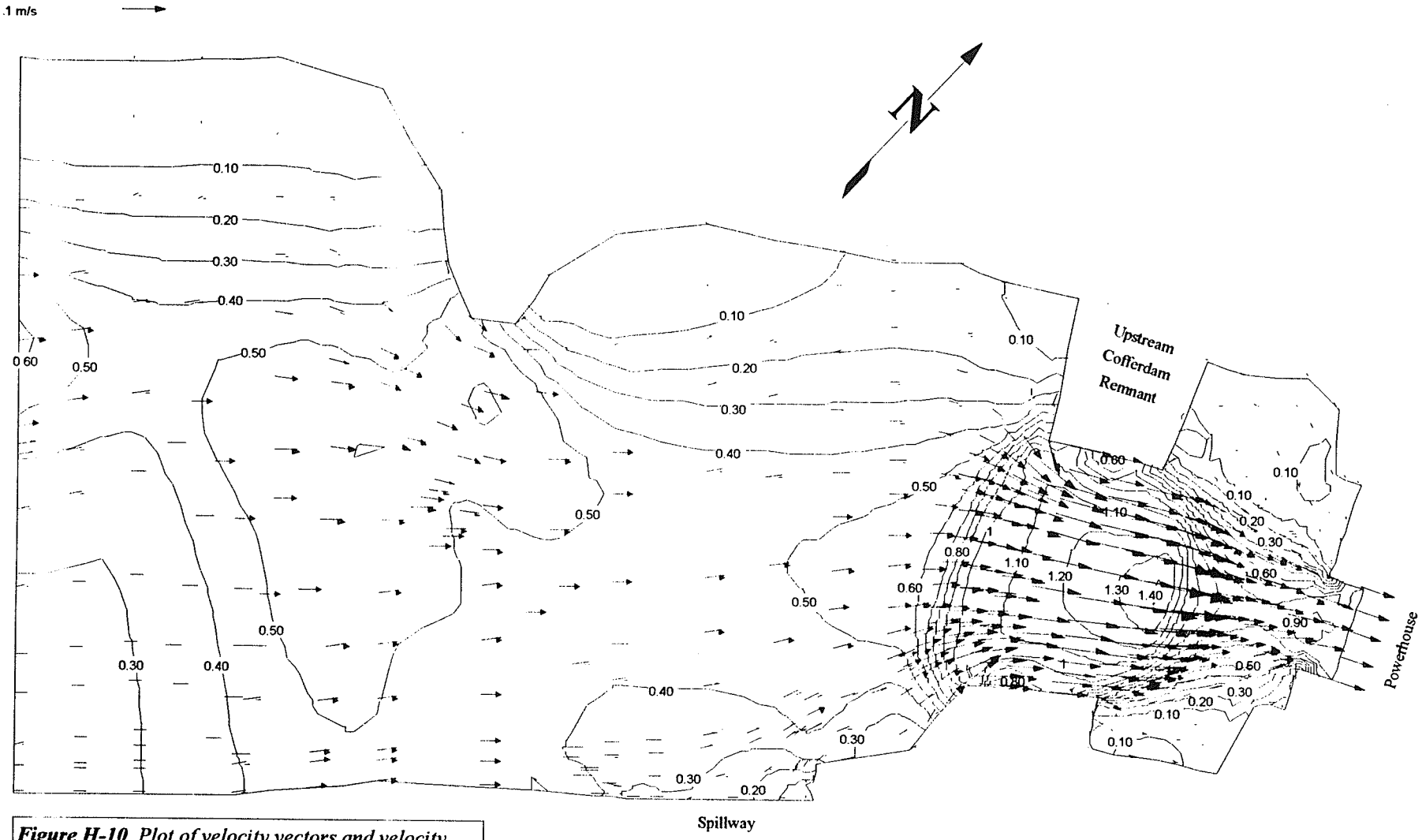

Figure H-10 *Plot of velocity vectors and velocity contours for the upstream Notigi G.S. with Cofferdam Removal Scheme UC3c (invert = 245.4 m, width = 60 m) under a discharge of 1100 m^3/s and an upstream water surface elevation of 257.45 m.*

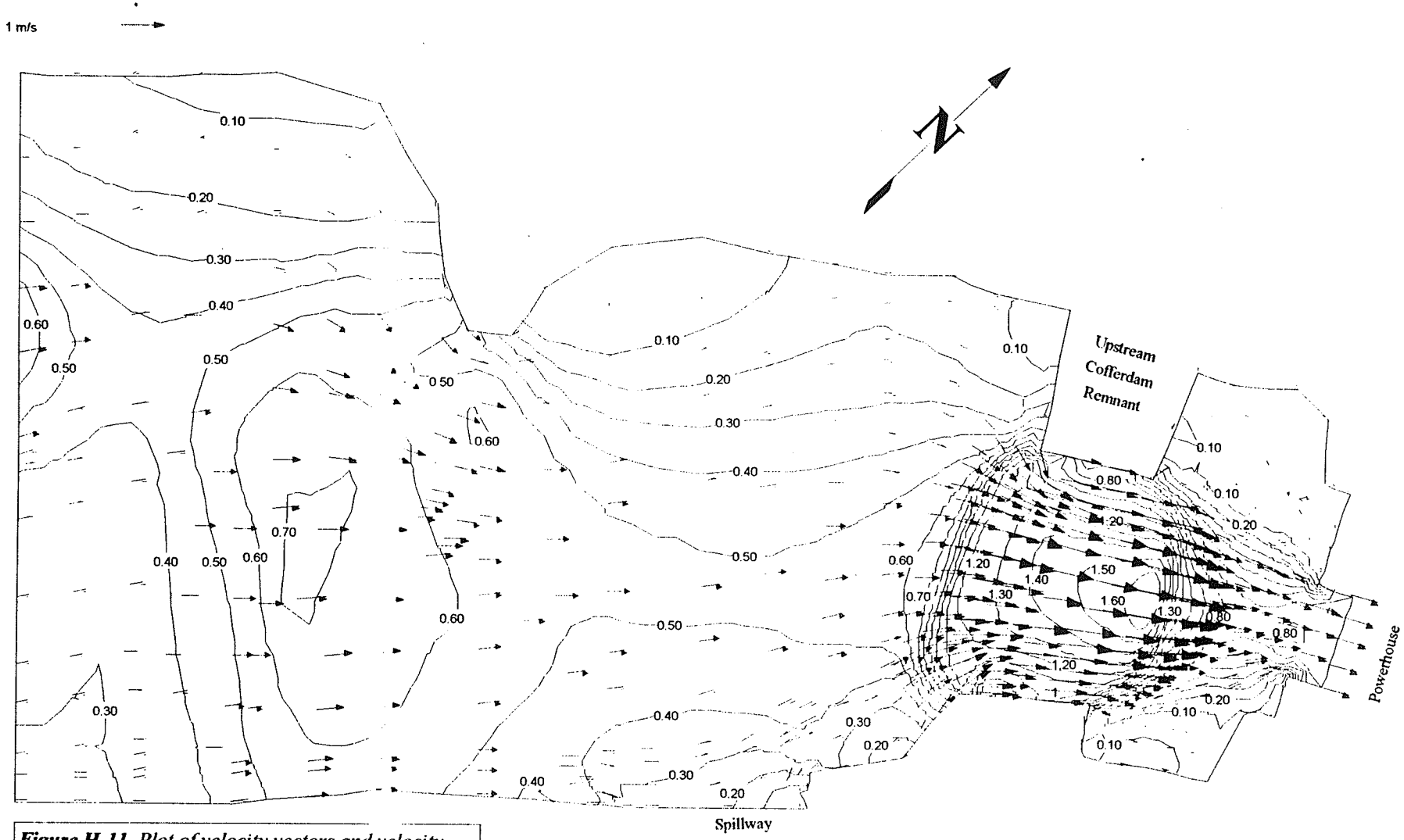

Figure H-11 *Plot of velocity vectors and velocity contours for the upstream Notigi G.S. with Cofferdam Removal Scheme UC3c (invert = 245.4 m, width = 60 m) under a discharge of 867 m^3/s and an upstream water surface elevation of 254.02 m.*

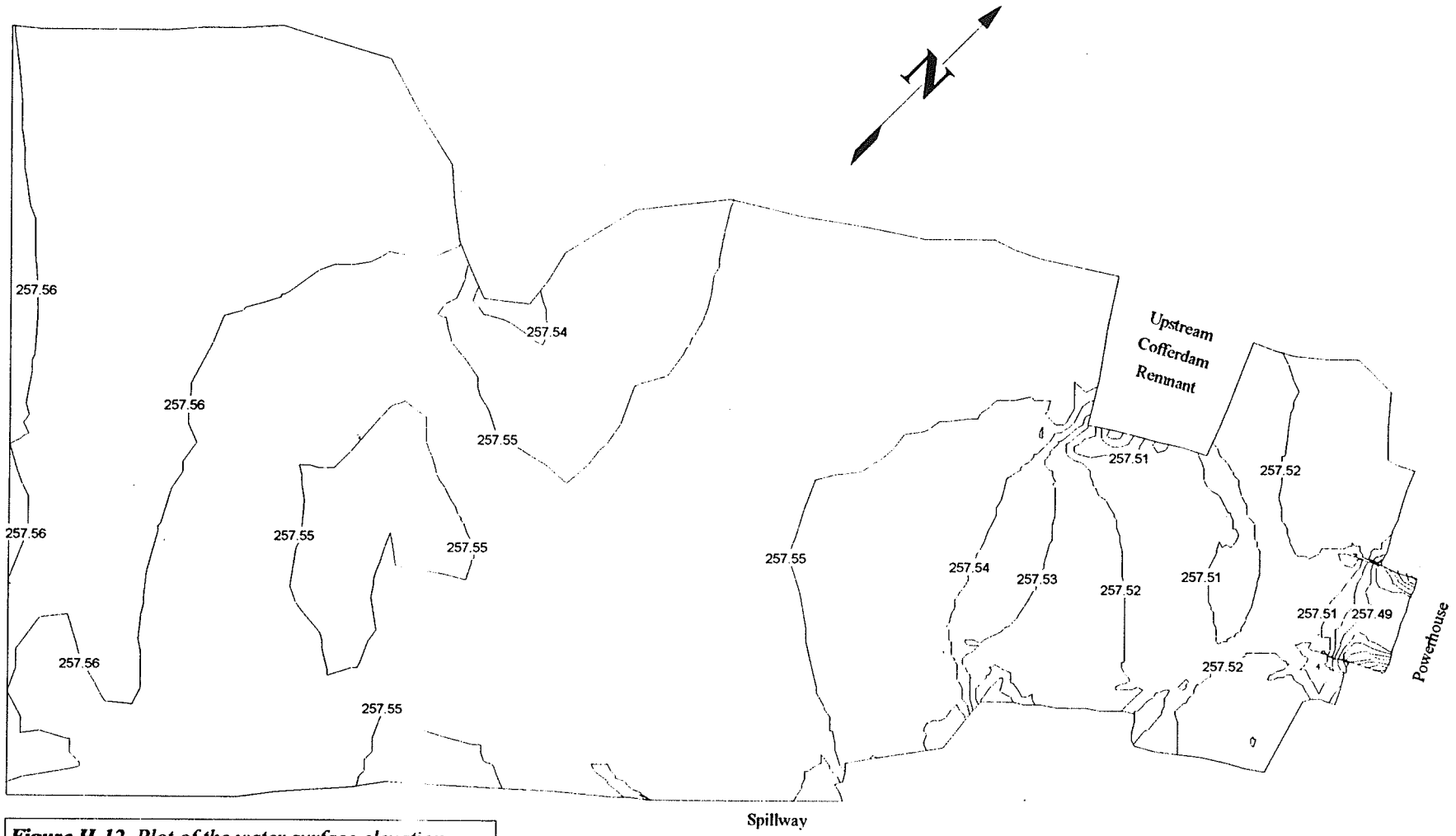

Figure H-12 *Plot of the water surface elevation contours for the upstream Notigi G.S. with Cofferdam Removal Scheme UC1b (invert = 239.8 m, width = 50 m) under a discharge of 1100 m^3/s and an upstream water surface elevation of 257.56 m.*

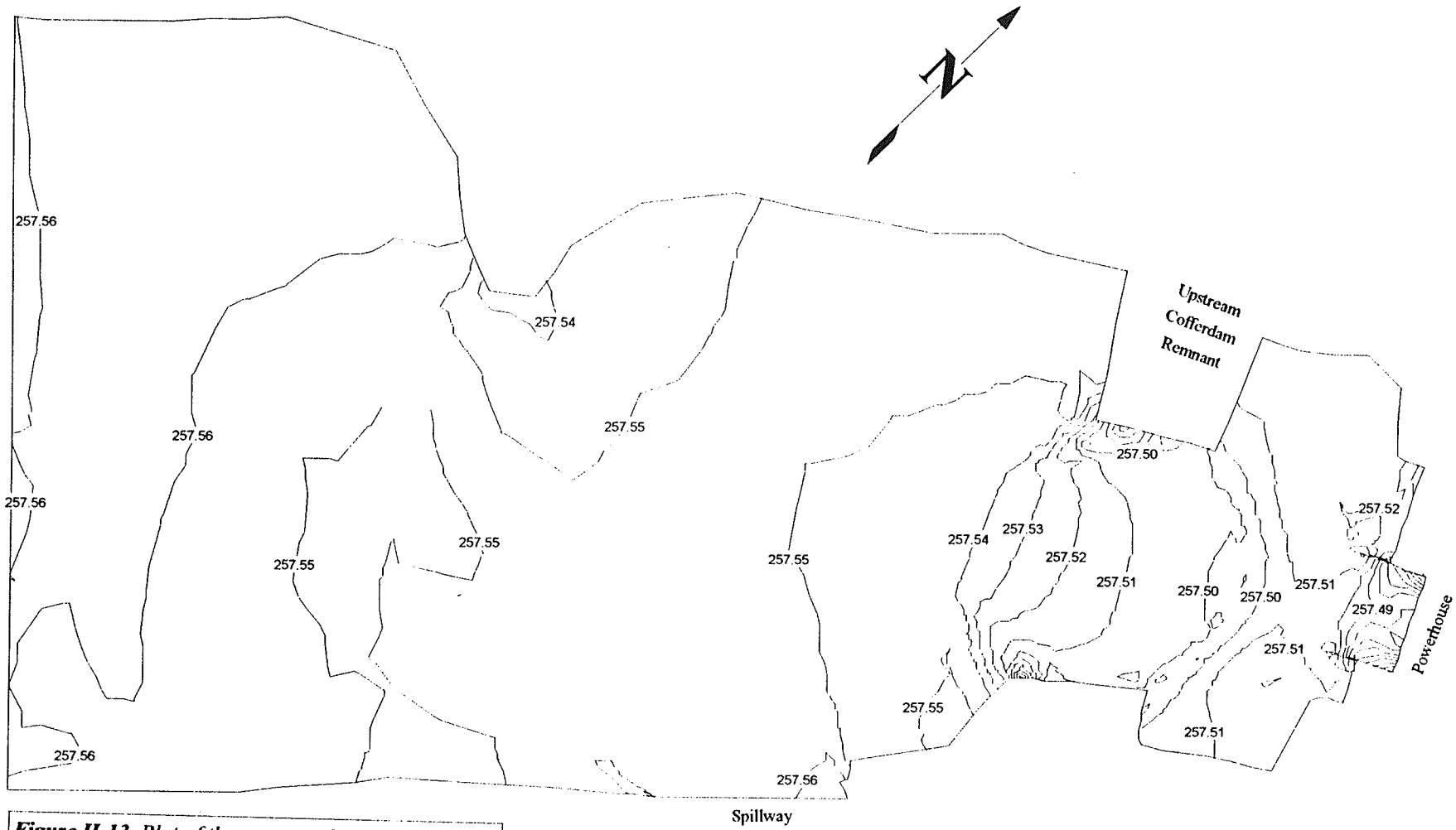

Figure H-13 *Plot of the water surface elevation contours for the upstream Notigi G.S. with Cofferdam Removal Scheme UC1c (invert = 239.8 m, width = 40 m) under a discharge of 1100 m^3/s and an upstream water surface elevation of 257.56 m.*

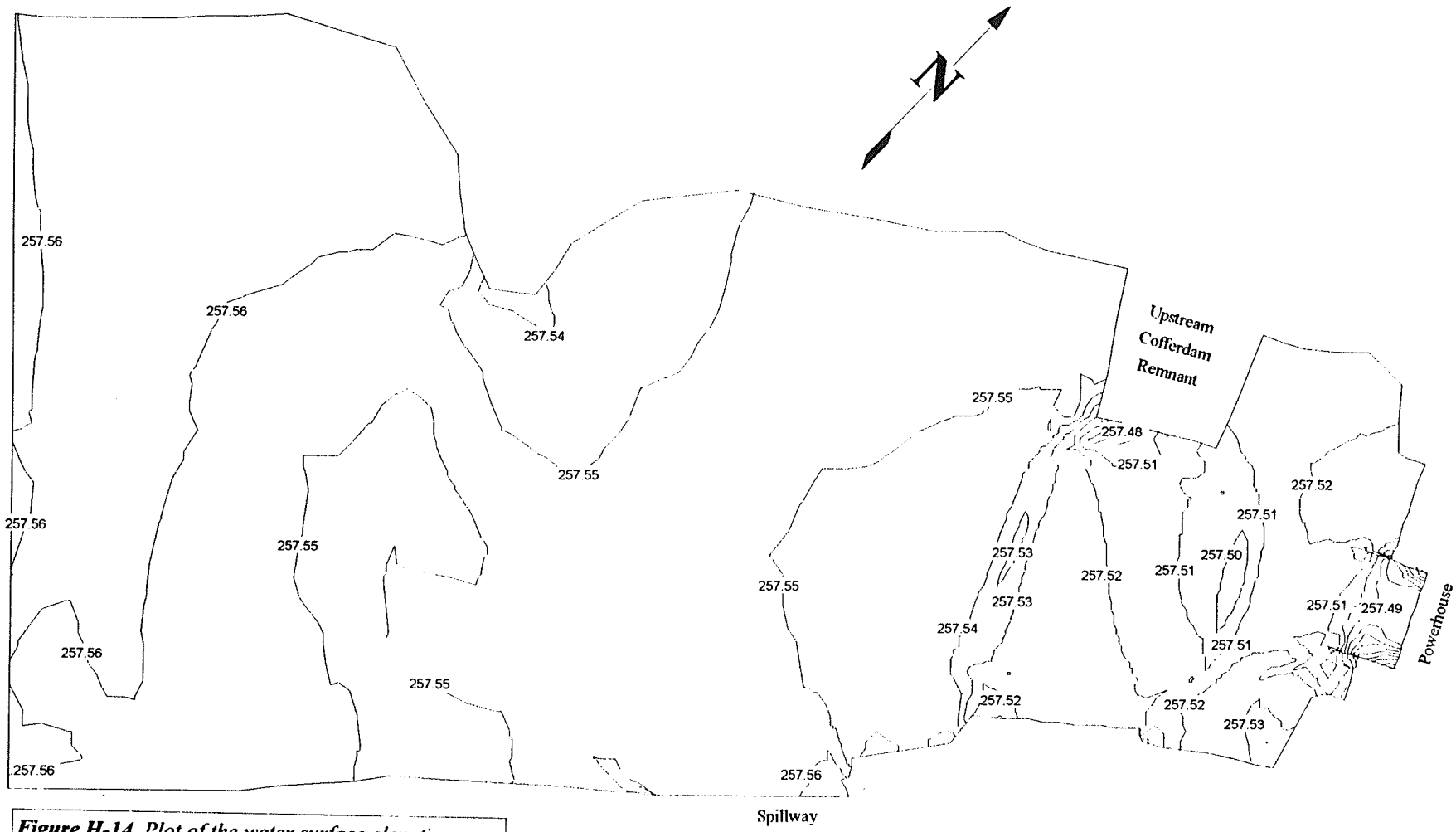

Figure H-14 *Plot of the water surface elevation contours for the upstream Notigi G.S. with Cofferdam Removal Scheme UC2a (invert = 242.8 m, width = 70 m) under a discharge of 1100 m^3/s and an upstream water surface elevation of 257.56 m.*

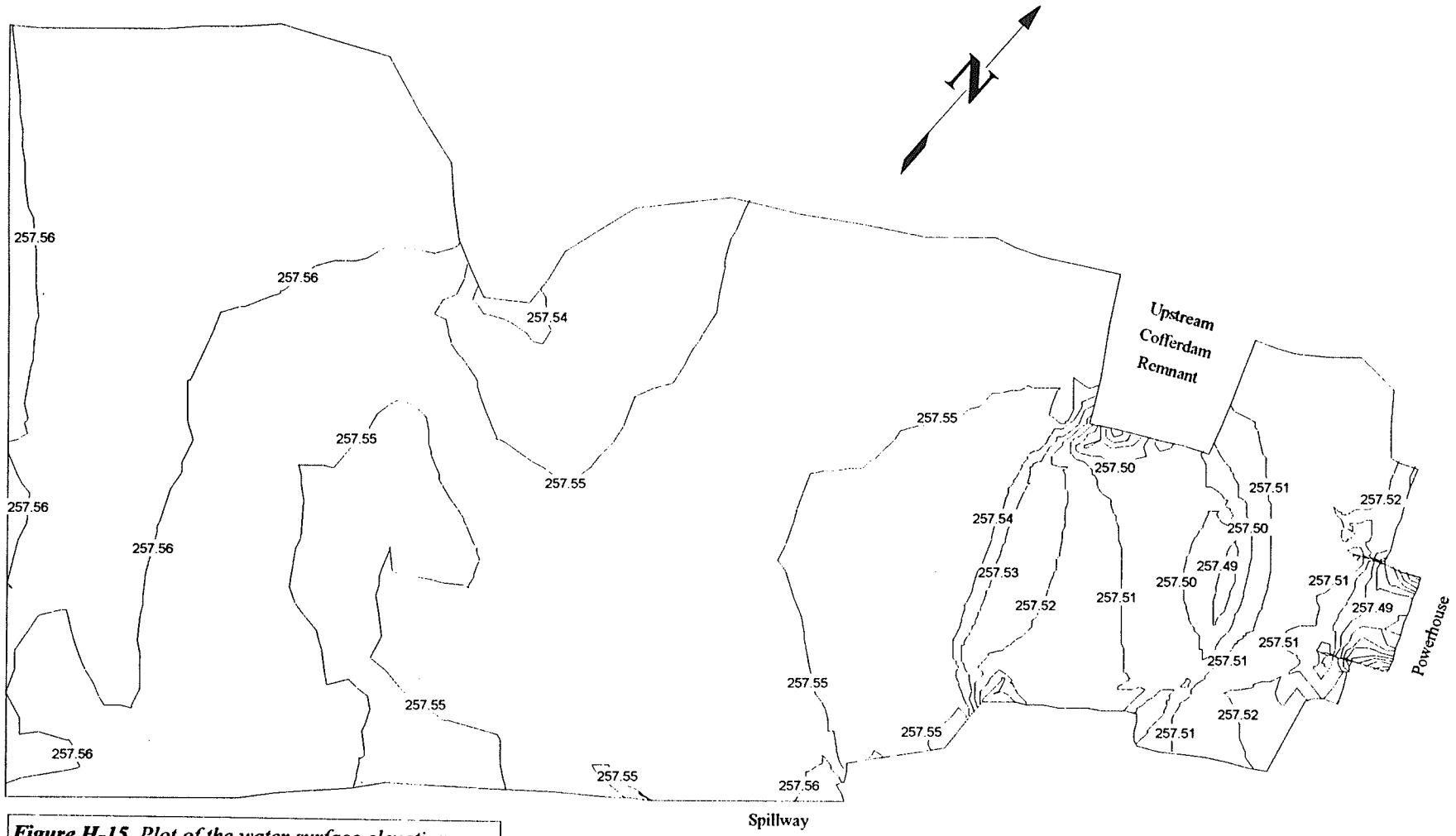

Figure H-15 *Plot of the water surface elevation contours for the upstream Notigi G.S. with Cofferdam Removal Scheme UC2b (invert = 242.8 m, width = 60 m) under a discharge of 1100 m^3/s and an upstream water surface elevation of 257.56 m*

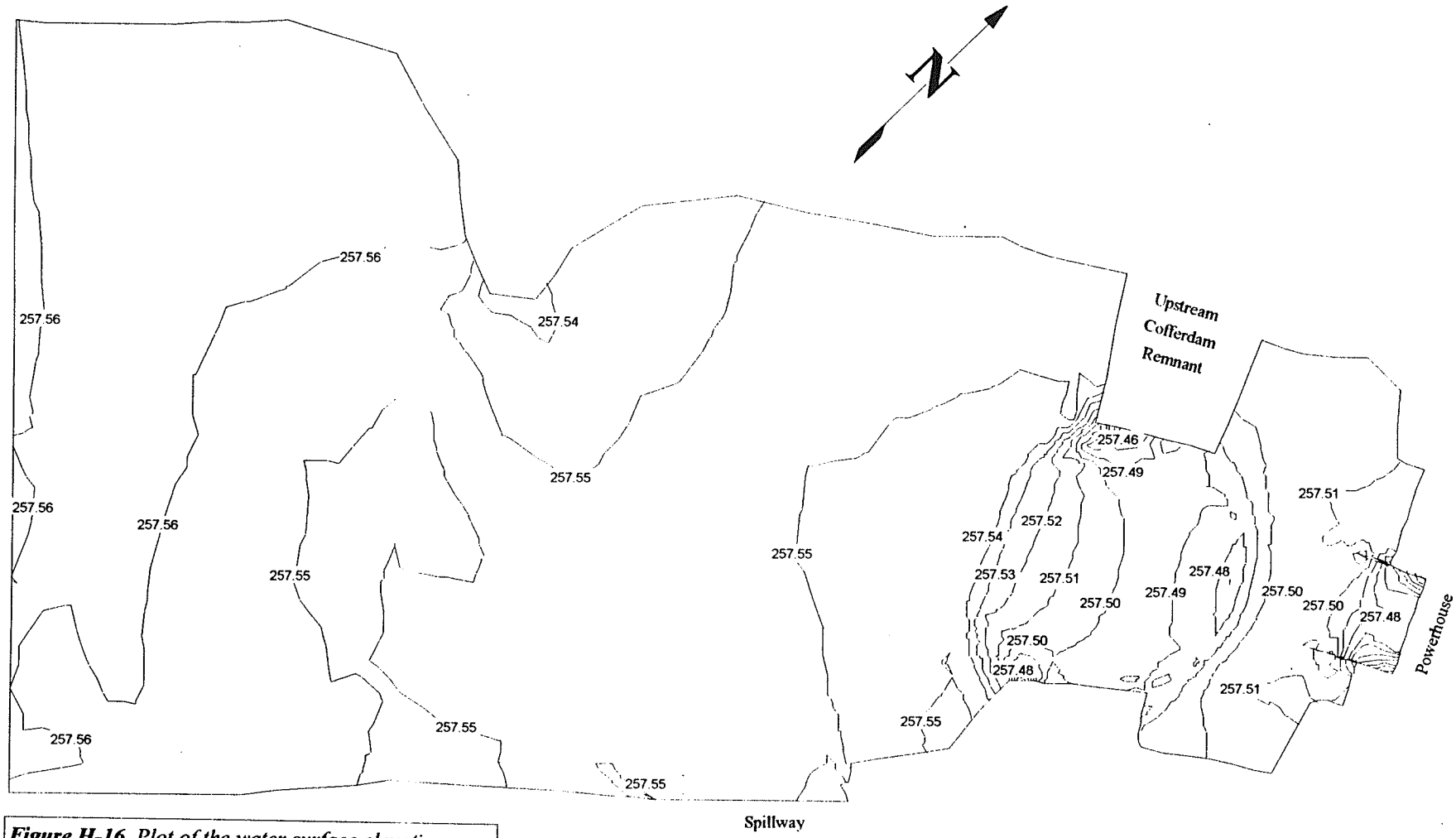

Figure H-16 *Plot of the water surface elevation contours for the upstream Notigi G.S. with Cofferdam Removal Scheme UC2c (invert = 242.8 m, width = 50 m) under a discharge of 1100 m^3/s and an upstream water surface elevation of 257.56 m.*

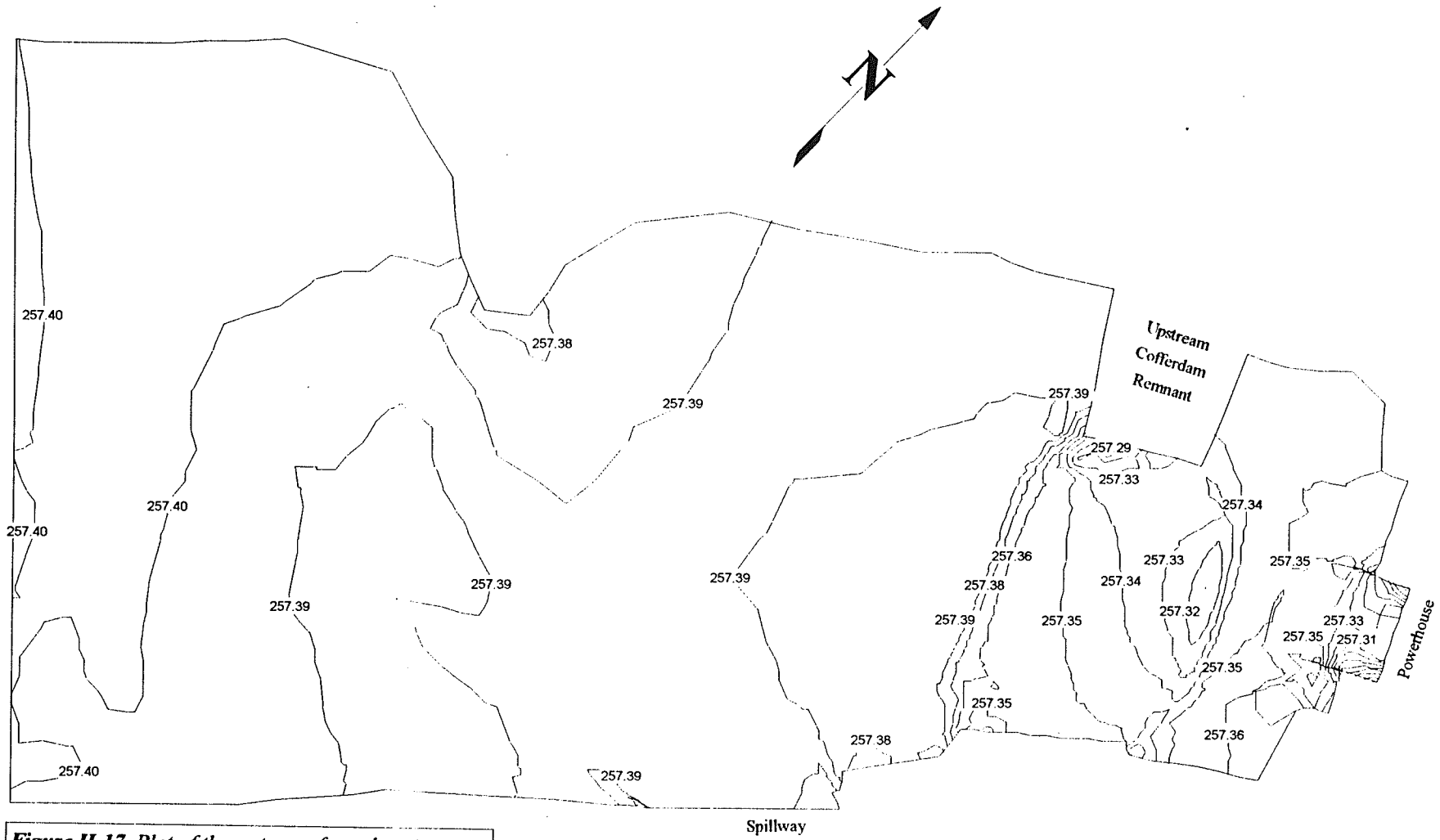

Figure H-17 *Plot of the water surface elevation contours for the upstream Notigi G.S. with Cofferdam Removal Scheme UC3a (invert = 245.4 m, width = 80 m) under a discharge of 1100 m^3/s and an upstream water surface elevation of 257.4 m.*

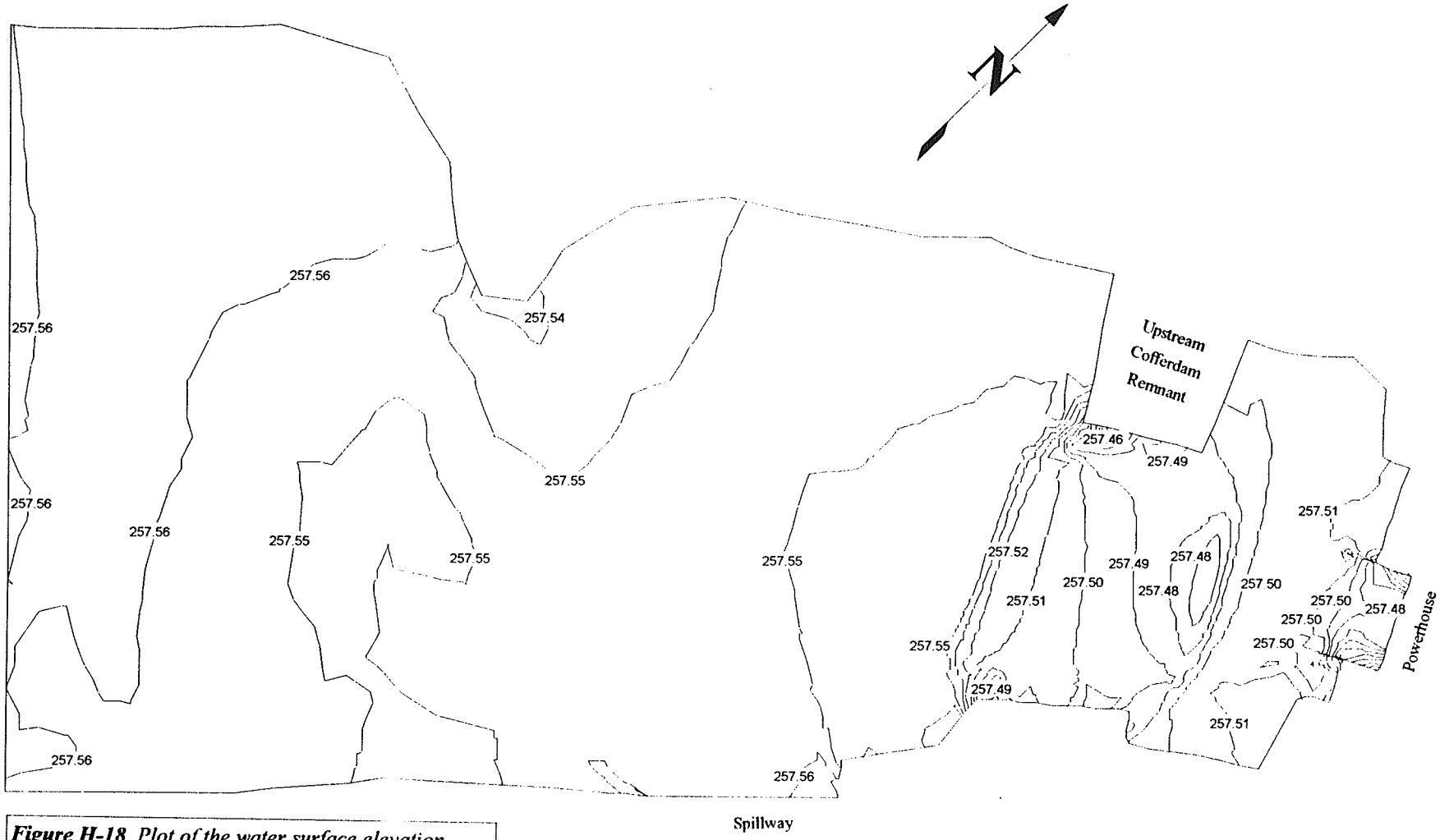

Figure H-18 *Plot of the water surface elevation contours for the upstream Notigi G.S. with Cofferdam Removal Scheme UC3b (invert = 245.4 m, width = 70 m) under a discharge of 1100 m^3/s and an upstream water surface elevation of 257.56 m*

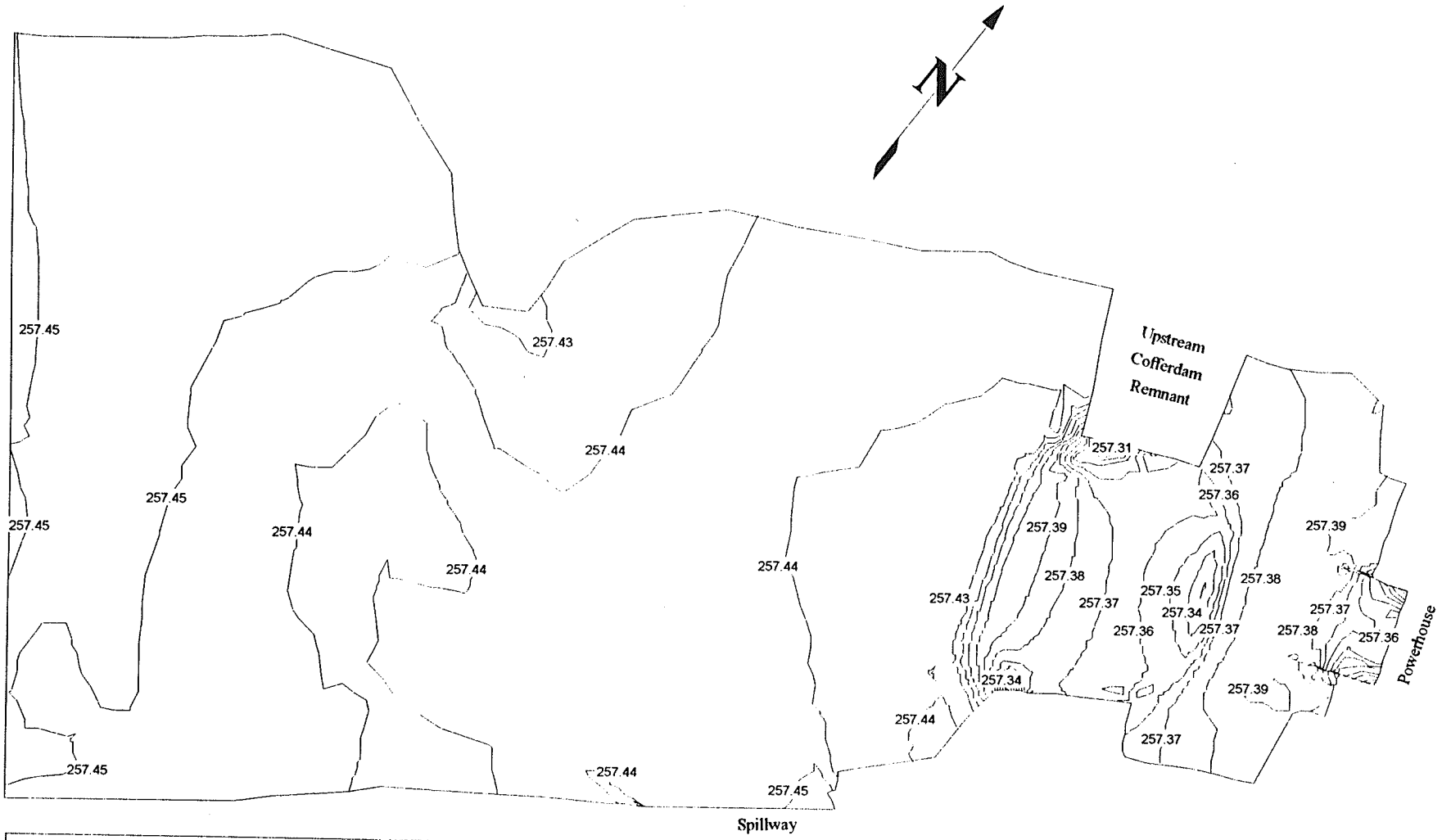

Figure H-19 *Plot of the water surface elevation contours for the upstream Notigi G.S. with Cofferdam Removal Scheme UC3c (invert = 245.4 m, width = 60 m) under a discharge of 1100 m^3/s and an upstream water surface elevation of 257.45 m.*

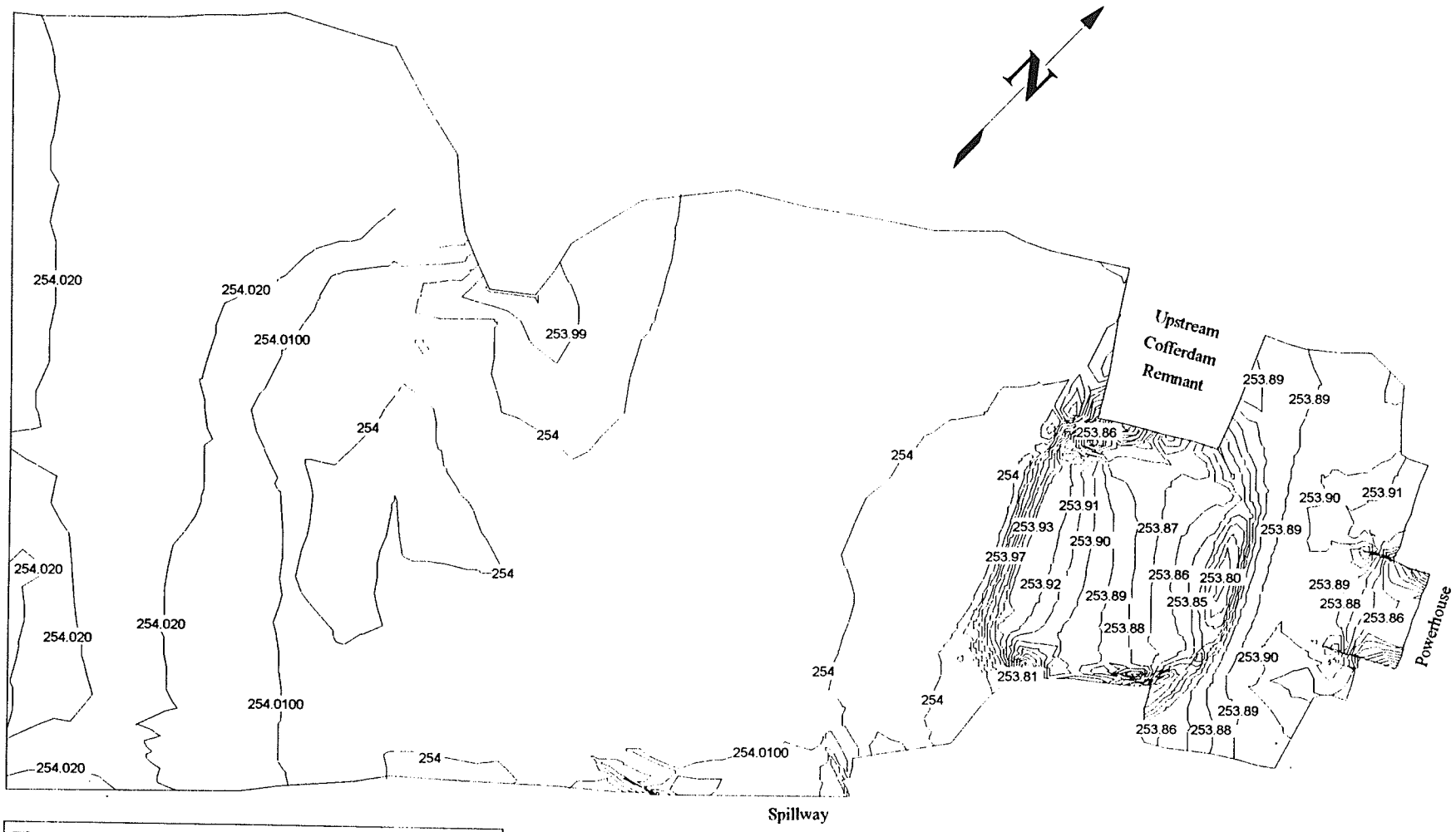

Figure H-20 *Plot of the water surface elevation contours for the upstream Notigi G.S. with Cofferdam Removal Scheme UC3c (invert = 245.4 m, width = 60 m) under a discharge of 867 m^3/s and an upstream water surface elevation of 254.02 m.*

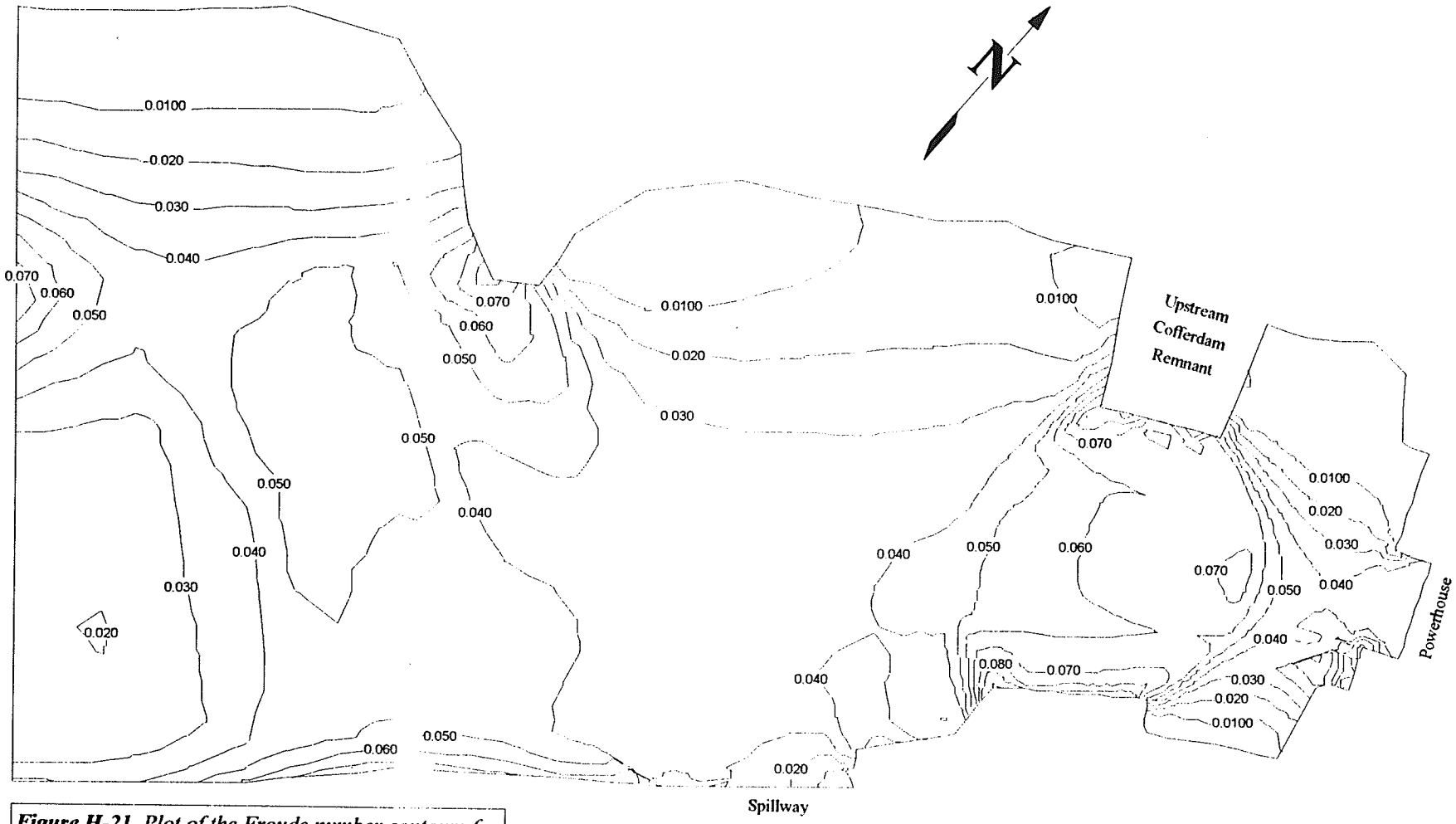

Figure H-21 *Plot of the Froude number contours for the upstream Notigi G.S. with Cofferdam Removal Scheme UC1b (invert = 239.8 m, width = 50 m) under a discharge of 1100 m^3/s and an upstream water surface elevation of 257.56 m.*

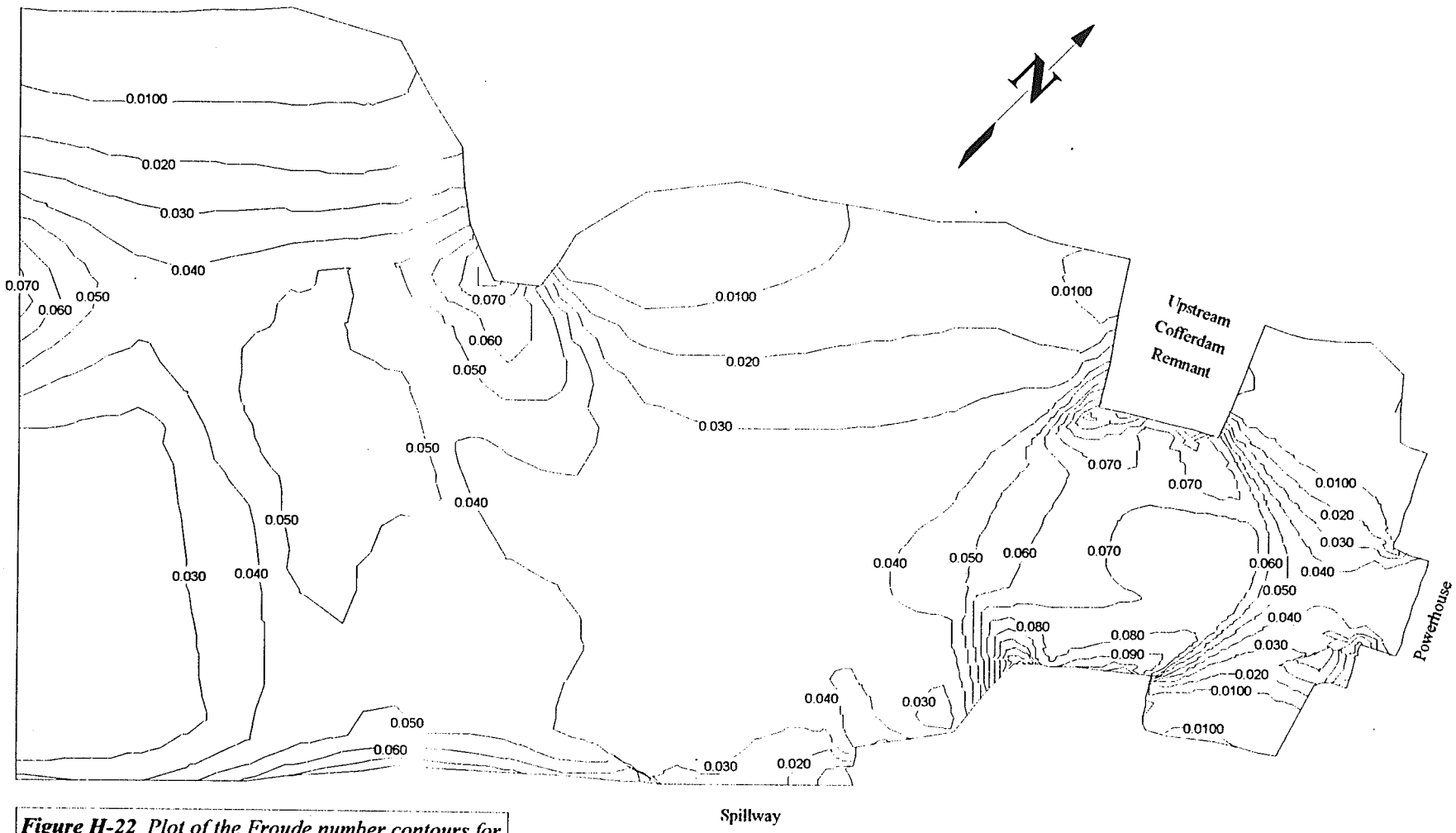

Figure H-22 *Plot of the Froude number contours for the upstream Notigi G.S. with Cofferdam Removal Scheme UC1c (invert = 239.8 m, width = 40 m) under a discharge of 1100 m^3/s and an upstream water surface elevation of 257.56 m.*

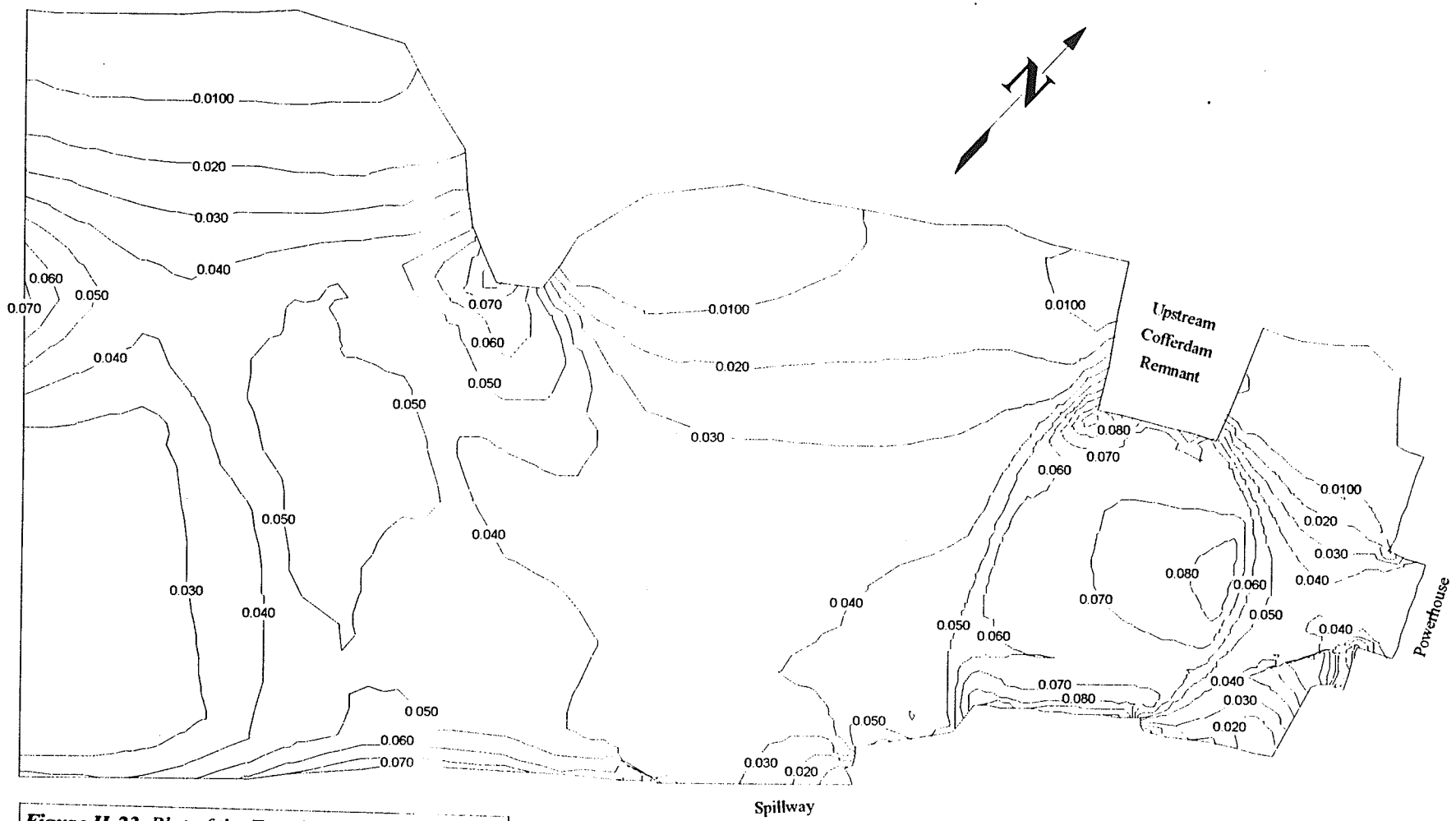

Figure H-23 *Plot of the Froude number contours for the upstream Notigi G.S. with Cofferdam Removal Scheme UC2a (invert = 242.8 m, width = 70 m) under a discharge of 1100 m^3/s and an upstream water surface elevation of 257.56 m.*

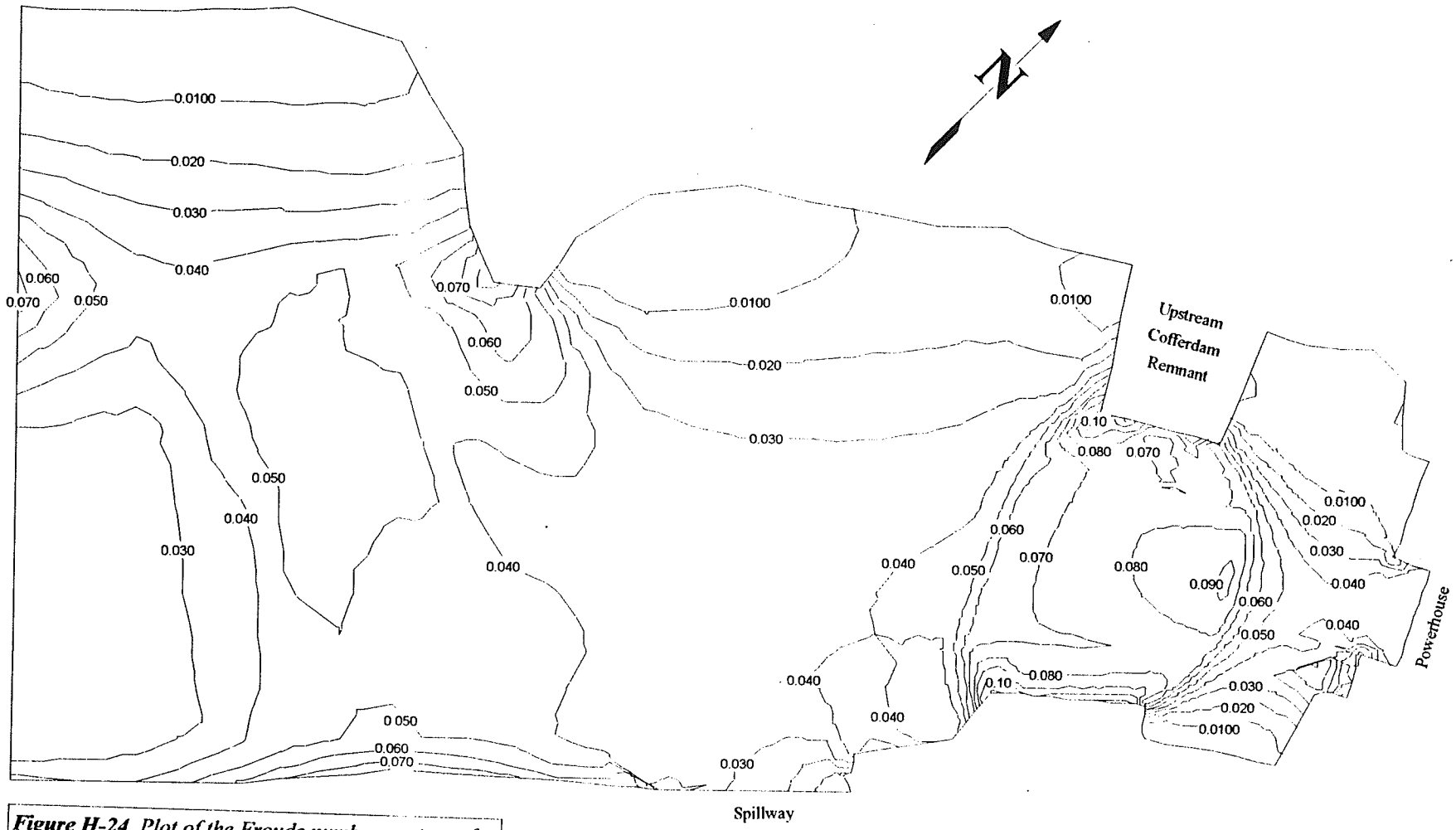

Figure H-24 *Plot of the Froude number contours for the upstream Notigi G.S. with Cofferdam Removal Scheme UC2h (invert = 242.8 m, width = 60 m) under a discharge of 1100 m^3/s and an upstream water surface elevation of 257.56 m*

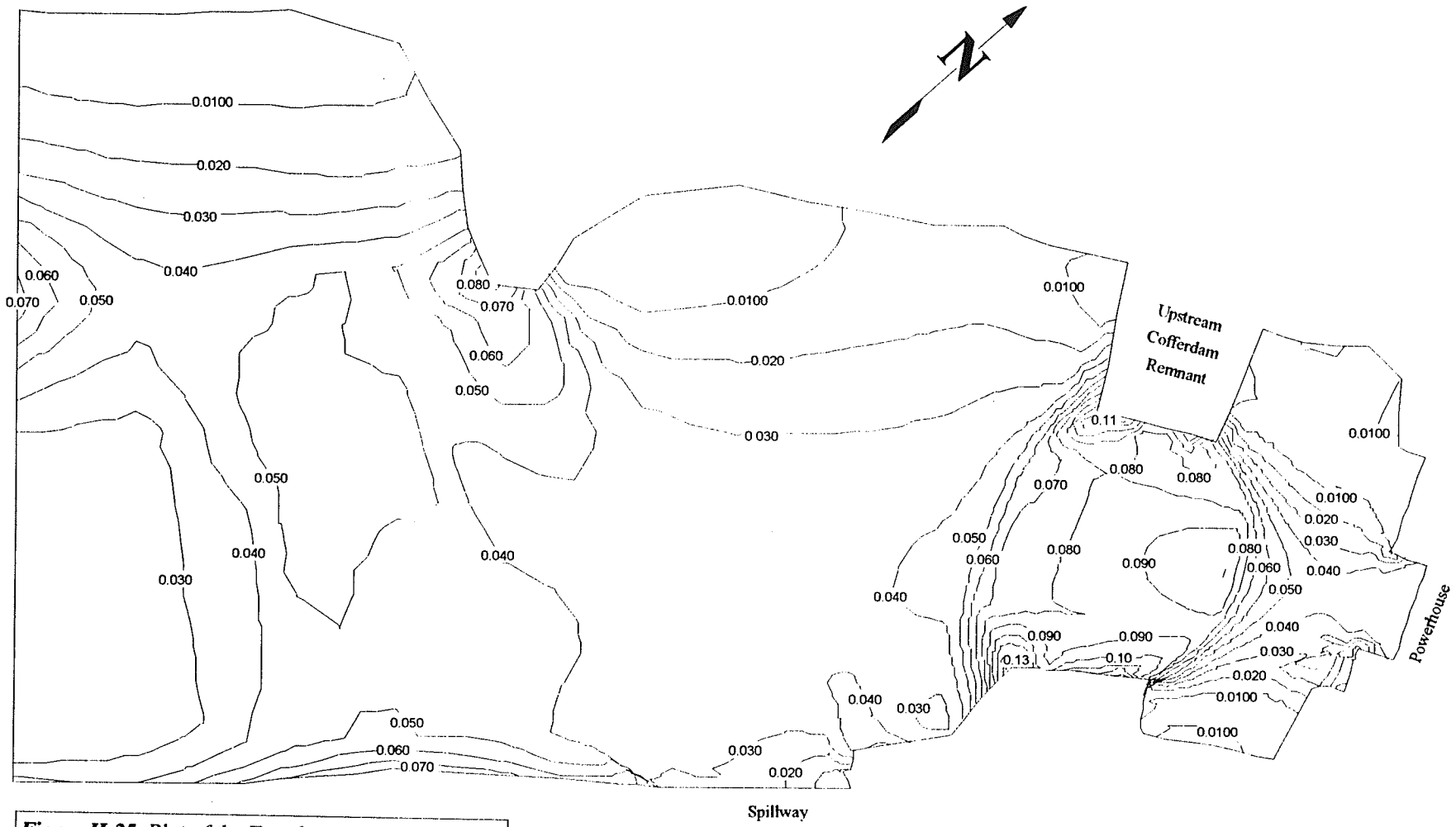

Figure H-25 *Plot of the Froude number contours for the upstream Notigi G.S. with Cofferdam Removal Scheme UC2c (invert = 242.8 m, width = 50 m) under a discharge of 1100 m^3/s and an upstream water surface elevation of 257.56 m.*

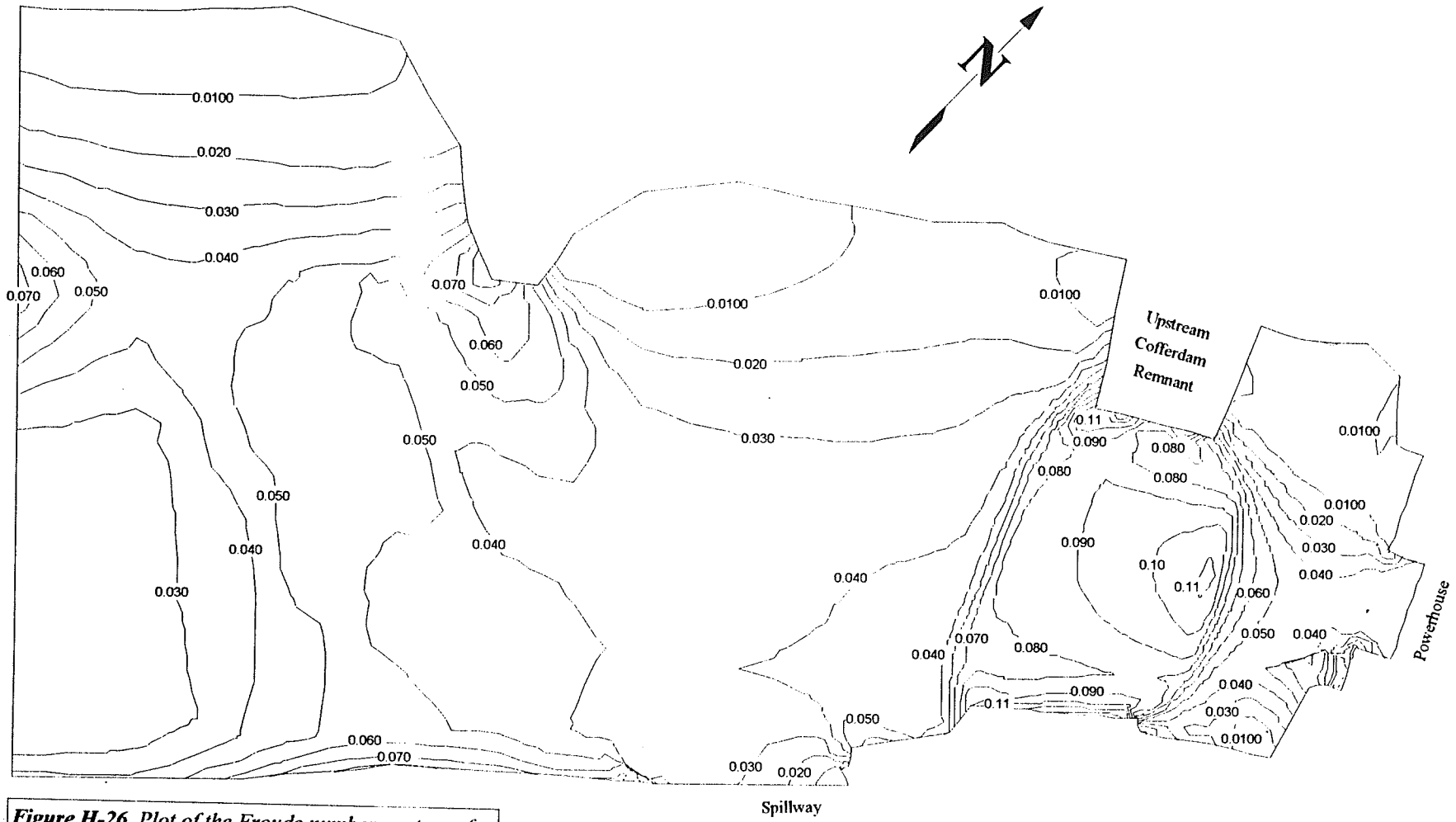

Figure H-26 *Plot of the Froude number contours for the upstream Notigi G.S. with Cofferdam Removal Scheme UC3a (invert = 245.4 m, width = 80 m) under a discharge of 1100 m^3/s and an upstream water surface elevation of 257.4 m.*

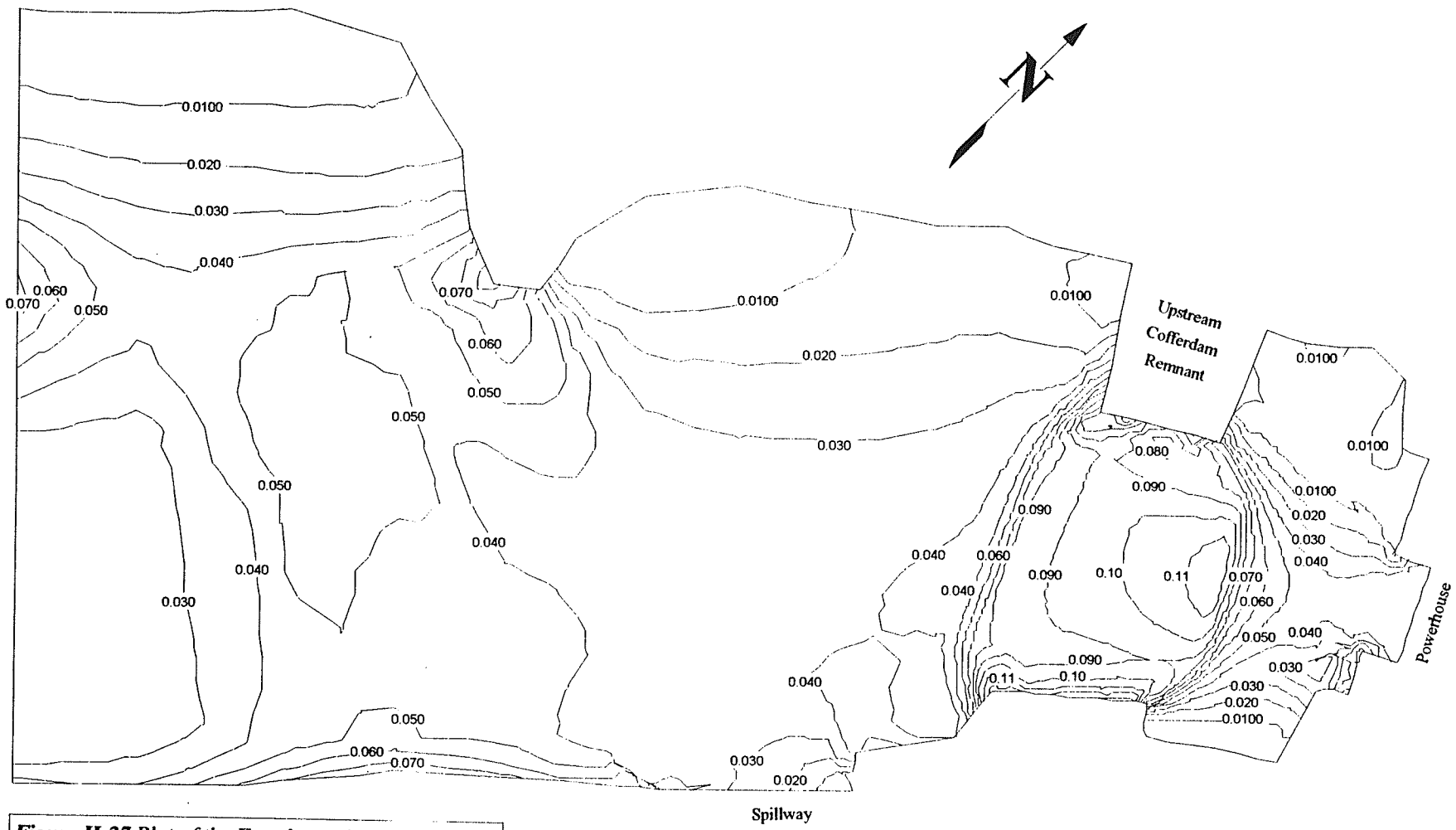

Figure H-27 *Plot of the Froude number contours for the upstream Notigi G.S. with Cofferdam Removal Scheme UC3b (invert = 245.4 m, width = 70 m) under a discharge of 1100 m^3/s and an upstream water surface elevation of 257.56 m*

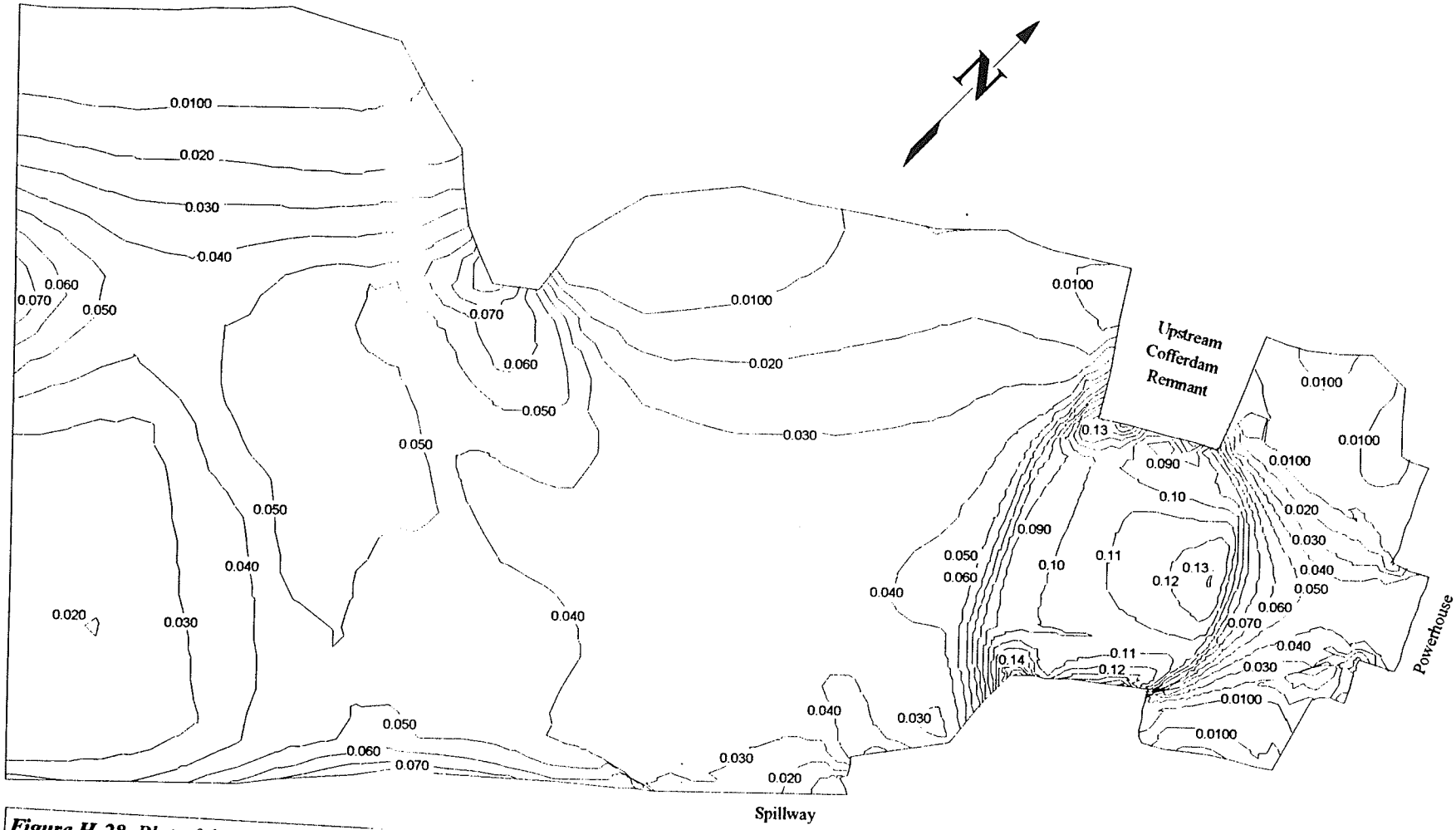

Figure H-28 *Plot of the Froude number contours for the upstream Notigi G.S. with Cofferdam Removal Scheme UC3c (invert = 245.4 m, width = 60 m) under a discharge of 1100 m^3/s and an upstream water surface elevation of 257.45 m.*

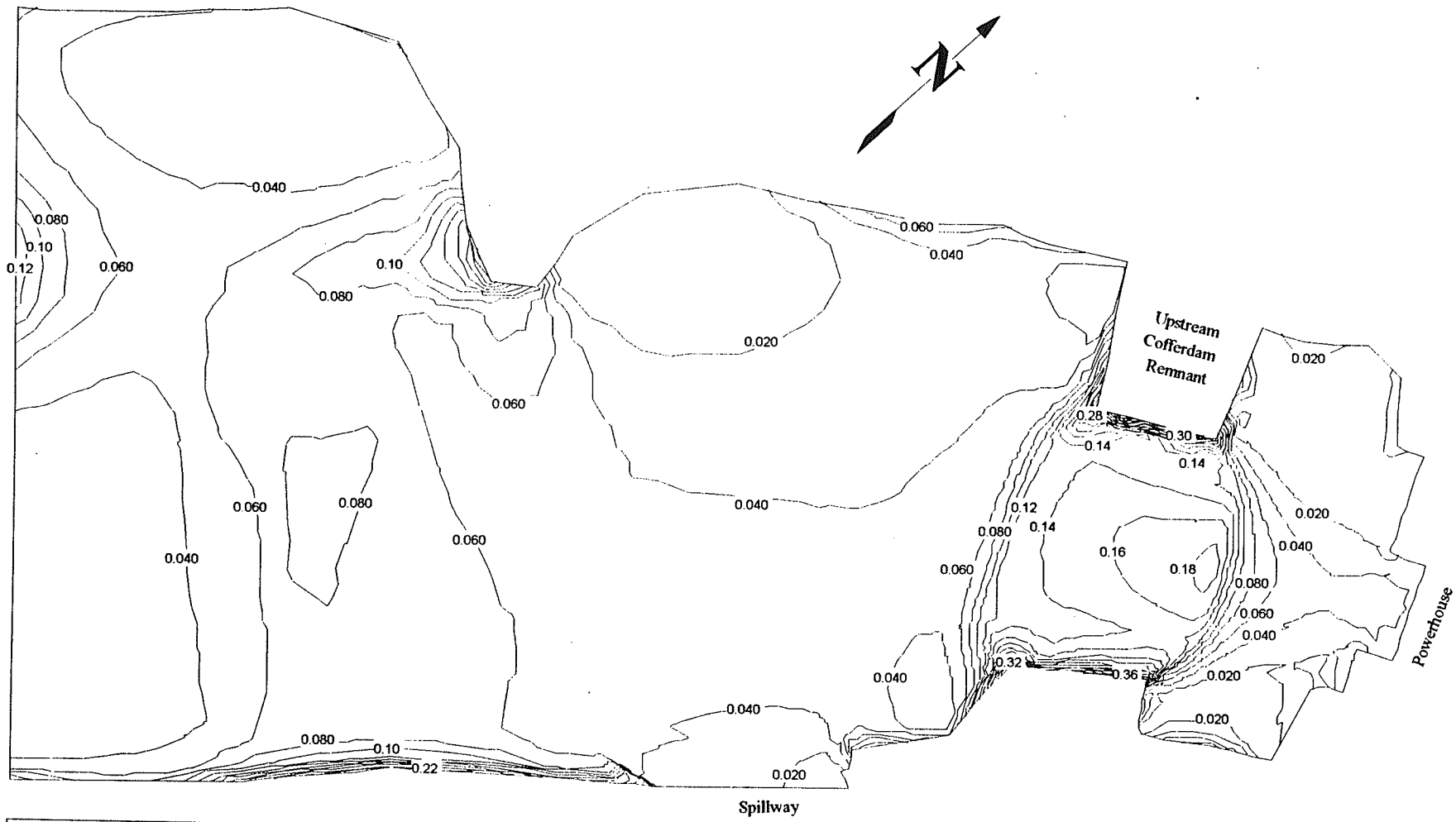

Figure H-29 *Plot of the Froude number contours for the upstream Notigi G.S. with Cofferdam Removal Scheme UC3c (invert = 245.4 m, width = 60 m) under a discharge of 867 m^3/s and an upstream water surface elevation of 254.02 m.*